



ASES SOLAR 20/20

Renewable Energy Vision

Virtual Conference
June 24-25, 2020

Official Conference Proceedings



AMERICAN
SOLAR
ENERGY SOCIETY



American Solar Energy Society National Solar Conference 2020 Proceedings

Edited by

Paulette Middleton, Elaine Hebert, Dara Bortman, Robert Foster, Carly Cipolla, and Carly Rixham
SOLAR 20/20 National Organizing Committee

Scott Sklar

Chair, SOLAR 20/20 National Solar Conference

Copyright © 2020 by the American Solar Energy Society

American Solar Energy Society

2525 Arapahoe Ave, Ste E4-253
Boulder, CO 80302

Email: info@ases.org

Web: www.ases.org

ISBN: 978-3-9820408-4-4

All rights reserved. No part of the publication may be reproduced, transmitted, in any form or by any means, electronic, mechanical, photocopying, recording or otherwise, without permission of the publisher, except in the case of brief quotations embodied in critical articles and review or where prior rights are preserved.

Produced by

International Solar Energy Society
Wiesentalstr 50
79115 Freiburg
Germany

Tel: + 49 761 45906 – 0

Fax: + 49 761 45906 – 99

Email: hq@ises.org

Web: www.ises.org

Notice

Neither the International Solar Energy Society and the American Solar Energy Society, nor any one of the supporters or sponsors of the American Solar Energy Society National Solar Conference 2020 (SOLAR 20/20) makes any warranty, express or implied, or accepts legal liability or responsibility for the accuracy, completeness or usefulness of any information, apparatus, product or process disclosed, or represents that its use would not infringe privately on rights of others. The contents of articles express the opinion of the authors and are not necessarily endorsed by the International Solar Energy Society, American Solar Energy Society or by any of the supporters or sponsors of SOLAR 20/20. The International Solar Energy Society and the American Solar Energy Society do not necessarily condone the politics, political affiliation and opinions of the authors or their sponsors.

Scientific Program

Proceedings

ASES SOLAR 20/20: Renewable Energy Vision Conference, Proceedings Introduction <i>Committee, N.O.</i>	1
A Framework to Reduce Dust Problems on PV Modules in the US Climatic Zones <i>Ragheb, A.</i>	2
Emergency Power For All Disasters <i>Young, B.</i>	10
Utilizing Solar Infrared-Induced Photothermal Heating on Building Windows in Winter <i>Zhang, E., Duan, Q., Wang, J., Zhao, Y.</i>	18
Long Term Output Deterioration of Grid-Tied PV Systems <i>Barber, E.</i>	27
New Ways to Combine Solar Thermal with Geothermal <i>Olson, G., Yu, Y.</i>	32
A New National Database for Solar Resource Assessment Compiled from Ground-Based Observations <i>Hall, J.</i>	40
Occupational Risks Associated with Solar Installations: A Review <i>Duroha, J., Brownson, J.R.S., Macht, G.</i>	49
Carbon Footprint in the Design Studio, a Paradigm Shift <i>Mansy, K., Brandvold, A., Phillips, J., Spector, T., Stivers, J.</i>	56
Is Hydrogen Energy Storage Ready for Prime Time on the North American Grid? A Guide for Bankers and Their Engineers <i>Stavy, M.</i>	63
Development of a Spectral Integral Method for Analyzing Solar Effects through Windows on Indoor Thermal Comfort <i>Wang, N., Feng, Y., Wang, J.</i>	74
Estimating Hourly Solar NIR Irradiance Using Meteorological Data for Sustainable Building Design and Engineering <i>Duan, Q., Feng, Y., Wang, J.</i>	80
Forecasting Carbon Emissions in Seven Eastern States of the United States: The Effects of Coal Deregulations <i>Khoie, R., Calderon, A.</i>	86
The Carbon Emissions of Wind Power: A Study of Emissions of Windmill in the Panhandle of Texas <i>Khoie, R., Bose, A., Saltsman, J.</i>	99
House in a House <i>Schwaen, R.</i>	110
Sustainable Solar Water Pumping for Irrigation in Bangladesh <i>Foster, R., Rahman, M., Sayeed, S.I.</i>	121
Zero Emissions Network: A Pilot Program for Carbon Emissions Reduction <i>Townes, S., Khoie, R., Stathopoulos, P.</i>	133

Emerald City 100% Renewable Energy Plan	
<i>Smiley, S.</i>	142
Hourly Solar Radiation Estimation Using DM and GRNN Models	
<i>Gebreyohannes, Y., Kahsay, M.B., Lauwaert, J.</i>	155

Proceedings

ASES SOLAR 20/20: Renewable Energy Vision Conference
Proceedings Introduction
National Organizing Committee

The world has changed and we must change with it, but our ultimate goal – a world run on clean, renewable energy – remains the same. What can we do together to ensure that the current global pandemic doesn't slow, but actually accelerates the transition to a clean energy world? What can we do to better integrate and connect concerns about social, economic and racial injustice with our ongoing efforts to improve access to clean air, clean water and clean energy for all? These were key questions addressed throughout the American Solar Energy Society's (ASES) first virtual conference on June 24 and 25. A major outcome of the conference is the Call to Action #MissionPossible #FossilFreeAndFlourishing. To sign the Call to Action and to view conference discussions, visit ases.org/conference

A key aspect of achieving the renewable energy vision is gaining public support for actions and policies that will rapidly advance the transformation to 100% renewables. During the kickoff session of the conference, the *Stronger Together Town Hall*, representatives from a wide array of organizations involved in advocacy and policy making highlighted how we can better work together to grow our constituencies and strengthen our movement to realize our common goals. The two conference keynote sessions, *Clear Vision for Worldwide Action* and *Citizen Action*, brought together diverse perspectives on global and national climate actions aimed at drawing together policymakers, leaders in all sectors, and advocates to spur change.

The conference featured technical discussions on advances in buildings, including presentations from 2020 Solar Decathlon decathletes; PV, solar thermal, storage and system integration; as well as clean energy education, policy, and finance. Many of these presentations have been developed into papers for these proceedings.

Special forums included the longstanding Women in Solar Energy (WISE) Forum highlighting women who are leading and inspiring others across the solar industry space; the Emerging Professionals Forum connecting young people new to the renewable workforce through networking opportunities; and the Spirit and Sustainability Community Forum in which everyone was invited to share their thoughts about how we can move toward a cleaner, healthier, and more equitable society as efficiently, safely, and quickly as possible. The interactive conference platform provided opportunities for participants to network with each other through chat platforms, engage in live and recorded sessions with dozens of speakers, and learn more about conference partners and sponsors in the exhibit hall.

During the conference, attendees were invited to sign the Call to Action which stresses:

- ◆ A world run on 100% renewable energy is possible; and
- ◆ Being fossil free leads to a thriving economy, planet and people worldwide; and
- ◆ Progress to 100% renewable energy is accelerated by working together.

To sign the Call to Action pledge for your organization and yourself, and to view conference discussions, visit ases.org/conference

A Framework to Reduce Dust Problems on PV Modules in the US Climatic Zones

Ash Ragheb, PhD

Lawrence Technological University, Southfield, Michigan, United States

Abstract

The peak of energy demand, oil prices, and impending climate change are critically driving the adoption of solar photovoltaic (PV) as a sustainable, renewable and less impact energy alternative. The installation of PV systems for optimum yield is primarily dictated by its geographic location (latitude and available solar insolation), and installation design (tilt angle, orientation, and altitude) to maximize solar exposure. Once these parameters have been addressed appropriately, there are other externalities that contribute to the system performance (efficiency and output). Dust is a major factor that significantly influences the performance of the PV systems. Although substantial time and money have been invested in PV systems to increase efficiency, a far less time and money have been invested to address dust deposition on such systems.

This paper provides an overview of soiling problems; primarily those associated with dust or sand and combined dust-moisture conditions that are associated with many of the most solar-rich geographic locations in the United States. It reviews and evaluates key contributions to the understanding, performance effects, and mitigation of these problems. More specifically, the paper reviews the impact of dust deposition on the performance of solar PV and identifies challenges to further research in this area. It highlights the status of research over seven decades of effort. Based on the research studies, the research outcome presents recommendations to guide in identifying the appropriate cleaning/maintenance cycle for PV systems. This is aligned with the prevalent climatic and environmental conditions in the United States' climatic zones based on ASHRAE classification.

Keywords: Photovoltaics (PV), Performance, Dust Impact, PV Cleaning, ASHRAE US Climatic Zones.

1. Introduction

The delivery of a solar-energy system is generally associated with the sun's availability, irradiance, as well as a variety of environmental and climatic factors and component performance. Soiling represents a problem that can be an obstacle for the viability of a solar installation. The deposition of dust, bird droppings, salty water stains can degrade the efficiency of the solar PV. Moreover, it is further reduced through losses in wiring, inverters by 10-25% due to these conditions (Denholm et al., 2010)

Research has been ongoing on this subject for more than seven decades. Yet, the impact and properties of dust on energy transfer and efficiency of PV is still not fully comprehended. Till today, the most effective mitigation technique is basically washing the PV surface with water or with some specialty solutions/detergents. This method is labor and water consuming as well, it has high operating cost. In most cases in the U.S. and abroad, the abundant solar regions are usually contingent with water scarcity which makes wet cleaning not an optimum mitigation approach.

Research has aimed to study the dust deposition primarily in the context of solar PV installations. Based on the nature of investigation into the impact of dust on PV system performance, the research can be categorized into the two main topics. First, the wind effects/directions and exposure time studies, primarily investigate solar system characteristics such as tilt angle, glazing, and its impact of dust accumulation. Second, are the

more comprehensive studies on dust particles physics and chemistry with deeper accuracy in experimental investigations.

2. Dust impact on performance: wind effects, exposure time, and tilt angle

The first studies on the effects of dust accumulation on the performance of solar collectors were conducted in the United States. Dietz (1963) tested glass samples (between 0° and 50°) and showed a reduction up to 5% of the solar radiation reaching the collector due to dust accumulation. Michalsky (1988) ran a study in Albany, NY that compared the performance of 2 pyranometers of which one was cleaned daily and the other was left un-cleaned for 2 months. The un-cleaned showed less than 1% reduction in performance. The results of these studies could not be generalized, except for these regions in the U.S. that have frequent rain and low dust. However, the industry accepted results as typical for the U.S and stopped the development till the energy crisis in early 1970s. During this period, technology and research has advanced in other critical areas where dust is more significant factor. These areas are Middle East, North Africa (MENA) and Asia as well, where desert, wind, and dusty environment are significant. Studies in these dusty areas have shown that few hours of exposure to dust can cause the same reduction in PV performance over months in more temperate areas like Northeast of U.S.

Among studies in this region, Sayigh (1978) conducted a study in Saudi Arabia and found a performance reduction of 30% in flat plate collectors after only 3 days without wiping/cleaning. Another study by Sayigh et al. (1985) conducted more comprehensive experiments examining the reduction in transmittance vs. tilt angle in Kuwait desert. They found a reduction in plate-transmittance by an amount ranging from 64% to 17% for tilt angles ranging from 0° to 60°, respectively after 38 days of exposure. In addition, a reduction of 30% in useful energy gain was observed by the horizontal collector after 3 days of dust accumulation (Fig.1).

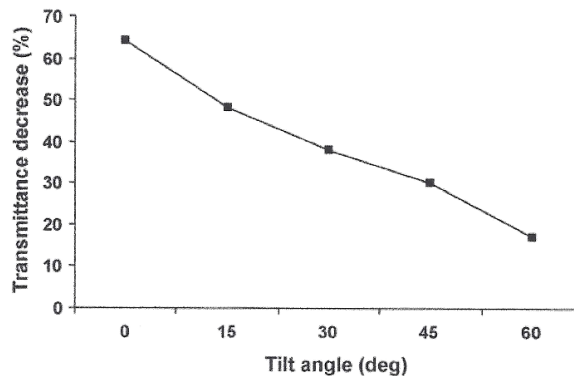


Fig. 1: Reduction in Solar Intensity for Various Particle Size Due to Dust Deposition (5)

3. Dust physical and chemical properties vs. PV performance

A critical factor to develop effective dust mitigation techniques is to understand the relationship between the physical properties of dust (size, geometry) and its chemistry (carbon, cement, limestone, etc) on performance of PV modules. This physical nature and deposition patterns vary by regions of the world. Not until early 1990s when this relationship was recognized, and research validated.

El-Shobokshy and Hussein (1993a, 1993b) investigated the physical properties of the dust accumulation and deposition density on their impact on parameters degrading PV efficiency. The experiment was entirely simulated with artificial dust (including limestone, cement, and carbon particulates) and halogen lamps. While keeping the solar (light) intensity constant and varying the different densities of dust the test was repeated

several times. The study revealed the impact of cement particles to be the most significant, with a 73 g/m² deposition of cement dust resulting in an 80% drop in PV short-circuit voltage; atmospheric dust with mean diameter 80 mm at 250 g/m² was found to reduce the short-circuit current by 82%. Fine carbon particulates (5 mm) were found to have the most deteriorating effect on the PV efficiency. The study also found the impact of finer particles to have a greater impact than coarser particles on PV performance (Fig. 2), for the same dust type. In addition, while the PV fill-factor reduced with excessive dust accumulation, it was found to respond to increase in solar intensity for both cleaned and un-cleaned conditions.

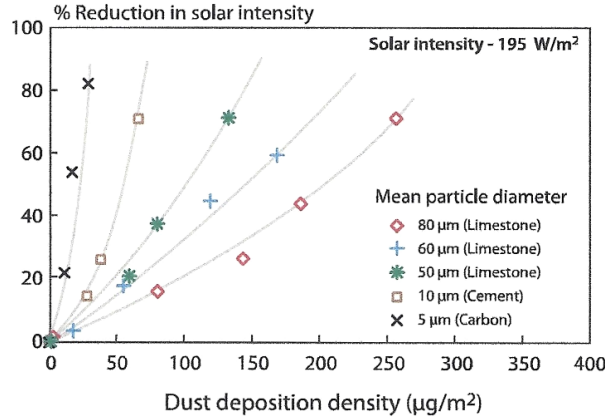


Fig. 2: Reduction in Solar Intensity for Various Particle Size Due to Dust Deposition (8,9)

Mailuha et al. (1994) conducted an evaluation on solar energy use in Kenya. Their PV module-based study focused on the impact of dust layer density, tilt angle, and solar intensity. They concluded that as solar intensity increased, PV performance due to dust accumulation decreased. As shown in Fig. 3, at 700 W/m², the reduction in output was almost negligible. However, when solar intensity dropped to 400 W/m², the loss was near 25% of initial power output (Fig. 3).

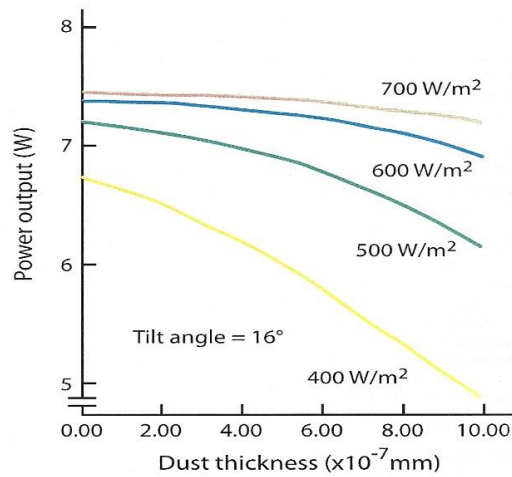


Fig. 3: Power Degradation of a PV Module for Various Intensities as a Function of Dust Thickness (10)

Hassan et al. (2005) studied the effect of airborne dust concentration on PV performance. They observed a decrease in efficiency from 33.5% to 65.8% for an exposure of 1-6 months, respectively. The study concluded that the degradation progress is dominant and proceeds rapidly during the initial 30 days of exposure to dust.

The experimental investigation conducted by Elminir et al. (2006) at the National Research Institute of Astronomy and Geophysics, Cairo, Egypt, experimented 100 glass plates with different tilt and azimuth angles. The glass transmittance was evaluated at regular intervals over a 7-month period for the prevalent wind conditions, including thunderstorms. The study revealed a reduction in dust deposition from 15.84 g/m² (for a 0° tilt) to 4.48 g/m² (for a 90° tilt) and a corresponding increase in transmittance from 12.33% to 52.54%. A governing equation between the dust deposition and reduction in transmittance was also derived. A critical observation revealed that differences in humidity led to the formation of dew on the PV surface which coagulated dust. Weekly cleaning cycle was recommended for moderately dusty places (Fig. 4)

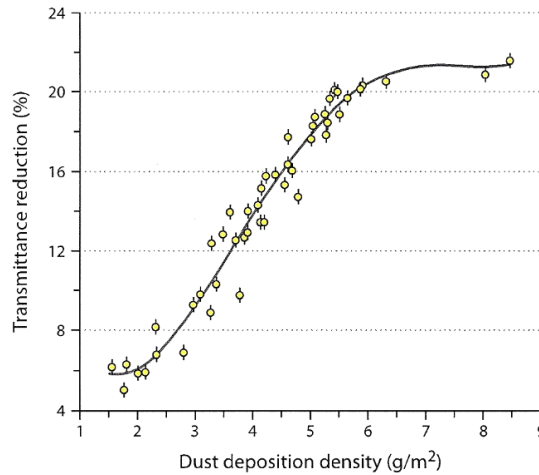


Fig. 4: Solar Transmittance Reduction as a Function of Dust Deposition Density (13)

Another study on dust physics and chemistry is conducted by Biryukov (1996) in the Negev desert. It evaluates particle size distribution using various microscopic techniques. A relationship was found between deposition rate, tilt angle, PV performance, and particle size. The study found that 90% of dust particle diameter ranges between 5 and 60 micron. The highest deposition rate per square centimeter per hour is found in particles that range between 15 and 25 micron. This supports the bigger the size, the slower the deposition rates in desert areas (Fig. 5).

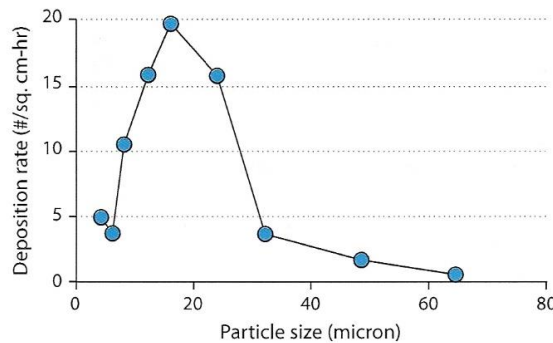


Fig. 5: Particle Size as a Function of Deposition Rate of a Solar Collector in the Desert Area.

4. United States climatic zones: ASHRAE classification

The American Society of Heating, Refrigerating and Air-Conditioning Engineers (ASHRAE) is an American professional association seeking to advance heating, ventilation, air conditioning and refrigeration (HVAC) systems design and construction. ASHRAE has more than 57,000 members in more than 132

countries worldwide. Its members consist of building services engineers, professors, architects, mechanical contractors, equipment manufacturers' employees, and others concerned with the design and construction of HVAC systems in buildings. The society funds research projects, offers continuing education programs, and develops and publishes technical standards to improve building services engineering, energy efficiency, indoor air quality, and sustainable development (2020, Jun 1). ASHRAE has some 87 active standards and guideline project committees, addressing broad areas as indoor air quality, thermal comfort, energy conservation in buildings, reducing refrigerant emissions, and the designation and safety classification of refrigerants.

ASHRAE climate zones (2013) for the United States (Fig. 6) represents the most familiar classification for architects, builders, engineers in the U.S. It uses numbers (0-8) and 3 letter system (A, B, C) to define U.S. climate zones. The first number represents a location's main climate type (temperature data): 1: Very Hot, 2: Hot, 3: Warm, 4: Mixed, 5: Cool, 6: Cold, 7: Very Cold, 8: Subarctic/Arctic. A second letter assigned to the weather zone based on precipitation: A: Humid, B: Dry, C: Marine. The United States has 8 of the 9 defined ASHRAE climate zones. Zones 0A, 0B, and 1B do not exist in the U.S. climate zones.

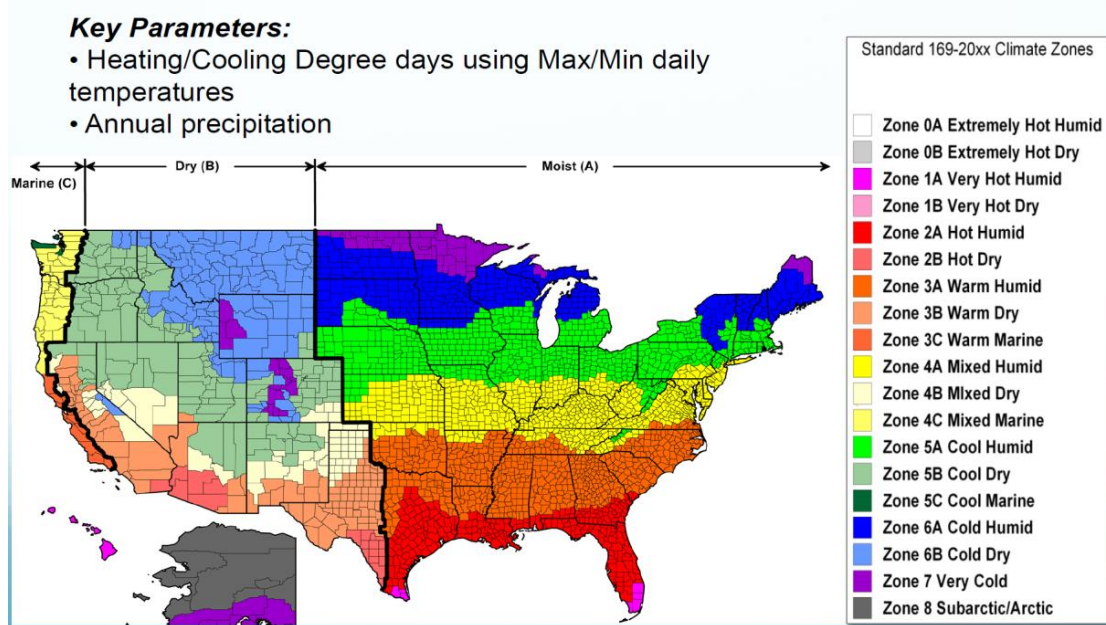


Fig. 6: ASHRAE climate zones of the United States

5. Dust reduction recommendations for U.S. climatic zones

The highest solar energy in the U.S. is located in the dry regions 2B, 3B, 4B, and southern part of zone 5B (NREL, 2018). These represent most of the southwest and west of the U.S. where solar energy exceeds 2000 kWh/m²/year. Dust deposition is a concern in these areas to utilize this high energy output. Therefore, most research focus on such climatic zones.

Based on the literature research provided earlier, Table 1 provides a basic guide to reduce dust deposition for U.S. climatic zones. It lists the characteristics of the weather in each zone and states that represent that zone (column 2). It provides the conditions that affect the PV installations in these specific zones (column 3), and recommendations for dust reduction as a rule of thumb for such zones (column 4). Nevertheless, dust deposition and soiling of PV modules remains a problem in search for better alternatives especially in the desert and arid climate in the U.S. and the world. These areas combine the best solar energy potential that unfortunately come with the worst dust accumulation conditions.

Table 1: Dust Reduction Recommendations for U.S. Climatic Zones

Climate Zone	Characteristics Location within the U.S.	Conditions Affecting PV Performance and Dust Deposition.	Cleaning Frequency Framework
1-A VERY HOT HUMID (TROPICAL)	Tropical climate: without frost, coolest month is warmer than 65°F (18°C) e.g. Extreme Southern FL, FL Keys, West Palm Beach area, Miami	Mostly low latitudes and require low tilt in PV systems to maximize energy Lower tilt angles tend to accumulate more dust deposition, therefore, tilt PV modules higher than latitude is recommended to reduce dust accumulation High annual rainfall minimizes dust accumulation	- Periodic washing by continuous annual precipitation reduces dust accumulation - Cleaning is recommended of a weekly/biweekly basis during dry season - Frequency depends on intensity of dust accumulation
2-A HOT-HUMID Warm winter	Wet- tropical: without frost, coolest month is warmer than 65°F (18°C) e.g. FL, Southern of GA, AL, MS, LA, SE of TX	Mostly low latitudes and require low tilt in PV systems to maximize solar energy PV systems with higher tilt angle are recommended in subtropical areas to reduce dust accumulation Utilize wind during the dry season to blow dust from the panels.	- Periodic washing by continuous annual precipitation reduces dust accumulation - Cleaning is recommended weekly for moderate dust accumulation in the dry season.
2-B HOT-DRY (ARID) Desert Mild/warm winter	Arid climate: evaporation exceeds precipitation Arid (desert): minimal annual rainfall Many regions: SW of TX, Southern AZ	Dusty desert environments and frequent dust storms reduces PV efficiency Low humidity and rainfall contribute to the problem High temperature reduces PV performance Has the max available, and intense solar radiation than any other regions	- Cleaning to respond to intensity of dust accumulation-at least a weekly cleaning is recommended - Immediate cleaning following dust storms is required - Application of dust-repelling coatings is highly recommended as preventative approach
3-A WARM- HUMID Mild/warm winter	Wet- semi-tropical: without frost, coolest month is warmer than 50°F (10°C) e.g. NC, SC, GA, AL, MS, LA, AR, OK	Mostly low latitudes and require low tilt in PV systems to maximize solar energy PV systems with higher tilt angle are recommended in subtropical areas to reduce dust accumulation Utilize wind during the dry season to blow dust from the panels.	- Periodic washing by continuous annual precipitation reduces dust accumulation - Cleaning is recommended weekly for moderate dust accumulation in the dry season.
3-B WARM- DRY Tundra (Savannah) Semi Desert Cool winter	Arid climate: evaporation exceeds precipitation Semi-arid (steppe): low annual rainfall Many regions: West TX, Parts of AZ, Southern and middle CA (away from ocean)	High latitudes require high tilt angle in PV system; a lower fixed tilt angle is recommended to optimize year-round solar gain Dust generally tends to fall off with an increased tilt angle Areas with higher rainfall would aid in cleaning the PV panels	- With low rainfall and high tilt angle, a moderate frequency cleaning cycle (weekly) is recommended - More frequent cleaning cycle is recommended with lower tilt angle (to maximize solar gain) - A less intense (weekly or biweekly) cleaning cycle is adequate for above 40° N
4-A MIXED- HUMID (TEMPERATE- HUMID) humid, no dry season warm summer cool winter	Temperate, subtropical climate: 8 months or more of average warmer than 50°F(10°C), rainfall all year MD, DE, VA, WV, KY, MO, KS.	A lower fixed tilt angle is recommended to optimize year-round solar gain in temperate areas. High latitudes require high tilt angle Dust generally not a problem unless combined with heavy moisture Heavy rainfall aids in cleaning the PV panels	- The least intense cleaning required- a monthly or bi-weekly cleaning cycle is adequate - Intense rainfall washes off the dust from the panels and maximize benefits of nature
4-B MIXED-DRY (TEMPERATE- DRY) tundra/dry warm summer cool winter	Temperate, subtropical climate: 8 months or more of average warmer than 50°F(10°C), Dry summer (Mediterranean) Northern TX, NM	High latitudes require high tilt in PV system; a lower fixed tilt angle is recommended to optimize year-round solar gain Dust generally tends to fall off with the increase in the tilt angle	- Recommended cleaning weekly or bi-weekly depending upon the rate of dust accumulation on the surface. - Regions with higher dust accumulation may need a daily cleaning
5-A COOL-HUMID 6-A / 7-A COLD/VERY COLD-HUMID humid, no dry season mild summer cool summer	Cool to Cold, temperate, moist, and forest: 4-8 months of average warmer than 50°F (10°C), rainfall all year 5-A: PA, OH, MI, IL, IA, NE 6-A: ME, NH, VT, WI, MN, ND, SD	Dust is less critical factor in comparison to maximizing solar gain in these regions Sun movable tracking may be needed to harness solar energy Colder temperature improves PV performance Dust generally tends to fall off at near-vertical tilt angles	- Weekly cleaning cycle is adequate - A less intense biweekly cleaning cycle is adequate for above 40° N - Intense rainfall washes off the dust from the panels and maximize benefits of nature - Removing snow accumulation needs to be frequent and immediate after snowstorms
5-B COOL-DRY 6-B VERY COLD- DRY mild summer cool summer	Cool to cold, mountain climate, changes rapidly, has same seasons of wet and dry periods of the immediate surrounding climate. e.g. Higher latitudes. 5-B: CO, UT, ID 6-B: MT, WY	High latitudes require high tilt angle closer to vertical Sun movable tracking may be needed to harness solar energy Colder temperature reduces PV cells heat and improves performance Dust generally tends to fall off at near-vertical tilt angle	- Weekly cleaning frequency is adequate - Removing snow accumulation needs to be frequent and immediate after snowstorms

6. How to clean and prevent dust

In areas of low-soiling conditions and/or periodic rain in the U.S., dust represents no major problem. Naturally, rain, or snow, would clean the surfaces periodically. This is valid in most of the United States except the southwestern regions where some other cleaning methods would take place. In areas of high moisture and heavy morning dews, performance is affected by compounding the dust problem. Light rain can collect particles and form a residue that stick to the collectors. This requires continuous cleaning and wash off the PV surface. These specific 2 cases (desert, heavy dew) require more advanced technology such as automated cleaning devices and robots to mitigate dust and keep the PV at its best efficiency performance.

In some instances, nature can be the most effective and least costly solution for dust problems in zone 3C and 4C of Pacific coast marine climate on the map (Fig. 6), where heavy rain washes off any dust deposition. Sandia National Labs and the solar thermal industry were among the first to develop mitigation techniques for dust and soiling problems in the United States

7. Conclusion

This paper reviewed the research development, challenges relating to the dust deposition on PV installations. It provides analysis on the environmental impact (wind, exposure) on dust deposition, and the dust particle analysis (physical and chemical properties) and how it affects PV performance. It analyzes United States climatic zones based on ASHRAE classification and discusses the characteristics of each zone. It provides conditions affecting PV performance and dust deposition for each zone (Table 1). It highlights the problems associated with desert climate in regions like the southwest of the U.S. (2B, 3B, 4B, and southern part of zone 5B on the map). These areas have growing potential in interest and investment but need to mitigate the dust accumulation problems associated with it. The paper finally provides a framework of recommendations for cleaning PV modules in each of the U.S. climatic zones based on variations of weather and precipitation conditions pertinent to each zone.

8. References

- ASHRAE, 2020. <https://en.wikipedia.org/wiki/ASHRAE>, accessed June 1, 2020
- ASHRAE 169-2013, Climatic data for building design standards, www.ashrae.org, accessed Jun 1, 2020.
- Biryukov S., 1996. Degradation of optical properties of solar collectors due to the ambient dust deposition as a function of particle size. *Journal of Aerosol Science*: 27: p 37–8.
- Denholm P, Drury E, Margolis R, Mehos M., 2010. Solar energy: the largest energy resource. In: Sioshansi FP, editor. *Generating electricity in a carbon-constrained world*. California: Academic Press, p. 271-302.
- Dietz A., 1963. Diathermanous materials and properties of surfaces. In: Zarem A, Erway D, editors. *Introduction to the Utilization of Solar Energy*. New York: McGraw-Hill; p. 59–86.
- Elminir H, Ghitas A, Hamid R, El-Hussainy F, Beheary M, Abdel- Moneim K., 2006. Effect of dust on the transparent cover of solar collectors. *Energy Conservation and Management* 2006; 47:3192-203.
- El-Shobokshy M., Hussein F., 1993a. Degradation of photovoltaic cell performance due to dust deposition on its surface. *Renewable Energy* 1993; 3:585–90.
- El-Shobokshy M., Hussein F., 1993b. Effect of dust with different physical proper- ties on the performance of photovoltaic cells. *Solar Energy* 1993; 51:505–11.

Hassan, A., Rahoma, U., Elminir, H., Fathy, A., 2005. Effect of airborne dust concentration on the performance of PV modules. *Journal of the Astronomical Society of Egypt*, 2005; 13 (1), 24–38.

Mailuha J., Murase H., Inoti I., 1994. Knowledge engineering-based studies on solar energy utilization in Kenya. *Agriculture Mechanization in Asia, Africa, and Latin America 1994*; 25:13–6.

McKnight, Tom L; Hess, Darrel, 2000. "Climate Zones and Types". *Physical Geography: A Landscape Appreciation*. Upper Saddle River, NJ: Prentice Hall.

Michalsky J, Perez R, Stewart R, LeBaron B, Harrison L., 1988. Design and development of a rotating shadow band radiometer solar radiation/daylight network. *Solar Energy* 1988; 41:577–81.

National Renewable Energy Lab (NREL), 2018. Solar Resource Data, Tools, and Maps. <https://www.nrel.gov/gis/solar.html>, accessed Jun 1, 2020.

Sarver et al., 2013. A comprehensive review of the impact of dust on the use of solar energy: History, investigations, results, literature, and mitigation approaches. *Renewable and Sustainable Energy Reviews* 2013 (22): 698-733.

Sayigh A., Al-Jandal S., Ahmed H., 1985. Dust effect on solar flat surfaces devices in Kuwait. In: *Proceedings of the international symposium on thermal application of solar energy*. Hakone, Japan ; 1985. p. 95–100; Furlan C, Mancin N, Sayigh A, Seraphin B, editors. *Proceedings of workshop on the physics of non-conventional energy sources and materials science*. ICTP, Trieste, Italy. 1985. p. 353–67.

Sayigh A., 1978. Effect of dust on flat plate collectors. Sun, mankind's future source of energy. In: *Proceedings of the international solar energy society congress*; 1978. p. 960–4.

Emergency Power For All Disasters

ASES Solar 2020

William Young

SunTreeFarm, Titusville, Florida, USA

Abstract

Anytime and anywhere, a man-made or natural disaster can happen. The impact can be as minor as a lightning strike temporarily knocking out power or as major as a hurricane affecting thousands of people, damaging homes, businesses and civic infrastructure. Electrical utilities can be damaged or destroyed, leaving people without power for water, sanitation, medical services, refrigeration and communications.

In 1989, following Hurricane Hugo, portable solar-powered consumer items such as lamps, chargers and radios were first used in response to a disaster. At that time, there were a few solar-powered homes and business and passive natural energy buildings. These homes and businesses had solar electric systems which included batteries for storage and were connected to the utility grid. When disaster struck and utility power was out, these buildings generated their own electricity. Since then, the use of photovoltaic with or without storage has become more common and is moving towards becoming mainstream in various configurations.

Also, growing is the application of zero-energy building design with energy efficient appliances and passive energy design. These buildings, powered by the sun, can achieve real resilience and sustainability. Distributed generation of passive and renewable energy balances generation with conservation in a holistic design approach. With the introduction of enhanced building codes and fortified structural designs, plus the implementation of sustainable renewable energy, it is now possible to minimize the impact of disasters and climate change.

Keywords: Disaster, Emergency, Outage, Power, Photovoltaic, Electricity, Solar, Resilience, Sustainability.

1. Introduction

Disasters, man-made or natural, can happen at anytime, anywhere. Major disasters can leave several hundred thousand people homeless and disrupt power utilities, water works, businesses, medical services and communication. Impacted businesses, industry, government and homes may not recover for days, weeks and even years before services can be fully restored. Although the American power utilities and industry are some of the best in the world, the Federal Emergency Management Agency plans for full recovery efforts to take up to three years.

Based on reliability and low lifecycle cost, the National Aeronautics and Space Administration (NASA) has used photovoltaics (PV) on satellites since 1958; the U.S. Coast Guard uses PV on navigation devices for remote power.

Since Hurricane Hugo in 1989, solar technology has been used to provide backup electricity during and following disasters. In response to Hugo, portable consumer-powered solar items were deployed, such as lamps, chargers, water pumps, radios and small camping refrigerators. Early solar adopters already owned stand-alone solar-electric systems with batteries integrated into their remote cabins and homes. A few utility interactive systems with batteries for grid connected systems were being used in homes and businesses in urban settings. This relatively small group of people had not necessarily planned to use solar in disasters, but found their motive to be independent and sustainable rewarded them well.

By the year 2000, technology and codes had taken a new direction. Net metering was introduced and batteries were eliminated from many photovoltaic (PV – solar electric) system designs to lower costs. A new configuration of grid-tied inverters on PV systems without on-site storage became common. Simpler design and installation made solar more accessible and less expensive, as the utility acted as storage. But disasters have a way of revealing flaws in preparedness, as did Hurricane Charlie in 2004. Grid-tied PV systems did not provide a consistent power supply when the local utility connection went down. The concept of utility interactive or solar+batteries began to look more appealing. Critical power distribution panels were added to meet emergency power needs such as medical equipment, lighting, refrigerators and communications. These three PV configurations (stand alone, utility interactive and grid-tied) address most of the energy needs of the general public and businesses.

The all-electric home was introduced in the 1980s, as electric utilities worked to corner the power market. This movement has advanced as older devices and equipment are replaced by electronic “smart” technologies. Building science and passive design technology have also advanced and zero-energy building design fulfills goals of sustainability and resilience. As the cost of photovoltaics goes down, a ‘competition’ exists between choices of adding PV power or investing in energy efficiency. Whatever happens to the power utility should not impact people in a disaster-resistant home or business. A zero-energy building is both disaster-resistant and sustainable. To achieve true sustainability and resilience without an external energy source other than the sun, all technologies must be integrated and a building should generate as much energy as it consumes.

Building survival is dependent upon enhanced building codes and fortified structural designs. While today’s structural design options can complete the concept of full disaster resistance and efficiency, these features increase costs, creating potential tension between the goals of resilience and profitability for real estate brokers and building contractors. This paper does not address the politics or economics of this issue; rather the concept of creating sustainable and resilient buildings.

In the 1800’s, various organizations began gathering data on weather, disasters, population growth and other factors affecting American lives. In 1870, The National Weather Service was formed and collected data on extreme weather, including hurricanes. The Federal Emergency Management Agency was formed in 1979, as the number of declared disasters in this country had increased in frequency by over 400 percent.

Hurricane Donna crossed Florida in 1960, damaging many homes. As Florida became more and more appealing as a retirement destination, a few home builders began to offer “hurricane houses” as a marketing advantage over other builders. Houses were built with a lower rise roof angle and secondary power panels for critical load items and an electrical outlet was added for connecting a fossil fuel generator for backup power.

In 1992, Hurricane Andrew caused such damage in Miami, Florida, that building codes were strengthened by adding mitigation requirements. Miami now has the strongest building codes in the country. The adoption of new codes is controversial, as realtors and builders struggle for lower costs and insurance companies and emergency managers struggle for safety and disaster preparedness. The rapid succession of Hurricanes Charley, Jeanne, Frances and Ivan in 2004 changed the way the United States does business and the way FEMA responds to disasters. The most deadly, destructive and costly storm in the US was Hurricane Sandy in 2012. Sandy was a category 3 hurricane with winds over 115 mph, causing 285 fatalities and over 65 billion dollars in damage in 24 states and the Caribbean. Each disaster poses new challenges as lessons are learned and changes made.

2. Resources in Play

Emergency management suggests all families assemble a disaster kit that includes water, food, lights and first aid items and to be prepared to follow safety practices outlined in the “Are You Ready?” program. Local, state and federal emergency management organizations have a plan for response, recovery, mitigation and preparedness that provides guidance on maintaining and restoring a community to a point where the community can rebuild itself.

The most critical time for survivors after a disaster strikes is the first 72 hours when people are fending for themselves until help arrives. First responders must evaluate needs and move into place quickly with the right resources. FEMA teams with many disaster response organizations, like the American Red Cross, Salvation Army, Volunteer Organization Active in Disaster, International Association of Emergency Managers and religious and citizen organizations. It takes about three days to a week to respond to a disaster, as much as three months to start recovery and in some cases three years for people to rebuild.

FEMA promotes mitigation over response as being more cost effective and safer. Before a disaster, mitigation means building structures to higher than minimal codes and paves the way for safer disaster operations. After a disaster, FEMA promotes rebuilding to safer practices and codes.

Additional organizations have a stake in the process as well, particularly insurance companies, that have research institutes and test facilities that evaluate historical data on damage caused by disasters. The Institute for Business and Home Safety (IBHS) offers a Fortified Building Program with standards beyond traditional building safety codes with three levels of design for creating stronger, safer buildings. They research and test materials and technologies to save lives and property through mitigation. National building codes are minimal based on historical averages related factors such as wind speed, temperature, and ground density. The IBHS plan is to reduce disaster-related damage and financial loss by creating buildings that are truly disaster-resistant and built beyond present codes. One of their programs promotes the construction of safe rooms in which to shelter.

Another non-profit, the Federal Alliance for Safe Homes (FLASH), was formed after Hurricane Andrew. They are a consumer advocacy organization that encourages safety and resilience through education. They empower the community with knowledge and resources designed to foster preparedness and mitigation.

Research completed by the Florida Solar Energy Center, in conjunction with other organizations, confirms solar systems designed and constructed to code will survive the destructive forces of most disasters, tornados being the potential exception. Given the many safety, fire, electrical and building codes applied to components and systems today, owners of solar equipment can be encouraged about their investments' functionality and resilience.

3. Energy Efficiency

The U.S. Department of Energy (DOE) and Environmental Protection Agency (EPA) offer excellent programs for your home's comfort and energy-efficiency. One such program is Energy Star which helps consumers, businesses and industry save money and protect the environment through the adoption of energy-efficient products and practices. The EPA manages products and the DOE manages energy usage. The goal is to design energy efficient applications and use natural passive energy resources to reduce energy consumption, as shown in Fig 1.

Leadership in Energy and Environmental Design (LEED) is another DOE energy efficiency program that looks long term at the holistic impact of building materials and lifestyle processes. LEED promotes best practices in green building strategies proven to reduce energy and water use, lower operating costs, reduce liability, improve indoor air quality and increase user comfort and productivity. LEED buildings typically consume 18% to 39% less energy than conventional methods of construction. Though initial up-front costs average 2% more, following LEED guidelines yields over ten times that in savings.

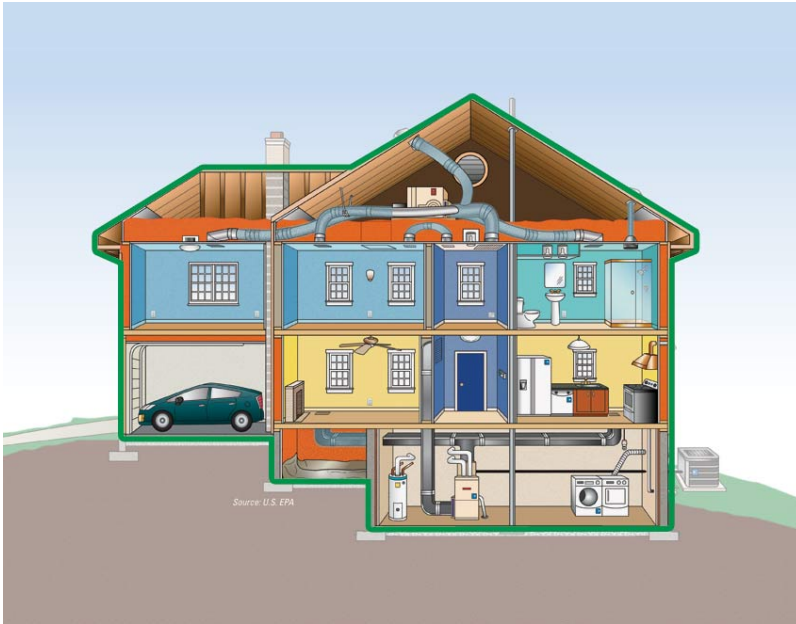


Fig. 1. Building Energy Efficiency, 2011 (DOE/EPA)

Many benefits are enjoyed by people who occupy a resilient, energy efficient building. During a power outage, inhabitants are not as uncomfortable or concerned about safety as in a conventionally designed building. Utility power bills are lower. With building power consumption reduced, the cost of a renewable energy supply to produce the needed power is also lower.

Various alternative energy sources can be added such as biomass, geothermal, biogas and others. Wood stoves and heaters using wood pellets can be use when available locally. Of course, solar energy in its many forms, like solar thermal or photovoltaic systems, are now main stream and cost effective.

4. Solar Design

The sun provides energy in different forms that are quiet, environmentally sound, abundant, and free. One form of solar energy is solar thermal for heating water. Solar hot water systems were actually patented in the early 1890s. Another application of solar energy is the photovoltaic cell, first developed in 1954 by Bell Telephone Laboratories, which converts photons of light into direct current (DC) electricity. Photovoltaic systems range from a few watts to as large as 100s of megawatts.

Early solar applications for disaster response included portable solar-powered devices for people who lost electricity for lights, medical equipment, communications, and refrigeration. Portable PV consumer items deployed included lanterns, flashlights, battery chargers, radios, portable power units, and trailer-mounted generators. Many of these items were low voltage direct current (DC) devices producing less than 5 watts which were carried to tent camps, damaged homes, businesses, and shelters. None of the items were designed for disaster relief, but camping equipment and portable/mobile stand-alone systems were adaptable to disaster relief applications. In 1998, FEMA purchased and tested trailer mounted stand-alone 1.8 kw PV systems to meet larger emergency power needs. Though solar consumer items were readily available and useful, they were not as cost effective as integrating solar into buildings.

PV power systems for buildings are much larger than mobile, portable and consumer items. Power used in buildings is alternative current (AC) electricity at voltages from 120 to 1500 or more. An inverter is used to transform DC to AC at 60 cycles sine waveform, commonly known as ‘home power’. A typical photovoltaic system consists of a PV array, controller, inverter, batteries, and conventional electrical equipment, comprising the balance of system (BOS) components, as shown in Fig 2. The BOS components consists of fuses, circuit breakers, a combiner box, power panel, wire, disconnects, and conduit.

As mentioned above, three major PV system configurations are in common use today: stand-alone, grid-tied, and utility-interactive/solar+batteries. Stand-alone PV is for remote locations without utility power and operates on its own. Grid-tied PV is interconnected with a utility power plant distribution system and requires grid current to operate and produce the utility electricity waveform. Utility interactive/solar+batteries combines the two configurations and can operate with or without the utility waveform. There are other system configurations; one such alternative system is called grid-tied with secure power, where the inverter produces single phase electricity without the grid during a power outage, as long as the sun shines. Hybrid systems where PV is combined with wind, fossil fuel engine generators or another power source are also available.

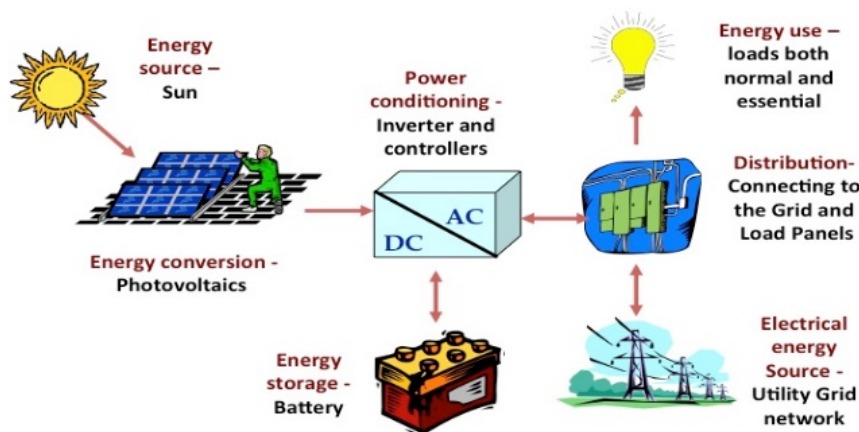


Fig. 2. Typical PV System Diagram (FSEC)

Grid-tied systems became more prevalent when net-metering law was amended in 2000 to provide compensation at the average retail utility energy rate. Grid-tied systems without storage are less expensive and less complex. However, the 2004 hurricane season brought forward the value of battery storage when grid-tied systems did not work during power outages.

Photovoltaic systems have advanced in efficiency, performance and reliability and rival anything utilities can do, in a more environmentally sound and cost-effective manner. PV systems are subject to similar failure issues as utility power plants, such as extreme weather interruption, fallen trees, loose or corroded connections, and heat stress. Like any other equipment, a preventive maintenance program can keep these failures at a minimum. The benefits of solar are that sunlight is free, renewable and produces no noise or pollution.

5. Designing for Disasters

Strong codes provide strong PV systems that can withstand the impacts of a disaster. Many PV systems have survived disasters and continued to work during resulting utility power outages. But resilience is more than strong codes. This author practices a design philosophy learned while working at Kennedy Space Center for manned space flight. The design concept is fault-tolerant architecture, that when applied to PV systems, provides power through any failure.

In 2003, the Florida Solar Energy Center implemented a DOE Solar for Schools Program which called for installation of PV systems on schools for educational purposes. By 2010, the educational mission was enhanced to a more meaningful objective to put PV on schools designated as shelters. The PV systems had a 10 kWp PV array connected to the grid with battery storage. This configuration was installed on 118 schools in Florida for solar education and emergency power. The SunSmart E-shelter for Schools became a real life, viable application, as shown in Fig 3. These utility interactive systems used a net meter connected to grid power to reduce the school's electric bill during normal times and to provide emergency power for critical/essential loads during utility outage. A critical load power panel for lights, communications, and special needs equipment was powered by the PV system during emergencies and normal times, as shown in Fig 4. The battery pack was kept full at all times to be able to provide emergency power through a bi-modal inverter for two days.

The PV array had fourteen PV strings of 3 modules to minimize array losses from shading, damage, or other failure in a fault-tolerant PV design configuration. When a string is damaged, only a small proportion of power is lost and not the whole array. There were three inverters, so an inverter loss did not cause a complete system failure. Since 2010, these PV systems have proven their worth each hurricane season.



Fig 3. SunSmart E-shelter school – (FSEC)

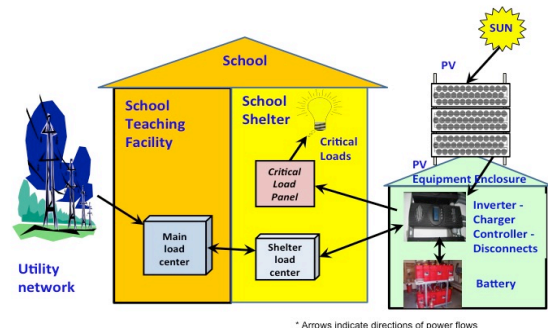


Fig 4. Essential school loads and supply - (FSEC)

6. Distributed Generation

Roof-top PV systems have advanced into other configurations such as solar farms that rival conventional utility power plants in size, with some as large as 100 mega watts. They may or may not have storage, but they are very large power plants that feed the utility grid distribution system. Community solar is usually smaller than solar farms and is dedicated to a community that is generally closed to outsiders, but have arrays in the mega watt size. Micro-grids are smaller arrays and produce power for facilities or small complexes that may not have a utility distribution system. Large storage systems in the mega watt range are coming into use as the cost of batteries becomes lower and can offset utility 'peaker' power plants. These varied, large systems are being integrated into distributed

generation configurations for utility providers to utilize diverse resources for the economy, power outages and load demands. Additionally, smart grid technology integrates all available sources together, greatly enhancing the resilience of the modern grid.

7. Conclusion

Disasters can be very destructive, leaving thousands of people without shelter, power, water, sanitation, and communication. Renewables are viable in all four phases of a disaster: preparation, mitigation, response, and recovery. Through the years, the solar industry has learned about energy needs precipitated by disasters and disaster organizations have learned about the value of solar applications. Disaster-resistant building construction, low energy consumption, and renewable energy-powered buildings can mitigate the effects of a disaster and save on energy expenses during normal times.

Renewable energy applications, such as solar thermal, photovoltaics, micro-grids, community-solar, wind, and battery storage are making homes and businesses and the grid more resilient and sustainable. Conventional utilities are advancing to become more resilient and sustainable as they incorporate renewables into the grid through distributed generation of energy sources. Designing to fault-tolerant architecture concepts enhances the disaster resistance of PV systems. As these systems become more resilient and sustainable, they become more disaster resistant.

First, building to enhanced building codes and fortified structure design leads to physical disaster resistance. Then, integrating energy efficiency, renewable power sources, distributed generation connections, energy storage, and modern mitigation practices completes the process. Roof-top photovoltaics on homes should produce as much power as it consumes. This sustainability concept will lower costs and provide safe living conditions during any disaster as man grivels with climate change. Every home should be a hurricane home. Using these technologies and practices lessens man's exposure to the effects of changing weather patterns and natural and manmade disasters and makes meaningful inroads into mitigating the impact of traditional energy usage on planet Earth.

8. Acknowledgements

I would like to thank the Florida Solar Energy Center for many opportunities to gain solar experience. Also, my wife Betty for her editing assistance.

9. References

- (1) W. R. Young, "Photovoltaic Application for Disaster Relief", Florida Solar Energy Center, Cocoa, Florida, FSEC-849-95-C, November 1995, and February 2006.
- (2) Young, William, and Susan Schleith, Florida's Emergency Shelters Go Solar, ASES Solar 2007 Conference, American Solar Energy Society, Cleveland, Ohio, July 2007.
- (3) Fact sheets and data Status Summary, Federal Emergency Management Agency, [online], <http://fema.gov/fact-sheets/td>.
- (4) Hotchkiss, Eliza, National Renewable Energy Laboratory, October 24, 2017, How is Solar PV Performing in Hurricane Struck Location?, <http://nrel.com/technical-assistance/bolg/post/pvhurricanestruck> .

- (5) Young, William, Distributed PV Design for Emergency Power, ASES Solar 2016 conference, American Solar Energy Society, San Francisco, July, 2016.
- (6) Michael, Hordeski, Emergency and Backup Power Sources: Preparing for Blackout and Brownouts, CRC Press, Boca Raton, Florida, 2005.
- (7) Ali, Keyhani, Smart Power Grid Renewable Energy Systems, Institute of Electrical and Electronic Engineers, John Wiley & Son, Hoboken, New Jersey, 2011.
- (8) Guidelines for Hurricane Resistant Residential Construction, Institute for Business and Home Safety, Tampa, Florida, 2009.
- (9) A Homeowner's Insurance Guide to Natural Disasters, Federal Alliance for Safe Homes, Tallahassee, Florida, 2015.

Utilizing Solar Infrared-induced Photothermal Heating on Building Windows in Winter

Enhe Zhang, Qiuhua Duan, Yuan Zhao, Julian Wang*

Department of Architectural Engineering

104 Engineering Unit A

The Pennsylvania State University

University Park, PA 16802

* Corresponding author: Julian Wang

Abstract

Single-pane windows still account for a large percentage of the US building energy consumption. In this paper, we introduced a new solution incorporating the photothermal effect of metallic nanoparticles ($\text{Fe}_3\text{O}_4@\text{Cu}_{2-x}\text{S}$) into glazing structures to utilize solar infrared and then enhance the window's thermal performance in winter. Such spectrally selective characteristics of the designed photothermal films were obtained from lab measurements and then integrated into a thermodynamic analytical model. Subsequently, we examined the thermal and optical behaviors of the photothermal single-pane window and compared its overall energy performance with the conventional low-e coated single-pane window, in which typical window properties, dimensions, winter boundary conditions, and solar irradiance were adopted. The numerical analysis results demonstrated that the photothermal window systems could yield 20.4% energy savings relative to the conventional low-e coated windows. This research paves an underlying thermodynamic mechanism for understanding such a nanoscale phenomenon at the architectural scale. From the implementation perspective, the designed photothermal film can be added into the existing single-pane windows for energy-efficient retrofitting purposes.

Keywords: Building windows, Solar radiation, Photothermal effect, Energy savings, Optical behaviors, Thermodynamics.

1. Introduction

It was reported that the buildings are responsible for 41% of primary energy consumption in the United States.¹ The physical properties of building envelopes may have an impact on building energy consumption. In general, 30 ~40% of current building windows are single-pane, even in northern areas in the USA, and they are responsible for over 50% of the total energy loss in the United States.² To improve the performance of building windows, adding low emissivity (low-e) coating on existing windowpanes is one of the main practical strategies. The low-e coating is a micro-thin layer of thermally reflective materials that can be applied to the surface of the glass. The low-e coated windows can not only reduce radiative heat transfer by reflecting solar radiation to the exterior in summer but also lower heating needs in winter by keeping the heat from radiating to the outside. Consequently, adding low-e coatings or window films may decrease HVAC energy consumption so that they have been commonly recommended to retrofit existing building windows.³ However, Wang and Shi demonstrated that it had been a great challenge to achieve coincident high solar-infrared transmittance and low emissivity in longwave radiation.⁴ As such, even the high solar heat gain coefficient (SHGC) low-e coating (e.g., single silver unit) may reflect about 50% solar near-infrared (NIR) to outdoor, which may offset the solar heat gain benefits for indoor heating energy savings in winter.

In this research, we introduced and then analytically examined a new spectrally selective nanostructure, based on metallic nanoparticles' photothermal effect discovered in recent years, that can be added on the existing low-e window systems and utilize the solar NIR for heating energy saving purposes in winter.

2. Photothermal effects and heating experiments under simulated solar light

The photothermal (PT) effect has been investigated for biomedical applications in the past two decades, such as the studies on sensing, imaging, therapies, and drug deliveries.^{5,6} The PT effect includes two stages, the photonic energy absorption, and photon-induced heat generation. The first stage usually happens in the way of absorption and may exist in other photonic extinction due to the microstructure of the material, such as multiple scattering. The second stage is the conversion of absorbed light energy to thermal energy. For metal or some semiconductor nanoparticles, Localized Surface Plasmon Resonance (LSPR) is believed to be the main reason for their photothermal effect.⁷ As

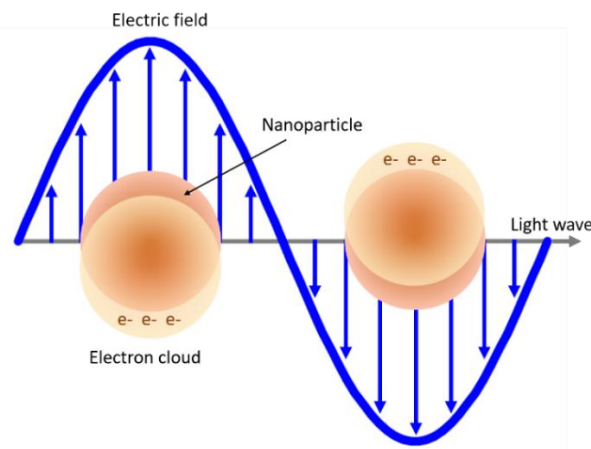


Figure 1. Schematic diagram of LSPR.

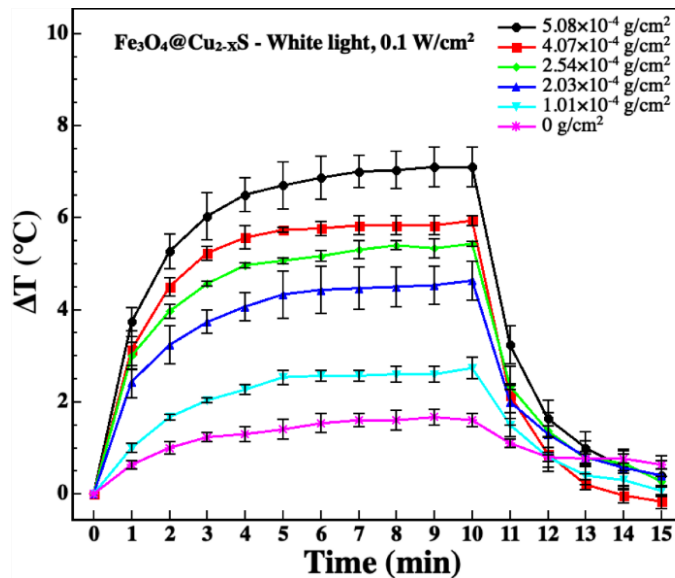


Figure 2. Temperature Change diagram.

shown in Figure 1, LSPR is driven by photoexcitation when the incident frequency matches the natural frequency of the oscillating surface electrons. This excitation causes an inhomogeneity in the electron density of a conductor,

generating a local electrical field that tends to drive charge equilibration. Electrons accelerating through this field can pick up enough energy to overshoot equilibrium configuration and effectively switch the local electric field, causing an oscillation. This oscillation is not perpetual, thus requiring photoexcitation for maintenance. More importantly, various research efforts have been focused on manipulating the absorptions into the desired regions, which provides strong potential in solar infrared modulation for building applications. While controlling transmitted solar infrared thermal radiation, an ideal window should be capable of sufficient transmission of visible light, which is associated with the window's optical property of visual transmittance (VT). A higher VT brings more daylight to the interior and may offset electric lighting, especially for spaces with a great lighting demand. It has been reported that window's VT ranges from above 90% to less than 10%, determined by glazing type, number of panes, and glass coatings or films.⁸ Solar NIR-induced photothermal effect may independently modulate the solar heat without (or with slight) compensation of the visible transmittance. However, before incorporating such photothermal effect into building windows, it is necessary to perform an in-depth energy-saving analysis to understand its energy impacts and associated thermal and optical behaviors.

Note that the energy-saving analysis of this study was based on experimental results in our previous report.⁹ Specifically, $\text{Fe}_3\text{O}_4@\text{Cu}_2\text{-xS}$ nanoparticles were synthesized and coated on glass substrates ($2.54 \times 2.54 \text{ cm}^2$). Samples are made in specific average visible transmittance (AVT): 65%, 70%, 75%, 80% and 85%. The coated samples were irradiated by 0.1 Wcm^{-2} simulated solar light by a Newport 150W solar simulator, as shown in Figure 2. The temperature was monitored by a FLIR E6 infrared camera. In particular, FC-75% achieved a $5.43 \text{ }^\circ\text{C}$ temperature increase, which was then utilized in the following analytical analysis.

3. Energy-saving analysis of photothermal single-pane windows

Solar radiation interaction with the earth atmosphere results in four solar components: direct normal irradiance (DNI), diffuse horizontal irradiance (DHI), global horizontal irradiance (GHI), and reflected ground radiation (R_g).¹⁰ For vertical windows of a building, the average global radiation can be estimated by Liu-Jordan isotropic model.¹¹ Solar radiation on windows is either transmitted, absorbed, or reflected in varying amounts depending on the wavelength. Solar heat gains through a window system can be determined from the overall transmittance and the absorptance of each pane or layer as a function of the angle of incidence. The transmitted solar radiation may directly reduce indoor heating energy use. In contrast, the absorbed solar radiation may partially flow inward from the panes to indoor, which may also increase the temperature of indoor, and consequently improve heating energy savings in winter. In brief, compared with the low-e coated windows, the addition of photothermal coatings may slightly reduce the transmitted amount of solar radiation but theoretically lead to a significant increase of the inward flowing heat due to the photothermal effects through absorbing the solar radiation. In this work, we firstly used OPTICS of the WINDOW program to build the low-e coated single-pane window (as the baseline or called Type 1) and the photothermal window (Type 2). Then we output the spectral characteristics of the two types of window models developed. Combing the spectral properties derived and the calculated incident solar radiation, we then calculated the transmitted and absorbed solar radiation. Subsequently, the PT effect yielded in our previous material experiments was successfully incorporated into thermodynamic analyses and calculations of the inward flowing thermal radiation. This computation was completed by using a thermal transfer analytical model built in Matlab. Finally, we compared the net energy based on the heating loads in terms of transmitted solar gains and inward flowing thermal radiation, of the two types of windows.

3.1 Incident solar irradiance on vertical window surfaces

The total ("global") hemispherical radiation on a plane, G or GHI, is defined as Equation (1). It is the combination of the direct normal radiation multiplied by the cosine of the incidence angle θ (between the normal to the plane and the

direction from the base of the normal to the center of the solar disk), $DNI \cos(\theta)$ or $B \cos(\theta)$, plus the diffuse sky radiation DHI or D .¹²

$$G = B \cos(\theta) + D \quad (\text{eq. 1})$$

For a titled plane with titled angle β , diffuse irradiance D is defined as Equation (2) by using Liu-Jordan isotropic model.¹¹ Meanwhile, the global (total) hemispherical irradiance on the tilted plane should consider the reflected ground radiation R_g so that G can be obtained by Equation (3).

$$D = D_h * 0.5 * (1 + \cos\beta) \quad (\text{eq. 2})$$

Where, D_h is diffused horizontal irradiance.

$$G = B \cos(\theta) + D + R_g \beta \quad (\text{eq. 3})$$

$$R_g = \rho \cdot G_h \cdot R_h \beta \quad (\text{eq. 4})$$

Where, ρ is foreground's albedo, G_h is global horizontal irradiance, R_h is the ground reflected horizontal irradiance $R_h = 0.5 \cdot (1 - \cos\beta)$, β is a tilted angle.

We selected solar spectra data collected by using ASTM G173-03 Reference Spectra Derived from SMARTS v. 2.9.2,¹³ and considered a vertical window façade facing south in State College, Pennsylvania at noon on December 21st, 2019, the incident angle for solar θ is 26° , the titled angle for vertical windows β is 90° . We obtained the incident global solar irradiance $G = 636 \text{ W/m}^2$ on the vertical window surface, and the solar irradiation curve on the vertical plane is shown in Figure 3. Please note that this simplified method of calculating incident solar irradiance on the vertical surface may overlook the effect of ground reflection and the complexity of sky conditions. However, this would not significantly affect our next comparisons between the two types of windows as long as the same solar irradiance data for those two windows were utilized.

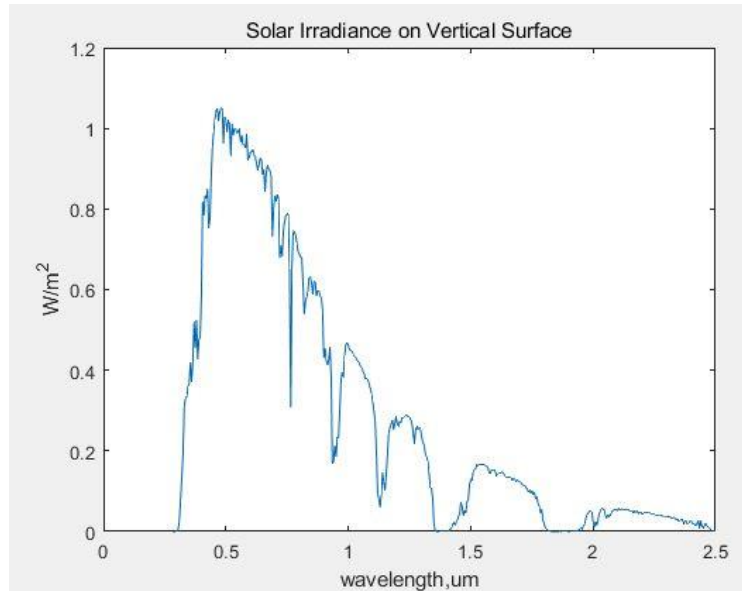


Figure 3. Solar Irradiation Curve.

3.2 Window modeling and spectral properties

We designed two types of single-pane glazing in OPTICS software, which was developed by the Lawrence Berkeley National Laboratory (LBNL). Type 1 was low-e coating single-pane glazing, which was made up of clear glass (NFRC

ID 8203) and low-e coating (NFRC ID 1511). Type 2 was the photothermal low-e single-pane glazing, which consisted of Type 1 plus a photothermal film. The photothermal film was the above-mentioned FC-75% Fe₃O₄@Cu_{2-x}S film, and its spectral data measured in the lab was loaded manually in OPTICS. An import data can be customized by several key parameters, including transmittance, reflection front, reflection back, thickness, conductivity, and emissivity. The photothermal film layer was placed on the external surface of the low-e coated glass. Figure 4 illustrates the structures of Type 1 and Type 2, and Figure 5 displays their spectral properties (spectral transmission curve and absorptive curve).

As shown in Figure 5, Type 2 window had a 45.1% higher absorption (α), and it absorbed more solar radiation, mainly focusing on the solar NIR band. As a tradeoff, it has a 6.6% lower visible transmittance (τ), which allowed slightly less solar radiation to be transmitted through the window. Furthermore, the window properties, including solar heat SHGC, VT, U-factor, and solar transmittance (Ts) were obtained using OPTICS and WINDOW, as shown in Table 1. The results indicate a similar property performance, and the comparison for each parameter needs to be done before we can move on to the capability of temperature increasing. Type 1 and Type 2 have the same U-factor that is related to the thermal resistance of each layer of the window structure, which can be explained by the fact that the thin layer coating added did not have much influence on the thermal resistance. Type 2 has a slightly lower visible transmittance than the value of Type 1, which also influences SHGC. By simply calculation of the transmitted solar gains using the above solar transmittance calculated from the WINDOW OPTICS, we found that Type 1 window transmitted 335.95 W m⁻², while Type 2 window transmitted 323.01 W m⁻². In other words, the addition of the PT coating reduced 12.94 W m⁻² solar gains to the interior.

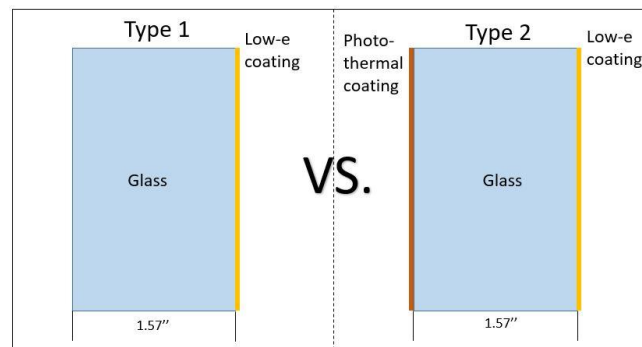


Figure 4. Window System Diagram in Optics software.

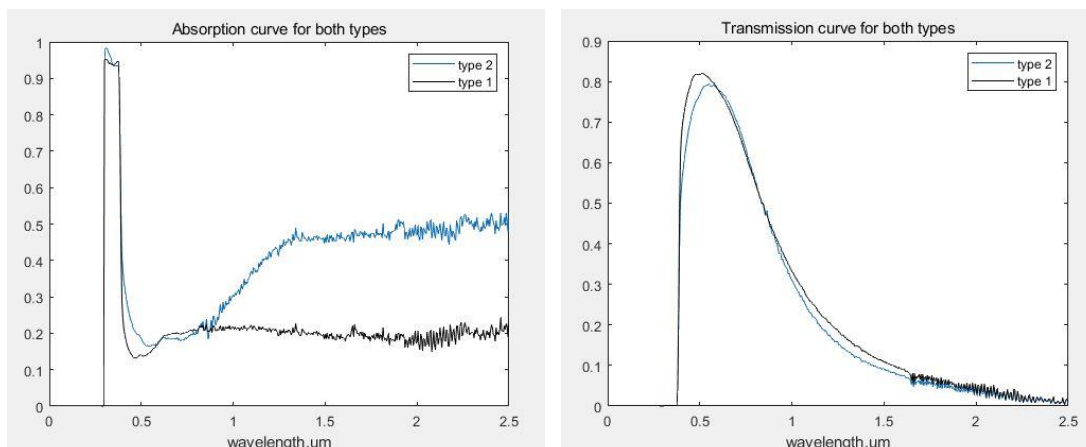


Figure 5. a) Absorption curves for both types in Optics. b) Transmission curves for both types in Optics.

In summary, the differences in the visible and full spectral transmittances of solar radiation in both types of windows were very minimal, which were about 2.1% and 3.6%, respectively. The significant difference is in the solar NIR band that was absorbed by Type 2 but reflected by Type 1.

Table 1. Window optical Properties.

	U factor, W m⁻² K⁻¹	SHGC	Tvis	Ts
LowE+glass, type 1	3.496	0.537	0.799	0.504
LowE+glass+PT, type 2	3.496	0.533	0.782	0.486

3.3 Analytical studies for thermal behaviors

Without solar radiation involvements, the thermodynamic analysis is quite straight forward, which can be completed based on the given indoor and outdoor boundary conditions and glazing properties. However, in this study, due to the existence of solar irradiance, non-negligible absorbed solar energy, and incorporation of the photothermal effect, more comprehensive thermodynamic analytical models were needed.

First, the transmitted solar radiation, Q_{trans} , could be simply calculated by Equations (3) and (5) with the given glazing area. Similarly, the solar radiation absorbed Q_{abs} by the glazing system could be obtained by Equations (3) and (6), which might increase the glazing system's temperature, especially for the photothermal windows (Type 2).¹⁴

$$q_{trans} = G_h * \tau \quad (\text{eq. 5})$$

$$q_{abs} = G_h * \alpha \quad (\text{eq. 6})$$

The thermal energy-driven temperature change could be expressed as Equation (7) based on the specific heat capacity formulas:¹⁵

$$Q_{mal} = \int_t^{t+1} c * m * \Delta T * dt \quad (\text{eq. 7})$$

Where heat capacity c is in a unit of J gm⁻¹ K⁻¹, m is the material mass in gm, ΔT is the temperature change for the material in a time-period t , indicated as $(T_{t+1}-T_t)$.

Second, under-designed internal and external boundary conditions, all three (conductive, convective, and radiative) types of heat transfer were calculated. In this case, with negligible forced convection, the convection and conduction were referred to buoyancy force called free convection flows.¹⁶ The governing equations involved in Nusselt number, Prandtl number, Grashof number, and Reynolds number that were related to the thermal conductivity of air to the temperature changes. The convection and conduction occurred among the surrounding air; the assumption was that the window materials are isothermal. The conductivity of air is related to the temperature shown in the following equations.

For external free convection flows (vertical plate) could be obtained in Equations (8), (9), and (10):¹⁷

$$Nu_L = 0.68 + \frac{0.670 * Ra_L^{1/4}}{[1 + (0.492/Pr)^{9/16}]^{4/9}}, Ra_L \leq 10^9 \quad (\text{eq. 8})$$

Ra_L is the Rayleigh number calculated in Equation (9), Nu is the Nusselt number,¹⁶

$$Ra_L = GR_L * Pr = \frac{g * \beta * (T_s - T_\infty) * L^3}{v * \alpha} \quad (\text{eq. 9})$$

In the function above, g is the gravity on earth, L is the height of the window surface, β is expansion coefficient = $1/T_f$, T_f is the absolute temperature = $(T_s + T_\infty)/2$, T_s is the glass surface temperature including both surfaces $T_{in,s}$ and $T_{out,s}$, T_∞ is the ambient temperature including both inner and outer $T_{in,\infty}$ and $T_{out,\infty}$. v is the kinematic viscosity = μ/ρ , α is thermal diffusivity = $k/(\rho * Cp)$,¹⁸ where μ , k , Cp , ρ , and Pr are dynamic viscosity, thermal

conductivity, specific heat, density, and Prandtl number factors related to the surface air temperature (100 K to 3000 K).¹⁹ Free convection from the panel to the surroundings is given by Newton's Law of cooling as well as conduction and radiation are shown in Equation (10), (11) and (12), respectively.¹⁶

$$Q_{conv} = hA_s(T_s - T_\infty) \quad (\text{eq. 10})$$

Where $h = Nu_L * k / L'$, A_s is the area of the glass surface. $L' = A/P$.

The net rate of radiation heat transfer between the glass and the surroundings is,

$$Q_{rad} = \varepsilon\sigma A_s(T_s - T_\infty) \quad (\text{eq. 11})$$

ε is the emissivity, σ is Stefan-Boltzmann constant $5.67E-08 \text{ W m}^{-1} \text{ K}^{-1}$.

$$Q_{cond} = kA_s(T_s - T_\infty)/L' \quad (\text{eq. 12})$$

L' is the thickness of the glass. But use the same assumption as conduction

Third, based on equations (6), (7), (10), (11), and (12), the thermal balance model can be written as in two equations (13) and (14):

$$Q_{abs} = Q_{conv} + Q_{cond} + Q_{rad} + Q_{mal} * t \quad (\text{eq. 13})$$

$$Q_{abs} = q_{abs} * A_s \quad (\text{eq. 14})$$

In the comparison of Type 1 and Type 2, they all placed under the same solar irradiation conditions, which were based on the reference solar spectra. The outdoor temperature was 0°C , and the indoor temperature remained 25°C . The dimension of this glazing system was 1.2m by 1.5m. Besides, the surrounding relative humidity was set as a constant 50% RH. Also, in this comparison, we ignored other effects by window frames, glazing edges, condensation risks, etc.

By using the above governing functions, we then derived the window surface temperatures and the inward flowing thermal radiation values. As shown in Table 2, the total solar absorption Q_{abs} are 183.83 W m^{-2} and 139.38 W m^{-2} for Type 1 and Type 2, respectively. Type 2 gained 44.45 W m^{-2} more than Type 1 on absorption. Affected by the PT effect, that difference resulted in a 23.84 K temperature increase for the inner window surface temperature of Type 2, compared with that temperature of Type 1, as shown in Table 2. The temperature difference between the window's inner surface temperature and interior ambient temperature formed thermal transfer that could be calculated using Equations (10), (11), and (12). As shown in the results Table 2, the heat transfer to the indoor area through convection, conduction, and radiation were -10.19 and 69.18 W m^{-2} for Type 1 and Type 2, respectively. The negative sign of heat transfer represents a heat loss from the indoor area to outside. It also indicated that the PT effect significantly increased the inner surface temperature and even became a thermal radiation source for the interior.

Table 2. Window thermal properties.

In winter	Q_{abs} , W m^{-2}	Q_{trans} , W m^{-2}	Material T, K	$T_{in,s} / T_{out,s}$, K		Heat transfer to indoor, W m^{-2}
Type 1	139.38	335.95	294.08	294.29	293.86	-10.19
Type 2	183.83	323.01	317.92	318.14	317.71	69.18

3.4 Heating energy saving analysis

Combining the results from the above sections 3.2 and 3.3, we were able to calculate the net energy based on the solar heat gains and the building heat loss through windows: 325.76 W m^{-2} for Type 1, and 392.19 W m^{-2} for Type 2. The

net energy amounts are shown in Table 2: 325.76 W m⁻² and 392.19 W m⁻² for Type 1 and Type 2, respectively. In short, this represents that the photothermal window (Type 2) could achieve 20.4% energy savings than the baseline window (Type 1) in winter and with solar radiation situations.

4. Conclusion

In this paper, we proposed a solution of using a photothermal thin film to enhance the thermal performance of low-e coated single-pane windows. Then, we focused on the development of a comprehensive thermodynamic analytical model into which we incorporated the photothermal effect. Through this analytical model and computation, we concluded that compared with the low-e coated windows, 20.4% energy-savings could be yielded by the photothermal windows in winter. Notably, this energy-saving was not achieved by increasing the thermal insulation but rather by the spectrally selective design of glazing materials and utilization of solar NIR. Our future works include three trajectories. First, further work of this model is looking to bring more flexible inputs such as the variability of ambient temperature into the models. Also, the wind speed was negligible in the model to avoid forced convection calculations in this study. Second, we plan to apply hourly weather data, including the solar NIR value, and then predict annual energy savings. We will incorporate our previous study of solar NIR modeling into this annual energy analysis.²⁰ Last, in addition to the energy savings due to the PT effect, the PT effect may also reduce the risks of window condensation by increasing the temperature of the window's inner surface. The condensation occurred on building windows, especially low-e coated single-pane windows, which may lead to significant thermal loss from indoor to outdoor.²¹ Therefore, the combined energy savings on window condensation improvements and enhanced solar heat gains need to be investigated with more thorough and dynamic energy analysis methods.

6. Acknowledgements

We acknowledge the financial supports provided by the National Science Foundation CMMI-1847024 and National Science Foundation CMMI-1953004.

References:

1. Zimmer A, Ha. H. Buildings and Infrastructure from a Sustainability Perspective. *Sustain Heal Communities Program-Theme 41*. 2014;1:2016-09.
2. Carmody J, Selkowitz S, Lee Eleanor S., Arashteh D, Willmert T. Window System for High-Performance Buildings. *WW Norton&Company*. 2004.
3. LOW-EMISSIVITY WINDOW FILM. https://www.gsa.gov/cdnstatic/GPG_Findings_032-Low-E_Film.pdf. Accessed July 12, 2020.
4. Wang J (Jialiang), Shi D. Spectral selective and photothermal nano structured thin films for energy efficient windows. *Appl Energy*. 2017;208:83-96. doi:10.1016/j.apenergy.2017.10.066
5. Kim M, Lee JH, Nam JM. Plasmonic Photothermal Nanoparticles for Biomedical Applications. *Adv Sci*. 2019. doi:10.1002/advs.201900471
6. Zhao Z, Yuan J, Zhao X, Bandla A, Thakor N V., Tan MC. Engineering the Infrared Luminescence and Photothermal Properties of Double-Shelled Rare-Earth-Doped Nanoparticles for Biomedical Applications. *ACS Biomater Sci Eng*. 2019. doi:10.1021/acsbomaterials.9b00526
7. Link S, El-Sayed MA. Shape and size dependence of radiative, non-radiative and photothermal properties of gold nanocrystals. *Int Rev Phys Chem*. 2000. doi:10.1080/01442350050034180
8. Wang J, Caldas L, Chakraborty D, Huo L. Selection of energy efficient windows for hot climates using genetic algorithms optimization. In: *Cities, Buildings, People: Towards Regenerative*

- Environments*. In Proceedings of PLEA 2016, International Conference on Passive and Low Energy Architecture 2016; 2016:11-13.
9. Lin J, Zhao Y, Shi D. Optical thermal insulation via the photothermal effects of Fe₃O₄ and Fe₃O₄@Cu₂-xS thin films for energy-efficient single-pane windows. *MRS Commun.* 2020. doi:10.1557/mrc.2020.4
 10. Myers DR. *Solar Radiation: Practical Modeling for Renewable Energy Applications.*; 2017. doi:10.1201/b13898
 11. Liu BYH, Jordan RC. The long-term average performance of flat-plate solar-energy collectors. With design data for the U.S., its outlying possessions and Canada. *Sol Energy.* 1963. doi:10.1016/0038-092X(63)90006-9
 12. NREL. Global Horizontal Radiation. <https://www.nrel.gov/grid/solar-resource/solar-glossary.html>.
 13. NREL. *Air Mass 1.5: ASTM G-173-03.* <https://www.nrel.gov/grid/solar-resource/spectra.html>.
 14. Marion W, Wilcox S. *Solar Radiation Data Manual For Buildings.* Golden Colorado <https://www.nrel.gov/docs/legosti/old/7904.pdf>.
 15. Reif F, Scott HL. Fundamentals of Statistical and Thermal Physics. *Am J Phys.* 1998. doi:10.1119/1.19073
 16. Incropera FP, De Witt DP. Fundamentals of heat transfer. 1981. doi:10.13182/nse65-a18809
 17. Spalding DB. Handbook of heat transfer. *Int J Heat Mass Transf.* 1975. doi:10.1016/0017-9310(75)90148-9
 18. Bird RB, Stewart WE, Lightfoot. EN. *Phenomena Second Edition.* academia.edu
 19. Zografos AI, Martin WA, Sunderland JE. Equations of properties as a function of temperature for seven fluids. *Comput Methods Appl Mech Eng.* 1987. doi:10.1016/0045-7825(87)90003-X
 20. Duan Q, Feng Y, Zhang E, Song Y, Wang J, Niu S. Solar Infrared Radiation towards Building Energy Efficiency: Measurement, Data, and Modeling. *Environ Rev.* 2020.
 21. Duan Q, Zhao Y, Wang. J. Thermal performance and condensation risk of single-pane glazing with low emissivity coatings. *MRS Adv.* 2020:1-10.

Long Term Output of Grid-Tied Solar Electric Systems

An Interim Report

Everett. M. Barber, Jr.

Guilford, CT (USA)

everett.barber@gmail.com

Abstract

This is a report on the deterioration of the output of grid-tied solar electric systems over time. Commercial and residential systems are included. The capacities of the solar arrays range from 1.25 kW dc to 455 kW dc. Initially, 25 systems were in the study, 19 systems remain. The monthly output of each system has been recorded since the systems were installed. The most recently installed system is 10 years old; the oldest is 15 years old. All systems in the study are located in the northeastern US. The recorded output includes that of the inverter and the array. String-inverters are used exclusively. Excel's Trendline function is used to project system output from each system out to 20 years, based on recorded output. Causes for system output deterioration are given. Four different types of solar electric collector modules are included. Two studies of historical system output are referenced.

Keywords:

[Solar electric collectors, grid-tied solar systems, long term deterioration of solar electric systems, fixed-mount solar electric systems, sun-tracking solar electric systems, string inverters, interim report.]

1. Introduction

This is a report on the deterioration of the output of grid-tied solar electric systems over a period of 20 years. Charts were prepared to illustrate the rate of system deterioration. The study is a work in progress.

The oldest system has been tracked for over 15 years. Another iteration will be published in about 5 years, when the oldest study in this group of systems has been in operation for 20 years. The main factors affecting the output of the systems studied here are listed.

2. Timing

At the time this study was begun, 2006, other studies of grid-tied solar electric system deterioration were difficult to find. The first extensive study of the subject, referenced below, was published in 2012. It is quite thorough, but was not found until some years after this one was underway. By that time, continuing with this study seemed worthwhile.

3. Selecting The Systems

The systems included in the study were chosen mainly because the system owners agreed to make the output data from their system available on a monthly basis, for an extended period of time. That extended period could be for as long as 20 years. An effort was made to include about the same number of residential and commercial systems in the study. The capacities of systems studies range from 1.25 kW dc to 455 kW dc. Initially, 25 systems were in the study. That number was chosen to limit the time required for the study. The monthly output of each system has been recorded since the systems were installed. The most recently installed system is presently 10 years old; the oldest is 15 years old. All systems in the study are located in the northeastern US. Of the original 25 systems in the study 19 remain. Most owner's agreed to supply data on a monthly basis provided that their contact information not be made available to others.

4. Types of Cell in Arrays

Four Different Types of Cells are in the arrays:

- Single or mono-crystalline;
 - Multi or polycrystalline;
 - Amorphous silicon;
 - Semi-Crystalline,
-

5. Acquiring Data

Data is recorded monthly. The data supplied by the system owners includes the date and time of the reading, the inverter output in kWh. As a check on the inverter kWh meter, a utility-type meter is also included in several systems. Owners of the residential systems send in their data by email. The data for most of the commercial systems is obtained from webbased data logging sites. Owners of commercial systems that are not connected to the internet supply data in the same manner as the owners of residential systems. The output recorded includes that of the array plus the inverter. The two components are not read separately. String-inverters are used exclusively.

6. Soiling of the Glazing

No attempt was made to clean the collector glazings and thus improve the system output. Not because it isn't worthwhile but because few of the systems were available to the author. Also, after a few years of ownership few owners showed much enthusiasm for cleaning their collectors. Thus, the recorded output of the systems in this study reflects a worst case condition. at least due to soiling of the cover.

7. Analysis:

Monthly output data for each system is entered in a spreadsheet. The output is averaged yearly. Further, the rate of deterioration is projected for each system based on historical output. The Excel Trendline function is used to project the system output over a 20 year period.

8. Observed Causes of Output Deterioration

- Inverter mal-function: Many inverters have been replaced or overhauled after 10 years;
- Owner's inattention to system output & procrastination once output loss discovered;
- Owner's difficulty in finding a capable service contractor;
- Difficulty finding webbased data logging service;
- Subtile output loss due to shade caused by tree growth;
- Incorrectly sized replacement string fuses;
- Inverter fuse damage due to lightning;

Everett Barber/ ASES National Solar Conference 2020 Proceedings

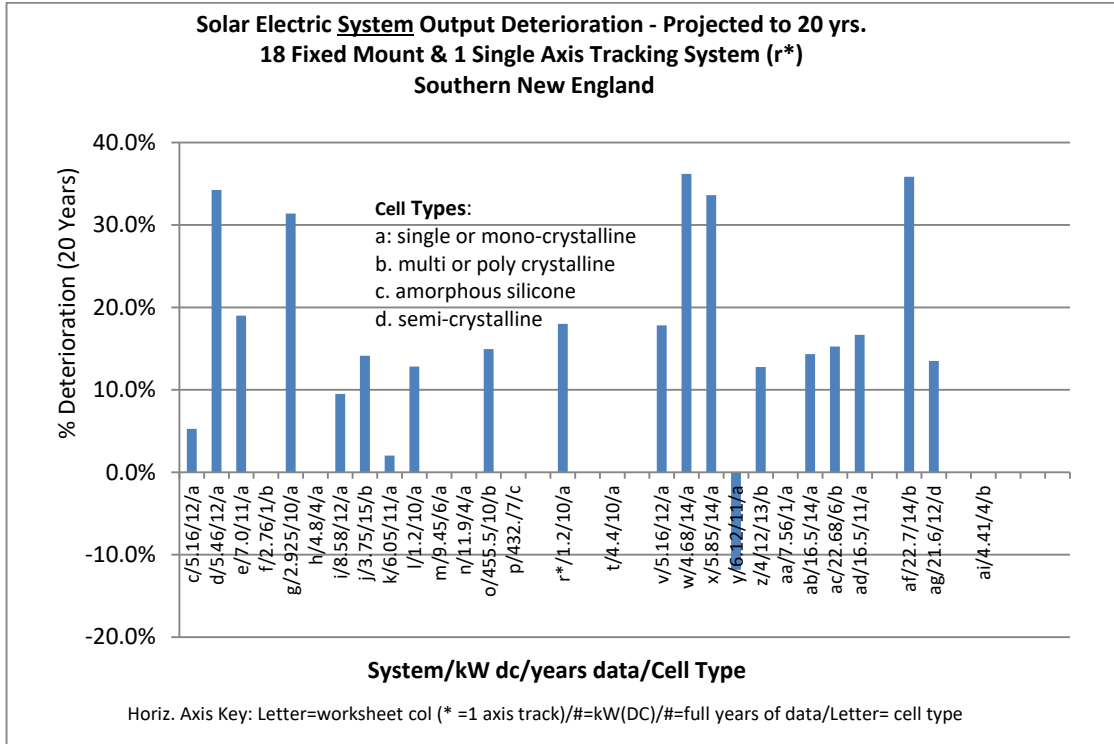
- Electrical shorting due to squirrels chewing on wiring insulation underneath the modules;
 - Long term deterioration of the cells in the modules;
 - System shut off for reasons such as: building vacant; backup generator testing; maintenance; then owner neglecting to turn system on again;
 - Array removed due to reroofing, remounting delay due to unexpected cost; system abandoned by owner due to remounting cost;
 - New inverter required due to owner enlarging original array which eliminated system from this study;
 - Ownership changed, new system owner ceased reporting output data.
-

9. An Output Anomaly

System 'y' in Fig. 1 below shows a gain in system performance over 11 years of observation. This is contrary to all the other systems and contrary to what is to be expected. The gain over the 11 year period seems to be due to the approximate 4 year-long reduction in system output between about 2012 and 2014. During that time the owner struggled to find a competent service technician to correct the system problem. When one was found the technician determined the reduction in system output to be due to improperly sized string fuses installed between the inverter and the solar arrays. When fuses with the correct ampacity were installed the system output increased significantly. It remains to be seen if the longterm output trend is gradually downward after 2016.

Fig. 1: Projected Output of 19 grid-tied systems – kWh ac/m²/yr

Everett Barber/ ASES National Solar Conference 2020 Proceedings



As the systems continue to age the height of the above 'bars' are expected to lengthen.

References:

Dirk C. Jordan and Sarah R. Kurtz, June 2012. Photovoltaic Degradation Rates – An Analytical Review. Journal Article, NREL/JA-5200-51664, Contract No. DE-AC36-08GO28308.
Web Address: <https://www.nrel.gov/docs/fy12osti/51664.pdf> (last checked 7/12/2020)

Mark Bolinger, Will Gorman, Dev Millstein, Dirk C. Jordan, July 2020. System-level performance and degradation of 21 GW-DC of utility-scale PV plants in the United States, Journal of Renewable and Sustainable Energy; Vol 12, Issue

New Ways to Combine Solar Thermal with Geothermal

Gaylord Olson¹, Yao Yu²

¹ Seasonal Storage Technologies, Princeton, NJ (United States)

² North Dakota State University, Fargo, ND (United States)

Abstract

A more efficient and less costly method for heating and cooling of buildings is possible using any of several types of solar thermal collectors along with a geothermal or ground source heat pump (GSHP). This paper considers only shallow earth geothermal, as opposed to deep earth geothermal typically used for electricity generation. Although a variety of solar assisted ground source heat pump (SAGSHP) systems have been described in the literature in past years, none of these have become commercially viable products. It is possible that with a more optimum design, this general approach could become more cost-effective than conventional ground source heat pump systems and thereby become commercially viable. The general consideration is that there is a trade-off between the size and cost of a solar thermal collector array and the ground loop for the geothermal portion of the system. For parts of the world where the cost of drilling and installing ground loops is high, it is likely that the added cost of a solar thermal array (or possibly an air to liquid heat exchanger) will be lower than the cost of the portion of the ground loop which is eliminated. This could lead to commercial viability for a systems such as described herein.

Keywords: Solar Thermal Collector, Ground Source Heat Pump, Geothermal

1. Introduction

The U.S. consumes approximately 19% of the total energy of the world, in which buildings account for 41% of the U.S. energy consumption. However, only 9% of the U.S. building energy is renewable. Within the 41%, Heating, Ventilating, and Air Conditioning (HVAC) accounts for about 60% of U.S. building site energy consumption (Buildings Energy Data Book). A heat pump system is a type of HVAC system for buildings which provides heating and cooling using a conventional refrigeration cycle and is known to have higher system efficiency (especially for heating) compared to many other HVAC systems, such as systems with gas-fired furnaces or boilers.

Although a GSHP system has the potential for achieving a high system efficiency, the high initial cost is a major barrier for the broad application of GSHP systems in the market. Additional source(s) can be used within a heat pump system along with the ground, such as solar thermal, ambient air, water (lake, river, etc.). A heat pump system with more than one source is known as a multi-source heat pump system. Recent studies (Allaerts et al., 2015; Ermi et al., 2015; Corberán et al., 2018) indicate that the size of the underground loop of a conventional GSHP system can be reduced by about half without a reduction of system efficiency if an additional source is used along with the ground, such as a solar thermal collector or an air to liquid heat exchanger. Although all types of solar thermal collectors are capable of collecting thermal energy from the sun, certain types of collectors are suitable for collection of both heat and cold. Two of these types are unglazed plastic collectors (often used for swimming pool heating) (Anderson et al., 2011, 2013; Man et al., 2011) and photovoltaic/thermal (PV/T) collectors (Eicker and Dalibard, 2011; Pean et al., 2015). These collectors dissipate heat through both convection and radiation and thus would be suitable for use in any climate. The unglazed and PV/T types are functionally similar to air to liquid heat exchangers, also known as dry coolers. The word “cooler” is somewhat of a misnomer because these devices can collect heat just as well as dissipate heat.

The use of inexpensive solar thermal collectors or dry fluid coolers instead of more expensive ground loops contributes to the reduction of the overall system cost, thus providing a cost-effective way to overcome this barrier of GSHP systems. This paper introduces an innovative multi-source heat pump system design that is lower cost to build (much smaller ground loop) and use (higher average annual efficiency) compared to standard, conventional GSHP systems. All new concepts presented herein are currently either patented or patent pending.

2. System Design and Discussion

This paper builds upon three papers published in Europe recently and also one commercial heat pump product currently available in much of Europe. A group based in Spain (Corberán et al., 2018) describes a dual source heat pump system with two separate source fluid heat exchangers in the refrigerant loop, thus providing both an air source and a ground source mode (Figure 1). The mode selection is based on whichever source temperature is best at any given time. A conclusion of this paper is that the system has an efficiency similar to a conventional GSHP system but requires a one half size ground loop (about 50% lower ground loop cost). However, a limitation of this design is that since the air source heat exchanger uses refrigerant rather than water, it cannot provide preconditioning of the ground loop (i.e., to connect the air source heat exchanger and the ground loop directly to collect heat/cold from the ambient air and then transfer it to the ground to allow a certain level of underground thermal energy storage). This is a significant disadvantage, as will be discussed below.

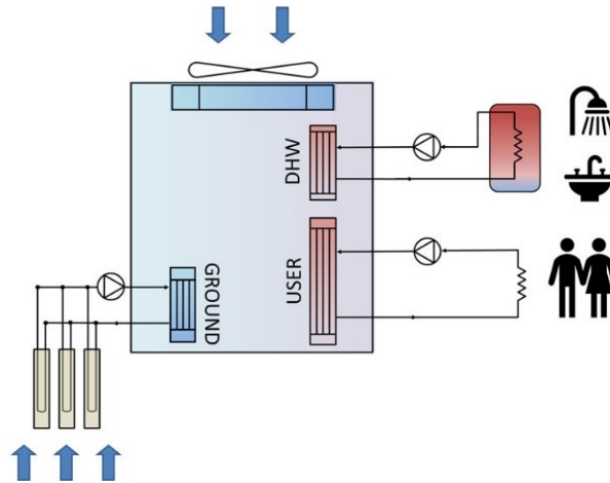


Fig. 1: Dual source heat pump system design (Corberán et al., 2018)

A multi-source system functionally similar to the system from Spain is now in production by a German company, Thermselect (THERMSELECT). This product differs from the Spanish design in that it has physically separate modules for the water and air source heat exchangers (one inside the building and one outside). The Thermselect system also has an option for use of solar thermal collectors. This product is designed for European electrical power standards, and thus is not available in North America. In common with the Spanish system, the Thermselect product cannot provide ground loop preconditioning since the air source heat exchanger uses refrigerant rather than water, and it is claimed that the ground loop needs to be only one half the size of a conventional GSHP loop (SmartHeat). For cold climate regions, a paper by Italian authors (Emmi et al., 2015) shows a simple SAGSHP system which also functions well with a much smaller ground loop. In contrast to the systems described above from Spain and Germany, this Italian design does provide for preconditioning of the ground loop, since the solar collectors and the ground loop both use water rather than refrigerant (Figure 2). This paper from Italy shows simulation results for six different cold climate cities. The worst case example (coldest) location was a city in northern Poland (Bialystok). Even with this coldest location, the summer preconditioning using solar thermal collectors gives a higher efficiency than a conventional GSHP system after seven years of operation, and this is with a 70 percent ground loop size reduction.

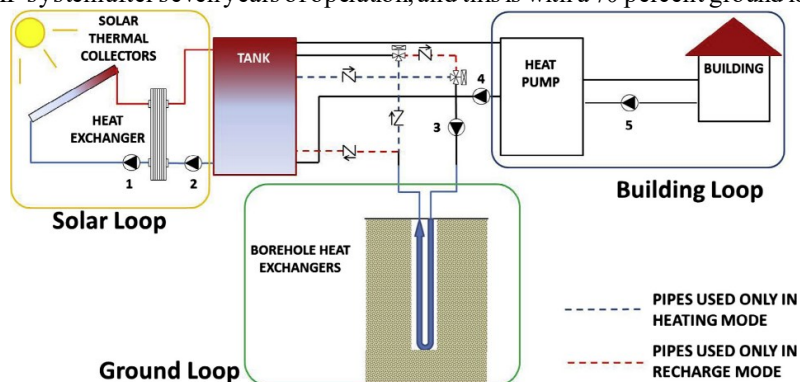


Fig. 2: SAGSHP system design (Emmi et al., 2015)

A much different type of multi-source system is described by the authors in Belgium (Allaerts et al., 2015). This system (Figure 3) uses a dry cooler with a water source heat pump, but it does not have or use an air source mode as do the systems from Spain and Germany. Instead of this it uses only preconditioning into two separate ground loops, one for hot storage and one for cold storage. This system has a somewhat complex valve design and it needs two separate water pumps for the source fluid. The system reverses the flow patterns for summer and winter seasons (Figure 3). On hot summer afternoons, the preconditioning pump supplies hot water into the warm ground loop while at the same time the other water pump sends cold water from the other ground loop to the heat pump. On the coldest winter nights this is reversed, with preconditioning of very cold water (or antifreeze solution) into the cold ground loop while much warmer water is used by the heat pump. This selection of modes provides a significant benefit for both efficiency and total ground loop size. Even though this Belgian design has two separate ground loops, the summation of size for both loops together is approximately half the size of a conventional single loop GSHP design. It should be noted that the dry cooler as proposed by the Belgian authors could instead be an unglazed solar or PV/T array. The relative cost-effectiveness of solar collector use versus dry cooler use will require further study.

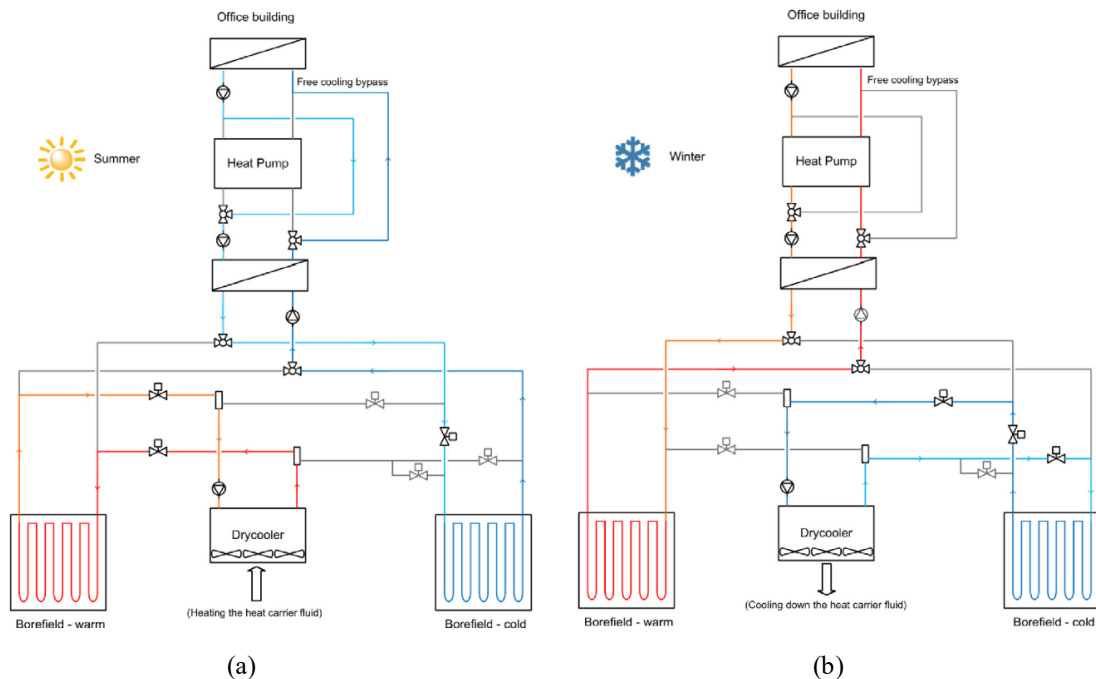


Fig. 3: Multi-source system design: (a) cooling mode (b) heating mode (Allaerts et al., 2015)

Figure 4 shows a simplified diagram of the Spanish/German system approach on the left versus the Belgian approach on the right. The Spanish/German approach simply allows a choice between an air source mode or a ground source mode (no preconditioning of the ground loop). The Belgian approach does not have an air source mode into the heat pump, but it does have preconditioning into two separate ground loop regions. Since both of these approaches have been shown to give about a 50 percent ground loop size reduction (with equal or better system efficiency), the use of both concepts in a single system should give something better than 50 percent. This combination in a single system could reasonably have a 60 percent ground loop size reduction.

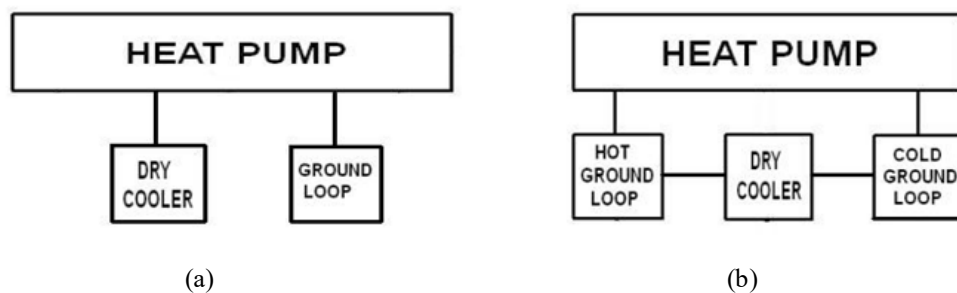


Fig. 4: Dual source system design options: (a) Spanish/German system approach (b) Belgian approach

Figure 5 shows a possible design that includes all of the concepts discussed above. The top water pump in Figure 5 is used for supplying source water to the heat pump. The bottom water pump is used for preconditioning into either or both of the ground loops. Both water pumps are in use when the air source mode is selected. The three ball valves in Figure 5 give at least twelve different modes of operation. These modes are delineated in a recent patent application for this system. A very similar design, also using three valves, is described in US 10724769.

The three valves in Figure 5 are all identical types, and use what is known as an internal T-port configuration (ValveMan). The valves and pumps are assumed to be electrically actuated and computer controlled. The T-port ball valves have four different settings with 90-degree angular increments of the internal ball. If the valve is oriented such that the connections are in an east-west-south arrangement, the four settings are as follows:

1. Flow is allowed in or out of all three connections.
2. Flow is allowed only between east and west connections.
3. Flow is allowed only between west and south connections.
4. Flow is allowed only between east and south connections.

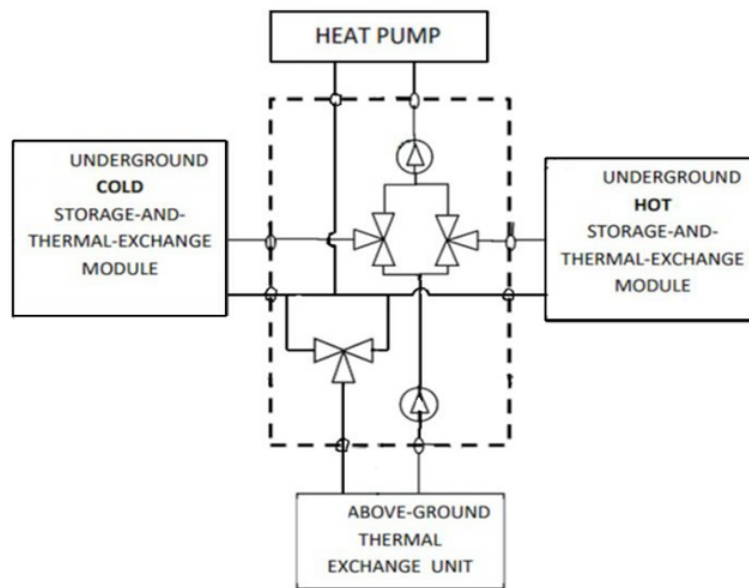


Fig. 5: Revised multi-source system design

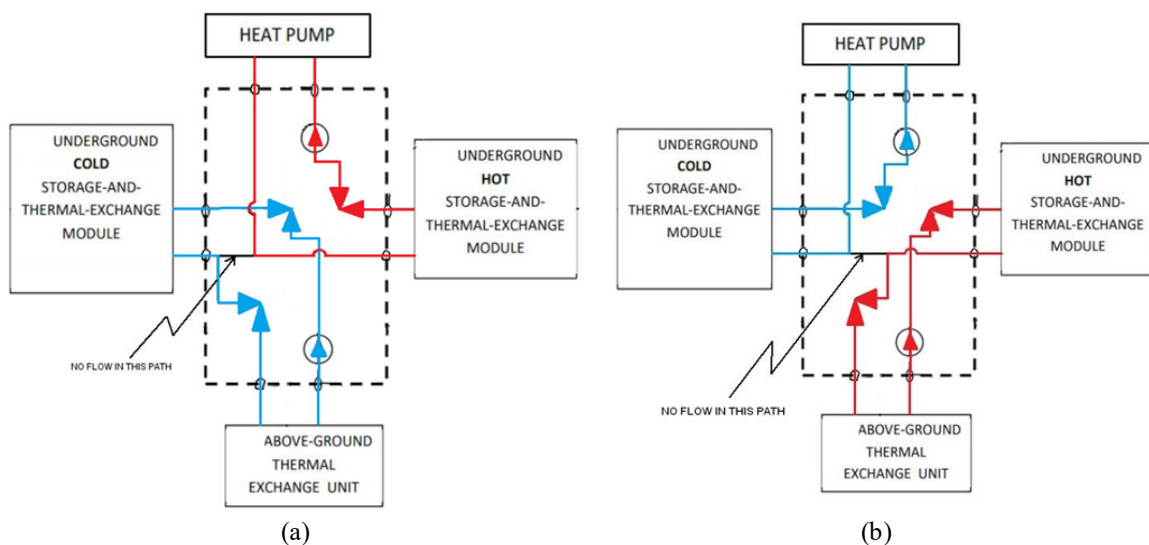


Fig. 6: Flow paths during (a) the coldest winter night and (b) the hottest summer day

It is expected that both water pumps in this design are variable speed types, although most of the functionality is possible with single speed pumps. It is also expected that there will be a control computer and at least two temperature

sensors. Both outdoor ambient and source input temperatures would be recorded in the computer at regular intervals, and these two temperature histories would determine the best settings for valves and pump speeds. It is assumed that when the heat pump is in a heating mode, a maximum source input fluid temperature is desired and vice versa for the cooling mode.

Figure 6 shows the valve settings that will accomplish what the paper from Allaerts et al. (2015) describes. The blue color is intended to show cold fluid and the red color much warmer fluid. These would be the modes most appropriate for the most extreme ambient temperature conditions. Consider now the situation where the outdoor ambient temperature is beginning to rise above an extreme cold condition. There will likely be an ambient temperature at which the above ground thermal exchange unit (dry cooler or solar thermal element) will give a higher source input temperature than that from the ground loop. A simple approach would be to switch from ground source mode to above ground mode at this point. Although simple, this approach is not optimum. A better strategy is to use a parallel mode at and near this temperature crossover point. The parallel mode is indicated in Figures 7 and 8. If it is desired to have equal flow rates from the above ground unit and from the ground loop, the top water pump would be adjusted to have a flow rate which is double the flow rate of the bottom pump. As shown in Figure 8, the parallel mode red and green curves give a significantly higher temperature than the simpler case where the parallel mode is not used. The graph of Figure 8 is for the case of the heat pump being in a heating mode. A similar graph would exist for the case where the ambient temperature is coming down from an extreme hot condition.

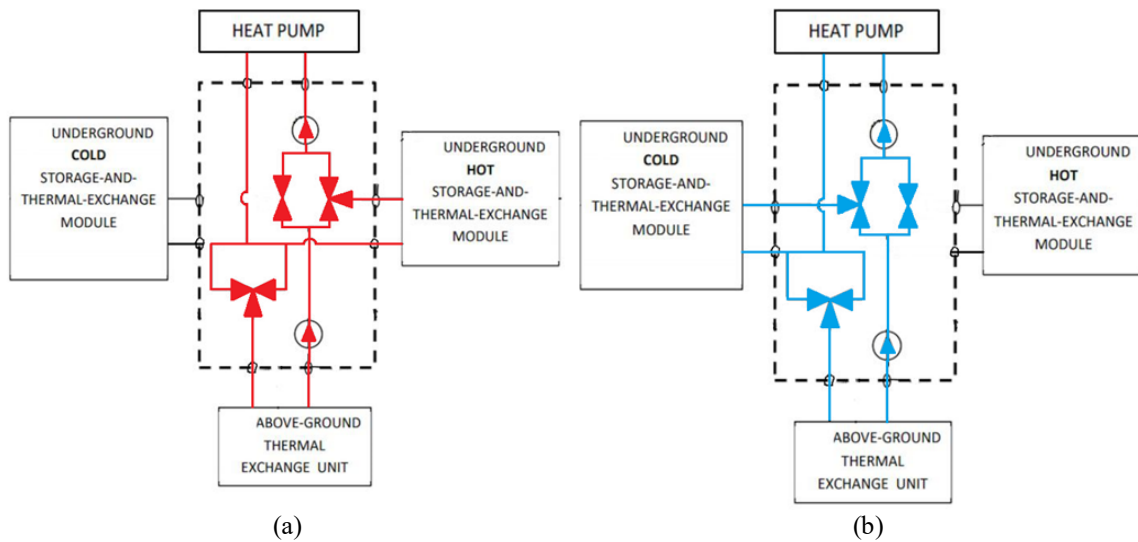


Fig. 7: Parallel modes using (a) hot module and (b) cold module

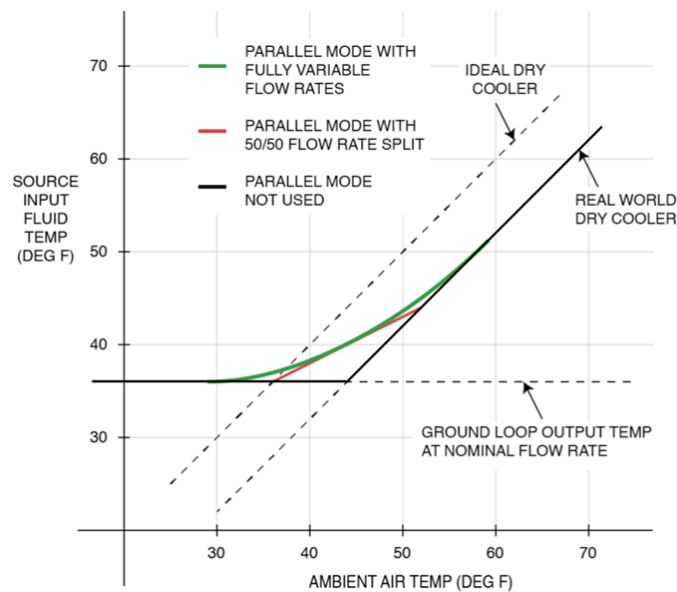


Fig. 8: Temperature curve

Valve settings for the air source mode are shown in Figure 9. Both water pumps are used, and there will be no flow through either of the ground loops. In case where there is just one ground loop, two of the valves are not needed. In this case, the configuration could be as shown in Figure 10. Even with this simpler configuration, there are still four modes possible: ground source, air source, parallel, and preconditioning.

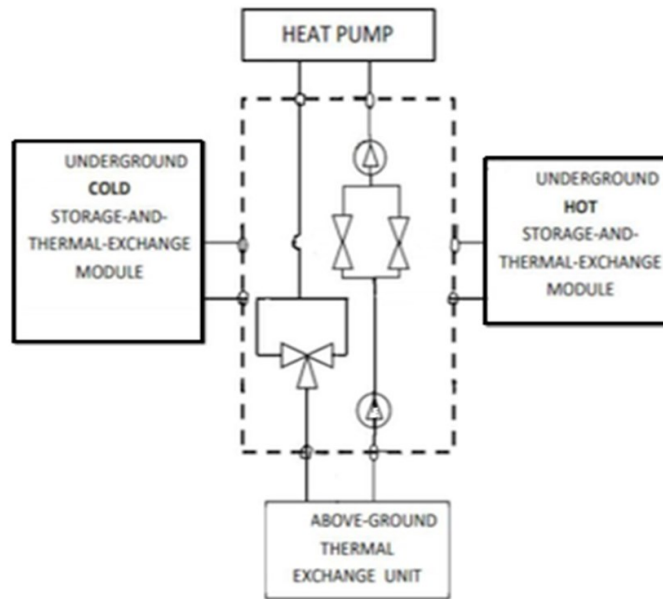


Fig. 9: Air source mode flow paths

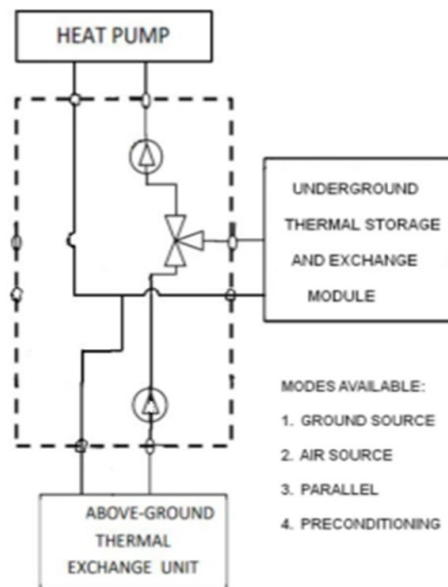


Fig. 10: Modification for a single ground loop

As shown in the paper by Allaerts, et al. (2015), ground loop preconditioning might lead to ground loop temperatures such that the heat pump and compressor are not needed for space conditioning. This is very likely the case at the start of the cooling season, after a winter of cold loop preconditioning. In this case the heat pump can be bypassed, resulting in very cost-effective cooling. This might best be done using a water source heat pump which has an internal design with a water side economizer capability.

Regarding the physical implementation of the system described above, there are four possible configurations:

1. Place the three valves and two water pumps in a separate box, allowing interface to many different heat pumps and many different above ground units.

2. Place the valves and pumps in the same box as the above ground unit, allowing interface to many different water source heat pumps.
3. Place the valves and pumps in the same box as a water source heat pump, allowing interface to many different above ground units.
4. Place all components of all elements of the system in a single box, most likely to be located outdoors.

Although all of the figures above show a connection to a single heat pump, this can be changed such that multiple heat pumps are supplied with a flow of water around a closed loop. This could be a two-pipe loop or a one-pipe loop. A one pipe loop is shown in Figure 7 of the patent referenced above (US 10724769). This figure shows the use of a reversing valve at the primary loop pump, to make sure that all heat pumps in the loop have the same long-term average efficiency. To make this idea practical, reversible flow fixtures are used in place of closely spaced tees for all interfaces to the loop. This means that the heat pump in all the figures above would be replaced with a reversible flow fixture which interfaces with the primary loop. As long as temperature in this primary loop can be kept between 40 and 80 degrees F, all heat pumps will have good efficiency for both heating and cooling. Reversible flow fixtures can be constructed in many ways, but a specific type is commercially available from Taco Comfort Solutions (Taco LoadMatch). This product is available in a wide size range and has the brand name Twin-Tee.

3. Conclusion

This paper describes a possible design that can be used to advance the development of a high-efficiency, multi-source heat pump system. This system consists of a heat pump(s) with two underground regions (one for heat and one for cold) and above-ground thermal exchange unit(s), such as solar thermal collector(s), dry cooler(s), etc. A variety of control strategies have been discussed in the paper with the goal of not only providing enough heating and cooling to buildings but also maximizing system efficiency. This type of system design has the potential for reducing the overall system cost without sacrificing system efficiency compared to a conventional GSHP system, thanks to the significant reduction of the borehole size (more than 50%) realized by using inexpensive above-ground thermal exchange unit(s) as well as optimized control strategies. This study provides a cost-effective way to design and use a multi-source heat pump system. It has the potential for a wide application when used in dense urban areas due to its requirement of smaller ground loop areas. More simulation and experimental work will be performed in the future to further verify the design and optimize the size of system components.

4. Acknowledgments

We hereby acknowledge the assistance and encouragement of Dr. Roy J. Rosser.

5. References

- Allaerts, K., Coomans, M. and Salenbien, R., 2015. Hybrid ground-source heat pump system with active air source regeneration. *Energy Conversion and Management*, 90, pp.230-237.
- Anderson, T.N., Duke, M., Carson, J.K. 2011. Performance of a building integrated collector for solar heating and radiant cooling. *Solar 2011, the 49th AuSES Annual Conference*, November 30th – December 2nd, 2011.
- Anderson, T.N., Duke, M., Carson, J.K. 2013. Performance of an unglazed solar collector for radiant cooling. *Australian Solar Cooling 2013 Conference*, Sydney.
- Buildings Energy Data Book. U.S. Department of Energy. <http://web.archive.org/web/20130214024505/http://buildingsdatabook.eren.doe.gov/ChapterIntro1.aspx> (accessed: July 5, 2020).
- Corberán, J.M., Cazorla-Marín, A., Marchante-Avellaneda, J. and Montagud, C., 2018. Dual source heat pump, a high efficiency and cost-effective alternative for heating, cooling and DHW production. *International Journal of Low-Carbon Technologies*, 13(2), pp.161-176.
- Eicker, U. and Dalibard, A., 2011. Photovoltaic-thermal collectors for night radiative cooling of buildings. *Solar Energy*, 85(7), pp.1322-1335.
- Emmi, G., Zarrella, A., De Carli, M. and Galgaro, A., 2015. An analysis of solar assisted ground source heat pumps in cold climates. *Energy Conversion and Management*, 106, pp.660-675.
- Man, Y., Yang, H., Spittle, J.D., Fang, Z. 2011. Feasibility study on novel hybrid ground coupled heat pump system with nocturnal cooling radiator for cooling load dominated buildings. *Applied Energy*, 88, 4160-4171.

Pean, T.Q., Gennari, L., Olesen, B.W. and Kazanci, O.B., 2015. Nighttime radiative cooling potential of unglazed and PV/T solar collectors: parametric and experimental analyses. In 8th Mediterranean Congress of Heating, Ventilation and Air-Conditioning.

SmartHeat. <https://www.smartheat.de/waermepumpen/serie-therms electr.html> (Accessed: July 13, 2020)

Taco LoadMatch. http://apps.taco-hvac.com/uploads/FileLibrary/REV_LoadMatchTwinTee_Catalog_100-6.8_031119.pdf (Accessed: July 13, 2020)

THERMSELECT. www.therms elect.de (Accessed: July 13, 2020)

ValveMan. <https://valveman.com/blog/understanding-tport-vs-lport-directional-flows/> (Accessed: July 13, 2020)

A New National Database for Solar Resource Assessment Compiled from Ground-Based Observations

James W Hall, PhD

JHtech/SolarDataWarehouse, San Antonio, FL, USA

Abstract

A new solar radiation resource with complete coverage of the United States has been created from ground-based observations of global irradiance from 2005 to the present. Daily and hourly data have been collected from over 7000 professionally maintained weather stations. These sites belong to nearly 100 different federal, state and university networks. The average distance between sites in the continental US is about 37 km - somewhat farther in the great plains and closer in more populated areas. They have been combined into a “network of networks” so the accuracy of each individual site can be judged by comparing to nearby neighbors, often from other networks. Advanced filtering and sensor fusion techniques common in artificial intelligence are used to identify sensors that are not performing correctly and filter errors from the data stream. Validation tests have shown that the daily and hourly measurements of global irradiance in this ground-based resource have roughly half the uncertainty, half the observation error and half the bias error compared to the satellite based observations in the National Solar Radiation Database (NSRDB-PSM). Accuracy, bias and uncertainty at the monthly and annual levels are comparable. This new solar resource can be combined with existing data, or used as a stand-alone database, to enhance site planning, production forecasts and on-going monitoring of solar projects.

Keywords: solar radiation resource, solar radiation database, ground-based solar measurements, National Solar Radiation Database, NSRDB

1. Introduction

The solar power sector relies on accurate assessment of resource throughout the life cycle of a solar power plant. This reliance begins with site selection, continues through design and acceptance testing, and persists as efficient operation is validated to the end of the plant’s service life. Historically, the industry has relied on satellite-based solar resource since it is readily available, has global coverage and long-term measurements. However, due to the known limitations of satellite data, most significant projects also require additional ground-based, site-specific measurements of solar resource to tune the satellite data and lower the uncertainty in energy production estimates. This merging of satellite data with ground observations is often referred to as creating a bankable solar dataset.

Solar irradiance measurements from thousands of ground-based sites are publicly available. However, solar irradiance is among the most difficult of meteorological measurements, especially in a production setting. Some have questioned the direct use of these public sites for solar resource due to concerns about sensor maintenance, sparse distribution and the lack of validation methodologies.

SolarDataWarehouse has recently completed a new bankable, long-term solar resource based on ground measurements with complete coverage of the United States – the US Ground-Based Solar Irradiance Database (GSID). This paper explains how artificial intelligence (AI) filters and sensor fusion were applied to lower the uncertainty and quality control the observations from professional ground sites. Detailed validation of this new resource followed the same procedure used to validate National Solar Radiation Database Physical Solar Model (NSRDB-PSM version 3). In this validation, the ground-based observations in the GSID had roughly half the bias error, half the observation error, and half the uncertainty at hourly and daily levels compared to the satellite-based data in the NSRDB-PSM for the years 2005-2018. The GSID is therefore a ground-based

solar resource that can be used as a stand-alone dataset, or in conjunction with other resource data, for the planning and monitoring of solar power projects.

2. A Network of Networks

There are many different professional networks in the US that measure solar radiation. These networks have been established by the federal government, state governments and universities for a specific purpose such as climate research, resource management and agriculture. Each entity establishes their own criteria for site selection, maintenance and data quality control. Examples of these networks include:

- US Climate Reference (USCRN) – A network of over 130 sites across the US providing high-quality, long-term data for climate research.
- The University of Oregon’s Solar Radiation Monitoring Laboratory (SRML) – a network of 37 sites designed to provide high-quality solar resource data for the Pacific Northwest.
- California Irrigation Management Information System (CIMIS) – a network of over 200 stations across California to help manage water resources more efficiently.

Taken separately, each network fulfils specific, local purposes for which it is operated. However, no single network provides nationwide solar coverage, and generally the sites are located too far apart to cross-validate observations with other sites in the network. The Ground-Based Solar Irradiance Database (GSID) is a compilation of data from nearly 100 different overlapping networks, professionally operated and maintained with over 7000 individual sites (Figure 1). Merging these networks into one provides complete spatial coverage across the US. The average distance between sites is 37 km, with somewhat greater spacing in the Great Plains and tighter spacing in more populated areas.



Fig. 1: The US-GSID is a network of networks, combining solar observations from over 7000 sites and nearly 100 networks

The many individual sites contained in the GSID database provide good coverage in key solar areas such as California, with 1350 sites at an average spacing of 18 km. The coastal and mountainous regions of California often contain microclimates that have proved challenging for satellite models. Researchers have demonstrated that significant improvement in solar resource for California can be obtained by utilizing ground-based data rather than relying solely on satellite observations (Anders Nottrott and Jan Kleissl, 2010, 2014).

Ingesting and merging the data from nearly 100 different networks into a single database presents challenges. Networks are constantly adding, decommissioning, or on occasion re-locating sites. Each network is built and operated for specific professional tasks - public data access is never the primary purpose and is generally limited to one site at a time. The networks measure different parameters, have different sampling rates, time

may be expressed differently and measurements expressed in different units. Web access and website formats change regularly, so constant modifications to the ingest software are required.

3. Reducing Error Via Artificial Intelligence and Sensor Fusion

In addition to complete spatial coverage, this dense network of professional ground sites provides an extensive amount of solar resource data. As with any large set of measurements, there are always errors. Rather than rejecting the data as a viable resource because of these errors, one can learn to identify specific data patterns associated with the errors and use modern processing techniques to filter them. Artificial Intelligence (AI) is particularly well suited to this task.

A common technique in artificial intelligence is sensor fusion: combining data from multiple sensors to compensate or correct for the deficiencies of individual sensors. It relies on multiple sensor sites or multiple types of sensors viewing the same event. Such an approach is data driven rather than model driven. Intelligent algorithms process the data and fuse it into a data stream with lower uncertainty than the original sensors might have. The algorithms also give an indication of sensors that are not performing correctly so they can be removed from the data stream until repaired.

For a basic example: the calibration of a solar irradiance sensor is conventionally done via side-by-side comparison to a high-quality reference. This works well for an initial calibration, but is not feasible for on-going performance monitoring. A data-driven method to monitor sensor performance is to compare a sensor's output to that of neighboring sensors viewing the same event. Clear sky days are an instance when all neighboring sensors should be seeing the same event.

There are several physics-based models for estimating clear sky radiation from solar position and atmospheric conditions, however, accurate knowledge of atmospheric conditions may not be available at the desired location and date. One data-driven alternative is plotting a large number of ground-based solar observations for a specific location over a period of time. To illustrate, the daily GHI observations from four ground sites near Kennewick, WA are in Figure 2. From such plots, one can estimate the average clear sky global irradiance at that location for any day of the year. Similarly, time histories of hourly data can be used to estimate clear sky global irradiance for any hour at a specific location and date. This type of analysis can also be used to quantify a bias error in any of individual sensors.

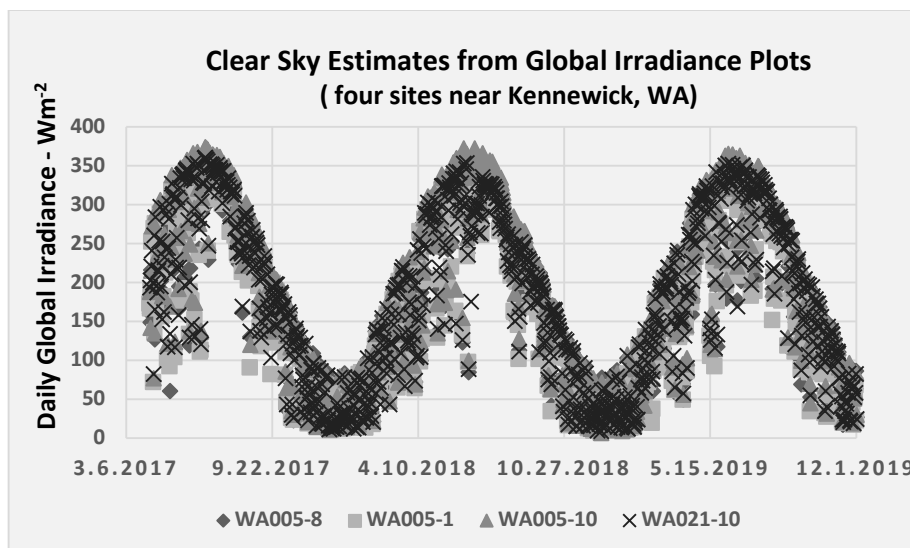


Fig. 2: Estimating clear sky global irradiance from observations near Kennewick, WA

Once the historical clear sky irradiance is known, clear sky events can be identified in real-time. On clear sky days, a deviation by one sensor from the mean of the neighboring sites can indicate a malfunction, and the amount of uncertainty for the malfunctioning sensor can be quantified using traditional statistical methods.

Figure 3 shows a simple example of a malfunctioning sensor near Sacramento, CA on October 2, 2013. Daily GHI observations of 17 ground sites from five different solar networks are shown. The circle indicates a 40 km radius. The site in the center of the circle is in disagreement with the surrounding sites, and is removed from the data stream until future observations indicate it has been repaired.

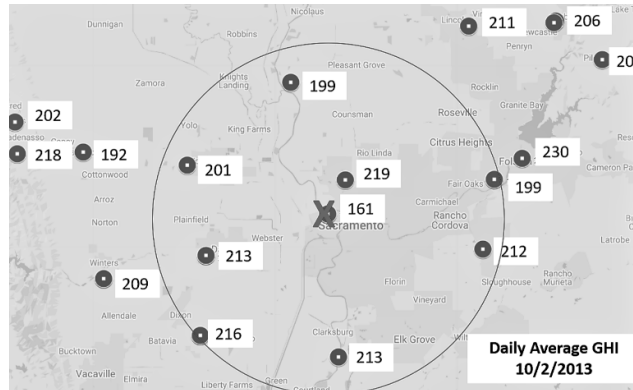


Fig. 3: A malfunctioning sensor near Sacramento was identified by comparing nearby sites on a clear sky day.

Analysis of hourly irradiance on clear sky days can identify improper siting or sensor misalignment (Figure 4). A repeated pattern of hourly observations below the historical envelope occurring at the same time of day can indicate shading of the sensor. A skewed curve, with recurring deviations below the historical envelope in the morning and above the envelope in the afternoon is a pattern typical of sensor misalignment. Artificial Intelligence (AI) algorithms are well suited to finding these patterns in large datasets.

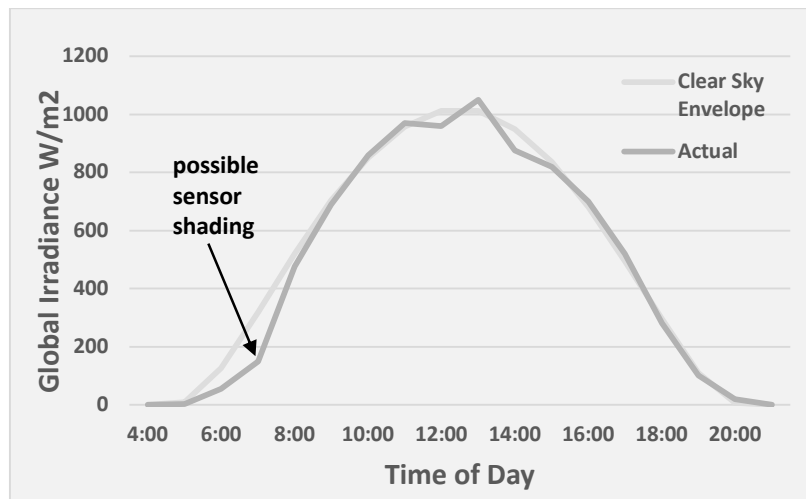


Fig. 4: Identifying siting or sensor installation problems from hourly data

Sensor fusion can perform complex quality control of the sensor data. For example, an algorithm for sensor soiling can learn the historical patterns in the time histories of neighboring sensors. Fusing precipitation data with solar observations enables the algorithm to identify sensor soiling from the pattern changes following a major precipitation event.

Each of these examples of finding and filtering out sensor errors requires pattern recognition. For small datasets, this can be performed by a skilled practitioner. However very large datasets require the type of automated pattern recognition offered by AI tools.

4. Validation Methodology

The validation of the GSID duplicated as closely as possible the methodology used to validate the NSRDB-PSM (Sengupta, et al., 2015; Habte, et al., 2017; Habte, et al., 2018). High-quality data from seven sites in the Surface Budget Radiation (SURFRAD) network (Figure 5) were downloaded from the NOAA website and used as the reference. Data from all SURFRAD sites were intentionally excluded from the GSID so they could be used for validation purposes. For this comparison, data from the GSID ground site closest to each SURFRAD site were used. NSRDB-PSM satellite-based data (version 3.0.1, 2005-2018) was downloaded from the NREL's NSRDB Data Viewer (see <https://maps.nrel.gov/nsrdb-viewer>) by entering the latitude and longitude of each SURFRAD site into the viewer. The hourly data was aggregated into daily, monthly and annual values. The only material difference in the validation methodology was that NREL excluded observations where solar zenith angles were less than 80 degrees in the original NSRDB-PSM validation. This validation procedure excluded observations where global irradiance at the reference site was less than 50 W/m². Both methods were intended to exclude errors that can occur under low-light conditions near sunrise and sunset.

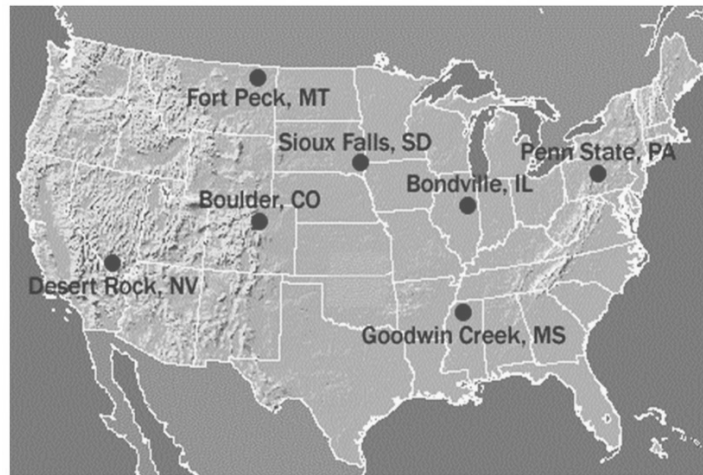


Fig. 5: SURFRAD sites used to validate the National Solar Radiation Database (image courtesy of Surface Radiation Budget Network)

5. Validation Results

The primary validation statistics were Mean Bias Percent Error (an indicator of long-term bias in the observations), Mean Absolute Percent Error (an indicator of the average error in the observations) and the Overall Uncertainty at 95% confidence (a confidence interval for the observations). These statistics were calculated using the following equations:

$$\text{Percent Error: } \%E = 100 \times \frac{(\text{observed} - \text{true})}{\text{true}} \quad (\text{eq. 1})$$

$$\text{Mean Bias Percent Error: } MB\%E = \frac{1}{n} \sum_1^n (\%E) \quad (\text{eq. 2})$$

$$\text{Mean Absolute Percent Error: } MA\%E = \frac{1}{n} \sum_1^n |\%E| \quad (\text{eq. 3})$$

$$\text{Root Mean Square Percent Error: } RMS\%E = \sqrt{\frac{1}{n} \sum_1^n (\%E)^2} \quad (\text{eq. 4})$$

$$\text{Overall Uncertainty at 95\% Confidence: } U_{95} = \pm 2 \sqrt{\left(\frac{U_{ref}}{2}\right)^2 + \left(\frac{MB\%E}{2}\right)^2 + \left(\frac{RMS\%E}{2}\right)^2} \quad (\text{eq. 5})$$

In these equations, n represents the number of observations and U_{ref} is the estimated uncertainty in the SURFRAD reference data. This validation used 5% for U_{ref} , as did the NRSDB validation.

The validation statistics for all seven sites combined are shown in Figures 6-8. The Appendix contains a table of the statistics for the individual comparison sites.

Mean Bias Errors for the NSRDB-PSM and GSID are shown in Figure 6. It can be seen that the GSID had significantly lower observation bias at the hourly, daily, monthly and annual levels.

Mean Absolute Errors for the NSRDB-PSM and GSID are shown in Figure 7. The GSID had almost half the observation error at the hourly and daily levels. Monthly and annual observation errors were similar for both datasets.

Overall Uncertainties at 95% Confidence for the NSRDB-PSM and GSID are shown in Figure 8. The NSRDB observations had twice the uncertainty of the GSID observations at the hourly and daily levels. Monthly and annual confidence intervals were similar for both datasets.

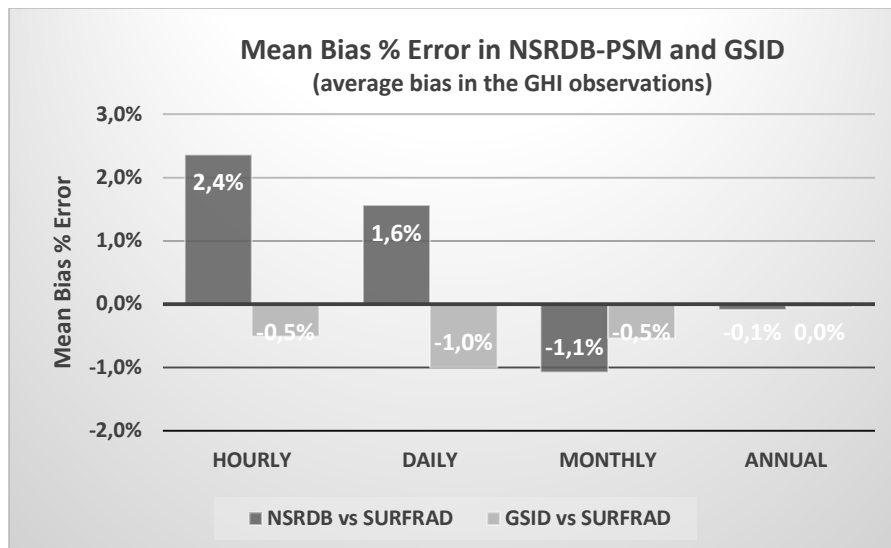


Fig. 6: Global irradiance: Mean bias errors (%) for the NSRDB-PSM and the GSID database

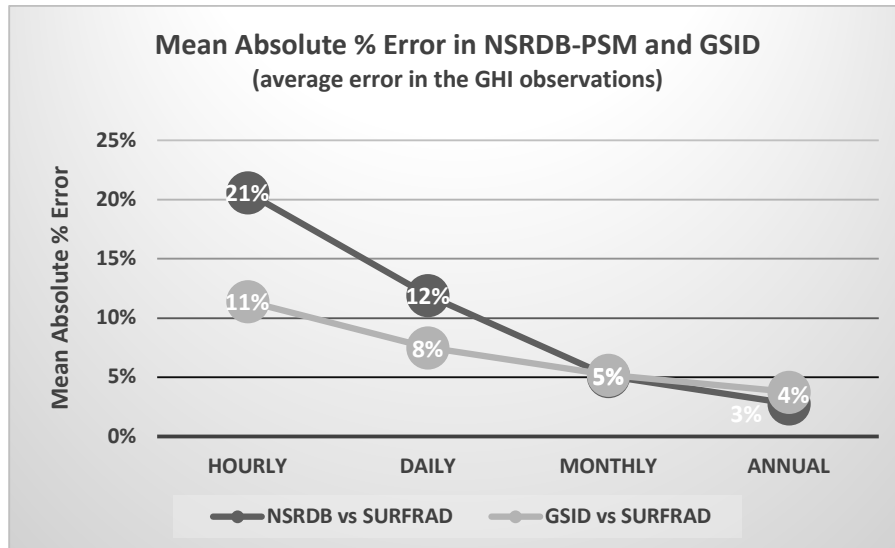


Fig. 7: Global irradiance: Mean absolute errors (%) for the NSRDB-PSM and the GSID database

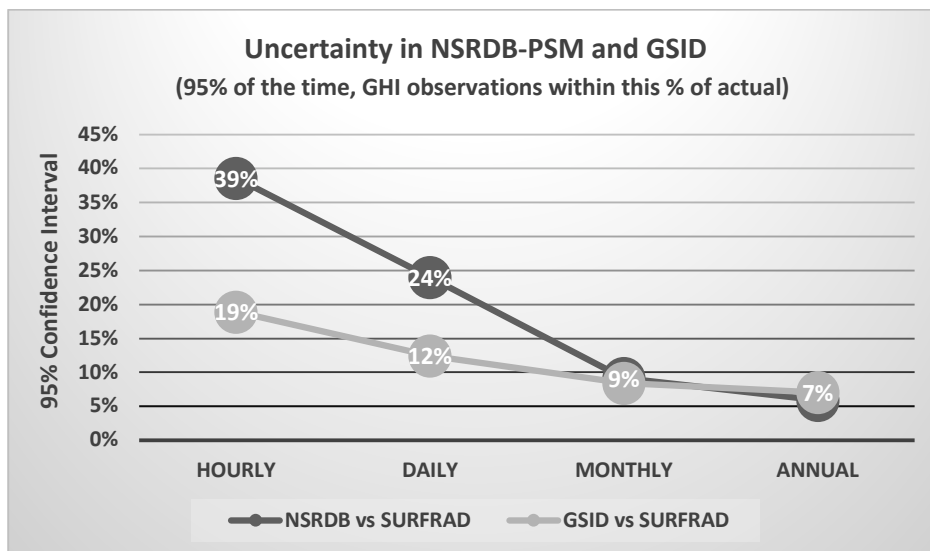


Fig. 8: Global irradiance: Overall uncertainty (%) at 95% confidence for the NSRDB-PSM and the GSID database

These statistics confirm that the GSID database has lower bias and is significantly more accurate than the NSRDB-PSM at the hourly and daily level. For applications requiring only monthly or annual resource data, either dataset would be acceptable.

One derivation of the daily GSID data, available without cost, is a gridded database (0.1-degree increments) of the continental US, Alaska and Hawaii for the years 2005-2018 (see www.SolarDataWarehouse.net). The full GSID database contains additional daily and hourly resource for measured global irradiance, estimates of beam irradiance, diffuse irradiance, and other meteorological measurements at over 7000 locations for the years 2005-present. The GSID also includes a suite of tools that can provide further data analysis, quality control, filtering, gridding, etc. that can be tailored to the specific needs of the end user.

6. Summary

A new solar resource with complete US coverage from 2005-present has been generated from ground-based observations: the GSID. The dataset has been quality controlled using AI technology and verified using the

same validation procedure as NREL’s National Solar Radiation Database. The validation statistics confirm that the GSID database has lower bias and is significantly more accurate than the NSRDB-PSM at the hourly and daily level. For monthly or annual resource data, the GSID and NSRDB-PSM are comparable. The GSID can be used stand-alone, or combined with other solar resource for a variety of projects including site selection, power output simulations and on-going monitoring of solar plants.

7. References

Anders Nottrott and Jan Kleissl (2010). Validation of the NSRDB-SUNY Global Horizontal Irradiance in California. Solar Energy Volume 84, Issue 10, October 2010, Pages 1816-1827

Anders Nottrott and Jan Kleissl (2014). Validation of the National Solar Radiation Database in California. <https://ww2.energy.ca.gov/2014publications/CEC-500-2014-017/CEC-500-2014-017.pdf>, accessed June 2020

Aron Habte, Manajit Sengupta, Anthony Lopez (2017). Evaluation of the National Solar Radiation Database (NSRDB Version 2): 1998–2015. <https://www.nrel.gov/docs/fy17osti/67722.pdf> accessed June 2020

Aron Habte, Manajit Sengupta, Anthony Lopez, Yu Xie and Galen Maclaurin (2018). Assessment of the National Solar Radiation Database (NSRDB 1998-2016). <https://www.nrel.gov/docs/fy18osti/71607.pdf> accessed June 2020

Sengupta, M.; Weekley, A.; Habte, A.; Lopez, A.; Molling, C.; Heidinger, A. (2015). Validation of the National Solar Radiation Database (NSRDB) (2005–2012). <https://www.nrel.gov/docs/fy15osti/64981.pdf> accessed June 2020

Appendix: Statistical Results

Table 1: Statistical Results at Varying Time Averages for the National Solar Radiation Database and the US Ground-Based Solar Irradiance Database (relative to USCRN ground reference sites)

		observations	NSRDB vs SURFRAD			GSID vs SURFRAD		
			MB%E	MA%E	RMS%E	MB%E	MA%E	RMS%E
Bondville	Hourly	52,112	4.1	20.3	37.9	0.4	6.9	11.0
	Daily	5,076	4.7	12.7	27.3	0.2	6.3	10.2
	Monthly	168	0.3	4.1	6.5	1.6	4.9	7.9
	Annually	14	1.0	2.0	2.2	2.1	3.9	5.9
Desert Rock	Hourly	56,715	-1.5	11.1	24.9	-0.4	4.4	6.7
	Daily	5,060	-1.9	4.9	9.4	-0.4	3.3	4.9
	Monthly	168	-2.3	2.5	3.1	-0.3	3.1	4.5
	Annually	14	-1.9	1.9	2.0	-0.3	2.7	4.0
Boulder	Hourly	54,641	-1.6	22.9	39.9	1.6	31.6	48.9
	Daily	5,079	-4.0	10.9	18.6	-1.0	16.0	25.0
	Monthly	168	-5.0	5.4	7.4	-0.2	6.8	8.6
	Annually	14	-3.8	3.8	4.3	0.7	4.4	4.9
Ft Peck	Hourly	53,254	-3.2	22.6	39.1	-0.2	5.8	8.2
	Daily	5,088	-5.4	14.6	25.0	-0.4	4.9	6.9
	Monthly	168	-6.4	8.8	14.7	0.8	3.7	4.5
	Annually	14	-3.0	3.6	4.5	2.3	2.9	3.2
Goodwin	Hourly	52,785	6.9	19.0	38.7	-4.0	14.9	24.7

	Daily	5,025	7.2	10.6	25.9	-3.5	11.0	13.9
	Monthly	168	3.2	3.9	5.6	-3.3	9.3	10.9
	Annually	14	3.2	3.2	3.5	-3.8	6.9	8.6
Penn St	Hourly	51,313	9.2	26.4	45.9	-1.8	9.4	18.1
	Daily	5,071	8.7	15.3	30.5	-2.9	7.3	11.1
	Monthly	168	4.4	5.1	6.5	-3.6	5.7	7.3
	Annually	14	3.6	3.6	4.0	-2.4	3.6	5.7
Sioux Falls	Hourly	52,909	2.7	21.8	41.3	0.9	6.7	10.3
	Daily	5,080	1.7	14.4	27.6	1.0	3.8	7.8
	Monthly	168	-1.8	5.9	9.5	1.2	2.9	3.8
	Annually	14	0.3	1.4	1.7	0.9	2.1	2.5
Averages	Hourly		2.4	20.6	38.2	-0.5	11.4	18.2
	Daily		1.6	11.9	23.5	-1.0	7.5	11.4
	Monthly		-1.1	5.1	7.6	-0.5	5.2	6.8
	Annually		-0.1	2.8	3.2	0.0	3.8	5.0

Occupational Risks Associated with Solar Installations: A Review

Jesse C. Duroha¹, Jeffrey R. S. Brownson², and Gretchen A. Macht¹

¹ Mechanical, Industrial & Systems Engineering, University of Rhode Island, Kingston, RI 02881
USA

² Energy Engineering, Pennsylvania State University, University Park, PA 16802 USA

Abstract

It is crucial to continuously review and assess the occupational risks associated with rooftop and ground-mount photovoltaic (PV) installations in the United States (U.S.) Solar industry. The Engineering, Procurement, and Construction sector of the U.S. Solar industry is growing rapidly and the current literature that investigates the occupational risks PV installers are exposed to is limited. This paper explores the musculoskeletal disorder (MSD), falls from elevated working surfaces, electrical, and heat stress risks installers face during PV installations. The environmental factors and working conditions that increase the severity of these risks are identified. Practical solutions are then presented regarding the engineering, administrative controls, and Personal Protective Equipment (PPE) required to mitigate these risks. Where published literature is lacking, the effects of these risks in comparable occupations with similar tasks to PV installers is explored in order to propose solutions. This research can aid occupational safety and health professionals to develop safety protocols that can reduce occupational hazards and ensure worker safety during PV installations.

Keywords: occupational risks, photovoltaic, installations, safety, ergonomics

1. Introduction

There is a core need to review and assess the occupational risks associated with rooftop and ground-mount photovoltaic (PV) installations within the Engineering, Procurement, and Construction (EPC) sector of the United States (U.S.) Solar industry. PV installers are exposed to (i) musculoskeletal disorder (MSD) risks from repetitive work at awkward postures (Hanson & Thatcher, 2020), (ii) falls from elevated working surfaces, (iii) electrical risks and hazards (e.g., electric shock, burns, electrocution and arc flash hazards), and (iv) heat stress from working for prolonged periods in hot temperatures (Hanson & Thatcher, 2020; Solar Energy Industries Association [SEIA], 2006). Injuries resulting from these risks can lead to a loss of income, a decrease in productivity, an increase in workers' compensation premiums for employers, discomfort, pain, and death (Fatality Assessment and Control Evaluation Program [FACE], 2020; National Institute for Occupational Safety and Health [NIOSH], 2013; SEIA, 2006).

The EPC sector of the U.S. solar supply chain is growing rapidly. In the past decade, the volume of PVs installed has grown at an average rate of 48% annually (SEIA, 2020) and the installation workforce has increased by 269% (The Solar Foundation, 2020, p. 23). A key component in sustaining the growth and continuous improvement of the solar EPC sector is understanding and mitigating occupational injuries. However, there is a lack of literature that addresses the effects of occupational risks and injuries directly on PV installers. Solar safety manuals and investigations tend to focus on falls from elevated working surfaces and electrical risks but do not extensively address musculoskeletal disorders (MSD) or the heat stress risks installers face (FACE, 2020; SEIA, 2006). Moreover, available solar worker accident reports indicate that insufficient Personal Protective Equipment (PPE), administrative and engineering controls are significant causes of PV related occupational injuries and fatalities (FACE, 2020). Consequently, this paper aims to review the occupational risks associated with rooftop and ground-mount PV installations and provide practical solutions (i.e., safety engineering, administrative controls, and PPE) to mitigate them. Where published literature lacks research

directly related to PV installation, practical solutions are proposed based on similar occupations with comparable tasks. This research can serve as a foundation to guide future investigations into the occupational injuries associated with PV installations. Furthermore, it can help occupational safety and health professionals develop safety protocols that reduce occupational hazards and increase productivity on-site while also providing an overall safe environment for PV installers.

2. Musculoskeletal Disorder (MSD) Risks

Musculoskeletal disorders (MSDs) are injuries that damage the musculoskeletal system (i.e., muscles, nerves, tendons, joints, ligaments). They are caused by performing tasks that involve repetitive motion, force, vibration, and awkward postures (Albers & Estill, 2007). The 2018 survey of occupational injuries and illnesses reported that work-related musculoskeletal injuries account for 30.3% of days-away-from-work cases in the U.S. private industry (U.S. Bureau of Labor Statistics, 2019, p. 20). During both rooftop and ground-mount PV installations, installers are exposed to MSD risks associated with performing repetitive manual handling tasks and the frequent use of vibrating hand and power tools. Hanson and Thatcher (2020) point out that solar panels can be challenging to handle due to their size and weight. Manual handling tasks that are typically involved in PV installations include, but are not limited to, lifting, lowering, pushing, pulling, and carrying panels and their constituent parts from one location to another within the installation area (Solar Energy Solutions Group, 2008). These tasks can increase the risk of sprains, strains, and soft tissue injuries (NIOSH, 2013). These injuries are normally involved with manual handling tasks in the residential construction domain, whose manual handling tasks are similar to solar installers. Thus, common soft tissue injuries that are likely associated with these types of manual handling tasks for solar installation work include, but are not limited to, shoulder injuries (e.g., rotator cuff bursitis, tendinitis, and tears), and back injuries (e.g., hip-low back strain, bulging or herniated discs, pinched nerves, L5-S1 damage) (NIOSH, 2013). Moreover, PV installers are also exposed to the risk of contracting Hand-Arm Vibration syndrome (HAVS) (Vergara et al., 2008; Weir & Lander, 2005) from the frequent use of vibrating hand and power tools such as drills and saws (U.S. Bureau of Labor Statistics, 2020). These MSD risks can be exacerbated by working in extreme weather conditions (e.g., heat, wind, rain) or on various angled working surfaces (i.e., flat, sloped, or elevated) (Hanson & Thatcher, 2020, p. 180).

The MSD risks associated with PV installations can be mitigated by conducting site-specific ergonomics programs and utilizing lifting tools and equipment to eliminate unnecessary lifting. Choi (2008), conducted a study to identify the work-related MSD and effective safety practices for construction workers. They emphasize the importance of employers creating and implementing a site-specific ergonomics program that identifies and educates workers about the lifting and manual handling hazards present in unique sites. Another strategy for reducing ergonomic stress during lifting is to store materials on the work-site strategically. Ergonomics manuals typically recommend storing materials close to their use location, between knee and chest height, for ease of lifting (NIOSH, 2013). Employers can also place restrictions on the maximum load an individual can handle based on various ergonomic safety factors. These factors include the workers' strength, fitness, medical health, lift duration, postures assumed during the lift, and the availability of lifting equipment (Choi et al., 2016; Health and Safety Executive, 2016). Workers should also be encouraged to take short breaks as needed during manual handling to rest their muscles and joints (NIOSH 2013) and regularly stretch and exercise (Ludewig and Borstad, 2003). Simple tools and equipment, such as dollies and carts, can be used to safely transport materials short distances (NIOSH 2013; Solar Energy Industries Association, 2006). Reduced vibration tools and anti-vibration gloves can be used to mitigate the risk of contracting HAVS (Albers & Estill, 2007). Powered and mechanical lifting equipment such as cranes, and fork trucks can be used to transport heavy materials for longer distances (NIOSH 2013). Hoists can be used to lift solar panels up to elevated working surfaces, manually lifting panels up to these surfaces can increase the risk of MSDs and also result in increased risks of workers falling from elevated working surfaces (SEIA, 2006).

3. Falls from Elevations

Falls from elevated surfaces are the most significant contributing occupational hazard to fatalities in the construction industry (Dong et al., 2019; U.S. Department of Labor, 1990). In 2018, 33.5% of occupational fatalities in the construction industry involved fall related accidents (Occupational Safety and Health Administration, 2018). PV installations performed on elevated working surfaces expose installers to the risk of falling from dangerous heights. Based on the most frequent fall accident locations and occurrences in the construction industry over time, falls from elevations are likely more prevalent among rooftop PV installers with the majority of falls occurring at elevations of 30 ft or less; from ladders, roofs, scaffolds, and floors with openings (Dong et al., 2019; Huang & Hinze 2003). Roofers, in particular, have the highest rates of fatal fall occurrences in the construction industry (Dong et al., 2019; Huang & Hinze 2003). Fall risks increase in extreme weather conditions (e.g., heat, wind, rain). In addition, working with electrical components can cause electrical shocks or trip hazards, which can increase fall risks (Romich & McGuire, 2015; Solar Energy Industries Association, 2006). Rooftop PV installations, in particular, have increased fall risks due to limited walking space, which can cause workers to walk closer to the edge of rooftop hatches and skylights (U.S. Department of Labor, n.d).

Fall occurrences can be reduced by training workers to recognize and safely respond to fall hazards. It is also crucial to provide workers with adequate fall safety devices to protect them during fall incidents. Huang and Hinze (2003) hypothesize that falls are more frequent from elevations of 30 ft or less because workers tend to “misjudge hazardous situations” and “lack or wear insufficient protective work clothing and equipment” at these elevations (p. 268). The Occupational Safety and Health Administration (OSHA) mandates that workers exposed to fall hazards at elevations of 6ft or more must be protected by either a guardrail system, safety nets, or personal fall arrest systems (U.S. Department of Labor, n.d). Workers should, additionally, be trained on how to adequately secure and use ladders as well as keeping the work site free from obstacles that may cause trip hazards (Solar Energy Industries Association, 2006). Although construction workers receive this training, 75% of fatal falls occur from roofs, ladders and scaffolding (Dong et al., 2019), more investigations are required to find the root cause of this phenomena. Regular safety inspections and audits should be performed by management personnel to ensure that the proper fall protection systems and practices are being utilized on-site (FACE, 2011). Prevention through design techniques can also be employed in building designs to prevent fall risks during future PV installations. Prevention through design is a technique whereby potential hazards are identified and mitigated in the design phase of a construction project (Dewlaney & Hallowell, 2012; Dong et al., 2019; Rajendran & Gambatese, 2013). For instance, installing parapets on roofs that comply with OSHA height requirements (Dewlaney & Hallowell, 2012; Rajendran & Gambatese, 2013) can serve as guardrails and reduce fall risks during PV installations. Even with all these protocols in place, there is a relationship between electrical components that can cause electrical shocks or trip hazards and falls.

4. Electrical risks and hazards

Tasks performed near electrical components and wiring expose workers to electrical risks and hazards, such as shock and electrocution. Electrocution is the third leading cause of fatalities in the U.S. construction industry accounting for 8.5% of construction fatalities in 2018 (Occupational Safety and Health Administration, 2018). Multitudes of electrical components are involved in installing PV systems, including but not limited to, combiners, inverters, transformers, and the PV modules themselves (SEIA, 2006; White & Doherty, 2017). Moreover, the PV modules themselves are always considered “live” due to their ability to create electricity when activated by sunlight, thus creating an environment where traditional regulations, such as Lockout/Tagout (LOTO), are no longer the primary safety solution. These modules and system components can expose installers to electrical shocks, burns, electrocution, and arc flash, especially when handled poorly insulated tools, and equipment (FACE, 2009; SEIA, 2006). Additionally, extreme weather conditions can exacerbate shock and burn risks. For instance, when manually handling PV modules, rainy conditions can increase shock risks (Romich & McGuire, 2015), while hot and windy conditions can increase the risk of burns (White & Doherty, 2017).

Safety measures to mitigate electrical risks and hazards include worker training and the implementation of good LOTO practices (United States Department of Labor, n.d.). Installers should be trained in identifying shock hazards and should use equipment and tools with proper insulation (SEIA, 2006). Site-specific emergency response plans should also be developed and communicated with local fire and rescue responders to aid preparations in case of emergencies. However, with constant PV activation in sunlight, other procedures for modules in combination with LOTO have been observed differently throughout time. Initially, other procedures considered covering the panels during installation (creating complexity and another element of which to be vigilant), or installing PVs during cloudy conditions (where diffuse light still activates the electricity generation process rendering the point moot) or even installing the systems at night (creating another set of safety issues entirely). These practices no longer occur because more modern installations and modules attempt to mitigate these risks by designing easy, quick-connect wire connections for safety and speed. Ultimately, when unsure about the “live” state of PV components and wiring, installers should assume they are electrically energized and proceed with caution (Romich & McGuire, 2015). When working with electrical components, the proper protective clothing includes rubber insulated gloves and leather protectors (White & Doherty, 2017), fire-rated clothing, arc flash protection, protective eyewear, and safety footwear (Romich & McGuire, 2015). Although these PPEs will mitigate installer risks with respect to electrical hazards, they can cause significant heat stress.

5. Heat Stress

Heat stress is caused by working in extreme heat conditions and can result in heat related illnesses such as heat cramps, exhaustion, and strokes (Acharya et al., 2018; Bonauto et al., 2007). In the U.S. over 600 people are killed from extreme heat annually (Center for Disease Control and Prevention, 2019), with workers in the construction industry historically being 13 times more likely to die from heat related illnesses (HRIs) than other industries (Gubernot et al., 2015). PV installers are exposed to HRIs from working in hot temperatures for prolonged periods. Solar panels are typically installed in geographic locations that have a high sun and heat exposure (Hanson & Thatcher, 2020), due to energy density and higher financial rates of return on investment, thus increasing the risk of HRIs. Further, the strenuous activities and PPE (e.g., safety helmets, reflective vests, and safety boots) involved in PV installations can make working in hot temperatures mentally and physically challenging (Acharya et al., 2018; Rowlinson et al., 2014; SEIA, 2006). Signs of HRI's include, but are not limited to, high body temperature, profuse sweating, confusion, slurred speech, and dizziness (Center for Disease Control and Prevention, 2018).

In order to reduce the risk of HRI's, installers need fluids and frequent rest in a shaded and cool area (California Department of Industrial Relations, 2015; Hanson & Thatcher, 2020). Work-rest cycles are essential to reducing the effects of heat stress on workers. Work rest schedules can be created for PV installation work using a heat stress index to measure heat effects. The most commonly used heat stress index is the Wet Bulb Globe Temperature (WBGT), which incorporates the air temperature, humidity, radiant heat, and wind speed to quantify heat stress levels (Acharya et al., 2018; Rowlinson and Jia, 2014; Rowlinson et al., 2014). To reduce the effects of heat stress, the workload on-site can start small and gradually increase to allow installers to acclimatize to their environment (Occupational Safety and Health Administration [OSHA], n.d.). It is also vital for employers to continuously monitor workers for signs of HRIs as they work in hot temperature conditions (Hanson & Thatcher, 2020; California Department of Industrial Relations, 2015; OSHA, n.d.). Workers can be monitored using physiological signs such as pulse rate, temperature, body weight, blood pressure, respiratory rate, and alertness; their workload adjusted based on these factors (OSHA, n.d.).

6. Conclusion

This paper explores the occupational risks associated with rooftop and ground-mount PV installations. By assessing these occupational risks, this paper aims to contribute to the continuous improvement of worker health and safety in the solar industry. These occupational risks can be mitigated significantly by solar EPC companies through continuously training installers to identify hazardous situations, developing and promulgating safety protocols that are easily accessible, and providing appropriate PPE to PV installers. When developing safety protocols, it is important to consider how specific occupational risks can exacerbate others. Safety protocols need to be comprehensive and account for the relationship between specific risks. For instance, strenuous lifting in hot conditions while wearing protective clothing can increase the risk of heat stress and, therefore, work-rest schedules should be augmented to address these conditions. Electrical shocks and burns on elevated surfaces can lead to falls from elevations and installers should, therefore, use both fall protection and the necessary electrical protective clothing in these situations. There is a lack of available investigation reports quantifying the rates at which these risks directly affect PV installers. Future work includes conducting questionnaires and worker interviews to assess the risks seen within the community in total, rates of occurrence of each of these risks amongst PV installers, and to understand from the installers perspective the factors that increase the severity and likelihood of these risks.

7. Acknowledgments

Thank you to the University of Rhode Island's Sustainable Innovative Solutions (SIS) Lab for their unwavering support.

8. References

- Acharya, P., Boggess, B., & Zhang, K. (2018). Assessing Heat Stress and Health among Construction Workers in a Changing Climate: A Review. *International Journal of Environmental Research and Public Health*, 15(2), 247. <https://doi.org/10.3390/ijerph15020247>
- Albers, J.T. & Estill, C.F. (2007). *Simple solutions: Ergonomics for construction workers* (NIOSH Publication No. 2007-122).
- Bonauto, D., Anderson, R., Rauser, E., & Burke, B. (2007). Occupational heat illness in Washington State, 1995–2005. *American Journal of Industrial Medicine*, 50(12), 940–950. <https://doi.org/10.1002/ajim.20517>
- California Department of Industrial Relations (2015, May 14) *Heat Illness Prevention Regulation Amendments*. <https://www.dir.ca.gov/dosh/documents/Heat-Illness-Prevention-Regulation-Amendments.pdf> (Accessed: 15 July 2020)
- Center for Disease Control and Prevention (2018, June 6). *Heat Stress- Heat Related Illness*. <https://www.cdc.gov/niosh/topics/heatstress/heatrelillness.html> (Accessed: 15 July 2020)
- Center for Disease Control and Prevention (2019, July 8). *Extreme Heat*. <https://www.cdc.gov/disasters/extremeheat/index.html> (Accessed: 15 July 2020)
- Choi, S. D. (2008). Investigation of Ergonomic Issues in the Wisconsin Construction Industry. *Journal of SH&E Research*.
- Choi, S. D., Yuan, L., & Borchardt, J. G. (2016). Musculoskeletal Disorders in Construction: Practical Solutions from the Literature. *American Society of Safety Engineers. Construction_Fatalities.pdf*
- Dewlaney, K. S., & Hallowell, M. (2012). Prevention through design and construction safety management strategies for high performance sustainable building construction. *Construction Management and Economics*, 30(2), 165–177. <https://doi.org/10.1080/01446193.2011.654232>

- Dong, X. S., Jackson, R., Varda, D., Betit, E., & Bunting, J. (2019). Trends of Fall Injuries and Prevention in the Construction Industry. *CPWR*.
- Fatality Assessment and Control Evaluation Program (2009, January 27). *Laborer dies when he falls 35 Feet from a scaffold after being electrocuted*. California Department of Public Health. <https://www.cdc.gov/niosh/face/pdfs/08CA006.pdf> (Accessed: 15 July 2020)
- Fatality Assessment and Control Evaluation Program (2011, April 27). *Solar panel installer dies when he falls off a roof*. California Department of Public Health. <https://www.cdph.ca.gov/Programs/CCDCPHP/DEODC/OHB/FACE/Pages/10CA003.aspx> (Accessed: 15 July 2020)
- Fatality Assessment and Control Evaluation Program (2020, January 22). *Preventing worker deaths in the solar industry*. California Department of Public Health. <https://www.cdph.ca.gov/Programs/CCDCPHP/DEODC/OHB/FACE/Pages/Solar.aspx> (Accessed: 15 July 2020)
- Gubernot, D. M., Anderson, G. B., & Hunting, K. L. (2015). Characterizing occupational heat-related mortality in the United States, 2000–2010: An analysis using the census of fatal occupational injuries database. *American Journal of Industrial Medicine*, 58(2), 203–211. <https://doi.org/10.1002/ajim.22381>
- Hanson, M., & Thatcher, A. (2020). Identifying Human Factors and Ergonomic Issues in Green Jobs: Facilitating Sustainable Green Jobs. In A. Thatcher, K. J. Zink & K. Fischer (Eds.), *Human Factors for Sustainability: Theoretical Perspectives and Global Applications* (pp. 171-192). CRC Press Taylor and Francis Group.
- Health and Safety Executive (2016). Musculoskeletal disorders: Manual handling. <https://www.hse.gov.uk/pubns/books/l23.htm> (Accessed: 15 July 2020)
- Huang, X., & Hinze, J. (2003). Analysis of Construction Worker Fall Accidents. *Journal of Construction Engineering and Management*, 129(3), 262–271. doi: 10.1061/(asce)0733-9364(2003)129:3(262)
- Ludewig, P.M. & Borstad, J.D. (2003). Effects of a home exercise program on shoulder pain and functional status in construction workers. *Occupational and Environmental Medicine*, 60(11), 841-849.
- National Institute for Occupational Safety and Health. (2013). Simple solutions for home building workers. <https://www.cdc.gov/niosh/docs/2013-111/default.html> (Accessed: 15 July 2020)
- Occupational Safety and Health Administration. (n.d.) *Using the Heat Index: A guide for Employers*. https://www.osha.gov/SLTC/heatillness/heat_index/pdfs/all_in_one.pdf (Accessed: 15 July 2020)
- Occupational Safety and Health Administration. (2018). Commonly Used Statistics. <https://www.osha.gov/data/commonstats> (Accessed: 15 July 2020)
- Rajendran, S., & Gambatese, J. (2013). Risk and Financial Impacts of Prevention through Design Solutions. *Practice Periodical on Structural Design and Construction*, 18(1), 67–72. [https://doi.org/10.1061/\(asce\)sc.1943-5576.0000129](https://doi.org/10.1061/(asce)sc.1943-5576.0000129)
- Romich, E., & McGuire, K. (2015). On-Farm Solar Electric System Safety. <https://ohioline.osu.edu/factsheet/CDFS-4105> (Accessed: 15 July 2020)
- Rowlinson, S., & Jia, Y. A. (2014). Application of the Predicted Heat Strain Model in Development of Localized, Threshold-based Heat Stress Management Guidelines for the Construction Industry. *The Annals of Occupational Hygiene*, 58(3), 326–339. <https://doi.org/10.1093/annhyg/met070>
- Rowlinson, S., YunyanJia, A., Li, B., & ChuanjingJu, C. (2014). Management of climatic heat stress risk in construction: A review of practices, methodologies, and future research. *Accident Analysis & Prevention*, 66, 187–198. <https://doi.org/10.1016/j.aap.2013.08.011>

- Solar Energy Solutions Group. (2008). Solar Power System Installation Manual. <https://www.solarelectricsupply.com/media/custom/upload/sharp-all-installation.pdf> (Accessed: 15 July 2020)
- Solar Energy Industries Association. (2006) *Solar Construction Safety*. https://www.coshnetwork.org/sites/default/files/OSEIA_Solar_Safety_12-06.pdf (Accessed: 15 July 2020)
- Solar Energy Industries Association. (2020) *Solar Industry Research Data*. <https://www.seia.org/solar-industry-research-data> (Accessed: 15 July 2020)
- The Solar Foundation. (2020) *National Solar Jobs Census*. <https://www.thesolarfoundation.org/national/> (Accessed: 15 July 2020)
- U.S. Bureau of Labor Statistics (2019, November 7). *2018 Survey of Occupational Injuries and Illnesses*. <https://www.bls.gov/iif/soii-charts-2018.pdf> (Accessed: 15 July 2020)
- U.S Bureau of Labor Statistics. (2020, April 10). *Solar Photovoltaic Installers - What Solar Photovoltaic Installers Do*. <https://www.bls.gov/ooh/construction-and-extraction/solar-photovoltaic-installers.htm#tab-2> (Accessed: 15 July 2020)
- U.S. Department of Labor (1990, November) *Analysis of Construction Fatalities-The OSHA Database 1985-1989*. <https://apps.dtic.mil/dtic/tr/fulltext/u2/a400187.pdf> (Accessed: 15 July 2020)
- U.S. Department of Labor. (n.d.). *Green Job Hazards: Solar Energy - Falls*. OSHA. https://www.osha.gov/dep/greenjobs/solar_falls.html. (Accessed: 15 July 2020)
- Vergara, M., Sancho, J.-L., Rodríguez, P., & Pérez-González, A. (2008). Hand-transmitted vibration in power tools: Accomplishment of standards and users' perception. *International Journal of Industrial Ergonomics*, 38(9–10), 652–660. doi: 10.1016/j.ergon.2007.10.014
- Weir E., & Lander, L. (2005). Hand-arm vibration syndrome. *CMAJ*. 172(8), 1001–1002. doi: <https://doi.org/10.1503/cmaj.045314>
- White, J. R., & Mike Doherty (2017). Hazards in the Installation and Maintenance of Solar Panels. *IEEE*. 10.1109/ESW.2017.7914834

Carbon Footprint in the Design Studio, a Paradigm Shift

Abby Brandvold¹, Khaled Mansy², John Phillips², Tom Spector², and Jerry Stivers²

¹ Walter P. Moore, Dallas (USA)

² Oklahoma State University, Stillwater (USA)
khaled.mansy@okstate.edu

Abstract

This paper reports on investigative academic work of the authors employing evidence-based design tools to teach students how to optimize their design for the combined impact of operational and embodied energy. An approach that recognizes the fact that at day zero of building operation, it has already contributed to energy consumption and carbon generation. Being aware of the optimization problem and their responsibility for training the new generation of designers, the authors integrate energy performance as a primary design goal in teaching a Comprehensive Design Studio that is required for senior students in Architecture and Architectural Engineering. The paper discusses life cycle carbon analysis, in association with other tools, as a means to evaluate design alternatives based on overall contribution to carbon footprint due to both operational and embodied energy. Minimizing operational energy, however, may be at odds with minimizing embodied energy. For example, a high window-to-wall ratio can be ameliorated by exterior aluminum shading devices, but these shading devices may actually have high embodied carbon. Therefore, energy performance and life-cycle carbon reductions must be treated as an optimization problem. To make this point clear, a case study in a student's evaluation of envelope design alternatives is presented.

Keywords: Carbon footprint, operational energy, operational carbon, embodied energy, embodied carbon.

1. Introduction

In 2019, four of the authors co-taught the Comprehensive Design Studio at the OSU School of Architecture. The studio has a long tradition of success in addressing integrative design and collaboration with professional practice. Continuously, the studio enjoys dedicated support from Oklahoma's architects and engineers, as well as design firms and professional societies that sponsor student awards. In 2004, the studio was awarded the National Council of Architectural Registration Boards (NCARB) Grand Prize for Creative Integration of Practice and Education in the Academy. In 2020, for its plans to address global warming, the studio was awarded the Association of Collegiate Schools of Architecture (ACSA) Course Development Prize for Architecture, Climate Change, and Society. One of the primary educational goals of the studio is to introduce students to performance-based design. In 2019, the authors explored expanding the scope of the studio to address performance not only to include operational energy, but also to include embodied energy, in a way that students may evaluate their design iterations based on carbon footprint as the primary measure of performance. This holistic approach to performance evaluation should help students make well-informed design decisions and better understand the interrelationship between architecture and national and global environmental issues.

2. Performance in the design studio

Driven by the emphasis on performance-based design, performance is addressed in the Comprehensive Design Studio in a multi-faceted fashion, i.e., in terms of structural performance, energy performance, and cost performance. Being the capstone studio for the architectural engineering students and the required studio before last in the architecture program, it is taken by well-prepared senior students towards the end of the curriculum when they have already taken all prerequisite architectural science and structural courses.

2.1 Preparation in lecture courses

In the program's technology track, students entering professional school are introduced to the universal concept of sustainability and the three economic sectors that consume energy, i.e., the industrial, transportation, and building sectors (residential and commercial) as shown in Fig. 1a (EIA, 2018), with building operation consuming around 38% of the total primary energy resources. Follow-up architectural science courses primarily focus on the building's operational energy, with less emphasis on the impact of the industrial and transportation sectors. Students become aware of the profession's relative success in capping energy consumption at 2005 levels and its more challenging task to reach zero-energy by 2030 as shown in Fig. 1b (Mazria, 2019). In the required structural courses, students are introduced to engineering science and design of timber, steel, and concrete structures, with less emphasis on the embodied carbon in structural materials due to manufacturing processes, transportation, and on-site construction. In the required professional practice courses, students learn the principles of project management and cost estimating. Indeed, there is a limited opportunity to introduce the concept of holistic performance in rather fragmented lecture courses. It is arguably a much better opportunity to do so within the design studio context where students can address all building systems (structural, mechanical, electrical, and the building service systems) and cost estimating in the same design project.

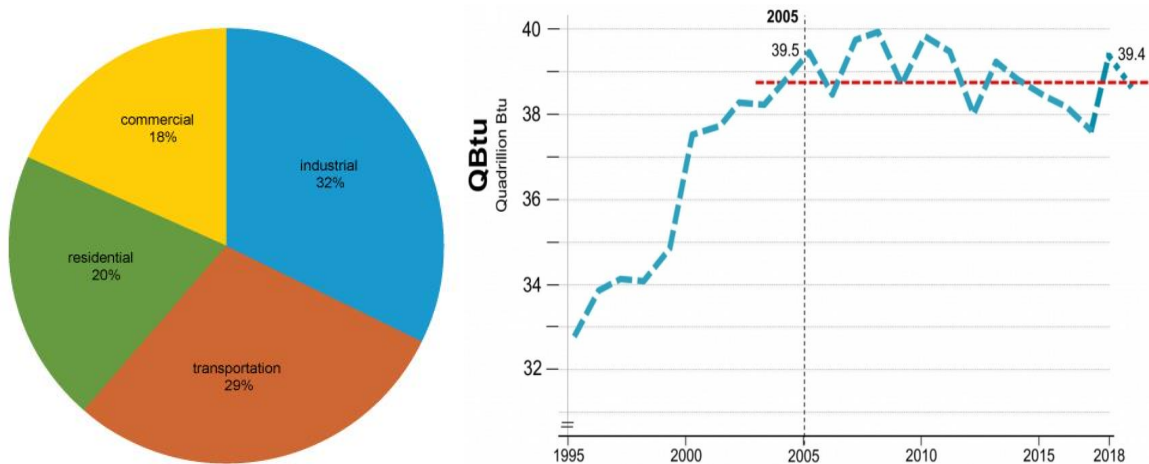


Fig. 1: (a) Shares of total US energy consumption by end-use sectors in 2017, and (b) US building sector operational energy consumption

2.2 Performance in the design studio

Understandably, most design studios in undergraduate architecture programs are limited in scope to just schematic design (SD). Usually, only one or two studios in each program extend beyond schematic design to cover design development (DD) and construction documents (CD). Only in upper level design studios the students become prepared to address DD design problems and systems integration. Indeed, students usually have limited opportunity to improve their skills in terms of performance-based design (Mansy, 2017).

In the Comprehensive Design Studio, the faculty articulate the scope and learning objectives to maximize students' exposure to building efficiency, structural performance, energy performance, and cost performance. During the second semester of the fourth year of the architecture curriculum and fifth year of the architectural engineering curriculum, students enroll in a 12-credit hour block of three interconnected courses, i.e., 6-hour comprehensive design studio, 3-hour concurrent technology seminar, and 3-hour project management course. In studio, the 15-week semester is divided into five weeks of SD when students work in teams and ten weeks of DD and CD when each student works on his/her own DD of a significant space within the building, which we call DD focus space.

For structural performance, during SD each student team is responsible for developing two structural schemes for their project, then selecting the better performing system. During DD, each student is expected to develop structural details necessary for the building envelope and foundations. Architecture students use simple rules-of-thumb and architectural engineering students use computer programs.

For energy performance, during DD, in addition to proving the building's code compliance with the International Energy Conservation Code (IECC), each student is expected to make sound performance-based decisions to design efficient mechanical, lighting and daylighting systems in his/her DD focus space. Course requirements include the four following tasks.

- Code compliance with IECC, either based on the code prescriptive values or based on performance (minimum of 15% energy cost saving)
- Electric lighting design in the DD focus space: verify performance in terms of recommended illuminance in foot-candles (fc) and light load in Watt/sf. Students may use hand calculations, online calculators, or an illumination design software.
- Daylighting design in the DD focus space: verify performance based on average illuminance and distribution when testing physical models under the artificial sky dome, or in terms of spatial daylight autonomy (sDA) and annual solar exposure (ASE) when using a daylighting simulation software.
- Cooling load: verify performance in terms of the building's energy use intensity (EUI), and peak cooling load in the DD focus space. Students may only use verified energy simulation programs.

For cost performance, at the end of DD, each student is expected to estimate the total construction cost of his/her building using RSMMeans. While typically there is no predetermined construction budget, this requirement greatly helps students to better understand the cost implications of their design decisions.

2.3 How to evaluate overall performance?

It can be claimed that the Comprehensive Design Studio addresses performance in a comprehensive fashion since it helps students to understand the performance implications of their design decisions regarding building design, structural design, energy design, and quantities of specified materials. The key observation, however, is that students' experience remains dissected into three different performance measures with no reasonable way to combine them into an overall quantitative measure. Due to the same disconnect between individual measures, another source of concern is the tendency of students to design buildings with a high to very high window-to-wall ratio (WWR). An overwhelming majority of students end up with a much higher WWR than what is allowed by IECC, which also results in higher EUI than what is permitted in order to comply with code. To bring the building into code compliance, a popular solution is specifying a better-than-code glass that is also more expensive and/or adding external shading devices that come with an added cost and embodied carbon. The apparent dilemma here is: is it a good idea to reduce operational energy at the expense of a higher embodied energy?

3. Life cycle analysis

In order to establish one measure of performance that combines all three performance measures in a meaningful way, carbon footprint seems to be a reasonable candidate. Life cycle analysis of the building can combine all factors affecting structural, energy, and cost performance. It is also capable of combining both operational and embodied energy, to calculate operational and embodied carbon, and estimate the building's global warming potential. Global warming potential per square foot of the building can be considered the primary measure of its environmental performance. The apparent dilemma here is that in professional practice design decisions are, understandably, made to optimize the cost as dictated by the client. Future research may investigate how cost may align with global warming potential. The next section (section 4), reports on the investigative case study performed in order to find the pros and cons of establishing global warming potential as the primary measure of performance in the design studio, and to explore the possibility of using life cycle analysis as a design-assisting tool during DD and not only at the very end of the design process.

4. Case study

In an independent study that is tied to the design development phase of her project, we helped one of our architectural engineering students (Abby Brandvold) conduct a comparative analysis of the performance of three alternative designs of the envelope of a significant space in her project (the DD focus space). The objective of this study was to investigate the possibility of conducting more comprehensive analysis than what is so far regularly required in studio, precisely, to assess performance of design iterations based on the overall impact of both operational and embodied carbon, a new approach in which the design's carbon footprint is considered the primary

measure of its environmental performance. Instead of only meeting the regular studio requirement of developing a baseline and one code-compliant envelope design, she developed a baseline and two code-compliant design iterations (Fig. 2) and estimated the overall carbon footprint of each of the two alternative designs. Below is a detailed description of the steps of the case study.

4.1 Step one: establishing the baseline and alternative envelope designs

Since the objective is to evaluate the impact of proposed design improvements compared to a reasonable baseline, the student developed energy models for the minimum code-complying design and two design iterations intended to reduce the cooling load in the focus space. For the purpose of this case study, this energy model is for a south-facing 20ft-high lobby for a museum in Oklahoma City (climate zone 3A). As for occupancy loads, all input data comply with relevant requirements in IECC-2018 and ASHRAE Standard 62.1-2016, as well as data available in ASHRAE Handbook of Fundamentals (ASHRAE, 2017). Below is the description of the three energy models.

- Standard reference design building

As defined in IECC-2018, this energy model (model #1 in Fig. 2) is a version of the proposed design (of the envelope design in the student's DD focus space) that meets the minimum requirements of the code, which is used to determine the maximum annual energy use requirement for compliance based on total energy performance (IECC-2018). Input data comply with all relevant prescriptive values required by IECC for a metal-framed building. Glass ratio is 40%, assuming compliance with requirements for increased vertical fenestration area with daylight responsive control. Thermal properties of all envelope components (fenestration, exterior wall, roof, and slab-on-grade) comply with tables C402.1.4 and C402.4 in IECC. Refer to Table 1 for a detailed list of input data.

- Proposed envelope design without external shading

This design iteration proposes a 90% window-to-wall ratio (WWR) of the envelope in the same focus space (model #2 in Fig. 2). The glass used is a high-performance glass having the thermal properties listed in Table 1. Using such glass is intended to reduce solar heat gain in order to reduce cooling loads. The lower-than code U-factor should help reduce both heating and cooling loads. However, because of the larger area of glass (compared to the standard reference design building), this design results in an increase of total length of the aluminum frame and mullions.

- Proposed envelope design with external shading

This design iteration proposes adding a horizontal external shading device (louvers) in front of the 90% glass in order to further reduce solar heat gain and, in turn, further reduce cooling loads (model # 3 in Fig. 2). Like the first design iteration, the lower-than code U-factor should help reduce both heating and cooling loads. Glass thermal properties are listed in Table 1. Adding the aluminum louvers does not only increase the quantity of aluminum used, but also requires additional structural support for the louvers.

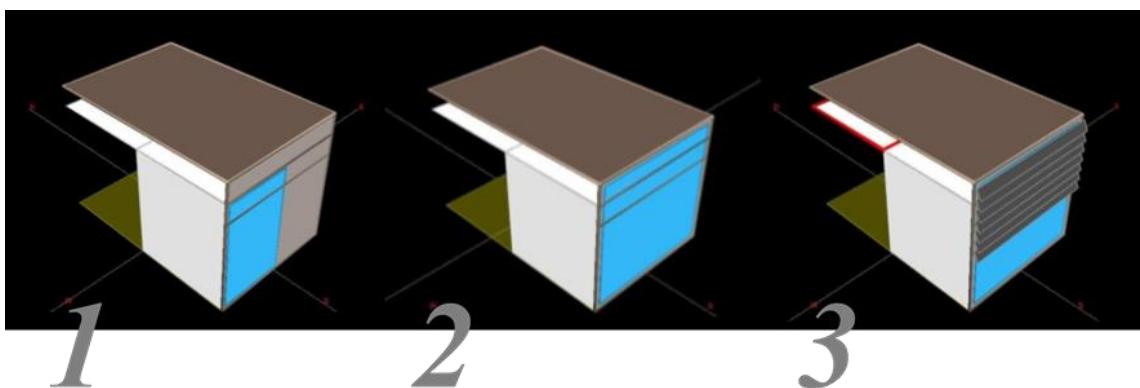


Fig. 2: Energy models of the standard reference design and two design iterations

4.2 Step two: energy performance (operational energy)

Energy modeling was performed using eQuest, which is an energy simulation program that is validated by the US Department of Energy (DOE, 2020). eQuest performs accurate hourly load calculations and produces both of the energy use intensity (EUI) and the peak load in every thermal zone. Based on the results of energy simulation, the

EUI of the standard reference design building (baseline for comparison) was 133.7 kBtu/sf.yr. The 90% WWR envelope design with high-performance glass resulted in EUI of 111.6 kBtu/sf.yr., achieving 16.5% energy savings compared to the baseline, while the partly-shaded 90% WWR envelope resulted in a lower EUI of 108.6kBtu/sf.yr., achieving 18.8% energy savings compared to the baseline (refer to Table 1). In conclusion, since both alternative design improvements result in energy cost savings greater than 15%, they both comply with the IECC based on performance (IECC-2018). In conclusion, based on EUI only, adding external shading results in higher environmental performance.

Although not related to code compliance, an interesting result that is worth-mentioning here is that while the two proposed design iterations resulted in considerable energy savings, only the partly-shaded envelope design reduced the peak cooling load in the perimeter thermal zone, which resulted in further cost savings due to downsizing of mechanical equipment.

Tab. 1: Input data and results of energy simulation, cost estimating, and carbon life cycle analysis

	Standard reference design	Design iteration without external shading	Design iteration with external shading
IECC climate zone	3A	3A	3A
Space use	Lobby	Lobby	Lobby
Exposure	South-facing	South-facing	South-facing
Floor-to-floor height	20 ft	20 ft	20 ft
Window-to-wall ratio	40%	90%	90%
Wall U-factor (Btuh/ft ² .°F)	0.064	0.064	0.064
Roof U-factor (Btuh/ft ² .°F)	0.039	0.0314	0.0314
Slab on-grade U-factor (Btuh/ft ² .°F)	0.73	0.4545	0.4545
Glass properties			
- U-factor (Btuh/ft ² .°F)	0.46	0.26	0.25
- Shading coefficient	0.29	0.14	0.195
- Visible Transmittance	0.275	0.06	0.21
External shading	None	None	Aluminum louvers
Occupancy loads			
- Lighting power (W/sf)	1.0	1.0	1.0
- Ventilation, CFM per person	5.0	5.0	5.0
- Ventilation, CFM per SF	0.06	0.06	0.06
- Set point temp in cooling (°F)	75	75	75
- Set point temp in heating (°F)	72	72	72
- Density (sf/person)	100	100	100
- People sensible load (Btuh/person)	250	250	250
- People latent load (Btuh/person)	200	200	200
Results of Energy Simulation			
- EUI (kBtu/sf.yr)	133.7	111.6	108.6
- Peak cooling load (CFM/sf)	1.25	1.52	1.24
Cost comparison			
- Cost estimate (\$/sf)	baseline	+165.67	+239.67
- Return on investment	NA	baseline	-3.57%
Global warming potential (kgCO ₂ eq/sf)	NA	24.98	156.30

4.3 Step three: cost performance

Cost analysis was performed by summing the cost of each individual component of each envelope design and determining the overall cost per square foot for that wall assembly. Cost data were collected from manufacturers and the most current RSMMeans. Cost of the 90% WWR design improvement adds \$164.67 per square foot, while cost of the partially shaded 90% WWR adds \$239.67 per square foot. After factoring in the energy savings due to the use of external shading (18.8% > 16.5%), using the current rates of natural gas and electricity from the OG&E (Oklahoma Gas & Electric Company), adding the external shading results in negative return on investment of 3.57%. In conclusion, based on financial analysis only, adding external shading is not economical over the useful life of the building.

4.4 Step four: embodied + operational carbon

Life cycle analysis was performed using Athena, the Impact Estimator for Buildings, which is developed by Athena Sustainable Materials Institute (Athena, 2019). The same input data used to perform cost analysis was used to calculate embodied carbon due to manufacturing and transportation of materials, on-site construction, operation, de-construction, demolition, disposal, and waste processing of the two design improvements. The global warming potential of the 90% WWR is 24.98 kgCO₂eq, while due to the added aluminum louvers and increased use of materials to attach them to the structure, it is 156.30 kgCO₂eq for the partially shaded 90% WWR. In conclusion, adding the aluminum external shading results in surprisingly high global warming potential, which should eliminate it as a possible design improvement.

4.5 Step five: case study conclusions

Apparently, the different measures of performance do not favor the same design iteration. While the aluminum external shading results in lower EUI and a smaller mechanical system, it is not cost effective (negative return on investment) when compared to the design without external shading. Furthermore, it results in a significant increase in global warming potential. In situations when different measures conflict, the design team may need to decide based on the client's highest priority. However, if carbon footprint is considered as the primary measure of environmental performance, then the decision is clearly to eliminate the aluminum external shading.

5. Conclusions

In conclusion, this investigative study sheds light on several issues that relate to performance-based design, climate change, architectural education, and professional practice. These issues can be explained as follows:

It is important to correct the practice of saving operational energy at the expense of embodied energy. It is counterproductive to design high performance buildings with high window-to-wall ratio. Increased glass ratio (than what is allowed by code) requires the use of more expensive glass that is also most likely of a higher embodied carbon (compared to other materials such as brick and gypsum board) and/or the use of external shading devices that also come with high embodied carbon.

Disagreement is possible between different measures of performance when considered in isolation. Conflicting feedbacks render a real challenge to students in making well-informed performance-based design decisions based on quantitative evaluation. In such situation, they will have to subjectively choose to follow the direction of one feedback and ignore the other(s). For example, design an envelope that yields higher energy savings although it is more expensive to build, or to design an envelope that is less expensive to build although it does not achieve the lowest energy consumption.

In light of the urgency of climate action and the quest to fight global warming, the carbon footprint, expressed as global warming potential per square foot, may be considered the primary measure of performance, which replaces the need for looking at different aspects of performance, e.g., structural, energy, and cost performance. The key advantage of using carbon footprint as the primary measure is that it takes into account structural materials, both of operational and embodied energy, and all specified materials to be used in construction. Furthermore, building performance expressed in global warming potential should provide students with more comprehensive understanding of the relationships to the other economic sectors, i.e., industrial and transportation (Fig. 1a).

In the sake of supporting pragmatic professional practice, future research is needed to test the correlation between design driven by climate action and the least cost design often desired by clients.

Using life cycle cost analysis as a design-assisting tool in studio faces several challenges. Such challenges are due to the lack of necessary information needed to quantify carbon during some of the cradle-to-grave stages, namely, building material production and transportation, on-site construction, and end of life (disposal, reuse, and recycle).

High performance buildings are the reason behind the profession's success in capping operational energy at 2005 levels. However, achieving zero operational energy by 2030 is impossible without reliance on renewable energy technology, which comes with its own high embodied carbon. In the future, a paradigm shift will happen when zero operational energy has been achieved and the environmental impact of buildings becomes solely due to embodied carbon. At that point, performance-based design will be all about the stages before and after the occupancy stage of buildings.

6. References

- ASHRAE, 2016. ANSI/ASHRAE Standard 62.1 Ventilation for Acceptable Indoor Air Quality, 2016.
- ASHRAE, 2017. ASHRAE Handbook of Fundamentals, 2017.
- Athena, 2019. Athena Sustainable Materials Institute, Athena Impact Estimator for Buildings, <http://www.athenasmi.org/>, accessed April 2019.
- DOE, 2020. US Department of Energy, Office of Energy Efficiency & Renewable Energy, Qualified Software for Calculating Commercial Building Tax Deductions, <https://www.energy.gov/eere/buildings/qualified-software-calculating-commercial-building-tax-deductions>, accessed March 2020.
- EIA, 2018. US Energy Information Administration, Monthly Energy Review, Table 2.1, preliminary data, 2018.
- IECC 2018. International Code Council, International Energy Conservation Code, 2018.
- Mansy, 2017. Energy Performance within Integrative Design, Barriers in Academia, ASES Solar 2017, Denver.
- Mazria, 2019. An Urgent Message from Ed Mazria, Architect (The Journal of the American Institute of Architects), June 18th, 2019.

Is Hydrogen Energy Storage Ready for Prime Time on the North American Grid? A Guide for Bankers and Their Engineers

Michael STAVY, MBA (Northwestern), CPA (inactive)¹

¹ Advisor on the Finances of Renewable Energy Projects, Chicago, IL (USA)

Abstract

A utility scale¹ energy storage plant can be used on the North American (NA) grid for the storage of solar (PV) electricity and/or to provide ancillary services. To help bankers and their engineers determine whether hydrogen (H₂) energy storage is ready for prime time², this paper presents a H₂ storage plant (HSP) levelized cost of storage (LCOS)³ financial algorithm for a model HSP. The LCOS algorithm is based on engineering economics and financial accounting principles. The algorithm only uses S. I. energy units for both the HSP's kinetic (electricity) energy and its potential energy (H₂). It converts US\$ values into € values. The paper discusses HSP technology focusing on the three phases of all HSP; charging the HSP by using a H₂ electrolyzer (HE) to produce H₂, storage of the PV electricity as H₂ in a "H₂ "Tank", and discharging the PV electricity from the HSP by using the stored H₂ as the fuel for a fuel cell (FC) to regenerate the PV electricity. The LCOS algorithm uses "project accounting" to compute a separate "LCOS" for each HSP phase. The LCOS algorithm is presented in the paper's Excel⁴ HSP LCOS Financial Algorithm Workbook. Based on the paper's LCOS algorithm and on the HSP specifications (specs, metrics) compiled for a base case "data set" for the model HSP, H₂ energy storage is not yet ready for commercial development on the North American grid. Low round trip HSP efficiency (η) and a high HSP CapEx do not allow a HSP to operate commercially on the North American grid.

Keywords: levelized cost of storage, LCOS, LCOE, hydrogen energy storage, North American grid, PV electricity, S.I. units, hydrogen electrolyzer, fuel cell, commercial energy storage, financial algorithm, engineering economics

1. The Levelized Cost of Storage (LCOS) Algorithm and its Excel Workbook

The goal of this paper is to determine if H₂ energy storage is ready for commercial development. To reach this goal, the author developed a HSP LCOS algorithm with a recognized uniform set of HSP specs that is based on generally accepted financial and engineering principles. Both "back of the envelope" simplicity and an accurate first approximation of the cost (US\$/MWh; €/MWh) of storing PV electric energy in a HSP are the two criteria for choosing a computational method. The paper's levelized cost (LC) algorithm meets both criteria.

The paper's HSP LCOS algorithm requires 22 HSP specifications (specs) [metrics]. The 22 HSP specs [independent variables] and the 76 dependent variables are all defined⁵ using the standard S.I. power (MW_{ELECT}) and energy (MWh_{ELECT}, MWh_{H2}) units.

The actual compilation⁶ of a public data base of the HSP specs for use by bankers (and their engineers) is not the primary goal of this paper (Electric Power Research Institute, Inc. (EPRI); Lazard; US DOE). The author has the much more modest goal of first presenting a recognized standard LC financial algorithm, second, using a base case for a model HSP to demonstrate to the reader how the LCOS algorithm works and third, using these base case specs and the LCOS algorithm to compare the PV electricity's LCOS with the grid's wholesale PV price for electricity.

While the paper discusses the 22 specs for a model HSP, there is also no case study to discuss how to compile⁶ the 22 HSP base case specs from the current authoritative data sources. Readers who want learn how to compile⁶ the 22 HSP specs for either their own base case (or to compile a public data base of HSP specs) should read the author's Cabin Creek Pumped Storage Plant spec compilation case study that is found in the author's Wind Europe 2018 paper (Task Committee..., Stavy, 2018).

¹ 100-2,500/MWh/day

² is currently ready for commercial development

³ not to be confused with the levelized cost of energy (LCOE) [Stavy, 2002]

⁴ a fully functioning Excel Workbook

⁵ required in these SOLAR 20/20 Conference Proceedings, but this is not the conventional practice in either the North American H₂ industrial gas industry or North American H₂ electrolyzer industry

⁶ assemble, organize, gather, create, publish

Putting the paper’s LCOS algorithm in an Excel Workbook allows the reader (author, banker, engineer) to quickly do sensitivity analysis. For the reader to follow this paper, the reader must download this paper’s Excel HSP LCOS Financial Algorithm Workbook from this paper’s Additional Material Section⁷ at SOLAR 20/20 Conference Proceedings Website: [Link]. This is because the paper refers to the worksheet (WS) lines on the four WS of the Excel HSP LCOS Financial Algorithm Workbook⁸.

A H₂ Electrolyzer (HE) is used in the HSP charging phase; a H₂ “Tank” in the HSP storage phase and a Fuel Cell (FC) in the HSP discharging phase. The Excel HSP LCOS Workbook has four WS: three WS are for the three HSP phases: WS # 1, Charging-H₂ Electrolyzer-HE; WS # 2, Storage-H₂ Storage “Tank”; WS # 3, Discharging-Fuel Cell-FC. WS # 4 is the Summary Page.

At the end of this paper is Fig. 1. A Schematic of a H₂ Storage Plant; Table 1. Acronym Meanings; Table 2. The 22 Specs of the HSP LCOS Algorithm and for those readers who cannot access this paper’s “Additional Material Section”, Table 3, WS # 4 Summary of the HSP Specs and the Key Computed Values.

The HSP LCOS Financial Algorithm uses “project accounting” to “fine tune” sensitivity studies. This also allows the Workbook user to do a sensitivity study of each phase separately. For each HSP phase (charging, storage and discharging), a separate “partial LCOS” is computed. By selecting different realistic values for the 22 specs of the model HSP, it has become clear to the author that there are two key dependent variables that determine whether a HSP is ready for commercial development; the HSP round trip efficiency (η) which is set too high in the base case to be realistic and the Total⁹ HSP CapEx which is set too low in the base case to be realistic. The reader can enter their own 22 HSP spec values in their Excel HSP LCOS Workbook and check their results.

In addition to the 22 HSP specs, the Excel HSP LCOS Workbook also requires a FX value. The base case uses US\$1.12987/€. (OANDA, 7 July 12, 2020) to convert the US\$ spec and dependent variable values into € values for readers in the € zone.

A HSP can be designed for the daily, weekly (seven days) or seasonal (180 days) storage cycle. The paper’s model HSP is basic. It is designed to have a daily energy storage cycle. The paper’s LCOS HSP financial algorithm only computes the LCOS (US\$/MWh; €/MWh) for the daily storage of solar electricity. Two of the 22 HSP specs (metrics) specify how many hours a day are used in the daily charging and discharging phases. The algorithm assigns the remaining hours of each day to the storage phase. The three phases of the model HSP do not operate at the same time. A HSP can be designed to have all three phases operate at the same time. A HSP can also be engineered to provide energy storage and/or ancillary grid services (voltage and frequency control and reactive power [var]) for the grid. This paper’s model HSP is not designed to provide ancillary services.

2. S. I. Energy Units and the H₂ Energy Units in the North American (NA) Industrial Gas and H₂ Electrolyzer (HE) Industries

The NA electric utility industry already measures production and prices electric power and electric energy in the S. I. units of the MW and the MWh. The NA industrial gas industry, however, measures the production and pricing of industrial H₂ in Kg_{H₂} (mass) or in Nm³_{H₂} (volume). The NA HE industry sizes and prices HE in MW_{ELECTin} of electric power into the HE and measures and prices the production of H₂ in Kg_{H₂} or in Nm³_{H₂}. These are the correct units for H₂ as an industrial gas but not for H₂ as an energy carrier in a HSP. Since MWh_{ELECTin} are charging the HSP and since MWh_{ELECTout} are discharged from the HSP, the paper’s HSP LCOS financial algorithm measures the production and price of the H₂ gas that is used to store the electricity in MWh_{H₂}. [H-TEC Systems; Universal Industrial Gases, Inc; US EIA). Even though the editors of these proceedings require S. I. units, the author considers the consistent¹⁰ use of the S. I. MW power unit and the MWh energy unit to be a major contribution to the “H₂ Economy” literature.

$$\text{MWh}_{\text{ELECT}} = \text{MWh}_{\text{H}_2}$$

3. The Three Phases of the HSP and the Algorithm’s LC Method Explained

⁷ Editor, I just checked some other journals that I am familiar with (i.e. the American Economics Review) and they allow additional material to be presented with the paper. I assume that the Solar 20/20 Proceedings also allow “additional material” to be downloaded by the reader from the Solar 20/20 Proceedings website

⁸ hereafter, referred to as the Excel HSP LCOS Workbook

⁹ Total CapEx refers to the sum of the CapEx of each of the three HSP phases (HE; H₂ “Tank”; FC)

¹⁰ without first converting to Kg_{H₂} (Nm³_{H₂}) for H₂ coming out of the HE and stored in the H₂ “Tank” and then converting the Kg_{H₂} (Nm³_{H₂}) back into MWh_{H₂} for the FC

This paper discusses H₂ storage technology focusing on the three phases of all HSP; one, the production of the H₂ with solar electricity, two, the storage of the H₂, three, the use of the stored H₂ as the fuel to regenerate the solar electricity. In a HSP, H₂ is used as the energy carrier. There is no carbon released (Stavy, 2005).

In the base case, the HE spec values, WS # 1, Lines 4, 6, 7, 8 & 9, have also been used as the H₂ “Tank” spec values, WS # 2, Lines 11, 12, 13, 14 & 15, and as the FC spec values WS # 3, Lines 18, 19, 20, 21 & 22¹¹. A specific example is WS # 1, Line 9, Cost of Capital, interest rate/ROE [WACC] is set at 6%, which is the author’s base case estimate. So are WS # 2, Line 15 and WS # 3, Line 22. Another example is, Line 8, HE Life-yrs, is set at 20, which is the author’s base case estimate for the typical “life” for power projects. So are WS # 2, Line 14 and WS # 3, Line 21. WS # 1, Line 1, HE hours/day operating and WS #3, FC hours/day operating are both eight hours. The algorithm assigns the remaining 8 hours/day to the H₂ “Tank”. This is done to have a straightforward base case. The paper’s Excel HSP LCOS Workbook allows the user to use different spec values for each HSP phase.

In the paper’s model HSP, solar electricity from the North America grid powers a HE. The HE uses the solar power to separate H₂O into H₂ and O₂. When the HE is producing H₂ with solar electricity, the HSP is charging. Currently no H₂ electrolyzer format is the most mature technology. The paper’s LCOS algorithm measures the “financial maturity” of HE with different technologies. The most important algorithm HE specs are WS # 1, Line A, HE Power Input (MW_{ELECTin}), WS # 1, Line 3, HE CapEx-US\$/MW_{ELECTin} (€/MW_{ELECTin}) and WS # 1, Line 4, HE efficiency (η).

The algorithm’s levelized cost method will now be explained using WS # 1, the HE phase.

WS #1 Line 9, Interest/ROE [WACC] is set at 6%. This is the cost (as a %) to invest the capital in the HE, WS # 1 Line D, Total HE CapEx. The HSP owner either provides the capital (equity) or borrows (debt) the capital to in order to own the HE phase. WS # 1 Line 8, HE Life-yrs is 20 years. During its physical life, as the HE phase operates the Total HE CapEx (WS # 1 Line D) must be recovered (depreciated) and the cost of capital (WS #1, Line 9) for using the invested capital must be paid. If borrowed money is used to construct the HE phase, the cost of borrowing the money is called the lender’s interest. If the HSP plant owner uses their own capital to construct the HSP, the cost of using the owner’s money is called the return on owner’s equity (ROE). The cost of capital (Line 9) is a weighted average percent for both the lender’s interest and for the owner’s ROE. Let us hypothesize that the HSP debt/owner’s equity ratio is 1:1; the interest on the debt is 4% and the required ROE is 8%; then the weighted average cost of capital (WACC), Interest/ROE Rate is 6%.

WS # 1, Line I is the capital amortization factor-CAF. It is computed to be 0.08720. This is the end of year annual payment computed for a financial annuity having US\$1.00 as the principal borrowed, a loan period of 20 years (WS # 1, Line 8) and an interest rate of 6% (WS #1, Line 9).

WS # 1, Line L is the annual capital amortization (ACA) in US\$/year. This computed to be US\$1,847,202/yr (€1,634,710/yr). Line L is the product of Line D multiplied by Line I.

The levelized cost (LC) method uses a financial annuity to compute Line L. The ACA-US\$/yr is one constant yearly payment for both the depreciation of Line B and for the payment of Interest/ROE (Line 9) over the physical life of the HE phase. This level (constant) capital amortization payment gives the method its name. The first year’s payment is almost all Interest/ROE, while the last year’s payment is almost all depreciation.

The algorithm’s LC method is the same in the H₂ “Tank” phase (WS # 2) and in the FC phase (WS #3).

In the paper’s model HSP, the solar electricity is stored as H₂ in a generic H₂ “Tank”. When the H₂ is in the storage H₂ “Tank”, the HSP is storing the solar electricity. There are various technologies for storing H₂. These include pressurized H₂ storage tanks, liquefied H₂ storage tanks, H₂ salt caverns (another type of H₂ storage tank), as ammonia (NH₃), with other H₂ rich chemicals or in metal hydrides. NH₃, metal hydrides, chemical storage, and H₂ in salt caverns are not yet mature enough technologies for a commercial HSP. High pressure and liquefied H₂ storage tanks are currently the most technically mature and most widely used technologies for industrial H₂ storage. The HSP LCOS algorithm measures the “financial maturity” of different H₂ “Tanks” (technologies). The most important algorithm H₂ Tank specs are WS # 2, Line I, H₂ “Tank” size (MWh_{H2}), WS # 2, Line 10, H₂ Tank CapEx-US\$/MWh_{H2} (€/MWh_{H2}), and WS # 2, Line 11, H₂ Tank efficiency (η).

In the paper’s model HSP, the H₂ is taken out of the H₂ Tank and is consumed as the fuel to power a FC that

¹¹ Table 2 on page 7 makes the relationships between the 22 HSP specs clear

regenerates the solar electricity which is then put back on the North American grid. When the FC is generating electricity with the stored H₂ as the fuel, the HSP is discharging the solar electricity from storage. There are various technologies for using the stored H₂ as the fuel to regenerate the solar energy as electricity. These include FC of various electro-chemistries and H₂ powered electric gas turbines in various formats (H₂ peaker turbine \approx NG peaker turbine; combined cycle H₂ turbine \approx combined cycle NG turbine (CCGT)). For a daily storage cycle, only a H₂ peaker turbine can be considered, but the H₂ peaker turbine is not yet a mature technology. This leaves FC of various technologies with different technical and financial maturities. The paper's HSP LCOS algorithm measures the "financial maturity" of different types of FC. The most important algorithm FC specs are WS # 3, Line XX, FC capacity (MW_{ELECTout}), WS # 3, Line 17, FC CapEx-US\$/MW_{ELECTout} (€/MW_{ELECTout}), and WS # 3, Line 18, FC efficiency (η).

4. Sensitivity Analysis

WS # 1, Line 5, Cost of the Solar Electricity to be Stored, US\$40.00/MWh (€35.40), is the cost of solar electricity generated a model PV plant. US\$40/MWh is the author's estimate of a model utility scale PV plant's LCOE (Stavy, 2002).

On WS # 3, Line LLL, the LCOS in the base case is US\$138.67/MWh (€120.99). This 246.7% increase from US\$40.00/MWh is too high for the market. Perhaps a carbon constrained North American grid would accept a time of day 20% increase to US\$48.00 (€42.48) for stored solar electricity but not much higher.

If the physical life of the HE (WS # 1, Line 8), H₂ "Tank" (WS # 2, Line 14) and FC (WS # 3, Line 21) are each set at 25 years instead of 20 years¹², the LCOS would be US\$130.19/MWh (€115.23). This is a 6.1% LCOS reduction from the base case of US\$138.67/MWh for a 25% increase in the physical life of the HSP. It is doubtful that a HSP would have a physical life of 25 years.

If the interest rate/ROE [WACC] of the HE (WS # 1, Line 9), H₂ "Tank" (WS # 2, Line 15) and FC (WS # 3, Line 22) are each set at 4% instead of 6%¹², then the LCOS would be US\$125.80/MWh (€111.34). This is a 9.3% LCOS reduction from the base case US\$138.67/MWh for a 33.3% decrease in the WACC. It is doubtful, however, that bankers or their engineers would risk funding a HSP at even 6% with the current state of HSP technical development.

Sensitivity analysis shows that currently the two key HSP specs in determining the HSP LCOS are the HSP Round Trip Efficiency (η) and the Total HSP Total CapEx.

On WS # 4, HSP Round Trip η -%, 72.9% is the product of 90% (WS # 1, Line 4, HE- η) X 90% (WS # 2, Line 11, H₂ "Tank"- η) X 90% (WS # 3, Line 18, FC- η). This is a very optimistic HSP Round Trip η because the HE, H₂ "Tank" and FC do not actually operate at $\eta = 90\%$. If the H₂ "Tank" were, in actuality, a high pressure H₂ storage tank or a liquefied H₂ storage tank, the storage phase η would be at most in the 70% range. If the phase η of the HE, H₂ "Tank" and FC are now each set at 80% instead of 90%¹² (an 11.1% reduction), the HSP Round Trip η would decline from 72.9% to 51.2% (a 29.8% decrease) while the LCOS would increase from the base case US\$138.67 to US\$179.78/MWh (€159.12), an 26.9% increase.

On WS # 4, Total⁹ HSP CapEx, US\$75,524,756 (€66,838,836) is the sum of US\$21,187,256/HE [WS # 1, Line D, HE CapEx] plus US\$27,000,000/H₂ "Tank" [WS # 2, Line BB, H₂ "Tank" CapEx] plus US\$27,337,500¹³/FC [WS # 3, Line AAA, Total FC CapEx].

The HE CapEx (WS # 1, Line D) is computed by multiplying the 38 MW_{ELECTin} of HE capacity (WS # 1, Line A) times the HE CapEx of US\$564,994/MW_{ELECTin} (WS # 1, Line 3). €500/kW_{ELECTin} (US\$573/kW) is the author's estimated cost of a modern commercial European MW scaled HE. The 38 MW_{ELECTin} (WS # 1, Line A) is computed by dividing the 300 MWh_{ELECTin} of solar electricity that charges the HSP each day (WS # 1, Line 2) with the 8 hrs. per day that the HE operates (WS # 1, Line 1).

The H₂ "Tank" CapEx (WS # 2, Line BB) is computed by multiplying the 270 MWh_{H2} H₂ "Tank" size (WS # 2, Line L) times the H₂ "Tank" CapEx of US\$100,000/MWh_{H2} (WS # 2, Line 10). US\$100,000/MWh is equal to US\$100/kWh which is the projected cost of a Tesla utility scale Li-ion battery. The H₂ "Tank" size is equal to the daily H₂ produced (WS # 1, Line B) by the HE. What is produced by the HE is stored in the H₂ "Tank".

The FC CapEx (WS # 3, Line AAA) is computed by multiplying the 27 MW_{ELECTout} of FC capacity (WS # 3, Line XX) times the FC CapEx of US\$1,000,000/MW_{ELECTout} (WS # 3, Line 17). The 27 MW_{ELECTout} (WS # 3, Line XX)

¹² and if all 19 of the other 22 specs remain the same

¹³ rounding errors appear in certain of the Workbook results

is computed by dividing the 219 MWh_{ELECTout} (WS # 3, Line YY) discharged by the HSP each day with the 8 hours per day that the FC operates (WS #3, Line 16). US\$1,000,000/MW_{ELECTout} is the author's estimate of the current cost of a utility scale FC.

If the CapEx of the HE (WS # 1, Line 3), H₂ "Tank" (WS #2, Line 10) and the FC (WS # 3, Line 17) are each reduced by 20%¹², the Total⁹ HSP CapEx would be \$60,419,813 (€53,575,013), a 20% reduction from the base case Total HSP CapEx of US\$75,524,756. The LCOS would be US\$122.07/MWh (€108.04), a 10.3% LCOS reduction from the base case of US\$138.67. This reduced Total HSP CapEx is caused by the 20% decrease in the CapEx of each HSP phase. The author estimates that the Total CapEx will have to go down by more than 60% for the model HSP to become commercially viable.

To get "hands on experience" in LCOS sensitivity analysis, the Workbook user should enter their own 22 HSP spec values on the paper's Excel HSP LCOS Workbook.

5. Conclusion

If you are a banker, or a banker's engineer, asking the author, is hydrogen energy storage ready for prime time on the North American grid?

Based on the research that the author did to assemble the following facts; the author's answer is **NO!**

1. There are no commercial HSP on the North American grid.
2. HSP specs for commercial North American HSP were not found in any current authoritative data source.
3. The author compiled the 22 base case specs for a model HSP. With the paper's LCOS financial algorithm, the author computed the LCOS but it was too high for the current development of a commercial North American HSP.
4. Sensitivity analysis showed that the HSP Round Trip η is not realistically presented by the author. He is too optimistic. His HSP Round Trip η is too high to be realistic. HSP Round Trip η should actually be about 60%; not the computed 72.9%.
5. Sensitivity analysis showed that the Total HSP CapEx is also not realistically presented by the author. He is again too optimistic. His HSP CapEx is too low to be realistic. Total HSP CapEx was too high for the LCOS to be less than 20% more than the cost of the solar electricity being stored but too low to reflect current HSP CapEx values.
6. Readers might want to compare the LCOS for current pumped storage plants as a benchmark for future HSP (Task Committee..., Stavy, 2018).

6. Acknowledgements

The author took (1960) the Physical Science Study Committee (PSSC) Course at Niles Township High School, Skokie, IL US where he learned how to do the S. I. Unit Analysis used in this paper. (MIT Institute Archives & Special Collections, 1956).

7. References

EPRI (Electric Power Research Institute, Inc) (2010), *Energy Storage Technology and Application Cost and Performance Data Base-2010*, Palo Alto, CA [Online] Available at; <https://tinyurl.com/ya6dsw15> (Accessed: 01 July 2020)

H-TEC Systems (undated), *Hydrogen Datacard-Tradeshaw Handout*, Lübeck Germany, Not Available at www.h-tec-systems.com (Accessed: 01 July 2020). The author has a copy of this Tradeshaw Datacard Handout

Lazard (2019), *Levelized Cost of Storage Analysis-Version 5.0*, New York City [online] Available at: <https://www.lazard.com/perspective/lcoe2019> (Accessed: 05 July 2020)

MIT Institute Archives & Special Collections; *Physical Science Study Committee, 1956* [Online] Available at <https://web.archive.org/web/20190513111535/https://libraries.mit.edu/archives/exhibits/pssc/> (Accessed; 10 July 2020)

OANDA Corporation, *Web Currency Converter*, [online] Available at: <http://www.oanda.com/> (Accessed: 07 July 2020)

Stavy, M. (2002), ‘A Financial Worksheet for Computing the Cost (¢/kWh) of Solar Electricity Generated at Grid Connected Photovoltaic (PV) Generating Plants’, *Journal of Solar Energy Engineering*, 124, p319-321.

Stavy M, (2005), ‘The Carbon Content of Hydrogen Vehicle Fuel Produced by Hydrogen Electrolysis’, *Journal of Solar Energy Engineering*, 127, p161-5

Stavy, M. (2018), ‘A Financial Algorithm for Computing the Levelized Cost (US\$/MWh; €/MWh) of the Bulk Storage of Wind Electricity (LCOS)’, *WindEurope 2018 Conference*, 25-28 Sept. Hamburg, Germany

Task Committee on Pumped Storage of the Hydropower Committee of the Energy Division of the ASCE (1993), ‘Cabin Creek Pumped Storage Plant’ in Roza, Jr, R (ed.) ‘*Compendium of Pumped Storage Plants in the United States*’, New York City, American Society of Civil Engineers, p199

US DOE (US Department of Energy), *Global Energy Storage Database*, Sandia National Laboratories [online] Available at: <https://www.sandia.gov/ess-ssl/global-energy-storage-database-home/> (Accessed: 05 May 2020)

US EIA (US Energy Information Agency), *Energy Units and Calculators Explained: Energy Conversion Calculators*, [online]

Available at: https://www.eia.gov/energyexplained/index.php?page=about_energy_conversion_calculator (Accessed: 05 May 2020)

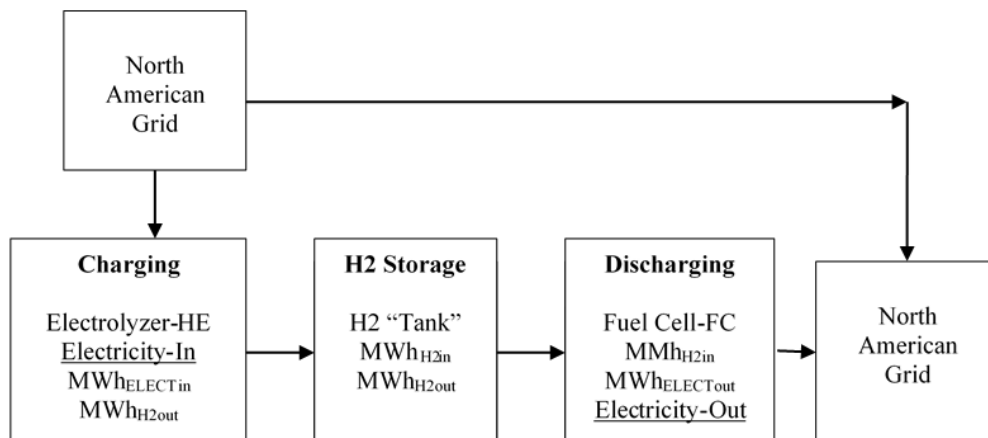


Fig. 1: Schematic of a H₂ Storage Plant (HSP)

Table 1: Acronym Meanings

Acronym	Meaning
CH ₃ =	ammonia
CCGT =	combined cycle gas turbine
η =	efficiency
EIA =	Energy Information Administration (USA)
FC =	fuel cell
FX =	foreign exchange
HE =	H ₂ electrolyzer
HS =	H ₂ storage
H ₂ =	hydrogen
HSP =	hydrogen storage plant
IEA =	International Energy Agency (OECD)
Kg _{H2} =	Kilogram-H ₂
LCOE =	levelized cost of energy
LCOS =	levelized cost of storage
MJ _{H2} =	megajoule-H ₂
lbs _{H2} =	pounds-H ₂
MW =	megawatt
MWh =	megawatt hour
mmBtu _{H2} =	million British thermal units-H ₂
NG =	natural gas
Nm ³ _{H2} =	nominal cubic meter-H ₂
O ₂ =	oxygen
PV =	photovoltaic
ROE =	return on owner's equity
scf _{H2} =	standard cubic foot-H ₂
SI =	Système International d'Unités
H ₂ O =	water
WACC =	weighted average cost of capital
WS =	worksheet

Table 2: The 22 Specs of the HSP LCOS Algorithm

spec #	<u>Charging</u> HE	spec #	<u>Storage</u> H ₂ "Tank"	spec #	<u>Discharging</u> Fuel Cell
1	HE hrs/Day Operating			16	FC hrs/Day Operating
2	Solar Energy to be Stored MWh/Day				
3	HE CapEx-US\$/MW _{ELECTin}	10	H ₂ "Tank" CapEx-US\$/MWh _{H2in}	17	FC CapEx-US\$/MW _{ELECTout}
4	HE Efficiency- η	11	H ₂ "Tank" Efficiency- η	18	FC Efficiency- η
5	Cost of the Solar Energy Stored-MWh _{ELECTin}				
6	Annual Fixed O & M-% HE Total HE CapEx-US\$	12	Annual Fixed O&M-% H ₂ "Tank" Total CapEx-US\$	19	Annual fixed O&M-% FC Total CapEx-US\$
7	HE Variable O&M-US\$/MWh _{H2out}	13	H ₂ "Tank" Variable O&M-US\$/MWh _{H2out}	20	FC Variable O&M-US\$/MWh _{ELECTout}
8	HE Life-yrs	14	H ₂ "Tank" Life-yrs	21	FC Life-yrs
9	HE Interest/ROE rate-%	15	H ₂ "Tank" Interest/ROE rate-%	22	FC Interest/ROE rate-%

¹ the Excel LCOS Workbook converts US\$ into € with the user selected FX rate

Table 3: WS # 4 Summary of the HSP Specs and the Key Computed Values

WS # 4

	US\$/€	d/m/y	Color Coding	
	US\$1.14610	13/01/19	From WS # 1	
			From WS # 2	
	WS # 1	WS # 2	From WS # 3	
	HE	H ₂ Tank	Result	
			Side Column Result	
quick key to HPS energy flow→	HE produces H ₂	H ₂ Tank stores H ₂	FC consumes H ₂	In €
Phase→	Charging	Storage	Discharging	HSP-η-%
HSP Phase-η-%	90%	90%	90%	72.9%
MWh _{ELECT} /day	300.00	←MWh _{ELECT} /day solar energy stored		
MWh _{H₂} /day	270.00	←MWh _{H₂} /day produced by HE		
MWh _{H₂} /day		270.00	←MWh _{H₂} /day stored	
MWh _{H₂} /day		243.00	←MWh _{H₂} /day released	
MWh _{H₂} /day			243.00	←MWh _{H₂} /day consumed by FC
MWh _{ELECT} /day			218.00	←MWh _{ELECT} /day solar energy regenerated
		proof ↓	72.9%	←HSP round trip η-%
MWh _{ELECT} /yr of solar energy stored→	109,500	72.9%	79,826	←MWh _{ELECT} /yr of solar energy put back on the grid

continued on next page

Table 3: WS # 4 Summary of the HSP Specs and the Key Computed Values

Phase →	WS # 1	WS # 2	WS # 3	Total hrs/day
	HE	H ₂ Tank	H ₂ FC	
Phase Operating hrs/day	Charging	Storage	Discharging	24
Only one phase operates at a time; HSP operates 24 hr/day; 365/yr				
US\$/MWh _{ELECT}	\$50.00			←US\$/MWh _{ELECT} cost (LCOE) of the solar energy to be stored
US\$/MWh _{H2}	\$63.55			←US\$/MWh _{H2} HE LC to produce H ₂
US\$/MWh _{H2}		\$63.55		←US\$/MWh _{H2} LC of H ₂ stored
US\$/MWh _{H2}		\$97.55		←US\$/MWh _{H2} LC of H ₂ released
US\$/MWh _{H2}			\$97.55	←US\$/MWh _{H2} LC H ₂ FC consumed
US\$/MWh _{ELECT}			\$138.67	← US\$/MWh _{ELECT} LCOS for solar energy
			246.7%	←% LCOS increased cost

continued on next page

Table 3: WS # 4 Summary of the HSP Specs and the Key Computed Values

WS # 4	WS # 1	WS # 2	WS # 3		
Phase →	HE	H ₂ Tank	H ₂ FC	€/MW _{ELECTIn}	€/MW _{ELECTOut}
	<u>Charging</u>	<u>Storage</u>	<u>Discharging</u>	↓	↓
	HE Power MW _{ELECTIn} ↓ 38	Tank Size MWh _{H2} ↓ 270	FC Power MW _{ELECTOut} ↓ 27	↓	↓
HE CapEx-US\$/MW _{ELECTIn}	\$64,994			€ 499,956	
Tank CapEx-US\$/MWh _{H2}		\$100,000			€ 87,252
FC CapEx-US\$/MW _{ELECTOut}			\$1,000,000		€ 872,524
CapEx -US\$/kW _{ELECTIn} ; US\$/kWh _{H2} ; US\$/kW _{ELECTOut}	\$565	\$100	\$1,000		
CapEx -€/kW _{ELECTIn} ; €/kWh _{H2} ; €/kW _{ELECTOut}	€ 500	€ 88	€ 885		
				Total ⁹ HSP CapEx ↓	
HSP CapEx-US\$/Phase	\$21,187,256	\$27,000,000	\$27,337,500	\$75,524,756	
HSP CapEx-€/Phase	€ 18,750,000	€ 23,894,080	€ 24,192,756	€ 66,836,836	
Fixed O&M Cost-% Phase CapEx	0.05%	0.05%	0.05%		
Variable O & M Cost-US\$/Phase MWh	\$0.25	\$0.25	\$0.25		
Phase Physical Life -Years	20	20	20		
Phase Interest/ROE Rate [WACC]-%	6.00%	6.00%	6.00%		

Development of A Spectral Integral Method for Analyzing Solar Effects through Windows on Indoor Thermal Comfort

Nan Wang, Yanxiao Feng and Julian Wang

Department of Architectural Engineering, Pennsylvania State University, State College (USA)

Corresponding Author: Julian Wang, julian.wang@psu.edu

Abstract

The interaction among the spectral characteristics of solar radiation, windows, and human skins may affect indoor thermal comfort. For analyzing such shortwave solar effects through windows on indoor thermal comfort, a more explicit method taking spectral features into account is indispensable. We built this new calculation methodology, called spectral integral method, upon a previous work that was mainly used to transfer the shortwave solar effect into the equivalent longwave effect to calculate indoor thermal comfort with the Predicted Mean Vote. Compared with the previous ones centered in the constant and simplified radiometric quantities, the uniqueness of this method is to provide the underlying radiometric calculation with the detailed and precise spectral contents and their variations of radiation sources, mediums, and receivers details. We adopted solar irradiance data from 8:00 to 18:00 with an interval of one hour in Denver, Colorado in a case study to verify the necessity of the spectral integral method relative to the constant method. The Predicted Mean Vote values with constant and spectral integral methods were then compared. The result of this work shows that using the spectral integral method could lead to quite different decisions of estimating indoor thermal comfort in some circumstances in terms of solar intensities and solar positions.

Keywords: Solar radiation, Spectral integral method, Indoor thermal comfort, Mean radiant temperature, Building windows

1. Introduction

Human thermal comfort has drawn increasing attention under the escalating demand for a high-quality and healthy living environment. The Predicted Mean Vote (PMV) model in ASHARE 55 standard (ASHARE, 2010) has been widely adopted to predict indoor thermal comfort by using six parameters, including indoor air temperature, mean radiant temperature (MRT), air speed, relative humidity, metabolic rate, and clothing level. On the other side, solar radiation, which is indispensable in daily life, possesses huge energy and is an essential factor in affecting thermal comfort. In particular, solar radiation may exhibit a heating effect on indoor occupants not only through longwave radiation emitted from the heated air, envelopes, and surrounding objects but also via shortwave radiation transmitted through windows to body surfaces, as stated in (Peter, 2000). When predicting thermal comfort, the quantitative contribution of longwave radiation could be represented by the parameter of MRT in the PMV model. However, the shortwave effect could not be simply and directly represented by any parameters in the PMV model. An equivalent conversion is needed to convert the thermal effect of shortwave radiation to the longwave radiation by eq. 1 (Edward, 2015). The quantitative contribution of the additional longwave radiation that is converted from the shortwave radiation is called mean radiant temperature delta (MRT delta). By adding the MRT delta to the previous longwave-based MRT, the thermal effect of the shortwave radiation could be involved in the PMV model.

$$\alpha_{LW}ERF_{solar} = \alpha_{SW}E_{solar} \quad (\text{eq. 1})$$

Where, E_{solar} is the shortwave solar radiant flux on human skin; α_{SW} is the shortwave absorptivity of human skin; ERF_{solar} is the transformed longwave radiant flux on human skin; α_{LW} is the longwave absorptivity of human skin.

Before converting the shortwave radiation to the equivalent longwave radiation, it is important to know the

amount of shortwave radiation that works on human thermal perception. There are multiple energy nodes in the energy transfer process from the solar to the human perception. Knowing the nodes is helpful to understand the parameters involved in such transfer processes. The first node is the amount of solar radiation that arrives at exterior building windows, which is determined by the irradiance emitted from the solar and the percentage of the emitted solar irradiance in the orientation of the windows. Afterward, it is the second node representing the amount of the shortwave radiation transmitted through the windows, which mainly depends on the spectral characteristics of the windows in use. Next, the third node is the amount of the incident shortwave radiation on occupant body surfaces, in which the position, posture, exposed skin surface areas, and the sky view factor of the occupant play important roles. The final node is the amount of the shortwave radiation absorbed by the occupant, being affected by the spectral absorptivity of the human skin.

In the context of the solar effects on indoor thermal comfort, the most representative work is done by Edward et al (2018). They have formed a program called SolaCal, which may quantify the effect by using eight parameters and derive two primary variables: ERF_{solar} and MRT delta. As such, the thermal comfort PMV indicators could be estimated. Those eight parameters include the posture of an occupant, solar altitude (β), solar horizontal angle relative to the front of a person (SHARP), direct beam (normal) solar irradiance (I_{dir}), total solar transmittance (T_{sol}), sky vault view fraction (fsvv), fraction of body exposed to the sun (fbes), average shortwave absorptivity (α). However, it is worth mentioning that among these parameters the total solar transmissivity and average shortwave absorptivity are the average optical properties based on the broadband, which ignores the spectral characteristics and the interactions of the radiation source (solar), medium (window), and the receiver (occupant). Notably, solar radiation has a spectral integral distribution, which means the photon carries different power at different wavelengths. Meanwhile, in the spectral range of solar radiation, building windows may have significantly different spectral features. For instance, as demonstrated in our previous studies (Julian, 2017), two spectrally selective glazing systems with very different spectral distributions may achieve very similar average transmittance under the standard solar light. Similarly, our body skins also have wavelength-dependent optical responses across different races and geographic regions. The superposition of the spectral features of solar radiation, window transmissivity, and human skin absorptivity can further complicate the resulting values. Figure 1 depicts the difference of superposition by wavelengths and by constant values, which uses constant spectra to represent constant values for comparing. Thus, in short, it is necessary to explore the influence of considering spectral characteristics of the parameters in predicting thermal comfort.

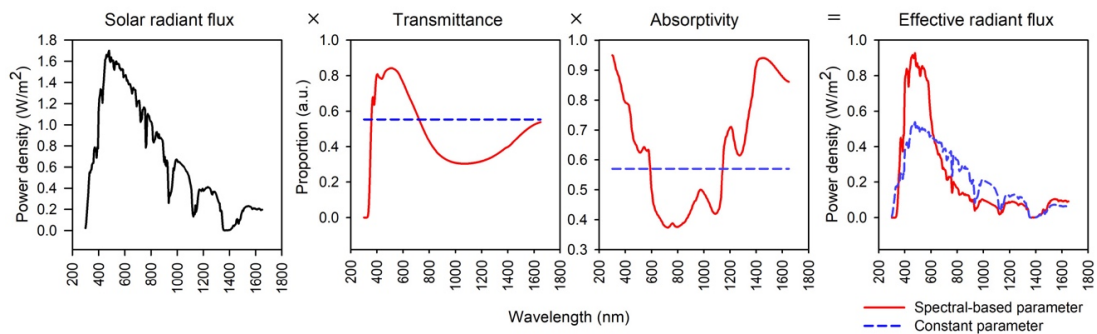


Fig. 1: Spectral difference of effective radiant flux between multiplying spectral integral and constant solar transmissivity of window and absorptivity of human skin

In this paper, we propose a spectral integral method to predict the solar effect on indoor thermal comfort, and we will also validate the necessity of the spectral integral method relative to the approach with corresponding constant values at different wavelengths (or called constant method in the following sections). The factors that influence the differences between the two methods are also explored. The unique contribution of this effort is to bring a more accurate analytical approach based on radiometry into the investigation of thermo-optical interactions among solar, glazing, and human.

2. Methods

2.1. Spectral integral method to predict human thermal comfort

The calculation for predicting human thermal comfort is by the PMV model. Among the six parameters in the PMV model, MRT could be related to the solar effect by adding the additional MRT delta term that converts the shortwave solar radiation to equivalent longwave radiation. The calculation to get the MRT delta value has been illustrated in the study mentioned above about SolarCal. Differently, for the two spectral integral parameters among eight predicting parameters in SolarCal, a spectral integral calculation in this work was proposed and then used instead of using provided or suggested constant values. We computed the spectral transmitted solar radiation that transmitted through the window by multiplying the spectral transmissivities of windows and the spectrum of the solar radiation by each wavelength and then summing the product at each wavelength together across all the wavelengths. The spectral integral solar transmissivity of the window (T_{sol_s}) would then be the spectral transmitted solar radiation that transmitted through the window over the incident solar radiation. In a parallel fashion, the final solar radiation absorbed by occupants was obtained through multiplying the above three factors: solar spectra, window's solar transmissivity, and human skin's spectral absorptivity by each wavelength, and then summing up the products. Then, the spectral integral absorptivity of human skin would be the final solar radiation absorbed by occupants over the total solar radiation incident on the human surfaces. Eq. 2 presents the calculation formula, and the propagation of solar radiation in the whole process is depicted in Fig. 2.

$$T_{sol_s} = \frac{\sum_{\lambda_1}^{\lambda_2} S \cdot T_{sol_spe} d\lambda}{\sum_{\lambda_1}^{\lambda_2} S d\lambda}$$

$$\alpha_s = \frac{\sum_{\lambda_1}^{\lambda_2} S \cdot T_{sol_spe} \cdot \alpha_{spe} d\lambda}{\sum_{\lambda_1}^{\lambda_2} S \cdot T_{sol_spe} d\lambda} \quad (\text{eq. 2})$$

where, S is the spectral power distribution of solar radiation; T_{sol_spe} is the spectral solar transmissivity of the window in use; α_{spe} is skin spectral absorptivity for the target occupant; λ_1 is the minimum wavelength in the calculation; λ_2 is the maximum wavelength.

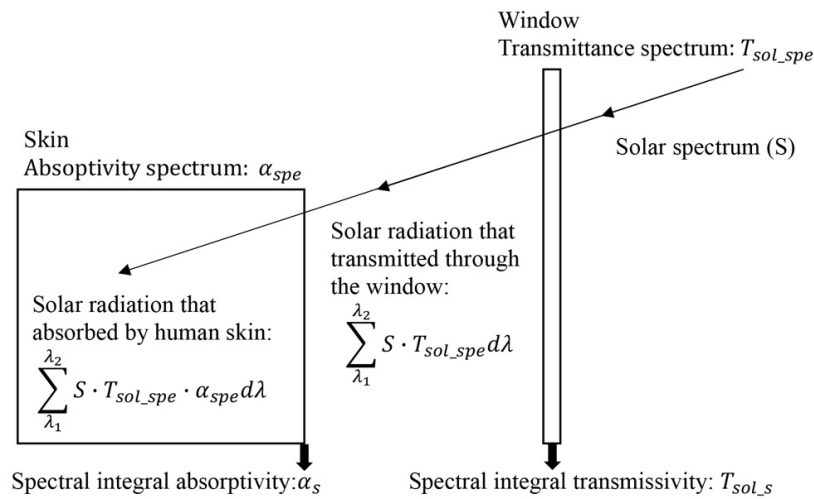


Fig. 2: The propagation of solar radiation into the human skin

2.2 Verification method

To verify the significance of using the proposed spectral integral method in the estimation of thermal comfort, different solar spectra were explored in this work. The variation of solar spectra at different times of day were taken into account. Thus, solar irradiance data at different times of day from 08:00 to 18:00 with an interval of one hour on June 1st in Denver, Colorado, was used. Next, we calculated the MRT delta and PMV values at different times of day by using the constant method and the spectral integral method, respectively. As a consequence, the results under the constant and spectral integral methods were compared.

Except for the spectral-related parameters, other parameters related to boundary conditions and situational contexts were maintained constant in all the calculations. The assumed values of the parameters unrelated to

spectrum variation are listed in Tabs. 1 and 2. Specifically, the parameters in Tab. 1 were adopted to calculate MRT delta, and those in Tab. 2 were set for accomplishing the calculation of PMV.

Tab. 1: The assumed values for not spectral-related parameters in calculating MRT delta

Posture	SHARP (°)	f_{svv}	f_{bes}
Seated	0	0.2	0.3

Tab. 2: The assumed values for not spectral-related parameters in calculating PMV

Air temperature (°C)	MRT (°C)	Air speed (m/s)	Relative humidity (%)	Metabolic rate (met)	Clothing level (clo)
25	25	0.1	50	1	0.6

3. Results

3.1. Mean radiant temperature delta

The direct beam (normal) solar irradiance (I_{dir}) and solar altitude angle (β) primarily shape the solar spectra at different times of day. A single-pane window with transmittance (T_{sol_c}) of 0.554 was selected in this case study. The color of the human skin in the calculation was assumed white, which has a suggested absorptivity (α_c) of 0.570. The spectral transmissivity (T_{sol_s}) and absorptivity (α_s) were calculated by eq. 2. The constant ($MRT\Delta_c$) and spectral integral ($MRT\Delta_s$) MRT delta values were calculated by the above parameters and assumed parameters in Tab. 1. Hence, Tab. 3 summarizes the results of the calculation and also shows the differences between the constant and spectral integral MRT delta values ($MRT\Delta_{diff}$).

Tab. 3: Constant and spectral integral mean radiant temperature values

Time	I_{dir} (W/m ²)	β	T_{sol_c}	T_{sol_s}	α_c	α_s	$MRT\Delta_c$	$MRT\Delta_s$	$MRT\Delta_{diff}$
08:00	468	14.4	0.554	0.5786	0.570	0.5746	3.8	4.0	0.2
09:00	669	25.6		0.5792		0.5777	5.6	5.9	0.3
10:00	622	37.1		0.5820		0.5798	5.5	5.8	0.3
11:00	914	48.5		0.5798		0.5787	8.3	8.8	0.5
12:00	922	59.4		0.5798		0.5774	8.3	8.8	0.5
13:00	115	68.5		0.5900		0.5731	1.0	1.1	0.1
14:00	448	72.4		0.5819		0.5757	4.0	4.2	0.2
15:00	745	68.0		0.5816		0.5785	6.6	7.1	0.5
16:00	399	58.7		0.5838		0.5783	3.6	3.8	0.2
17:00	435	47.7		0.5831		0.5760	4.0	4.2	0.2
18:00	116	36.3	0.6069	0.5934	1.0	1.2	0.2		

Note: $MRT\Delta_{diff} = MRT\Delta_s - MRT\Delta_c$

We could see from Tab. 3 that the differences between the constant and spectral integral transmissivities have a magnitude of 0.01. The differences between the constant and spectral integral absorptivities have a magnitude of 0.001. The differences are minor, while the aggregated variances between the constant and spectral integral MRT deltas could be ranging from 0.1 to 0.5, which may have significant influences on thermal comfort.

The $MRT\Delta_{diff}$ values are different across the time of day. To understand the factors that influence the

$MRT\Delta_{diff}$, we used linear regression to find out significant predictors for $MRT\Delta_{diff}$. The I_{dir} and $\sin(\beta)$ from Tab. 3, which we assumed to be the factors, were used to perform the regression. The parameters of I_{dir} (p value = 4.58×10^{-5}) and $\sin(\beta)$ (p value = 0.047) are all significant to predict the $MRT\Delta_{diff}$. The R-squared value 0.89 of the linear regression is also acceptable. Thus, we could conclude that the $MRT\Delta_{diff}$ is mainly dependent on the intensity of the solar irradiance and the altitude angle of the solar.

3.2 Predicted Mean Vote

The PMV values were calculated by processing the MRT delta values and assumed parameters in Tab. 2. MRT delta values were added up to the initial MRT values to get new MRT values. We then used the new MRT values to derive the PMV values in both constant and spectral integral methods. The calculation results are shown in Tab. 4.

Tab. 4: Constant and spectral integral Predicted Mean Vote

PMV	8:00	9:00	10:00	11:00	12:00	13:00	14:00	15:00	16:00	17:00	18:00
PMV_c	0.46	0.77	0.75	1.23	1.23	-0.01	0.49	0.94	0.43	0.49	-0.01
PMV_s	0.49	0.82	0.8	1.32	1.32	0	0.53	1.03	0.46	0.53	0.02
PMV_{diff}	0.03	0.05	0.05	0.09	0.09	0.01	0.04	0.09	0.03	0.04	0.03

Note: $PMV_{diff} = PMV_s - PMV_c$

The differences between constant and spectral integral PMV values ranged from 0.01 to 0.09. The results are also plotted within two zones in Fig. 3. The zone in gray is the thermal comfort zone with the PMV values between -0.5 and 0.5, while in red is the region represents that occupants may feel uncomfortably warm. Furthermore, when it comes to the accurate comparison of the comfort levels, the region that the PMV values locate in becomes more important than the differences of the PMV values under the constant and spectral integral methods.

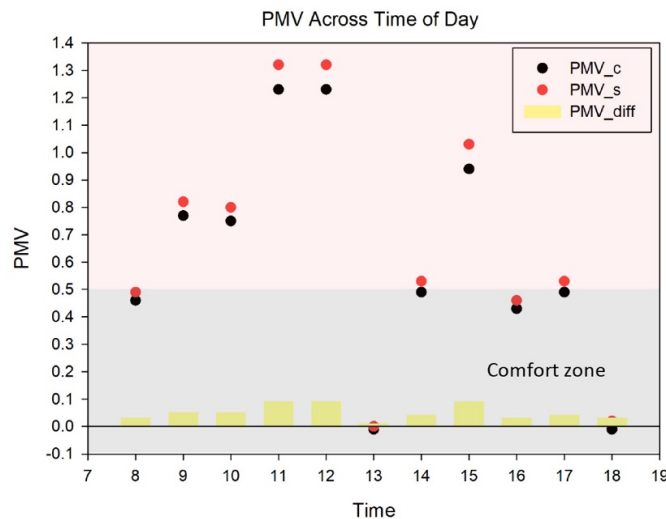


Fig. 3: The PMV values and PMV differences across times of day

At 14:00 and 17:00, the PMV_{diff} values were relatively minor, but different conclusions of the thermal comfort level are drawn for constant and spectral integral methods. The occupants are considered thermal comfort under the constant method, and uncomfortably warm under the spectral integral method. At 11:00 and 12:00, the PMV_{diff} values are relatively large, but they have the same thermal comfort level, which is both uncomfortably warm. Fig. 3 also states that the alteration of the thermal comfort level only happens at specific locations of the PMV values. As the spectral integral method is more complicated than the simplified constant method, the constant method is firstly suggested unless it is necessary to use the spectral integral method. In other words, the spectral integral method is only suggested to replace the constant method in certain cases. Thus, we should be able to determine the cases of constant PMV values that thermal comfort level might be

changed under the corresponding spectral integral method.

Another phenomenon that worth mentioning is that the PMV_{diff} values are all positive, which means the PMV values calculated with the constant method are underestimated the actual solar effects on thermal comfort. This could be problematic if a higher absorptivity is gained, such as the situations with a more intense solar irradiance, more transparent glazing, or higher skin absorptivity.

A simple linear regression modeling was also carried out to explore the factors that mainly influence the PMV_{diff} . The I_{dir} and $\sin(\beta)$ were assumed to be the factor in this analysis, and both of these parameters are significant, with p values 1.36×10^{-5} and 0.018 for I_{dir} and $\sin(\beta)$, respectively, to predict the PMV_{diff} . The R-squared value of the linear regression is 0.92, which looks reasonable. Thus, we could conclude that the PMV_{diff} is also related to the intensity of the solar irradiance and the altitude angle of the solar.

5. Conclusions

The spectral integral method was obtained by using spectral related solar transmissivity and absorptivity, which was calculated by eq. 2, instead of constant values provided or suggested.

By using the spectral integral method, the transmissivities were all higher than those using the constant method with a magnitude of 0.01. For absorptivities, the higher amount was about a magnitude of 0.001. The differences of transmissivities and absorptivities caused 0.1 magnitude differences in MRT delta values, and then PMV differences between the two methods had a magnitude of 0.01. The final differences in PMV values were minor but not negligible, as the actual indoor thermal comfort determined by the PMV values could be altered by using the spectral integral method. Thus, we verified that the spectral integral method becomes a necessity when the thermal comfort analysis is involved in solar effects, especially in some specific scenarios. Furthermore, we observed that the differences of the MRT delta and PMV values yielded by the constant and spectral integral methods were significantly influenced by the solar intensity that incident on the window and the solar altitude angle. These two parameters could be practical and helpful to appreciate the necessity of the spectral integral method. More guidelines are needed to judge the necessity of the spectral integral method so that we could determine the method to use before the calculation. Future work will form a few steps that could be directly used to give a preliminary judgment.

6. Acknowledgments

This project is supported by the NSF award: #1847024: CAREER: Understanding the Thermal and Optical Behaviors of the Near Infrared (NIR)-Selective Dynamic Glazing Structures.

7. References

- ASHRAE, A., 2010. *Standard 55-2010: Thermal environmental conditions for human occupancy*. 2010. American Society of heating, Refrigerating and Airconditioning Engineers: Atlanta.
- Arens, E., Hoyt, T., Zhou, X., Huang, L., Zhang, H. and Schiavon, S., 2015. *Modeling the comfort effects of short-wave solar radiation indoors*. *Build. Environ.*, 88, 3-9.
- Arens, E.D.W.A.R.D., Heizerling, D.A.V.I.D. and Paliaga, G.W.E.L.E.N., 2018. *Sunlight and indoor thermal comfort*. *ASHRAE J.*, 60(7), 12-21.
- Lyons, P.R., Arasteh, D. and Huizenga, C., 2000. *Window performance for human thermal comfort*. *Transactions-American Society of Heating Refrigerating and Air Conditioning Engineers*, 106(1), 594-604.
- Wang, J.J. and Shi, D., 2017. *Spectral selective and photothermal nano structured thin films for energy efficient windows*. *Appl. Energy*, 208, 83-96.

Estimating Hourly Solar Near-infrared Irradiance Using Meteorological Data for Sustainable Building Design and Engineering

Qihua Duan¹, Yanxiao Feng¹ and Julian Wang^{1,*}

¹ Department of Architectural Engineering, Pennsylvania State University, State College (United States)

* Corresponding Author Julian.wang@psu.edu

Abstract

Solar radiation is a key factor influencing sustainable building engineering, in terms of both optical and thermal properties of building envelopes. Solar irradiance data in a conventional weather data file are broadband, representing the total of ultraviolet (UV), visible light (VIS), and near-infrared radiation (NIR), three components of the solar spectrum; however, these three components play different roles in sustainable building design and engineering. For instance, solar VIS always provides benefits to indoor building energy savings (e.g., electrical lighting), while solar NIR is beneficial to building energy savings in winter but undesirable in summer. As a consequence, there is a need for reliable separate analyses focusing on individual solar radiation components. In this work, we explore and test classification-based modeling methods for decomposing hourly broadband global horizontal solar irradiance data in conventional weather files into hourly global horizontal solar NIR component. This model can then be conveniently implemented for sustainable building design and engineering purposes.

Keywords: Solar Radiation, Solar Building, Classification Trees, Prediction Model, Solar Energy, Building Energy

1. Introduction

Solar architecture is one of major category in the field of sustainable buildings, which makes the best possible use of locally available solar energy by employing both passive and active measures to achieve building sustainability and energy efficiency goals (Schittich 2012). The first solar building in America was proposed by Tod Neubauer in the 1950s.(Perlin 2013) Research in this field has addressed the theoretical background, simulation techniques, and experimental testing. Computational analysis in solar building design and engineering has been described and discussed widely in recent decades (Kisilewicz 2007). Usually an entire year's weather data are imported in a conventional format (e.g., Typical Meteorological Year 2 (TMY2), Typical Meteorological Year 3 (TMY3), Weather Year for Energy Calculations Version 2 (WYEC2)) into an energy simulation program to calculate the energy consumption of a building. Solar irradiance data in a complete weather file also include global horizontal irradiation (GHI), diffuse horizontal irradiation (DHI), and direct normal irradiation (DNI). Regardless of the three solar irradiance types noted above, the solar irradiance data are broadband and represent the total of ultraviolet (UV), visible light (VIS), and near-infrared radiation (NIR), three components of the solar spectrum.

With two known solar data components, the other component can be calculated via the mathematical relations among them. However, these three components play different roles in sustainable building engineering and design. Of these three major components, solar VIS always provides benefits to indoor building energy savings (e.g., electrical lighting), while solar NIR is strongly correlated to solar heat gains that are beneficial to building energy savings in winter but undesirable in summer (Eicker 2006). Similarly, the COVID-19 pandemic has heightened interest in the solar UV component and its potential impact on the spread and seasonality of disease. Therefore, in some in-depth building environment performance analyses, especially building energy simulation work, separate analyses focusing on each solar radiation component are desirable. With recent discoveries and engineering solutions emerging related to nanomaterials and nanostructures, independent band modulation of solar radiation on building envelopes (including glazing systems) has become increasingly viable as a potential means of improving building energy savings and indoor visual comfort (Wang et al. 2017). Meanwhile,

separated indicators or parameters related to solar light and heat have been integrated into the sustainable building design and engineering processes. For example, in our previous works solar heat gain coefficient and visible transmittance, two major building window properties, have been comprehensively studied in terms of their different impacts on building energy, potential conflicting effects, and measurement methods. (Feng et al. 2020; Wang et al. 2016). However, the meteorological data in conventional weather files do not normally include the spectral power distribution data of incident solar light because measuring the narrowband spectral distribution of sunlight is much more difficult and expensive than measuring broadband radiation (e.g., using pyranometers) (Duan et al. 2020). As a consequence, there is a pressing need for reliable performance estimations of spectral solar radiation control and response on a building scale. To assess this, we need band solar irradiance data as input.

To address this research gap and the practical need for sustainable building design and engineering, this work has developed an estimation model for the NIR component that can be captured efficiently from readily available datasets without the addition of new measurements and associated sensors; this can then be conveniently implemented into current practices and research activities related to solar building design and engineering. The methodology established in this work presents a new, efficient, and accurate method based on readily available weather data documented in conventional weather files, enabling more comprehensive and precise building energy and performance-related analyses, especially with respect to building elements and products that have NIR selectivity features.

2. Methodology

2.1 Data collection

Two major datasets, meteorological measurements (MM, in the TMY3 data format) and outdoor solar spectra data (WISER), were selected from the [Baseline Meteorological System \(BMS\)](#) database of [the National Renewable Energy Laboratory \(NREL\)](#) Solar Radiation Research Laboratory ([SRRL](#)) for the modeling done in this study (Andreas and Stoffel 1981). The MM dataset was used to retrieve and process the independent variables, including GHI, DNI, DHI, cloud coverage, dry-bulb temperature, dew-point, relative humidity, and wind speed, while the key dependent variables (i.e., solar NIR irradiance) were calculated from the WISER dataset (Andreas and Stoffel 1981).

The MM dataset for 2018 and 2019 was used in this project. It describes the basic solar radiation and meteorological elements with hourly timestamps. Note that the average value of all measured points each hour is defined as the MM value for the timestamp at the end of the one-hour interval (SOLARGIS, 2020). For example, the value at timestamp 08:00 in the MM dataset equals the average value of all measurements taken from 07:00 to 08:00. This dataset is well-organized and has been used widely to simulate the solar radiation and building energy performance in the architecture, engineering, and construction industries.

The WISER measurement database is formed from two spectroradiometers (i.e., MS-711 and MS-712) that are combined to measure global horizontal spectral solar irradiance data (Andreas and Stoffel 1981). MS-711 spectroradiometer covers the measurement range from 300 nm to 1,100 nm and MS-712 spectroradiometer focuses on the NIR range from 900 nm to 1,700 nm (Andreas and Stoffel 1981). We selected data from the same period: 2018 and 2019. The WISER database has a higher resolution measurement for both wavelengths (0.41 nm and 1.6 nm resolutions for the MS-711 and MS-712, respectively) and time intervals (typically 5 minutes, but occasionally 1 minute). To coordinate these two solar datasets from different sources, the 5-minute interval data were processed using the statistical computing software R. The hourly spectrum data were calculated by averaging the 5-minute interval data for each hour, following the criterion of timestamp calculation regulated in the MM dataset. The day-of-year time format was also modified to fit the time format of UTC (Coordinated Universal Time), as it was the same format used in the MM.

2.2 Data processing

First, to obtain the solar NIR component, we summed the spectral data for the corresponding wavelength ranges of 781 nm to 1,650 nm for NIR. We obtained the fraction of NIR/GHI by using the NIR values calculated from the WISER dataset and GHI values calculated from the MM dataset. Second, to potentially enhance modeling accuracy, we generated two additional predictor variables including Clearness index K_t and Cloud

transmittance T_{cld} . The mathematical expressions of these two parameters are as Equations (1) and (2):

- Clearness index K_t

$$K_t = \frac{GHI}{I_0 \cos(\zeta)} \quad (1)$$

where GHI is the horizontal global irradiance, I_0 is extraterrestrial solar radiation on the horizontal surface, and ζ is the solar zenith angle.

- Cloud transmittance T_{cld}

We formed a new parametric cloud transmittance T_{cld} based on our understanding of the physical behavior of solar irradiance transmission T_{cld} , defined as:

$$T_{cld} = \frac{(1-0.1T_{opq})(1-0.1T_{tot}+0.1T_{opq})}{1-0.05T_{tot}} = \frac{(1-0.1T_{opq})(1-0.1T_{trn})}{1-0.05T_{tot}} \quad (2)$$

where T_{opq} is the opaque sky cover transmittance, T_{tot} is the total sky cover transmittance, and T_{trn} is the translucent sky cover transmittance $T_{trn} = T_{tot} - T_{opq}$.

3. Results and Discussion

Classification and regression trees (CART) are a simple but powerful technique for modeling. In this study, we used the *rpart* package of CART method in R software to build regression trees for *NIR/GHI*. We split the entire dataset D into a training dataset (90% of D) and a test dataset (10% of D). The *rpart* implementation first fit a fully grown tree onto the training dataset with N terminal nodes. Then, it pruned the fully grown tree by k -fold cross-validation (default $k=10$).

3.1 CART results for the *NIR/GHI* fraction

1) Cross-validation error plot

Fig. 1 shows the cross-validation error plot for the *NIR/GHI* tree. From this figure, we can see that when $cp = 0.01$, the Size 10 regression tree has the minimum cross-validation error. This tree model is shown in **Fig. 2**.

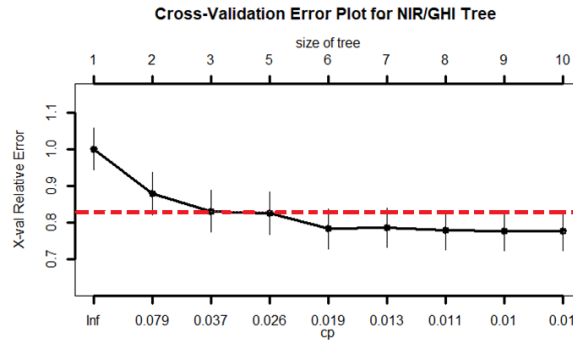


Fig. 1 Cross-validation error plot for the *NIR/GHI* tree.

(The red dotted line refers to the simplest tree, following the 1-SE rule).

2) Regression tree with minimum cross-validation error

The CART procedure generated a tree containing 10 terminal nodes for *NIR/GHI* (see **Fig. 2**), ranging from 0.1% to 33.5%. The first variable selected for splitting in this resulting tree was the clearness index K_t . If $K_t < 0.415$, the group was further split according to $RH \geq 82\%$ or $RH < 82\%$. If $K_t < 0.415$ and $RH \geq 82\%$, the group was further split according to $Dry -9.55^\circ\text{C}$ into two groups: the *NIR/GHI* values are 0.358 and 0.437. In another branch, if $K_t < 0.415$ and $RH < 82\%$, the group was further split according to the dewpoint temperature 15.3°C and yielded three more groups in which the *NIR/GHI* values are 0.391, 0.418, and 0.577, respectively. In the other major branch of this regression tree, if $K_t \geq 0.415$, the parameters of dewpoint

temperature, total cloudiness, and relative humidity were used to further form the groups, including 0.414, 0.42, 0.439, 0.456, and 0.743 for *NIR/GHI*.

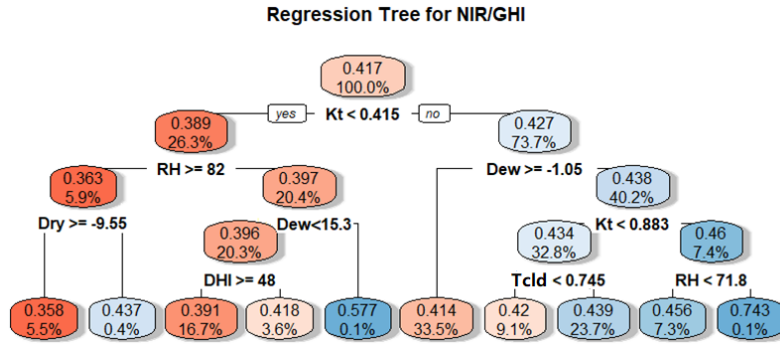


Fig. 2 Regression tree model for *NIR/GHI*.

3) Regression tree with the 1-SE rule

The dashed red line in **Fig. 1** shows the position of the 1-SE rule with the minimum $xerror + xstd$; **Fig. 3** shows that the pruned tree using the 1-SE rule for *NIR/GHI* contained three terminal nodes. The percentage of *NIR/GHI* ranged from 26.3% to 40.2% in these three groups. The first variable selected for splitting was the clearness index K_t . If $K_t < 0.415$, no further split was observed for Group 1: 26.3% of *NIR/GHI*, with a mean value of 0.389. If $K_t \geq 0.415$, the group was further split according to $Dew \geq -1.05^\circ\text{C}$ (Group 2: 33.5% of *NIR/GHI*, with a mean value of 0.414) or $Dew < -1.05^\circ\text{C}$ (Group 3: 40.2% of *NIR/GHI*, with a mean value of 0.438).

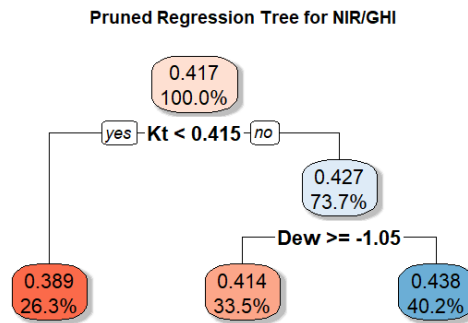


Fig. 3 Pruned regression tree model for *NIR/GHI*.

3.2 Estimation performance evaluation

The resultant tree models in **Figs. 2 and 3** are named Model 1 and Model 2, respectively. To further understand each model's estimated performance, we calculated the root mean squared error (RMSE) and the mean absolute error (MAE) of these two tree models on the test dataset with 758 observations. The \hat{y}_j variable was the prediction.

$$RMSE = \sqrt{\frac{1}{n} \sum_{j=1}^n (y_j - \hat{y}_j)^2} \quad (3)$$

$$MAE = \frac{1}{n} \sum_{j=1}^n |y_j - \hat{y}_j| \quad (4)$$

Table 1 Comparison of RMSE and MAE by Models

	<i>NIR/GHI</i>	
Regression Tree	Model 1	Model 2
Tree Size	10	3
RMSE	0.0391	0.0388
MAE	0.0213	0.0216

From **Table 1**, we can see that the RMSE decreased as the tree size decreased, but the MAE increased as the tree size decreased. Comparing Models 1 and 2, the RMSE decreased by 0.77% and the MAE increased by 1.4%. Regarding the changes in RMSE, since the errors were squared before they were averaged, larger errors receive a relatively higher weight. This means that the RMSE is more useful when significant errors are particularly undesirable. However, the RMSE did not necessarily increase with the variance of the errors. The RMSE increased with the variance of the frequency distribution of error magnitudes. Based on the information shown in **Table 1**, we can find the accuracy level differences among the models were negligible in this work. Both Models 1 and 2 had excellent prediction performances for *NIR/GHI*. This offers the opportunity to simplify the computation process if the weather data are insufficient.

4. Conclusion

This work demonstrated the feasibility and excellent prediction performance of regression tree models for hourly *NIR/GHI*. The solar spectra and conventional hourly weather data obtained from the BMS database of NREL's [SRRL](#) were utilized for model development. This research yielded models capable of converting the broadband solar irradiance data in weather files into NIR solar component, for building energy and performance-related studies in which independent solar spectra products are examined, such as analyses of spectrally selective glazing, transparent photovoltaic panels, etc. Solar components, especially NIR, are significantly affected by atmospheric parameters (e.g., water vapor levels), but these parameters are not very well documented observationally and dependent on local geographic and climatic features.

5. Acknowledgments

This project is supported by the NSF award: #1847024: CAREER: Understanding the Thermal and Optical Behaviors of the Near Infrared (NIR)-Selective Dynamic Glazing Structures

6. References

- Andreas, Afshin, and Tom Stoffel. 1981. *NREL Solar Radiation Research Laboratory (SRRL): Baseline Measurement System (BMS); Golden, Colorado (Data); NREL Report No. DA-5500-56488*. Golden, Colorado (Data); NREL Report No. DA-5500-56488. <http://dx.doi.org/10.5439/1052221> (May 20, 2020).
- Duan, Qihua et al. 2020. "Solar Infrared Radiation towards Building Energy Efficiency: Measurement, Data, and Modeling." *Environmental Reviews*.
- Eicker, Ursula. 2006. *Solar Technologies for Buildings*. John Wiley & Sons.
- Kisilewicz, Tomasz. 2007. "Computer Simulation in Solar Architecture Design." *Architectural Engineering and Design Management* 3(2): 106–23.
- Perlin, John. 2013. *Let It Shine: The 6,000-Year Story of Solar Energy*. New World Library.
- Schittich, Christian. 2012. *Solar Architecture: Strategies, Visions, Concepts*. Walter de Gruyter.

Solargis. 2019. "Data Format." <https://solargis.com/docs/product-guides/time-series-and-tmy-data/data-format> (May 20, 2020).

Wang, Donglu Shi, Julian(Jialiang) Wang, and Donglu Shi. 2017. "Spectral Selective and Photothermal Nano Structured Thin Films for Energy Efficient Windows." *Applied Energy* (208): 83–96.

Forecasting Carbon Emissions in Seven Eastern States of the United States; The Effects of Coal Deregulations

Rahim Khoie¹, and Antonio Calderon¹

¹Department of Electrical and Computer Engineering
University of the Pacific
Stockton, CA 95211
rkhoie@pacific.edu

Abstract

The 2008 through 2016 were the years of implementation of increasingly restrictive regulatory policies on climate change, and particularly on carbon emissions by coal-burning power plants. Some of these regulations were imposed by states (in the form of Renewable Portfolio Standards, RPS) and majority of them were imposed by Obama Administration. These regulations, among other factors, resulted in a significant drop in the U.S. total emissions; 12% drop from 2007 to 2016. The current Administration has taken several actions in reversing, relaxing, or repealing many of these regulations, and particularly regulations on use of coal in electricity generation. In this paper we present Two ARIMA models to forecast the potential effects of these deregulations on future carbon emissions of states of Ohio, Pennsylvania, North Carolina, Tennessee, Kentucky, Virginia, and West Virginia. These states were chosen in part because they rely heavily on electricity generated from coal and their RPS targets are among the lowest in the nation.

The results of our simulations over a large number of scenarios, based on a series of emission data in the years 1980 through 2014 clearly shows the significant role that the regulatory policies of the 2008-2014 era plays in significantly lowering these states' emissions by the year 2025. In particular, our results show that the continued implementation of the regulatory policies of Obama Administration could lower the states' emissions from coal generation from 2007-level of 588 million metric ton (MMT) to 189 MMT in 2025, a 68% drop. And conversely, reversal and or repeal of these regulations by the current Administration could result in the emissions of states to reach 713 MMT in 2025, an increase of 21% over the 2007-level.

Keywords: *Carbon Emissions, Coal Deregulations, Autoregressive Integrated Moving Average Model, Renewable Portfolio Standards*

1. Introduction

Taking the United States out of the historic 2016 International Paris Agreement is only one among a long list of actions taken by the current Administration in reversing many years of climate policies, especially those implemented by the Obama Administration (Adler, 2011) and (McCarthy and Copeland, 2016). The list of the deregulatory actions taken by the current Administration in coal industry include: (Brookings Institution, 2019) and (National Geographic, 2020):

- Relaxing the rules on emission of greenhouse gases in new coal-fuel power plants.
- Relaxing the rules on producing mercury and other air-toxins by coal-burning power plants.
- Repealing Clean Power Plan, and

- Postponing enforcement of many Environmental Protection Agency (EPA) regulations.

The National Oceanic and Atmospheric Administration in its 2018 Report on “Climate Change: Current and Projected Impacts on the U.S.” called for the need for removal of existing carbon from the atmosphere to prevent the projected climate disasters by 2050 (NOAA, Fahey 2018). In light of this warning, it is imperative that we investigate the effects of coal deregulations on carbon emissions, especially in those states in the United States who rely heavily on electricity generation from coal.

The total U.S. carbon emissions had been on a declining trend in the past several years, as shown in Fig. 1 (Energy In Depth, 2017).

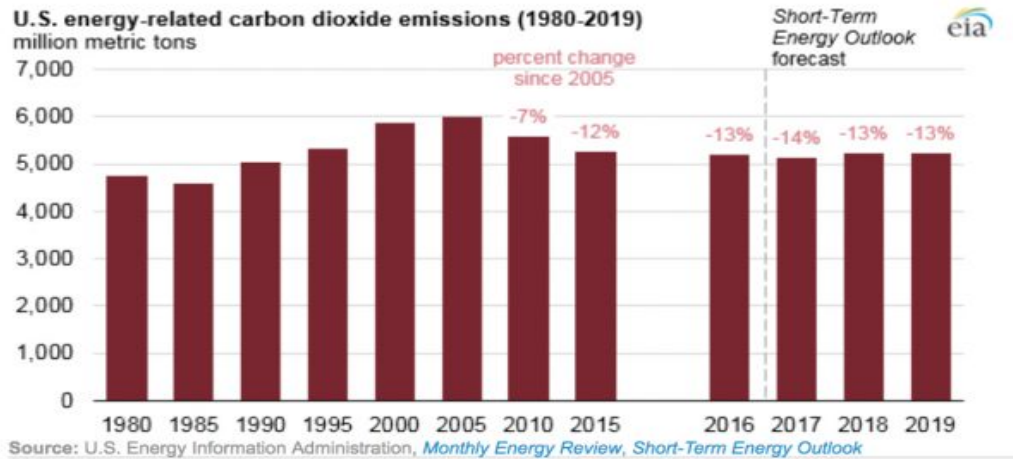


Fig. 1. The U.S. total carbon emissions from 1990 to 2016 (Energy in Depth, 2017)

After peaking at 5983 Million Metric Tons (MMT) in 2007, the total U.S. carbon emissions reached a trough of 5171 MMT in 2016. In fact compared to 2005-levels, the total U.S. emissions dropped by 7% and 13% in 2010 and 2016, respectively. The drop continued in 2017 at 14% below 2005 levels. This is a significant decline by any measure. Various researchers have cited reasons for this decline, including:

- decline in the U.S. economy output in the years following the financial crisis of 2008-2009 (Peters, et. al. 2012) (Guardian, 2010), and (Murray and Maniloff, 2015).
- increase in use of natural gas (Feng, et. al., 2015) and (De Gouw, et. al., 2014)
- federal regulations imposed by Obama Administration (Adler, 2011) (McCarthy and Copeland, 2016),
- and state-mandated regulations, and in particular, the Renewable Portfolio Standards (LBL, 2016).

In the absence of any federal mandate on reducing the U.S. carbon emissions, and in light of recent federal energy deregulations by present administration, and in particular, deregulation of coal industry, the role of states in mandating emission reduction is now more essential. A large number of states in the U.S. have enacted legislations mandating Renewable Portfolio Standard (RPS) requiring utility companies to produce a certain percentage of their electricity from renewable resources (U.S. EIA, 2012). While the state of Hawaii has the most ambitious target of 100% renewable electricity by 2045 (Hawaii State Energy Office, 2018), the state of California has set a goal of 50% renewable power production by the year 2030 (California Public Utility Commission, 2018). The state of Colorado requires production of 30% renewable electricity by 2020 (Colorado Energy Office, 2018). Overall, 29 states and the District of Columbia have adopted mandatory RPS along with 7 states that have voluntary goals (See Fig. 2) (LBL, 2016). The remaining states have no clear renewable energy policy including, ironically, the State of Florida, which has one of the most abundant supply of renewable resources, especially in solar energy (Khoie and Yee, 2015). Among other states without RPS laws are the states of Kentucky, Tennessee, and West Virginia which are among the seven eastern states that are studied in this work.

A number of researchers have developed forecasting models for investigating possible future trends in carbon emissions of the U.S. and other countries. Using state-level data on carbon emissions, Auffhammer and Steinhauer (2012) compared a large number of models for forecasting the U.S. CO₂ emissions. Other researchers have used ARIMA models for forecasting long-term trends in carbon emissions. Silva (2013) used a combination of various models, including Autoregressive Integrated Moving Average (ARIMA) model for short-term projection

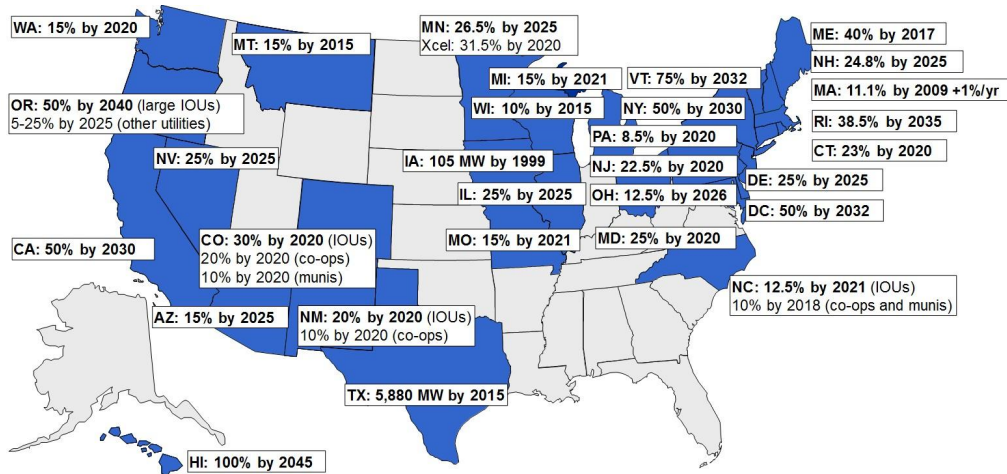


Fig. 2. Renewable Portfolio Standards of United States (LBL, 2016).

of the U.S. carbon emissions. Yuan, et. al., (2016) developed an ARIMA model for forecasting China’s energy consumption while comparing the results to those of Grey Model (GM) and concluded that the results of ARIMA model are less sensitive to temporary fluctuations in the past data. A similar comparative study was performed by Pao and Tsai (2011) for carbon emissions in Brazil. Other researchers have used ARIMA models for forecasting carbon emissions in countries such as Indonesia (Prananda et. al., 2015), Iran (Lotfalipour, et. al., 2013), and India (Sen, et. al., 2016). ARIMA models have also been used for forecasting near-term trends in stochastic processes such as wind power generation (Chen, et. al., 2010).

We (Khoie and Calderon, 2019) previously presented four ARIMA models for forecasting the future trends in carbon emissions of the three states of Hawaii, California, and Colorado whose RPS laws set the most ambitious renewable targets, and the State of Florida, which has no RPS laws. In this paper, we present ARIMA models for forecasting the future trends in carbon emissions of seven neighboring eastern states. These states are: Ohio, Pennsylvania, North Carolina, Tennessee, Kentucky, Virginia, and West Virginia. These states were chosen for two reasons: (a) they either do not have any RPS laws (KY, TN, and WV) or their RPS targets are among the lowest in the nation (see Table 1), and (b) they rely heavily on electricity generated from coal (U.S. EIA, 2018).

Table 1: The RPS and target year of the seven states (NCSL, 2019)

State	Year of RPS Enactment	RPS Target	RPS Target Year
Ohio	2008	12.5%	2026
Pennsylvania	2004	8.5%	2020
North Carolina	2007	12.5	2021
Tennessee	-	-	-
Kentucky	-	-	-
Virginia	2007	15%	2025

West Virginia	2007 (Repealed 2015)	-	-
---------------	----------------------	---	---

2. Recent Emissions Trends

In the first eight years of 2000's, the seven states of NC, OH, PA, KY, TN, VA, and WV, individually and collectively relied heavily on electricity generation from coal. Fig. 3 shows the total electricity generation of the seven states in the years 2001 thru 2016. While hovering around 850 million MWhr a year, the total electricity generation of the seven states reached a peak of 875 million MWhr in 2007 after which it declined by about 9% to 794 million MWhr in 2016. During this period, the electricity generation from coal peaked at 614 million MWhr in 2007 after which it declined by about 56% to 347 million MWhr in 2016, as shown in Fig. 4.

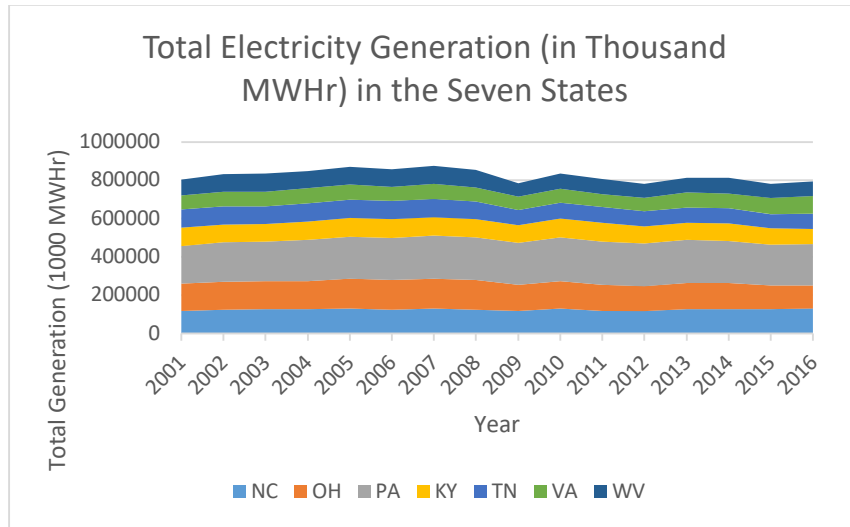


Fig. 3. Total electricity generation in each of the seven states between 2001 and 2016 (U.S. EIA, 2018).

Therefore, in the 8 years between 2001 and 2008, the percentage of electricity generation from coal in all seven states hovered around 70% (See Figs. 5 and 6). In the next 8 years (2008 to 2016) the percentage of electricity generation from coal in all seven states dropped from 70% in 2008 to 44% in 2016. This was a substantial drop in coal generation over the 8 years of the Obama Administration. In the meanwhile, the total emissions of the electricity generation from coal in all of the seven states (shown in Fig. 7) peaked at 588 MMT in 2007 after which it declined to 421 MMT in 2014 which is a 29% drop in emissions. This drop is significantly higher than the national average drop of about 11% during the same period.

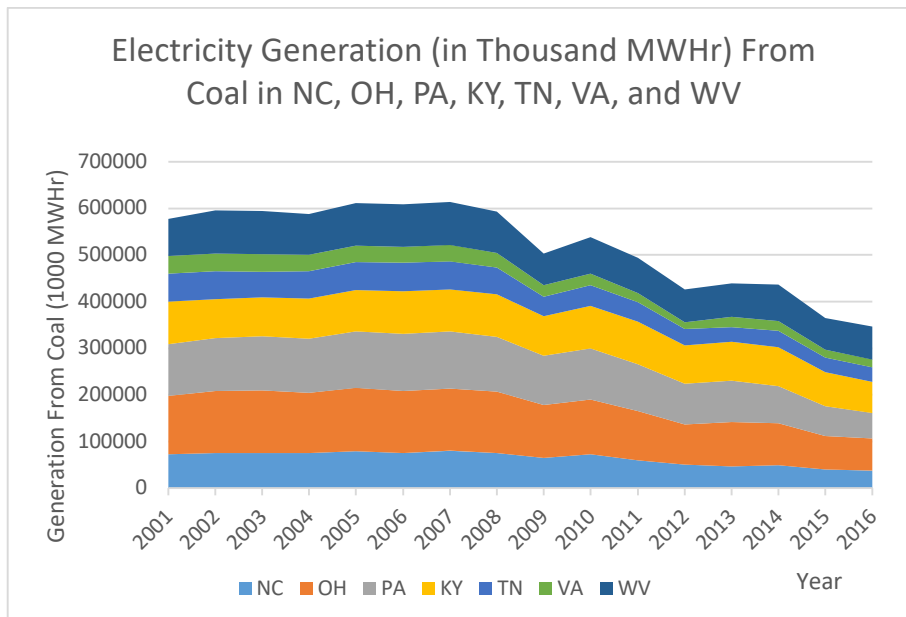


Fig. 4. Electricity generation from coal in each of the seven states between 2001 and 2016 (U.S. EIA, 2018).

The declining trends in coal generation and carbon emissions in these states in the years 2008 to 2016 correlate to four possible factors mentioned in the Introduction. These factors are downturn in the U.S. economy in 2008-2010, increase in use of natural gas, enactment of RPS laws in the prior years in most of these states, and increasing coal and emission regulations by the Obama Administration. To investigate the possible effects of coal regulations on carbon emissions by coal power plants we developed two different ARIMA models described below. We then used these models to forecast carbon emissions through 2025 with 8 different scenarios.

- In scenario 1, we use the combined emission data for all seven states in the years 1980 to 2007 and predict the combined emissions of all seven states in the years 2008 to 2025.

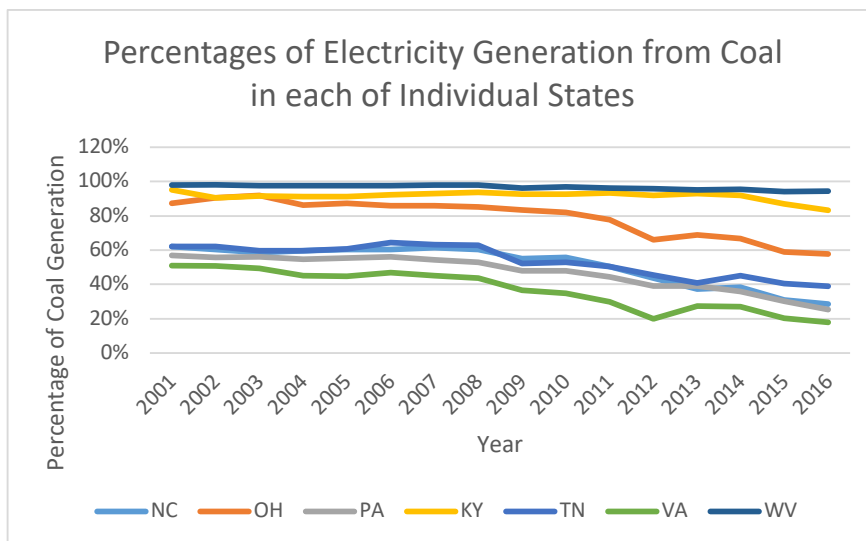


Fig. 5. Percentages of electricity generation from coal in each of the seven states between 2001 and 2016 (U.S. EIA, 2018). West Virginia and Virginia are the two extremes in percentage of coal generation.

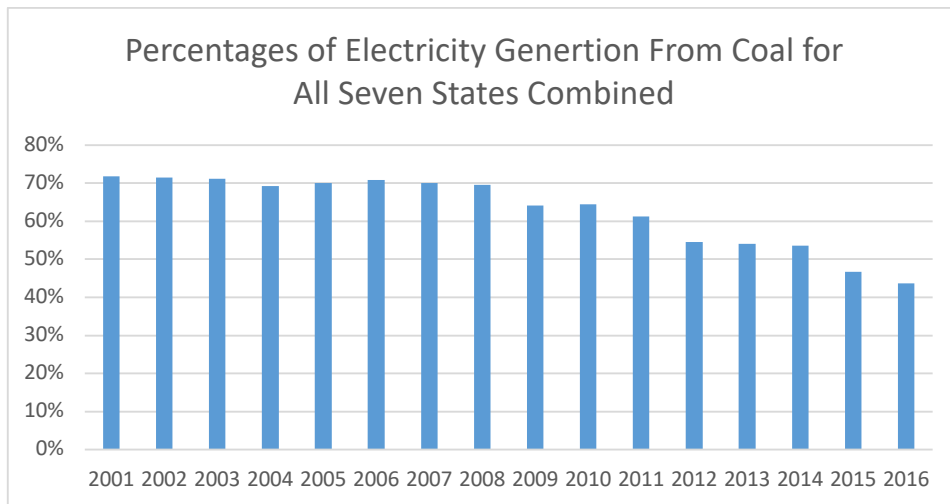


Fig. 6. Percentages of electricity generation from coal for all the seven states combined between 2001 and 2016 (U.S. EIA, 2018).

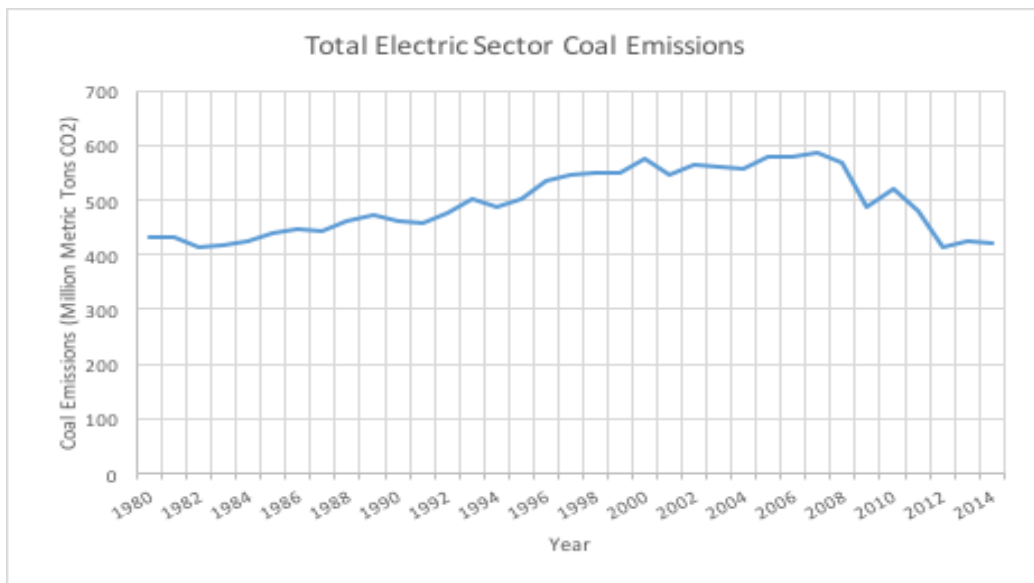


Fig. 7. Total carbon emissions of electricity generation from coal for all the seven states combined from 1980 to 2014 (U.S. EIA, 2018).

- In scenario 2, we use the combined emission data for all seven states in the years 1980 to 2008 and predict the combined emissions of all seven states in the years 2009 to 2025.
-
- In scenario 7, we use the combined emission data for all seven states in the years 1980 to 2013 and predict the combined emissions of all seven states in the years 2014 to 2025.
- In scenario 8, we use the combined emission data for all seven states in the years 1980 to 2014 and predict the combined emissions of all seven states in the years 2015 to 2025.

Obviously, the known values of emission data for the years 2008-2014, and especially emission data for the years 2015, 2016, and 2017 are used to validate our projections and adjust the ARIMA models' parameters for the minimum error between the predicted values and actual known emission data.

3. The ARIMA Models

The general form of the ARIMA model is given by (Chen, et. al, 2010):

$$y_t = \mu + \varphi_1 y_{t-1} + \varphi_2 y_{t-2} + \dots + \varphi_p y_{t-p} - \theta_1 \varepsilon_{t-1} - \theta_2 \varepsilon_{t-2} - \dots - \theta_q \varepsilon_{t-q} \quad (1)$$

Where:

- y_t is the predicted value for year t ,
- y_{t-1} is the predicted value for year $t - 1$,
- μ is a constant term for a non-zero average trend,
- φ_p terms are autoregressive term (AR),
- p is the order of autoregressive process,
- θ_q terms are moving average parameters (MA),
- q is number of lagged forecast errors in prediction model,
- ε_q terms are forecast errors.

In order to stationarize the predicted trends and mask seasonal variations, the order of differencing parameter, d was determined to be:

$$d = 2 \quad \text{then} \quad y_t = (Y_t - Y_{t-1}) - (Y_{t-1} - Y_{t-2}) = Y_t - 2Y_{t-1} + Y_{t-2}$$

In the above equations, y_t is the predicted value for the year t and Y_t is the value of original data at year t .

The parameters p , and q represent the number of AR and MA terms, respectively. In other words, p represents the tendency of the data to return to the mean value, and q represents the shock response of the data to a sudden change. The higher the order of these terms, the more past data is used to calculate the predicted value. The parameters p , and q are determined based on a Box-Jenkins (Chen, et. al., 2010) method using series of simulations resulting in least prediction error of known years. The adaptive nature of the model ensures that historical trends associated to policy changes are reflected in future trends. For more details of our ARIMA models see (Khoie and Calderon, 2018).

Using the total emissions data of all seven states, and testing various ARIMA models for various scenarios described in the above section, we determined the following two models:

- ARIMA ($p= 0, d= 2, q= 1$) and
- ARIMA ($p= 4, d= 2, q= 0$)

to have the best fit based on Akaike Information Criterion (AIC). The fitting process was done with the R package *forecast* which provides functions for AIC which is an integral step in model fitting (Yamaoka, et. al., 1978). The order of the fit was adjusted as appropriate to achieve a minimum absolute error between the predicted data and the known emissions data in the years 2008 through 2016 (as appropriate). The open-source statistical software R was used to facilitate the model fitting process and prediction to year 2025. For each of the eight scenarios described in the above section, we ran the two ARIMA models and produced prediction results which are described below.

4. Results

The two ARIMA models described above are simulated for the 8 scenarios producing 16 sets of forecasts. The results of the two ARIMA models for the two extreme scenarios, namely scenarios 1 and 8 (four sets of forecasts) are presented and discussed in this paper. The results of the other 6 scenarios fall somewhere in between these two extremes and are not presented here.

Fig. 8 Shows the forecast results of ARIMA (0,2,1) model for emissions of electricity generation from coal in all seven states through 2025. These results are based on emission data from 1980 through 2007 which exclude the emission data of the 2008-2014 era. These results show continued increase in emissions if the regulatory policy changes of 2008-2014 had not taken effect. The range of data for 80% and 90% confidence levels are also shown.

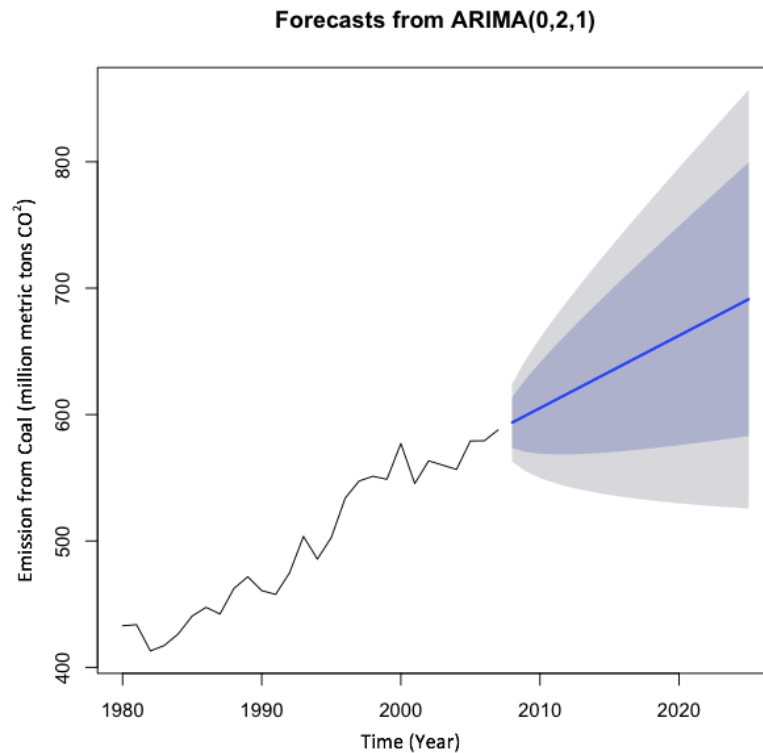


Fig. 8. Forecast of ARIMA (0,2,1) model for emissions of electricity generation from coal in all seven states through 2025. The results are based on emission data of 1980 through 2007 and show continued increase in emissions if the regulatory policy changes of 2008-2014 had not taken place. The range of data for 80% and 90% confidence levels are also shown.

Fig. 9 Shows the forecast results of ARIMA (0,2,1) model for emissions of electricity generation from coal in all seven states through 2025. These results are based on emission data of 1980 through 2014 and include the data for the 2008-2014 years in which increasingly more restrictive federal regulations and especially on coal power generation were implemented. These results show declining trends in emissions in years 2015-2025 in response to the regulatory policy changes of 2008-2014.

Fig 10 shows the results of ARIMA (4,2,0) model for emissions of electricity generation from coal in all seven states through 2025. Similar to the results shown in Fig. 8, these results which are based on emission data of 1980 through 2007 show continued increase in emissions in the years 2008 through 2025 had it not been for the regulatory policy changes of 2008-2014 period. And finally, Fig. 11 depicts the forecast results from the ARIMA (4,2,0) model based on emission data of 1980 through 2014 which includes the years of increasing regulatory actions by the federal government in electricity generation from coal. And again similar to the results shown in Fig. 9, this model also projects continued declined in emissions in response to the policy changes and regulations imposed by the Obama Administration in the years 2008 through 2014.

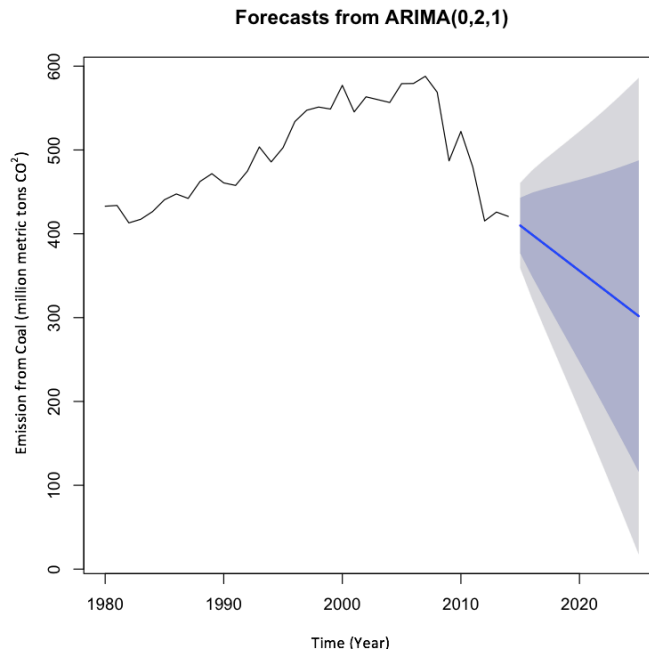


Fig. 9. Forecast of ARIMA (0,2,1) model for emissions of electricity generation from coal in all seven states through 2025. The results are based on emission data of 1980 through 2014 and show continued declined in emissions in response to the regulatory policy changes of 2008-2014.

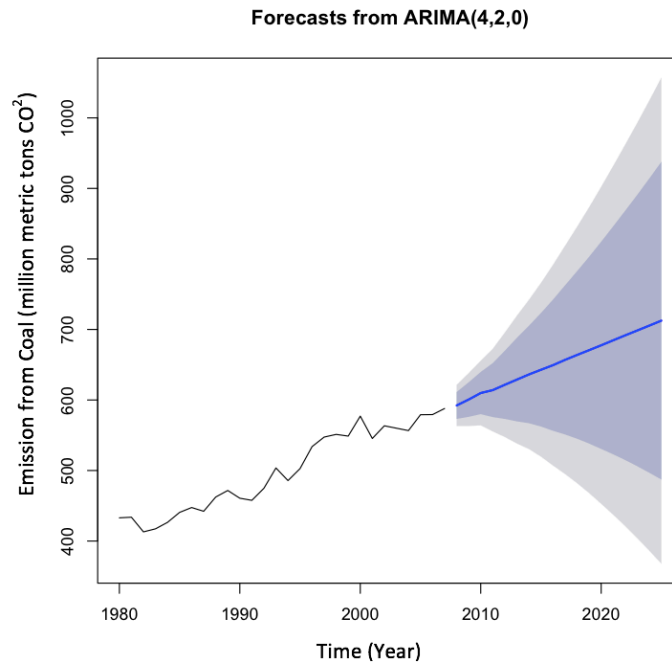


Fig. 10. Forecast of ARIMA (4,2,0) model for emissions of electricity generation from coal in all seven states through 2025. The results are based on emission data of 1980 through 2007 and show continued increase in emissions if the regulatory policy changes of 2008-2014 had not taken place. The range of data for 80% and 90% confidence levels are also shown.

The highlights of the four sets of data described above are summarized in Table 2 where we list the predicted values of the combined emissions of electricity generation from coal in all the seven states over the years 2008 through 2025. Also listed in this table are the actual known emission values in the years 2008 through 2016. As can be seen, in both models, the errors between the predicted value and the known value for the year 2008 in

scenario 1 are about 4%. However, in Scenario 8, the errors between the predicted value and known value for the year 2015 is about 15% in ARIMA (0,2,1) and about 6% for ARIMA (4,2,0), which is to be expected.

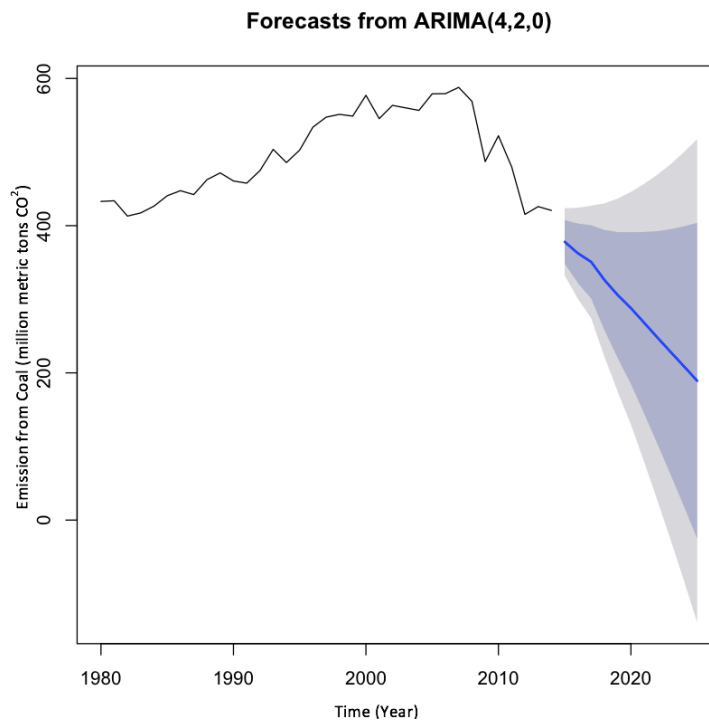


Fig. 11. Forecast of ARIMA (4,2,0) model for emissions of electricity generation from coal in all seven states through 2025. The results are based on emission data of 1980 through 2014 and show continued declined in emissions in response to the regulatory policy changes of 2008-2014.

5. Conclusions

In this study, we performed a series of simulations using two different ARIMA models to predict the impact of the Obama-era Environmental Protection Agency regulations on reducing CO₂ emissions from coal. To investigate the effect of federal policy changes on emissions from coal power generation, we created a large number of scenarios each using emission data of a specific period starting in 1980 and ending in the years 2007, 2008, 2009, and so on through 2014, resulting in 8 different scenarios. All these scenarios were tested with two somewhat of extreme ARIMA models, one almost a linear predictor, ARIMA (0,2,1) and another more nonlinear, ARIMA (4, 2, 0).

Both ARIMA models predicted similar trends, although with different precision and different confidence level. The forecast results of both ARIMA models for scenario 1 were based on data from 1980 to 2007, which were pre-Obama years. Both ARIMA models predicted that if the policies in effect in those years had continued in 2008 through 2014, the emissions from coal power generation in the seven states of NC, OH, PA, KY, TN, VA, and WV would have continued rising to extremely high levels (nearly 713 MMT in 2025). On the other hand, when we ran both ARIMA models with emission data in the Obama years included (scenario 8), the results showed sharp decline in emissions. Under the extreme scenario 8 which uses emission data from 1980 to 2014, the ARIMA(4,2,0) model predicted an emission level of 189 MMT in 2025 which would be 73% less than 713 MMT in 2025 predicted under scenario 1. These results support the conclusion that undoing, reversing, repealing, and or not enforcing the Obama-era coal regulations would result in reversing the recent declining trends in combined emissions of not only the seven states of NC, OH, PA, KY, TN, VA, and WV studied here, but also the of the entire United States.

Table 2: Emission results (in MMT) predicted by the two ARIMA forecast models for the two extreme scenarios 1 and 8. Both ARIMA models predict declining trends in emissions should regulatory policies of 2008 to 2016 continue.

Year	Forecast Scenario 1 ARIMA (0,2,1)	Forecast Scenario 8 ARIMA (0,2,1)	Forecast Scenario 1 ARIMA (4,2,0)	Forecast Scenario 8 ARIMA (4,2,0)	Actual (MMT)
2008	594		592		569
2009	599		601		487
2010	605		610		522
2011	611		614		480
2012	616		622		415
2013	622		629		425
2014	628		636		421
2015	634	410	643	378	355
2016	639	399	650	362	340
2017	645	388	657	351	
2018	651	377	664	326	
2019	657	367	671	306	
2020	663	356	678	288	
2021	668	345	685	268	
2022	674	334	692	248	
2023	680	323	699	229	
2024	685	312	705	209	
2025	691	301	713	189	

The short-term energy outlook forecast by Energy Information Administration (shown in Fig. 1 (Energy In Depth, 2017)) indicates that the total U.S. carbon emissions in the years 2018 and 2019 are on the rise. This trend, and potential acceleration of such trend as result of continuation of the deregulatory environment created by current Administration are in sharp contrast to the warning issued by the current National Oceanic and Atmospheric Administration. To prevent projected climate disasters by 2050 (NOAA, Fahey 2018), we need to remove existing carbon from the atmosphere. With that as our goal, even the 189 MMT projected emission in 2025 (under our best scenario 8 with ARIMA (4,2,0) would still too much emission to have to be removed from the atmosphere.

6. References

- Adler, J. 2011. Heat expands all things: The proliferation of greenhouse gas regulation under the Obama administration. *Harvard Journal of Law and Public Policy*, 421. <http://heinonline.org/>, Accessed March 2018.
- Auffhammer, M., and Steinhauser, R., 2012. "Forecasting The Path of US CO₂ Emissions Using State-Level Information," *Review of Economics and Statistics*, MIT Press, Volume 94, Issue 1, February 2012, p.172-185.
- Brookings Institution, 2019. "Tracking deregulation in the Trump era," Friday, April 12, 2019, <https://www.brookings.edu/interactives/tracking-deregulation-in-the-trump-era/> Accessed: April 2019
- California Public Utility Commission, 2018. California Renewables Portfolio Standard, http://www.cpuc.ca.gov/RPS_Homepage/ Accessed: March 2018.
- Chen, P., Pedersen, T., Bak-Jensen, B. 2010. ARIMA-based time series model of stochastic wind power generation. *IEEE Transactions on Power Systems*. vol. 25, pp. 667-676.

- Colorado Energy Office, 2018. <https://www.colorado.gov/pacific/energyoffice/renewable-energy-standard>, Accessed March 2018.
- De Gouw, J. A., Parrish, D.D., Frost, G. J., and Trainer, M., 2014. "Reduced emissions of CO₂, NO_x, and SO₂ from US power plants owing to switch from coal to natural gas with combined cycle technology." *Earth's Future* 2, no. 2 (2014): 75-82.
- Energy In Depth, 2017. "EIA: U.S. Carbon Emissions Fall Again in 2017, 'Mainly' Because of Natural Gas," *Energy In Depth: Climate and Environment*, <https://eidclimate.org/eia-u-s-carbon-emissions-fall-2017-mainly-natural-gas/> Accessed April 2019.
- Feng, K., Davis, S., Sun, L., and Hubacek, K. 2015. Drivers of the U.S. CO₂ emissions 1997–2013. *Nature Communications*, 21 July 2015, Open Source. <https://www.nature.com/articles/ncomms8714.pdf>.
- Guardian, The, 2010. Global emissions of carbon dioxide drop 1.3%, say international Scientists. <https://www.theguardian.com/environment/2010/nov/21/carbon-emissions-fall-report>, Accessed March 2018.
- Hawaii State Energy Office. 2018. <http://energy.hawaii.gov/renewable-energy> , Accessed March 2018.
- Khoie, R. and Yee, V., 2015. A forecast model for deep penetration of renewables in the Southwest, South Central, and Southeast regions of the United States. *Clean Technologies and Environmental Policy*, Volume 17, pp 957–971.
- Khoie, R. and Calderon, A., 2018. "Forecasting Carbon Emissions in States of Hawaii, California, Colorado, and Florida; The Effects of States' Renewable Portfolio Standards," Published in *Proceedings of SOLAR 2018, American Solar Energy Society 47th National Solar Conference and Summit*, Boulder, Colorado, August 5-8, 2018.
- LBL, 2016. Electricity Markets and Policy Group. Renewable Portfolio Standards Resources. Lawrence Berkeley National Laboratory. 2016. Available: <https://emp.lbl.gov/projects/renewables-portfolio>. Accessed March 2018.
- Lotfalipour, M., Falahi, M., and Bastam, M., 2013. "Prediction of CO₂ emissions in Iran using Grey and ARIMA models, *International Journal of Energy Economics and Policy*; Vol. 3, pp. 229.
- McCarthy, J. and Copeland C. 2016. EPA Regulations: Too Much, Too Little, or On Track? Congressional Research Service, Library of Congress, December 30, 2016 <https://fas.org/sgp/crs/misc/R41561.pdf>, Accessed March 2018.
- Murray, Brian C., and Maniloff, P., 2015. "Why have greenhouse emissions in RGGI states declined? An econometric attribution to economic, energy market, and policy factors." *Energy Economics* 51 pp. 581-589.
- National Geographic, 2020. <https://news.nationalgeographic.com/2017/03/how-trump-is-changing-science-environment/>. Accessed June 2020.
- National Oceanic and Atmospheric Administration, 2018. David Fahey, "Climate Change: Current and Projected Impacts on the U.S.," *ASES SOLAR 2018, Pathways to the Renewable Energy Transformation*, August 5-8, 2018, Boulder, CO. See: <https://www.noaa.gov/climate-data-and-reports>.
- NCSL, 2019, National Conference of State Legislators, "State Renewable Portfolio Standards and Goals," <http://www.ncsl.org/research/energy/renewable-portfolio-standards.aspx> , Accessed April 2019.

Pao, H., and Tsai, C., 2011. "Modeling and forecasting the CO₂ emissions, energy consumption, and economic growth in Brazil," *Energy*, Volume 36, Issue 5, May 2011, Pages 2450-2458.

Peters, G. Marland, G., Le Quéré, C., and Boden, T. 2012. Rapid growth in CO₂ emissions after the 2008–2009 global financial crisis. *Nature Climate Change*, 2012, <https://www.nature.com/articles/nclimate1332>, Accessed March 2018.

Prananda, J., Hantoro, R., Nugroho, G., 2015. "The Prediction of Carbon Dioxide Emission Using ARIMA for Support Green Energy Development in Surabaya Municipality, *Knowledge E*, Vol. 2, pp. 106-110.

Sen, P., Roy, M., Pal, P., 2016, "Application of ARIMA for forecasting energy consumption and GHG emission: A case study of an Indian pig iron manufacturing organization," *Energy*, Volume 116, Part 1, 1 December 2016, Pages 1031-1038.

Silva, E., 2013. "A COMBINATION FORECAST FOR ENERGY-RELATED CO₂ EMISSIONS IN THE UNITED STATES," *International Journal of Energy and Statistics*, Vol. 1, Issue 4, December 2013.

U.S. Energy Information Administration, 2012. Most States Have Renewable Portfolio Standards. February 2012. <https://www.eia.gov/todayinenergy/>. Accessed: March 2018.

U.S. Energy Information Administration, 2016. Environment, U.S. Energy-Related Carbon Dioxide Emissions. <https://www.eia.gov/environment/emissions/carbon/>. Accessed: August 2018.

U.S. Energy Information Administration, 2018. "State Carbon Dioxide Emissions Data, <https://www.eia.gov/environment/emissions/state/>, Accessed April 2019

Yamaoka, K., Nakagawa, T., and Uno, T., 1978. "Application of Akaike's information criterion (AIC) in the evaluation of linear pharmacokinetic equations," *Journal of Pharmacokinetics and Biopharmaceutics*, April 1978, Volume 6, Issue 2, pp 165–175.

Yuan, C., S Liu, S. Fang, Z, 2016. "Comparison of China's primary energy consumption forecasting by using ARIMA (the autoregressive integrated moving average) model and GM (1, 1) model," *Energy*, Volume 100, 1 April 2016, Pages 384-390.

The Carbon Emissions of Wind Power; A Study of Emissions of Windmill in the Panhandle of Texas

Rahim Khoie¹, Andrew Bose,² and Joshua Saltsman²

¹Department of Electrical and Computer Engineering

²Department of Mechanical Engineering

University of the Pacific
Stockton, CA 95211
rkhoie@pacific.edu

Abstract

The National Oceanic and Atmospheric Administration in its 2018 Report on “Climate Change: Current and Projected Impacts on the U.S.” called for the need for removal of existing carbon from the atmosphere to prevent the projected climate disasters by 2050 (NOAA, Fahey, SOLAR 2018 Conference). This warning necessitates an examination of the carbon footprint of renewables, especially solar photovoltaic and wind generation. The electricity generation from both wind and solar photovoltaics has been on the rise globally in recent years. In this paper we study the carbon footprint of wind generation from a 1.3 megawatts (MW) located in the wind sweet spot of the U.S., namely, Panhandle of Texas. We are also investigating the carbon footprint of solar photovoltaics and will report the results in the near future.

Our model includes the carbon cost of manufacturing, transportation, installation, operation, and maintenance of windmills. Our results show that a 1.3 MW windmill operating in the Panhandle of Texas produces 14.45 grams of carbon dioxide for each kilowatt (kWh) of generated electricity. Compared to carbon dioxide intensity of 792 grams CO₂ /kWh of electricity produced by an average coal power plant, wind power generation produces 1.8% emissions, a substantial 98.2% reduction in emissions. However, with 286.8 billion kWh wind generation in 2019, this amount to 4.13 million ton (MT) of annual emissions by wind, which will increase substantially as deeper levels of wind generation is achieved in the next several decades. Our results agree well with those reported by others.

Keywords: *Wind Power Generation, Carbon Footprint of Wind, Wind Power in Panhandle of Texas*

1. Introduction

The wind power in the United States has been expanding rapidly over the last several years. For the twelve months ending September 2019, the United States generated 286.6 terawatt-hour of wind power, roughly 7% of all generated electricity (Wind Power Monthly, 2020A). A similar trend is seen in China (GWEC, 2019) and Europe (Wind Power Monthly, 2020B) which is expected to continue over the next several decades. More specifically, as shown in Fig.1, the total installed wind capacity in the U.S. at the end of first quarter of 2020 was 107,319 MW (U.S. EERE, 2020). Just in the first quarter of 2020, the wind industry installed 1,821 MW of new wind power capacity, which is a 117% increase over the first quarter of 2019. Obviously, the continued increase in wind capacity is a major step toward reducing carbon emissions. However, there are two reports that should be considered as strong warnings on the global emissions and climate change. One is the report by U.S. EIA (2020) in which it was reported that the U.S. total emissions, after ten years of decline (from 2007 to 2017) went up by about 2.5% in 2018 (See Fig. 2).

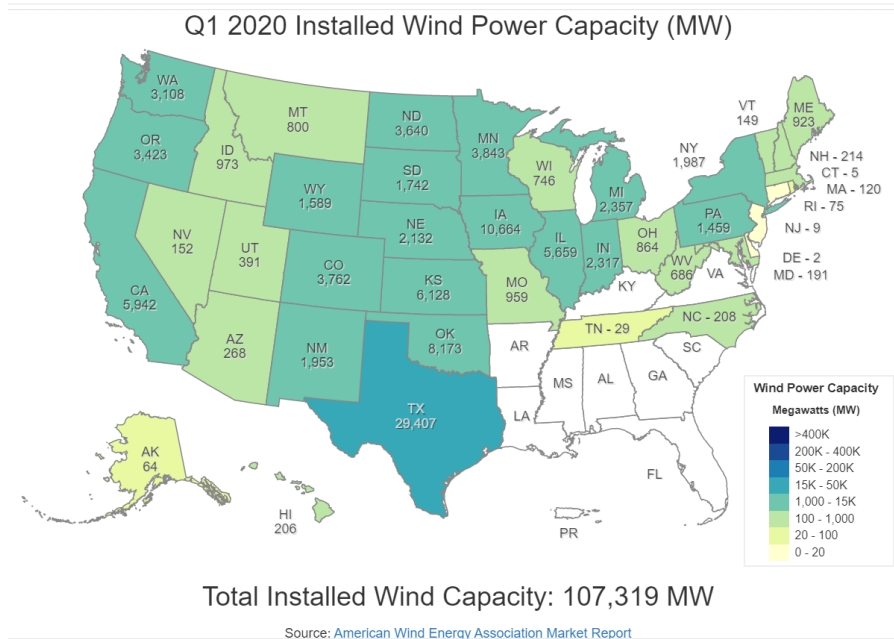


Fig. 1. U.S. Installed Wind Power Capacity in 2020 (U.S. EERE, 2020)

We have studied the effects of recent coal deregulations on the emissions of seven eastern states in the U.S. and projected an even faster rate of increase in emissions in the next several years (Khoie and Calderon, 2020).

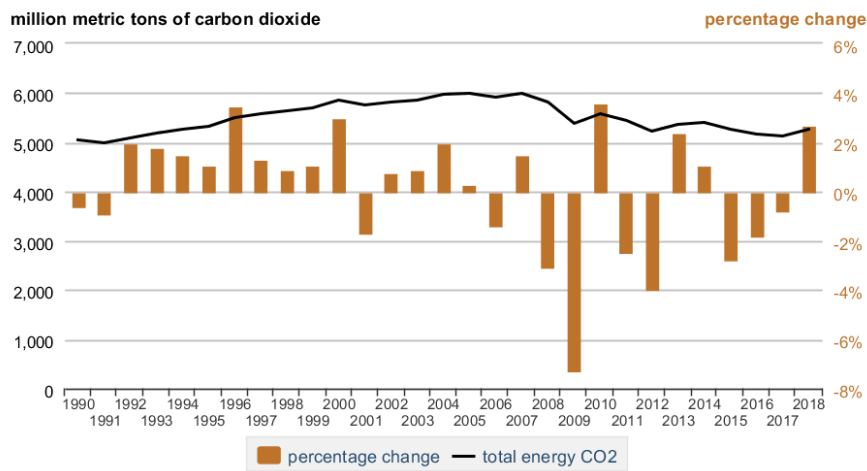


Fig. 2. Total and percentage of change in the U.S. energy-related carbon dioxide emissions. (U.S. EIA, 2020)

The second report is the National Oceanic and Atmospheric Administration 2018 Report on “Climate Change: Current and Projected Impacts on the U.S.” in which it was concluded that the time has reached for the need for removal of existing carbon from the atmosphere if we are to slow down the catastrophic consequences of continued rise in total global emissions and prevent the projected climate disasters by 2050 (NOAA Fahey, 2018). As such, there is no longer a debate that electricity generation from coal and other fossil fuels must be stopped immediately. There is also no doubt that our electricity generation should become 100% renewable as

soon as possible (Khoie, et. al., 2019). The warning by the National Oceanic and Atmospheric Administration necessitates a careful study of the carbon-neutrality of renewable generation in the U.S. and across the globe. This paper aims to analyze the carbon footprint (or carbon cost, or emissions intensity which is defined as CO₂ produced per kWh of electricity generated), and in particular, the emissions intensity of a 1.3 megawatts (MW) wind power located in the wind sweet spot of the U.S., namely, Panhandle of Texas.

2. Life Cycle Assessment

A number of researchers have developed models for Life Cycle Assessment of wind turbines mostly following International Organization for Standardization ISO Standard 14040 (ISO, 2006) by which the turbine is analyzed from cradle-to-grave including steps such as manufacturing, commissioning, operation, and retirement (Wind Energy, 2020), as shown in Fig. 3.

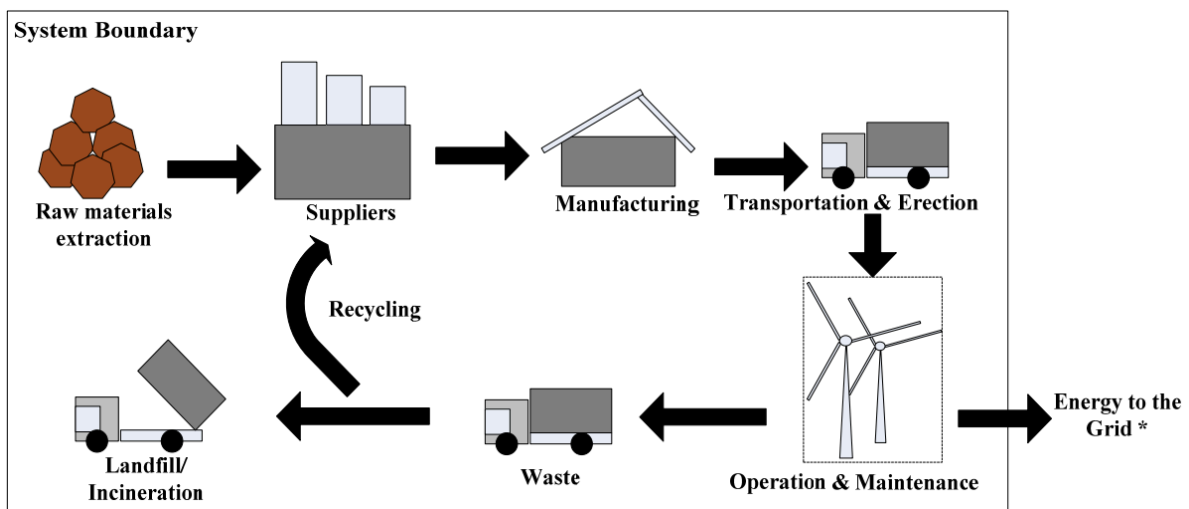


Fig. 3. Cradle-to-grave process in life cycle assessment of wind power generation (Garabedian, 2020).

Two distinct methods are generally used to quantify the carbon emissions produced throughout the lifespan of a turbine. The first method which is most commonly used is process-analysis (PA) which calculates the emissions based on the mass of the actual materials used in production. This method is a bottom-up approach that calculates the energy used in the materials in construction of a wind turbine including energy used in processes such as manufacturing, material handling, and transportation. This method focuses only on analyzing materials that are used in substantial quantities, thereby introducing errors in the results due to lack of consideration of materials that are not used in large quantities (Aversen and Hertwich, 2012). In spite of that, this method is generally considered a reliable approach to calculate the carbon emissions intensity.

The second method is the environmentally-extended input-output analysis (EEIOA) which calculates the emissions intensity using economic data. This method is a top-down approach that treats the entire economy as a system and calculates the emissions cost associated with transactions between various sectors of the economy. The emissions produced are then determined by calculating monetary value produced by each economic sector (Lieberman, 2003). This method tends to be more comprehensive but relies on the simplification that each sector produces one average product. Both methods have advantages and disadvantages, however, better accuracy can result by combining these two methods in various processes involved in wind power generation. In a comprehensive literature search we did, we found that of forty three studies, thirty six used process analysis, three used EEIOA, and four used a hybrid of both methods, in which various processes in wind power generation are modeled using either of the two methods depending on the availability of the data for each

specific process. The model described in this paper uses a hybrid analysis of various processes involved in wind power generation.

The actual power generated by wind is dependent on two major factors. The first is the size of the turbine. A search of literature shows that there is no linear (or even clear) relationship between the carbon emissions intensity of a wind turbine and its size, (Crawford, 2009), (Lenzen and Munksgaard, 2002), and (Aversen and Hertwich, 2012). Obviously, smaller turbines (below 750 kW) generally have higher emissions intensity with substantial fluctuations. No discernable trend can be found for any range of turbine size. Crawford (2009) found no significant difference in carbon emissions intensity in an 850 kW and a 3.0 MW turbine, with Lenzen and Munksgaard (2002) making the same observation and concluding that small turbines have roughly three times the intensities of larger turbines. Aversen and Hertwich (2012) found a logarithmic drop in intensities for turbines up to 1.8 MW. Our literature review determined a wide range of values for carbon emissions intensity of wind turbines of different sizes. The statistical data on the variation of reported intensities versus turbine size are tabulated in Table 1, showing substantial variation in reported data in the literature. In this study, we have selected a 1.3 MW wind turbine since its various parameters are more readily available in the literature.

Table 1: The range of values found from the wind power LCAs evaluated in literature review of forty three studies done by others.

Distribution Parameters	CO ₂ Intensity (g/kWh)
Minimum	3
Mean	13.6
Median	10.7
Maximum	34.4
Standard Deviation	7.76

The second important factor in the power generation of a windmill is its location. Various researchers have performed life cycle assessment of wind power in locations around the world including China (Liang, et. al., 2013), Europe (Tremeac and Meunier, 2009), (Guezuraga, et. al., 2012), and India (Lenzen and Munksgaard, 2002). In a study of renewable potential of the 18 southern states of the U.S., we (Khoie and Yee, 2015) reported a maximum renewable potential of state of Texas with 6,527 billion kWh of renewable resources, most of which in wind energy. As such we have selected the Panhandle of Texas as the location for this study.

3. The Hybrid Model

The model used in this study is a hybrid model in which carbon emissions intensity of various processes in the life cycle of wind turbine are determined using process analysis (PA) for raw materials and the environmentally-extended input-output analysis (EEIOA) for manufacturing, transportation, construction, and overhead/profit operations. We have selected a 1.3 MW Nordex N60/1300kW (Nordex, 2020) wind turbine (80 feet hub height) installed in the Panhandle of Texas. The main specifications of this wind turbine are listed in Table 2.

Table 2: Major specifications of Nordex N-60/1300 kW wind turbine. (Nordex, 2020)

Manufacturer	Nordex
Model	N-60 (80)
Hub Height (m)	80
Rated Power Output (kW)	1300
Rotor Diameter (m)	60
Rotor Swept Area (m ²)	2828
Cut - in Wind Speed (m/s)	3-4
Cut - out wind Speed (m/s)	25

Generated Power: The generated power by a wind turbine is given by Eq. 1: (Kalmikov and Dykes, 2020)

$$P = Cp \frac{\rho A v^3}{2} \quad Eq. (1)$$

where P is generated power (in W), Cp is the power coefficient (dimensionless with values ranging from 0.25 to 0.45), A is the blade swept area (in m^2) and v is the wind speed (in m/s).

Wind Speed: The wind speeds are taken from National Renewable Energy Laboratory using Typical Meteorological Year 3 -TMY3- data (NREL, 2015). Using the specifications provided by Nordex, the power curve of the Nordex N-60 turbine is then calculated as shown in Fig. 4.

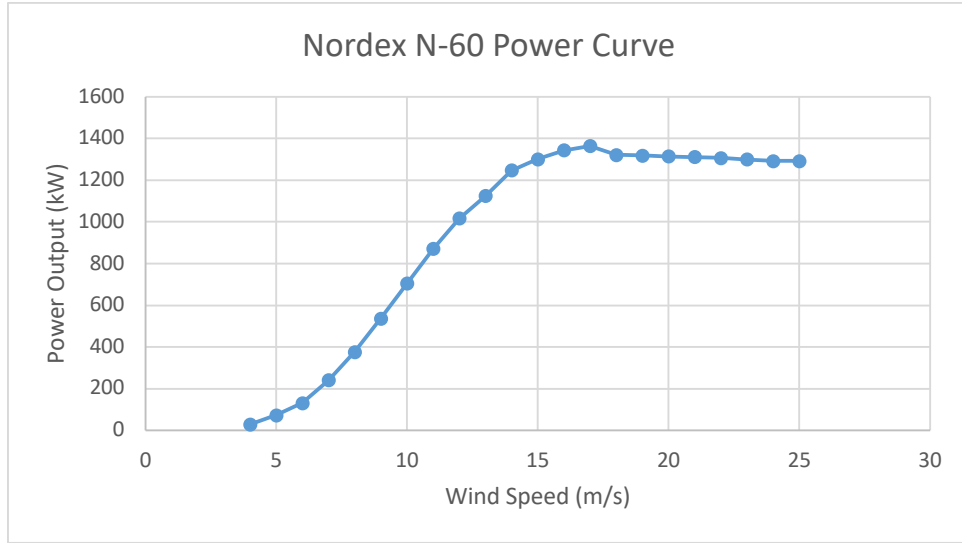


Fig. 4: Power curve of a Nordex N-60 wind turbine, generated power as a function of wind speeds. Data calculated from information provided by (Nordex, 2020).

Total Lifetime Energy Production: The lifetime energy production of the windmill is simply determined from the power curve of the wind turbine as given by Eq. 2:

$$Lifetime\ Energy\ Produced = \left(\sum_{1/1\ 1:00}^{12/31\ 24:00} Power\ Curve(Wind\ Speed) \cdot 3600s \right) \cdot 20yrs \quad Eq. (2)$$

The variables in Eq. 2 are:

Wind Speed: calculated from TMY3 hourly data.

Lifetime Energy Produced: calculated from Nordex power curve (Fig. 4) multiplied by 3600 seconds in each hour, summed over all the hours starting at 1:00 AM on January 1st ending at 12:00 midnight on December 31st, multiplied by a 20-year lifespan.

Life span of the turbine: taken to be 20 years (Crawford, 2009), (Lenzen and Munksgaard, 2002), and (Aversen and Hertwich, 2012). Using the wind speed data from Amarillo International Airport, the lifetime energy production of the Nordex N-60 wind turbine was determined to be 467 billion KJ.

CO₂ emissions Intensity: Eqs. (3) defines the emissions intensity of the wind turbine:

$$CO_2\ Intensity = \frac{Total\ CO_2\ Produced\ (g)}{Total\ Annual\ Electricity\ Production\ (kWh)} \quad Eq. (3)$$

The values of total CO₂ produced in various processes are calculated using either process analysis (PA) method or environmentally-extended input/output analysis (EEIOA) as described below.

Process Analysis (PA): is used to determine the CO₂ emissions resulting from the production of **raw materials** used in the wind turbine. In order to perform the process analysis the mass composition of the materials used in Nordex N-60 wind turbine, as well as the CO₂ emissions factors of each raw material are needed. The mass composition of the materials used in construction of the nacelle, rotor, and tower of the wind turbine (Including copper, steel, and glass-fiber reinforced plastic used in blades, hub, transformer, and gear-box) are provided by Liberman (2003). The materials used in the construction of the foundation are primarily concrete and steel rebar, which varies rather significantly based on the soil conditions. Nonetheless, we chose a 350 metric ton concrete which is right at the mean value of the range of 100 to 600 metric ton range of concrete foundations used in installation of the Nordex N-60 turbine. The mass of steel rebar used in the foundation is a dependent on the amount of concrete used. The mass of concrete ranges from 21.8 to 41.5 times the mass of rebar (Liberman, 2003). To study a worst case scenario, we used the 21.8 ratio and determined the mass of rebar to be 16 metric ton. The five primary materials used in the wind turbine are steel, glass-fiber reinforced plastic (GRP), concrete, copper, and oil products. The CO₂ emissions factors of each material were assigned based on various probability distributions (Liberman, 2003) and are tabulated in Table 3.

Table 3 - Assigned CO₂ emissions factors for raw materials used in the wind turbine. (Liberman, 2003)

Material	Assigned CO ₂ Emissions Factor (kg CO ₂ -eq/kg)
Steel	2.5
GRP	3.0
Concrete	0.2
Copper	6.33
Oil Products	1.44

Given the mass composition of materials used in the Nordex N-60 and CO₂ emission factors of each material as shown in Table 3, the emissions are then calculated for each material using:

$$CO_2 \text{ Emissions} = \text{Mass} * CO_2 \text{ Emissions Factor} \quad (Eq. 4)$$

where *Mass* is the mass of the material (kg), *CO₂ Emissions* are the CO₂ emissions resulting from production of the raw material (g), and *CO₂ Emissions Factor* is the CO₂ emissions resulting from raw material extraction/refining per unit mass (g CO₂ / kg material). The total emissions from each type of raw material is then summed over all materials used in the turbine.

Environmentally-Extended Input/Output Analysis (EEIOA): is used to determine the CO₂ emissions in various life stages of a windmill based on the cost of various components of the turbine. These components are: **manufacturing, transportation, construction, and overhead/profit**. The CO₂ emissions are given by:

$$CO_2 \text{ Emissions (g - CO}_2) = \text{Component Cost (\$)} * \text{Emissions Economic Factor} \left(\frac{g - CO_2}{\$} \right) \quad (Eq. 5)$$

where *Component Cost*, and *Emissions Economic Factor* for select materials are given in Tables 4 and 5 (Liberman, 2003) and (U.S. DOC BEA, 2020). Additional details of the model is presented elsewhere (Khoie, et., al., 2020).

Table 4: Samples of environmental factors in select manufacturing components. (Liberman, 2003)

Manufacturing Sector	CO ₂ Emissions Factor (kg- CO ₂ /\\$)
Transmission Equipment	0.86

Fabricated Steel Plate Work	1.16
Plastics	2.07

Table 5: Unit cost of select materials used in wind turbine. The data shown are mean values reported by others. (U.S. DOC BEA, 2020)

Material	Unit Price (\$/mt)
Copper and copper-base alloy	6,340
Steel castings	2,196
Carbon steel, plate, cut lengths	488
Carbon steel, wire rods	387
Lubricating oils	340
Concrete	48.5

Assumptions and Limitations of the Model:

The model used in this study has the following limitations based on either simplifying assumptions or worst case scenarios:

- 1) Offshore turbines are excluded due to complexities associated with offshore transportation and materials used for foundation.
- 2) The model assumes an unobstructed turbine, which neglects losses due to a reduction in the kinetic energy of wind as it passes through an entire wind farm.
- 3) This study assumes the wind turbine is operated as a single unit in the Texas Panhandle. This prevents the additional complexity produced when wind turbines are subject to wake effects caused in a wind farm.
- 4) We have intentionally chosen worst case scenarios including a 20-year lifespan of the windmill, (as compared to other who have assumed a 25-year lifespan (Kabir, et. al., 2012).
- 5) The carbon emissions of the following steps in the life cycle of the turbine are not included in our model: connection to the grid, de-commissioning and dismantling, recycling, and transportation after de-commissioning and landfill. While these steps contribute to the emissions, others have shown them to be either negligible or minor factors, or requiring rather complicated modeling (Aversen and Hertwich, 2012) (Guezuraga, et. al., 2012) (Martinez, el. al., 2009).

4. Results

The results of the Process Analysis model for environmental impacts of production of raw materials used in a 1.3 MW wind turbine (the turbine and its structure) are shown in Table 6. The total emissions for production of raw materials is 715 Mg - CO₂, with steel being the biggest contributor.

Table 6: Total CO₂ emissions (Mg- CO₂) for raw materials determined from PA model.

Material	Total CO ₂ Emissions (Mg- CO ₂)
Steel	558
Glass fiber Reinforced Plastic	72.3
Concrete	70
Coper	12.6
Oil Products	1.81
Total Raw Materials (PA Model)	715

The results of EEIOA model for transportation, construction, overhead/profit, and manufacturing are listed in Table 7. As shown in Table 7, the transportation, construction, overhead/profit, and manufacturing are

responsible for 307, 72.6, 10.9, and 765 Mg- CO₂ emissions, respectively, during the 20-year lifespan of the windmill. Table 8 shows the results of total emissions for all processes in the 20 years lifespan of a 1.3 MW windmill operating in Panhandle of Texas.

Table 7: Total CO₂ emissions (Mg- CO₂) for major wind turbine components (other than raw materials) determined using EEIOA model.

Major Components	Sub - Component	Total CO ₂ Emissions (Mg- CO ₂)
Transportation	Sea Freight	174
	Truck	133
Construction	Site Prep	7.56
	Remote Monitoring	7.56
	Erection/Commissioning	22.7
	Foundation	34.8
Overhead/Profit	Overhead	10.9
Manufacturing	Mechanical Power Transmission Equipment	340
	Fabricated Plate Work	153
	Plastics Materials Resin	272
Total	(EEIOA Model)	1,155.52

Table 8: The results of total CO₂ emitted by a 1.3 MW wind turbine operating in the Panhandle of Texas for 20 years.

Material	Total CO ₂ Emissions (Mg- CO ₂)
Raw Materials (PA Model)	715
Manufacturing, Transportation, Construction, and Overhead/profit (EEIOA Model)	1,155.52
Total (Lifetime)	1,870.52
Total (Annual)	93.53

Table 9: The summary of results of CO₂ emissions intensity of a 1.3 MW wind turbine operating in the Panhandle of Texas for 20 years. Also included are those of a similar average coal power plant (Liang, et. al., 2013).

Energy	Total Energy Output (TJ)
Annual Energy Output	23.3 TJ/Year = 6,472,222 kWh/Year
Lifetime (20 Years) Energy Output	466 TJ/Lifetime = 129,444,444 kWh/Lifetime
Intensities	Amount/Total Energy Output
CO ₂ Emissions Intensity (Wind)	1,870.52 Mg CO ₂ /466 TJ = 14.45 g-CO₂/kWh
CO ₂ Emissions Intensity (Coal) (Liang, et. al., 2013)	792 g-CO ₂ /kWh

Table 9 shows these results in terms of CO₂ emission intensity. With an annual electricity production of 23.3 TJ/Year, a 1.3 MW windmill in a location near the Amarillo International Airport produces 466 TJ of electricity

(129,444,444 kWh) operating over 20 years. The lifetime CO₂ emissions of this windmill is 1,870.52 Mg- CO₂ resulting in emissions intensity of 14.45 g- CO₂ /kWh, respectively.

Compared to the average CO₂ emissions intensity of coal generated electricity of 792 g-CO₂ /kWh (Liang, et. al., 2013) and (Tang, et. al., 2014), this windmill produces only 1.82% emissions of a similar size coal power plant, which is while substantial (98.2%) savings in emissions, it is not insignificant, especially with high penetration of wind energy in electricity sector in the coming decades. Our result, while in general agreement with those reported by others, is higher than the mean value of 13.6 g-CO₂ /kWh for emissions intensity.

5. Conclusions

The results of this study shows that a 1.3 MW Nordex N-60 wind turbine operating near the Amarillo International Airport (in Panhandle of Texas) has carbon dioxide intensity of 14.45 g- CO₂ /kWh, respectively. When compared to the carbon dioxide intensity of 13.6 g - CO₂/kWh, reported by others, our model overestimates carbon emissions by 6.6%. This difference is in large part due to the assumptions we have made in our model as listed above. Compared to coal power plants the wind turbine studied here emits 1.8% of carbon dioxide.

For the twelve months ending September 2019, the United States generated 286.6 terawatt-hour of wind power, roughly 7% of all generated electricity (Wind Power Monthly, 2020A). Our study shows that this wind generation in 2019 has produced roughly 4.13 million tons (MT) of CO₂ emissions, which is 98.2% less emissions than if this power had been generated from coal power plants. Nonetheless, this 4.13 MT emissions needs to be removed from the atmosphere, for the wind power to be truly carbon neutral. With the projected deeper penetration of wind in the U.S. electricity portfolio, the issue of emissions by wind power will become even more pressing, especially if the goal is to remove carbon from the atmosphere as suggested in 2018 by the National Oceanic and Atmospheric Administration.

6. References

- (Aversen and Hertwich, 2012) A. Arvesen and E. G. Hertwich, "Assessing the life cycle environmental impacts of wind power: A review of present knowledge and research needs," *Renewable and Sustainable Energy Reviews*, vol. 16, pp. 5994-6006, 2012.
- (Crawford, 2009) R. H. Crawford, "Life Cycle energy and greenhouse emissions analysis of wind turbines and the effect of size on energy yield," *Renewable and Sustainable Energy Reviews*, vol. 13, pp. 2653-2660, 2009.
- (Garabedian, 2020) K. Garabedian, "Wind power life cycle assessment," <https://storymaps.arcgis.com/stories/>, Accessed June 2020.
- (Guezuraga, et. al., 2012) B. Guezuraga, R. Zauner and W. Polz, "Life cycle assessment of two different 2 MW class wind turbines," *Renewable Energy*, vol. 37, pp. 37-44, 2012.
- (GWEC, 2029) "China Wind Energy," Global Wind Power Council, Beijing, China, October 21-24, 2019. <https://gwec.net/china-wind-power-2019/>, Accessed: June 2020.
- (ISO, 2006) International Organization for Standardization, Environmental management - Life cycle assessment - Principles and framework, <https://www.iso.org/obp/ui/#iso:std:iso:14040:ed-2:v1:en> (Accessed: June 2020).
- (Kabir, et. al., 2012) M. R. Kabir, B. Rooke, M. Dassanayake and B. A. Fleck, "Comparative life cycle energy, emission, and economic analysis of 100 kW nameplate wind power generation," *Renewable Energy*, vol. 37, pp. 133-141, 2012.

- (Kalmikov and Dykes, 2020) A. Kalmikov and K. Dykes, "Wind power fundamentals," MIT, <http://web.mit.edu/windenergy/windweek/Presentations/Wind%20Energy%20101.pdf>, Accessed: June 2020.
- (Khoie and Yee, 2015) R. Khoie and V. Yee, "A forecast model for deep penetration of renewables in the Southwest, South Central, and Southeast regions of the United States," *Clean Technologies and Environmental Policy*, Vol. 17, No. 4, pp. 957-971, 2015.
- (Khoie, et. al., 2019) Rahim Khoie, Kyle Ugale, and James Benefield, "Renewable resources of the northern half of the United States: potential for 100% renewable electricity," *Clean Technologies and Environmental Policy*, Vol. 21, pp. 1809–1827, 2019.
- (Khoie and Calderon, 2020). Rahim Khoie and Antonio Calderon, "Forecasting Carbon Emissions in Seven Eastern States of the United States; The Effects of Coal Deregulations," Conference Proceedings of SOLAR 2020, *American Solar Energy Society 49th National Solar Conference and Summit*, Washington, DC, June 24-25, 2020.
- (Khoie, et. al., 2020) Rahim Khoie, Andrew Bose and Joshua Saltsman, "A Study of Carbon Emissions and Energy Consumption of Wind Power Generation in the Panhandle of Texas," Submitted to *Clean Technologies and Environmental Policy*, July 2020.
- (Lenzen and Munksgaard, 2002) M. Lenzen and J. Munksgaard, "Energy and CO2 life-cycle analyses of wind turbines-review and applications," *Renewable Energy*, vol. 26, pp. 339-362, 2002.
- (Liang, et. al., 2013) X. Liang, Z. Wang, Z. Zhou, Z. Huang, J. Zhou and K. Cen, "Up-to-date life cycle assessment and comparison study of clean coal power generation technologies in China," *Journal of Cleaner Production*, vol. 39, pp. 24-31, 2013.
- (Lieberman, 2003) E. J. Lieberman, "A LIFE CYCLE ASSESSMENT AND ECONOMIC ANALYSIS OF WIND TURBINES USING MONTE CARLO SIMULATION," Air Force Institute of Technology, Wright-Patterson Air Force Base, 2003. <https://apps.dtic.mil/dtic/tr/fulltext/u2/a415268.pdf>, Accessed: June 2020.
- (Martinez, et. al., 2009) E. Martinez, F. Sanz, S. Pellegrini, E. Jimenez and J. Blanco, "Life cycle assessment of a multi-megawatt wind turbine," *Renewable Energy*, vol. 34, pp. 667-673, 2009.
- (NOAA, Fahey, 2018) National Oceanic and Atmospheric Administration, 2018. David Fahey, "Climate Change: Current and Projected Impacts on the U.S.," ASES SOLAR 2018, Pathways to the Renewable Energy Transformation, August 5-8, 2018, Boulder, CO. Also See: <https://www.noaa.gov/climate-data-and-reports>, Accessed June 2020.
- (Nordex 2020), "N60/1300KW," Nordex, <https://www.yumpu.com/en/www.nordex-online.com> Accessed: June 2020.
- (NREL, 2015) Solar Resource Characterization Project, "NSRDB: 1991 - 2005 Update: TMY3," National Renewable Energy Laboratory, 19 January 2015. [Online]. Available: http://rredc.nrel.gov/solar/old_data/nsrdb/1991-2005/tmy3/. Accessed: June 2020.
- (Tang, et. al., 2014) L. Tang, T. Yokoyama, H. Kubota and A. Shimota, "Life cycle assessment of a pulverized coal-fired power plant with CCS technology in Japan," *Energy Procedia*, vol. 63, pp. 7437-7443, 2014.
- (Tremeac and Meunier, 2009) B. Tremeac and F. Meunier, "Life cycle analysis of 4.5 MW and 250 W wind turbines," *Renewable and Sustainable Energy Reviews*, vol. 13, pp. 2104-2110, 2009.
- (U.S. DOC BEA 2020) U.S. Department of Commerce, Bureau of Economic Analysis, Gross Output by Industry, <https://www.commerce.gov/data-and-reports/economic-indicators>, see <https://apps.bea.gov/iTable/iTable.cfm> Accessed: June 2020.

(U.S. EERE, 2020) U.S. Office of Energy Efficiency and Renewable Energy, WINDEXchange, “U.S. Installed and Potential Wind Power Capacity and Generation,” <https://windexchange.energy.gov/maps-data/>, Accessed: June 2020.

(U.S. EIA, 2020). U.S. Energy Information Agency, 2020. <https://www.eia.gov/environment/emissions/> Accessed: June 2020.

(Wind Energy, 2020) “LCA in Wind Energy: Environmental Impacts through the Whole Chain.” Wind Energy, The Facts, <https://www.wind-energy-the-facts.org/lca-in-wind-energy.html>, Accessed: June 2020.

(Wind Power Monthly, 2020A), “Wind was primary U.S. renewable source in 2019,” Wind Power Monthly, <https://www.windpowermonthly.com/article/1680622/wind-primary-us-renewables-source-2019>, Accessed: June 2020.

(Wind Power Monthly, 2020B), “European offshore wind investment to overtake upstream oil and gas by 2022,” Wind Power Monthly, <https://www.windpowermonthly.com/europe>, Accessed: June 2020.

House in a House

Regin Schwaen, MAA

Department of Architecture, School of Design, Architecture + Art, North Dakota State University
Fargo, ND (United States)
regin.schwaen@ndsu.edu

Abstract

There is a significant amount of existing domestic housing stock in the United States that is ready to be insulated and retrofitted for improved energy performance. These existing houses can be upgraded to be more climate responsive extending their efficient occupancy for many decades to come. Instead of replacing or demolishing existing dwellings, they should be retrofitted so the environment is not burdened with inefficient houses. This concept limits the deterioration of neighborhoods, landfills are not overwhelmed with waste, and ultimately reduces greenhouse gas emissions. This paper is a case study that demonstrates the strategies incorporated to make a dwelling more climate responsive. The upgrade includes a rainscreen in conjunction with a crisscrossing lattice system mounted on a sub-façade, plus the addition of an interconnected passive ventilation system at the roof ridge. This paper examines the techniques utilized to install the rainscreen and how this system mitigates heat gain from solar radiation on the sub-façade, roof, and insulation. The idea is to construct and live in a house in a house.

Keywords: Sub-façade, rainscreen, heat mitigation, ventilation box, passive cooling

1. Introduction

The project uses existing technologies that can be applied in an innovative, economical and to some degree, when compared to existing methods, more efficient way. The concept is to externally refurbish existing dwellings; making already constructed houses climate responsive with passive cooling. The question is how to execute the retrofit in a cost-efficient manner that addresses both winter and summer conditions.



Fig. 1: Refurbished north façade – House in a House

The problem in refurbishing existing dwellings with new insulation is, in most cases, limited to the existing 2x4 wall framing system. Instead of creating access to the old 2x4 structure, the existing dwelling in the case study was wrapped with a new 2x10 insulating structure. Homeowners that have excessive heating loads might want to retrofit and add insulation to their house, but often fear the expenses associated with an approach that in most cases is intrusive and cumbersome. The house in a house idea eliminates this problem.

In the case study presented here is a dwelling from 1919, wrapped in a modern structure that was completed in 2019. In this project, known as the Cloud House, new extends old. In this approach the environment is not burdened with old dwellings simply being tossed away, instead existing dwellings are given new resiliency, reinvigorating existing neighborhoods while reducing greenhouse gas emissions.

2. Passive cooling

This case study is presented in twelve steps that illustrate how one can easily apply passive heating and passive cooling to an existing domestic dwelling. Most figures are extracted from evidence-based deployment in the field.

One: The Cloud House is situated in Fargo, North Dakota. The north façade received a new brise soleil that was executed in cedar (see figure 1). A brise soleil is excellent for ventilation and providing shadow. The dimension of each cedar element is 1 x 2's, not stacked tightly, but mounted with a negative space that allows for wind to pass through. A brise soleil should be set on sleepers with fine mesh applied to the surface facing the sub-façade.



Fig. 2: Original dwelling and refurbished dwelling

Two: The case study house originally had a stucco façade and was not executed with any insulation in the walls. The building is located in a climate with +80 degrees Fahrenheit temperatures in the summer and -40 degrees Fahrenheit in the winter. The building was wrapped and retrofitted with a new structure that contains insulation and a new rainscreen that prioritizes passive cooling in its design (see figure 2). The addition to the Cloud House includes a brise soleil on the south façade, similar to the one on mounted on the north façade (see figure 1).

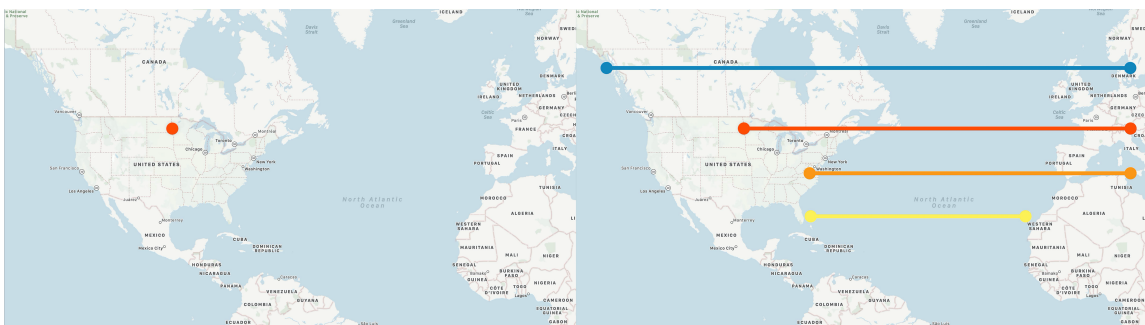


Fig. 3: Fargo, North Dakota and sunlight in relation to other areas

Three: In Figure 3, note that Fargo, North Dakota, is slightly north of Venice, Italy, Washington DC is at the same latitude as Palermo, Sicily, Miami is at the same latitude as Western Sahara, and the panhandle of Alaska is at the same latitude as Copenhagen, Denmark. The entire lower 48 states could learn from design solutions that many Mediterranean cultures developed when designing in relation to sunlight.

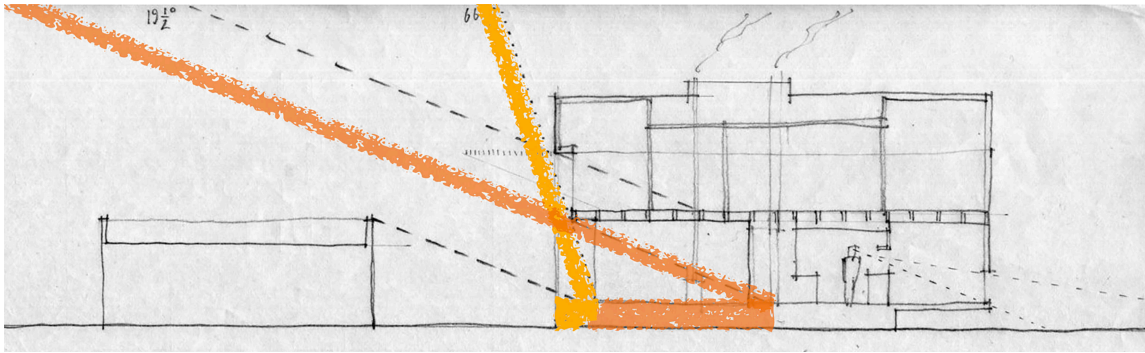


Fig. 4: Sketch regarding sunlight in summer and winter

Four: Early sketches of the Cloud House design account for the noon sun position on the 21st of June and noon sun position for the 21st of December (see figure 4). Sunlight should be considered and studied by architects and engineers when designing and working together. Designing and operating technical equipment for climate-controlled-interiors should include passive heating and passive cooling solutions as well. This sketch explores the geometry between sun and earth and how to invite sunlight into a building during winter and excluding direct sunlight from interior spaces during summer.

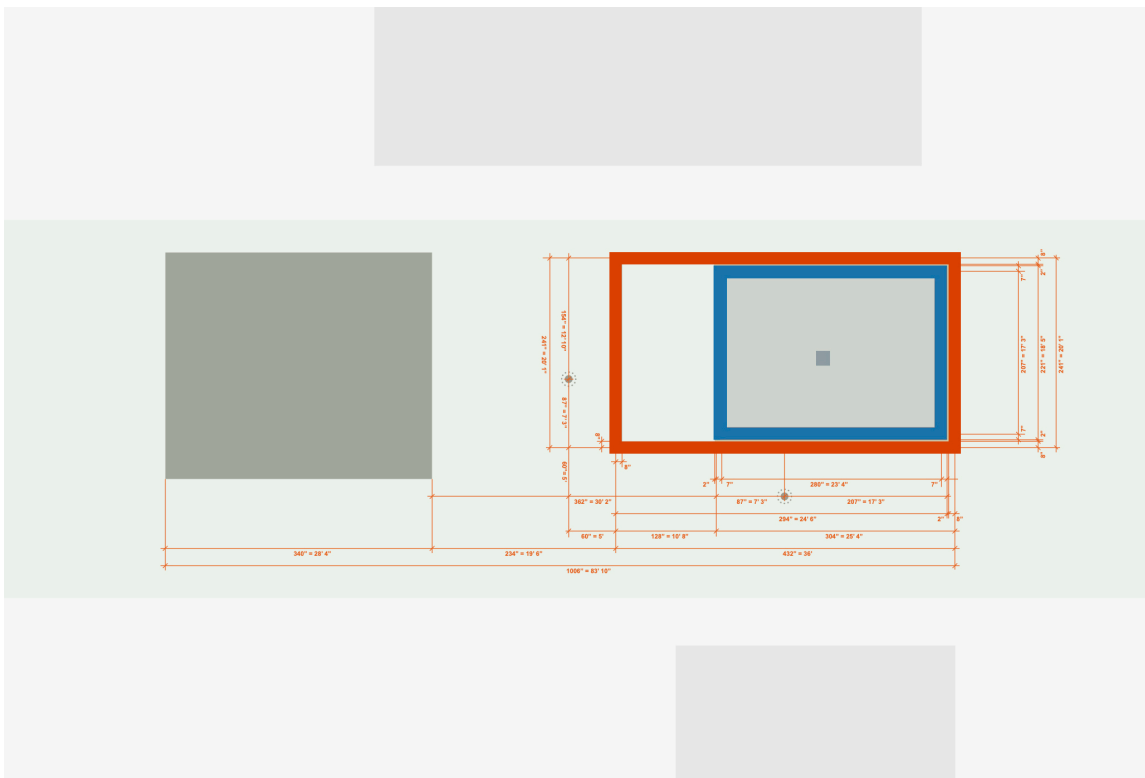


Fig. 5: Idea for a house in a house

Five: The plan in figure 5 is the essence of this concept for how to preserve and refurbish an existing dwelling with the house in a house approach. Almost any existing dwelling can be modified by expanding a new outer foundation in any direction. Zoning setback or urban context must be taken into consideration in any new design or alterations. The plan outlines the existing foundation in blue color and outlines a new foundation in red. The old foundation is framed by the new foundation creating a house in a house. Figure 5 also displays a garage to the left of the house, in dark gray. Neighboring houses, in light gray, can be seen outside the property indicated with a light green color. North is to the right.

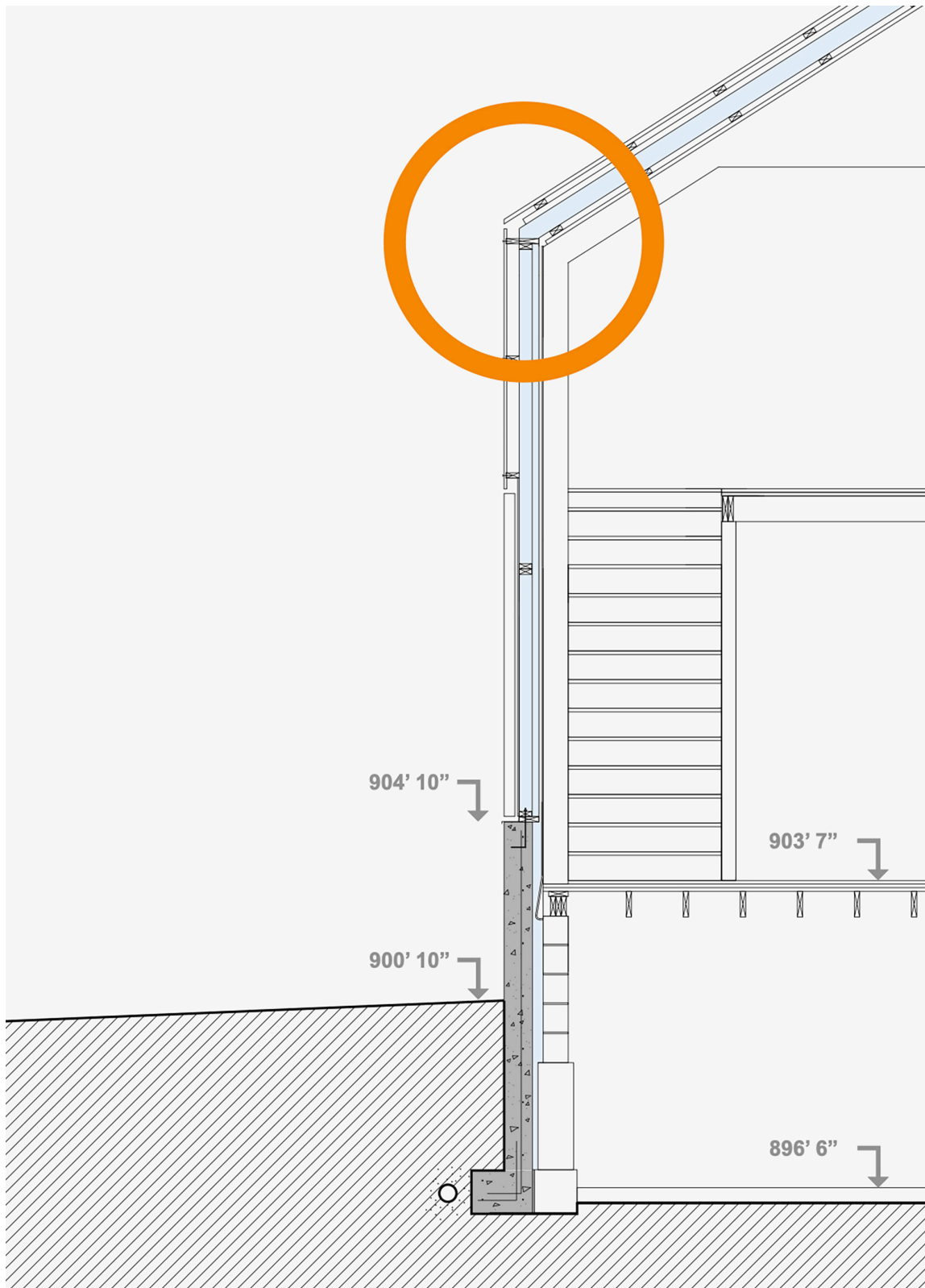


Fig. 8: Section of façade and roof

Eight: Figure 8 highlights a detail on how to mount rainscreen and roof, both floating on crisscrossing sleepers and latticework. The new structure is indicated in a very light blue color. The new rain gutter is missing in this drawing; refer to partly installed gutter as seen in figure 10 instead.



Fig. 9: Completing the crisscrossing lattice system for ventilation on façade

Nine: A layer of the 2x4 crisscrossing lattice system has been mounted on top of the sub-façade (figure 9, left). This is a simple and efficient solution to generate passive cooling behind a rainscreen. Notice that the large arrow in figure 9 points at the very first horizontal 2x4 that was mounted for the crisscrossing lattice system. The white lines indicate all the horizontal 2x4's that complete the crisscrossing lattice system that carry the rain screen. Simply mount any rain screen to a crisscrossing lattice system, in this case Galvalume was selected for the façade, and tie into a large ventilation box on ridge cap, and by doing so, create a cost-effective passive cooling system.



Fig. 10: Completing the crisscrossing lattice system for ventilation on roof

Ten: Almost all dwellings have a ventilation ridge, it is not a new idea, but they are rather simple and small in proportion. There are only very few design options for a ventilated ridge cap that targets residential buildings. The large ventilation ridge box not only collects all ventilation air behind the rainscreen, but also collects various other installations centrally, such as smokestack and pipes, eliminating perforation of roof or façades.



Fig. 11: Galvalume, crisscrossing lattice system, weather-resistant barrier

Eleven: A small sample of the brise soleil can be seen in the very right corner of the south façade in figure 11. When the brise soleil has been mounted on sleepers on top of the weather-resistant barrier that is protecting the sub-façade, it will help develop air convection initiating passive cooling. The brise soleil is constructed with a very fine mesh between sleepers and weather-resistant barrier preventing insects from entering the ventilation space. Notice the crisscrossing lattice system behind the ladder on the very left in figure 11, still exposed in this photograph, being applied a Galvalume siding that will complete the east and west façades. An efficient passive ventilation was made possible by combining the brise soleil with ventilation along all edges of the Galvalume and the ventilation box on the ridge.



Fig. 12: Passive cooling

Twelve: The façades, executed in wood on south and executed in metal on east and west, perform simultaneously and in unison regarding cooling (see figure 12). The orange arrow indicates how excessive hot air, generated behind the Galvalume, exits the ventilation box. The white arrows highlight the eastern area of the south façade; however, the arrows should be mirrored on the south façade, and applied to the north façade as well.

3. Cool aesthetics

The idea of a house in a house was first introduced to me when working on various design projects for architect Oswald Mathias Ungers in Berlin. The theoretical approach is full of temptations, but without deployment in the field there would not be any strategy, reflection, or feedback. The objective in this paper, to apply a rainscreen on a crisscrossing substructure generating passive cooling, emerged from an idea that originated from a very different problem. The ventilation box was primarily an aesthetic solution. It was first designed to merge all pipes that vent

the interior of the Cloud House. I wondered why roofscapes on dwellings are often poorly designed, or why so many architects would design a roof as a single membrane, only to see the rainscreen or roof be compromised by a number of penetrations? From a technical point a roof should never be compromised by installations that emerge from below; resulting in a potential leak. In the design of the Cloud House the lifespan of the roof is longer, as no surface of the roof has been compromised by poking large holes anywhere. The only compromise was to fasten the corrugated Galvalume to the crisscrossing substructure (figure 7, 9, 10, 12, 13 and 14). An unexpected benefit for the new ventilation box was that it could serve as a vehicle for passive cooling. When executed, it was easy to see why the house in a house approach would not be theoretical, or just an idea, but pragmatic. However, it is maybe a philosophical question instead: Should all existing dwellings be revitalized so we can live better tomorrow? The refurbishment of any project is to honor what is. It is an opportunity to alter and adjust what was set in motion decades or centuries ago. The future invites us to recognize that nature is not abundant, but limited to site, situation, seasons, and resources, encouraging architects to collaborate with engineers and experts to find a path to reshape current dwellings in a cost-efficient way. The house in a house is an idea, and an approach, for how to upgrade any dwelling in almost any location, however, from a professional point of view, it is especially joyful embracing areas of extreme exposure such as summer and winter on the Great Plains in North Dakota.



Fig. 13: The retrofitted dwelling seen from the northeast corner



Fig. 14: Upgraded south façade – House in a House

4. References

Media:

A place in the Clouds. Tammy Swift. The Forum. Newspaper. Fargo 2012. Section B. Pg. 1, pg. 3.

Cloud House, a flood proof home in Fargo. Paul Gleye. Design & Living Magazine. 2019. Pg. 77-81.

Fargo's Urban Cabins, Plains Art Museum Progressive Architecture. Tracy Nicholson. Midwest Nest. Ed. 26. 2019. Pg. 28-38.

Proceedings:

Fieldwork: The House as a Camera. Regin Schwaen, Meghan Duda. Working Out, thinking while building. 2014 ACSA Conference, Halifax, Nova Scotia, Dalhousie University, Canada. ISBN 978-0-935502-94-7. Pg: 16-23.

Books:

Oswald Mathias Ungers, Works and Projects 1991/1998, first ed. 1998, Electa, Milano, ISBN 1-904313-00-0

Salmela architect, Thomas Fisher, preface by David Salmela, first ed. 2005, University of Minnesota Press, USA, ISBN 0-8166-4257-5

Constructing Architecture: Materials, Processes, Structures; A handbook by Andrea Deplazes, second ed. 2008, Birkhäuser, ISBN 978-3-7643-8631-3.

SUSTAINABLE SOLAR WATER PUMPING FOR IRRIGATION IN BANGLADESH

Md. Sakil Ibne Sayeed¹, Robert E. Foster², Md. Mushfiqur Rahman³

¹ Project Director, Bangladesh Rural Electrification Board (BREB), Dhaka (Bangladesh)

² Team Leader, Sheladia Associates, Rockville, Maryland (USA)

³ Deputy Team Leader, Sodev, Dhaka (Bangladesh)

ABSTRACT

Solar water pumps (SWPs) are a mature, reliable, and economically attractive climate smart sustainable agricultural technology solution for responsible crop irrigation. The Government of Bangladesh (GoB) is implementing a large SWP project through Bangladesh Rural Electrification Board (BREB) named “Photovoltaic Pumping for Agricultural Irrigation (SPPAI)” project which is a subproject of Power System Efficiency Improvement Project of Asian Development Bank (ADB). The project aims to install 2,000 solar pumping systems in Bangladesh for irrigation with the objective to reduce the pollutants emitted by diesel driven pumps, reduction of grid power surges during irrigation season and diffusion of solar pumping systems throughout the country. Key challenges for SWP dissemination include market access, financing, and irrigation subsidies. This paper describes SWP technologies, lessons learned in Bangladesh, implementation challenges, project design, and economics, as well as key takeaways in providing reliable SWP solutions for a more sustainable agricultural sector in the age of climate change.

Keywords: Photovoltaics, solar water pumping, irrigation, sustainable agriculture, Bangladesh.

1. INTRODUCTION

Bangladesh is based on an agricultural economy which contributes about 20 percent of the national GDP. Approximately 3/4 of Bangladesh’s population and its workforce lives in rural areas and directly or indirectly relies on agriculture. At present, Net Cultivable area in Bangladesh is more than 8.5 million hectares whereas about 65% of the net cultivable area is irrigated (BADC, 2019). Currently there are more than 1.58 million pumps used in irrigation system of which 78.5% are operated by diesel engines; approximately 21.4% are operated by electricity; and approximately 0.2% are operated by solar (BADC, 2019). Diesel operated pumps yearly consumes 1 million ton of diesel (worth \$900 million) at a subsidized rate (World Bank, 2016) while emitting 3.22 million tons of CO₂. In addition, during the peak irrigation season 2,000 MW of power demand is solely required for running the electricity operated pumps (Al-Amin, 2017) which is provided at a subsidized rate for irrigation. A significant amount of subsidy could be reduced if a portion of diesel and electricity driven pumps could be replaced by SWPs.

Irrigation is an important component of the Bangladesh agriculture sector and allows smallholder farmers to increase yields and grow an additional crop a year, receiving higher off-season prices. Diesel water pumps are commonly used, but fuel and transport costs are high; as a result, without a government fuel subsidy, diesel irrigation would not be cost effective for farmers. Farmers using electricity operated water pumps for irrigation receives also a special subsidized tariff of about US\$0.04 per kWh but pumping restricted to off-peak utility load hours.

Bangladesh a low-lying delta river country, is vulnerable to climate change and already suffering saltwater intrusion along the coast. Despite that, Bangladesh is showing its leadership in climate change mitigation measures and stands as global champion to tackle adverse impacts of climate changes. The use of solar water pumps (SWPs) to displace contaminating diesel water pumps is a positive step in adopting a clean energy future. These diesel units are typically not very efficient (less than seven percent) and emit carbon emissions that further contribute to climate change. Diesel particulate emissions are highly damaging and proven carcinogens. SWPs are a logical solution to improve this situation. There are new opportunities emerging in the transition from diesel to solar power for Bangladeshi farmers.

The Bangladesh Agricultural Development Corporation (BADC) estimates that there are 1.24 million diesel-run pumps used for agricultural irrigation in Bangladesh (BADC, 2019). Operating costs for these pumps is about ~US\$900 million every year for the one million tons of imported diesel fuel needed to run Bangladesh diesel irrigation systems (World Bank, 2016). Diesel fuel is subsidized by about 30 percent by the Government of Bangladesh (GoB), totaling over US\$400 million per year in government subsidies (BADC, 2019). So for every liter of diesel fuel sold in Bangladesh, it costs GoB subsidy funding. Depending on the volatility of fuel

prices, diesel pumps cost about US\$0.40 per kWh to run, or nearly four times the cost of a SWP amortized over 20 years.

In Bangladesh there are also 338,870 electricity operated irrigation pumps (BADC, 2019). The subsidized electricity tariff for irrigation is BDT 4.0/kWh (US\$0.047/kWh) and a 20 percent rebate is provided from GoB at the end of the year. Considering the rebate, tariff rate becomes BDT 3.20/kWh (US\$0.037/kWh). The seasonal irrigation period is about 5 months (Nov-Mar) and total cost of irrigation is BDT 3,600 to 13,500 per year (US\$70/season).

SWPs are a mature, reliable, and economically attractive solution for water supply including for large-scale crop flood irrigation (IRENA, 2016). With ever increasing reliance on water pumping for food security needs in the age of climate change, and somewhat limited access to reliable electricity for many farmers, market development for pumping systems needs to be accelerated to further adoption through development programs such as this ADB/BREB project. Market access, financing and educational challenges for SWPs still exist in Bangladesh, which SPPAI activities aim to help overcome. Cost-effective off-season production using SWPs can help increase the competitiveness and bottom line of Bangladeshi farmers. SWPs can foster resiliency that helps farmers and market systems diversify risk to prepare for and thrive during economic, political, climate, and natural disaster shocks (Sheladia, 2019).

Water access is a key constraint for Bangladeshi farmers in the dry season, with water pumping required from about 3 to 4 months each year depending on location. Irrigation is critical to addressing food security challenges in the country. Bangladesh has ensured access to electricity for 97 percent of its population and by 2021 plans are to reach near 100%. GoB has improved reliability of the grid and taking necessary steps to improve it further. Diesel fuel costs are prohibitive to meet irrigation needs and only made possible with government subsidies, but solar powered irrigation systems can be economically deployed as an affordable and clean energy solution for agriculture sector and save GoB money on subsidized irrigation tariffs and diesel fuel subsidies. Climate smart irrigation using SWPs allows Bangladeshi farmers to farm an additional harvest and produce off-season vegetables and crops that garner higher prices. Climate smart agriculture couples an array of technologies besides SWPs, like shallow tube wells, lift irrigation, canal maintenance and rehabilitation, drip irrigation, sprinklers, water harvest tanks, and multi-use water systems.

Examples of successful large-scale SWP projects initiatives include projects in India, Nepal, Kenya, Mexico, etc. They demonstrate how to successfully overcome market barriers and demonstrate that challenges can be surmounted through public-private partnerships that take advantage of relative cost savings, increased reliability of both solar power and improved irrigation systems, and improved technology access through innovative financing or leasing arrangements (Foster, 2013). The initial ADB feasibility study (FS) indicates that up to 11 kW (pump size) is feasible (ADB, 2017), however did not initially consider on-grid options which could be economically expanded well beyond this size (Sheladia, 2019). The SPPAI team found many examples of 20 to 40 kWp solar and diesel water pumps already used in the field with the largest off-grid existing SWP system being ~65 kWp. In other countries like USA, grid-tied SWPs can exceed 100 kWp array size and offer an extra cash bonus to farmers selling energy back to the grid when not pumping.

Solar water pumping improves people's lives, protects the environment, increases economic activity, and helps safeguard people's health. The key to any successful project is to have a framework for long-term success. Solar-electric systems are commercially available today to meet a wide range of both urban and rural applications, from small to large scale. Institutional and market frameworks exist to successfully operate and maintain them. For long-term success of solar pumping systems, relevant mechanical and hydraulic aspects must be considered, during the phases of initial design, installation, and future maintenance.

2. SPPAI PROJECT BACKGROUND

Bangladesh Rural Electrification Board (BREB) is a non-profit semi-government autonomous organization, specializes in rural electrification and a pioneer in the field of diffusion of solar energy in Bangladesh. Over the last three decades BREB is playing a vital role in promoting environment friendly clean energy especially the solar energy in rural Bangladesh with the belief that "Energy Saved is Energy Produced". BREB pioneered the installation of Solar Home Systems (SHSs) through the first ever solar energy project in Bangladesh in 1993. Since then BREB has installed 15,250 Solar Home Systems (SHSs); 50,518 Solar Plants through consumers; 37 rooftop/hybrid type rooftop solar power plants; 40 solar powered irrigation pumps; 14 Solar Electric Auto Rickshaw Charging Stations; 191 solar plants connected to the national grid through net metering; and 4,000 solar streetlights. About 150 Solar Mini/Micro-grids are now being installed and 6,000 SHSs will be installed very soon.



The total capacity of the installed plants is about 24.2 MW_p. The main objective of BREB Renewable Energy program is piloting new type of renewable energy projects in the context of grid power limitations and promoting the uses of alternatives energy source. Considering the financial concept of PBS i.e. “No profit, No Loss” and cost effectiveness of solar systems, grant financing from development partners on renewable energy projects are always preferable.

In 2011-12, to introduce irrigation through solar energy, BREB installed 40 Solar Powered Irrigation Pumps with the support from Korea International Cooperation Agency (KOICA) and Climate Change Trust Fund (CCTF) of GoB. In recent years, steady awareness is growing on environmentally friendly irrigation using solar PV operated pumps in Bangladesh. With the objective to reduce the pollutants emitted by diesel driven pumps, reduction of any sudden surge of grid power during irrigation season through Solar Pumping Systems in the country, BREB is implementing a SWP project named “Solar Photovoltaic Pumping for Agricultural Irrigation Project” funded by GoB, BREB and ADB [Loan 2769-BAN, Grant 0583-BAN (EF) & 0584-BAN (EF)] to install 2000 solar irrigation pumps at 10 PBS area. The SWP project was originally conceived as a new additional component of ADB Loan 2769-BAN in 2018.

Initially the key objective of BREB is to disseminate 2,000 SWPs (~19.3 MW_p) under 10 Palli Biddyt Samity (PBS), local electric cooperative, commanding area in 10 districts, develop a sustainable business model and strengthen the rural economy by decreasing cost of irrigation in long term as well as increasing income from agriculture. The project was originally focused on rural off-grid areas, but many of these areas have now been electrified. Thanks to BREBs tremendous effort, 97 percent of rural Bangladesh has access to grid electricity.

3. BANGLADESH SOLAR RESOURCE

⁴ Among the different forms of RE potentials, at present solar energy seems to have the greatest potential in Bangladesh. It has a good solar resource which allows solar systems to generate significant energy over the year. SWPs tilted at latitude tilt maximize annual energy production, which for Bangladesh is about an 18-degree tilt. The latitude tilt annual solar resource shown below is about 4.5 to 5.0 kWh/m²/day as shown in Table 1. The solar resource is even up to 20 percent more during the irrigation season. The solar resource map below is estimated from satellite data and indicates that there is a good annual solar resource of about 1,300+ kWh/m² in most of Bangladesh in the BREB project areas. Solar resource is most greatly affected by cloudiness and monsoonal rainfall patterns. Fortunately, for SWPs, the proportion of rainfall is inversely proportional to the amount of water that needs to be pumped, i.e., when it is raining, there is no need for irrigation. Thus the advantage of grid-tied SWPs that can be injecting energy into the energy grid when not being used for pumping, which greatly improves their economic performance rather than having an idle solar power system for 7 or so months a year when irrigation is not needed (Sheladia, 2019).

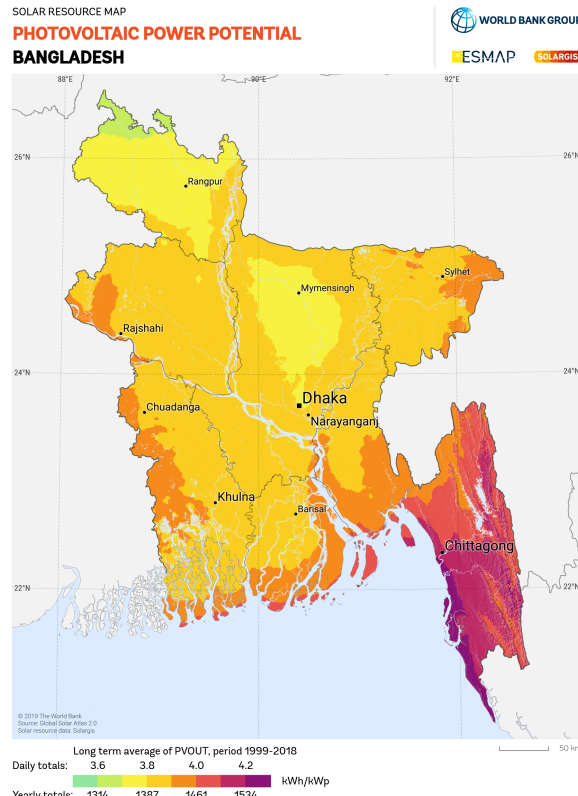


Fig. 4. Bangladesh satellite based solar resource data shows a good annual average solar resource The solar resource is even better than the annual average during the dry and sunny irrigation season. (Source: World Bank - ESMAP).

The solar resource data in the following table shows monthly GHI solar resource (Dhaka University, 1998). Note that there is not a great deal of solar resource variation in Bangladesh across the country as a whole (less than 10 percent nationally over the year) given its generally flat topography and tropical latitudes. There is about a 35 percent variation across the seasons over the year; however this is not as significant in the case of SWPs since there is no need to be pumping water during the cloudier monsoon rainy season, but in some cases may be supplying power to the grid through grid-connected SWPs.

Table 1. Monthly Global Solar Insolation for Bangladesh Regions (kWh/m²/day)

Month	Dhaka	Rajshahi	Sylhet	Bogra	Barishal	Jessor
Jan	4.03	3.96	4.00	4.01	4.17	4.25
Feb	4.78	4.47	4.63	4.69	4.81	4.85
Mar	5.33	5.88	5.20	5.68	5.30	4.50
Apr	5.71	6.24	5.24	5.87	5.94	6.23
May	5.71	6.17	5.37	6.02	5.75	6.09
June	4.80	5.25	4.53	5.26	4.39	5.12
July	4.41	4.79	4.14	4.34	4.20	4.81
Aug	4.82	5.16	4.56	4.84	4.42	4.93
Sep	4.41	4.96	4.07	4.67	4.48	4.57
Oct	4.61	4.88	4.61	5.65	4.71	4.68
Nov	4.27	4.42	4.32	4.35	4.35	4.24
Dec	3.92	3.82	3.85	3.87	3.95	3.97
Average	4.73	5.00	4.54	4.85	4.71	4.85

Source: Dhaka University, Dr. Shahida Rafique, recorded from 1988-98

4. BANGLADESH SOLAR WATER PUMPING LESSONS LEARNED

Over the past decade, there have been some pilot efforts to introduce SWPs in Bangladesh with mixed results. A small survey was conducted by SPPAI on existing SWPs and take lessons learned that can be applied to SPPAI.

KOICA and CCTF

BREB piloted twenty 5 HP SWPs (Installed PV Capacity is 6.72 – 7.2 kWp) in six districts during 2010-12 through the grant funding by KOICA and twenty more 5 HP SWPs (Installed PV Capacity is 5.16 kWp) in 8 districts during 2011-13 through the CCTF fund of GoB. Some of the KOICA and CCTF funded SWPs were not functional during the survey mostly due to inverter/ motor controller failures and a few cases of theft. The survey found that these pumps were designed to cover about 8 acres of land whereas farmers informed, they could only irrigate about 2 acres of land during Boro Rice season. It was insufficient water for the participating

farmers using these installed SWPs. Due to the technology available that time, some issues were identified as follows:

- Industrial VFDs used as pump inverters housed in a plastic box, which could not protect the VFD from dust, etc;
- Pump water delivery rate is 300 l/min which could draw maximum of 100,000 liters of water/day. A minimum need is ~65,000 liter/day of water to irrigate 0.3 acres of rice.
- Water is distributed through open soil drain resulting in wastage of 40-50 percent of water.
- Adequate training on usage, operation and maintenance was not provided to the farmers.

The SWPs were provided to the farmers at no cost but the responsibility for operation and maintenance of pumps lies with the farmer and the ownership of the pumps belongs to the PBSs. Farmers are also liable to pay a yearly lump-sum BDT 6,000 (US\$ 70.50) to the PBSs for using the SWPs. During the survey it was identified that the farmers do not own the SWPs and have no motivation to repair the SWPs since the revenue generated from the pumps was insufficient for repairs. Due to lack of budget for maintenance, it was not possible for the PBSs to take action to repair. Recently, BREB took initiatives to repair the pumps through PBS's own cost.



Fig. 5: KOICA financed Solar Pumping Project of BREB (5.16 kW_p PV array in a rice field powering a 3.7 kW submersible pump providing 300 l/min in Singair, Manikganj.

Infrastructure Development Company Ltd. (IDCOL)

IDCOL was founded in 1997 by GoB and is licensed by the Bangladesh Bank as a non-bank financial institution which is financing SWPs in Bangladesh. IDCOL's bridges the financing gap for developing medium to large-scale infrastructure and renewable energy projects. The company is a market leader in private sector energy and infrastructure financing. IDCOL channels grant and credit support to partner organizations comprised of NGOs and private investors. IDCOL receives funds from development partners such as World Bank, KfW, USAID, etc. IDCOL has financed about 1500 SWPs. IDCOL plans to promote a new ownership model for smaller-sized SWPs. Instead of buying water from POs, farmers will be able to own SWPs with credit and grant support from the project. By 2019 IDCOL has financed more than 1,500 solar irrigation pumps in operation with a cumulative capacity of about than 26.59 MW_p. IDCOL has set a target of installing 50,000 irrigation SWPs by 2025.



Fig. 6: IDCOL financed Solar Pump. 14.4 kW_p solar array powering a 10 HP submersible pump irrigating 72 bighas (~24 acres) of rice for 25 farmers in Biral, Dinajpur. The SWP installation cost was BDT 3,500,000 (~US\$41.1k)

Barind Multipurpose Development Authority (BMDA)

Surface SWP systems were financed by GoB and installed by BMDA, with over a hundred SWPs installed over the past four years that are operated on a pre-paid meter. BMDA originally installed ten pilot 11 kW

(15HP) centrifugal surface SWPs in 2016 in Godagari, Rajshahi with support from GoB. BMDA owns the pumps and sells water to farmers via a prepaid meter. Farmers use prepaid cards and are charged BDT 180/hour (US\$2.12/hr). All the BMDA SWP installations were found to be safe with proper overcurrent protection.

Based on good results, BMDA installed more surface centrifugal SWPs and owns 106 SWPs installed by 2019 around Rajshahi, Chapai Nawabganj and Naogaon. These SWPs are 11 kW (15 HP) surface centrifugal and vertical inline type pumps with a maximum discharge rate of 200 m³/hr. PV Capacity is 20.4 kW_p. Water is pumped from surface sources like rivers, ponds and canals for rice irrigation.



Fig. 7: BMDA 20.4 kW_p SWP in Godagari, Rajshahi installed in 2016. System is operated with pre-paid cards. GoB funded installation R BDT 2,400,000 or about US\$1.38 per W_p, including additional cost of 1,500 meters of 10” PVC pipe for BDT 700,000.



Fig. 8: BMDA 20.4 kW_p (300 W_p x 68) PV array used for rice irrigation in Rajshahi.



Fig. 9: BMDA Solar Surface Water Pumping System. MPPT Pump inverter with overcurrent protection for the DC strings. The pre-paid meter on the right uses AC circuit breakers. Note the green ground wire on the far left.

5. Common SWP Technical Issues and Lessons Learned in Bangladesh

Many existing Bangladesh SWPs have technical issues related to poor design and poor installation which can cause performance failures that lead to end-user dissatisfaction. A survey was conducted to identify these common problem areas as important to address for project implementation. Some common problem areas include the following:

Undersized SWP Systems

Some of the SWP systems were not designed properly omitting voltage crash due to hot temperatures, soil type needs, total dynamic head, and cropping patterns. A common result is undersized SWPs and insufficient water for the required irrigation area which makes farmers dissatisfied.

One solar pump operator Mr. Iqbal in Dinajpur stated that SWP operational and management costs are not affordable due to low revenue generation due to power disruption from the PV system and lack of timely technical support. The sponsor stopped to operate their SWPs and withdrew their staff from the field. In regard to the installation of SWPs, he mentioned that his organization had a plan to install more solar irrigation pumps but considering the experience observed from the existing pumps, the sponsor postponed their plans. The pump operator added that the BREB 100 percent electrification program funded by GoB, as well low irrigation costs from grid electricity due to subsidy caused the farmers to lose interest in SWPs and the sponsors were unable to repay on their installments. The SPPAI survey team found in general that the SWP projects were often not properly designed to fit the farmer water requirements as well as poor and unsafe installation quality.

Array shading: Vegetation sometimes grows up over the PV array, which causes poor system performance and can lead to module failures due to shaded cell hot spots. Also, we sometimes saw clods of dirt and plants from inattentive farmer weeding with hoes or dropped from birds can shade entire cells and create module hot spots and potential failures. Systems should be installed in anticipation of future vegetation growth and farmers trained to cut back on any offending plants that are shading the PV array.



Fig. 10: Banana tress have grown taller than this array on the north side and partially shaded a PV string on this Biral SWP system causing module shading and related current drop and module hotspots that can lead to premature failure.

No bonding and grounding: Most of the evaluated SWPs were not bonded to ground, which present a shock hazard to people. This also increases the likelihood of early failures from lightning strikes. This can present a high electrocution hazard especially in muddy rice paddy fields. It can be suspected some of the KOICA financed systems that failed had been from lightning strikes on systems that had loss of grounding due to lack of maintenance.

Poor or Improper wiring: Many SWP systems have undersized wires that cause high voltage drops. Also, many of the wires used outdoors are actually only rated for indoor use, so they will gradually deteriorate over time due to UV damage. Often systems showed poor workmanship, sometimes with wires carelessly strewn across the ground, and no use of conduit. This is usually the first indication that the installation is lacking.



Fig. 11: Example of poorly installed wiring. Wires dangerously and carelessly scattered across the ground; the farmers came back and installed loose wires on the wooden posts. There is no ground and no array string fuse, presenting a significant electric shock hazard. This 30 kW_p solar array powering a 20 HP submersible pump irrigating 48 bighas (~16 acres) of mostly boro and aman rice in Biral, Dinajpur. Water is sold to farmers at BDT 2,000 (US\$ 23.50) per bigha.

Improper or No Overcurrent Protection: Some SWP arrays were found have no string fuses on the DC source circuits. There are typically no surge protection devices (SPDs) to protect inverter circuits and pumps from lightning or other surges. Both string fuses and SPD ensure safety and a longer life. The SPPAI evaluation team also found a number of SWPs that improperly use AC circuit breakers in DC source circuits. The AC circuit breakers are not rated for DC circuits and can easily fail and result in frequent malfunctions or system failure. They are also not safe in DC circuits and can cause a fire and are an electrocution hazard. Good SWP design requires the use of listed DC components in DC circuits.



Fig. 12: Pump inverter used to power solar pump project in Setabjanj, Dinajpur. The system ran for 3 years and then a AC circuit breaker failed because it was inappropriately used in a DC circuit. It was replaced again with an AC circuit breaker in 2019 which can be expected to fail again.



Fig. 13: A SWP project in Biral, Dinajpur with a inverter with no string fuses or SPD to help protect from power surges.

Variable Frequency Drive (VFD) Inverters with No MPPT

Many SWP inverters installed use simple VFDs designed for 3 phase industrial induction motor applications and not for variable solar power generation. Good system reliability requires proportional integral-derivative (PID) controller synchronisation which varies the frequency and supply voltage for the motor. If VFD operates in a variable set-point mode, it must have array maximum power point tracking (MPPT). A VFD with no MPPT can cause the pump to start late in the morning and stop early in the afternoon. The SWP frequently turns on and off with passing clouds, The PV array is often way oversized PV array double or more of what is required and causes inefficient operation and less water to be pumped. This also shortens the inverter and pump life span.

6. Economics of Solar Water Pumps in Bangladesh

Solar power is a natural and symbiotic choice for water pumping and is one of the most economically attractive ways to power a pump with direct drive PV systems that can provide decades of reliable service. There is a good match between seasonal solar resource and seasonal water needs. There have been dramatic reductions in PV modules over the past decade, by over 90 percent. SWP is most cost-effective for steady pumping needs year round such as community water supply (Foster, 2013). For part-time pumping like for rice farmers in Bangladesh which only irrigate for about 5 months out of the year, grid-tied SWPs are the most attractive since they can provide power to the grid year round after the irrigation season is over.

In Bangladesh, pumps are most feasible where soil water retention capacity is at least three days or above in the case of rice cultivation. For other type of crops, it may not be as feasible an investment. The water head for most SWPs in Bangladesh is usually within ~5 m. Locations with water head greater than 5 m are still feasible, but with a smaller return on investment. A reasonable estimate for pump capacity is about 0.25 l/h. A 3 HP pump in Bangladesh costs only for BDT 15,000. 5 HP Pump price is BDT 25,000. This following analysis is for a 20.4 kWp SWP in Dinajpur.

Energy Generation

Capacity factor is the ratio of the PV energy produced in a given time to the energy that could be produced in that time if the plant had been continuously generating its fully rated output. Because PV plants can only produce during daylight hours, a capacity factor of about 20% can be expected for Bangladesh latitudes. The figure below shows the expected energy production for a 20.4 kWp grid-tied SWP in Dinajpur. The energy, which is not used by the pump is back fed into the power grid (anticipated to be about 245 days of the energy generation back to the grid).

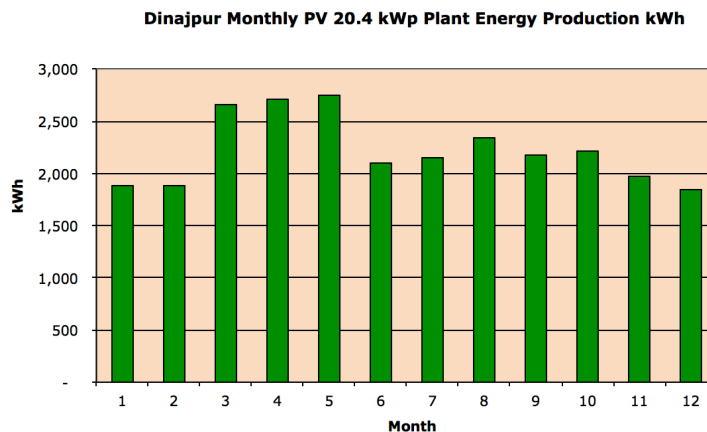


Fig. 14: Expected monthly energy generation from grid-tied SWP in Dinajpur (Year 1). Note that most of the energy Nov-March would be used for water pumping, while the rest of the year the system will be backfeeding the grid through net metering.

Array Degradation

Over time, the PV array will gradually degrade and performance and energy production will likewise drop. The SPPAI SWP array is assumed to degrade within PV module manufacturer specifications of providing 80 percent of rated power after 25 years, which implies an annual module degradation rate on average of 0.8 percent per year. Total first year expected energy production is about 26,682 kWh/year. Actual energy production will vary with solar insolation and overall PV plant availability and will gradually drop off slowly. The PV array will probably actually function at about 75% of nameplate rating even after 30 years.

Life Cycle Cost of Energy (LCOE)

For solar power systems, a life cycle cost of energy (LCOE) analysis is used to determine the economic value of a grid tied SWP. Using this methodology, including all future costs (O&M, replacements, and fuel), a comprehensive view of total system lifecycle costs is determined. LCOE analysis was made for a 20.4 kWp grid-tied SWP project looking at actual PV SWP system bid prices. We see a total solar system installed cost of about US\$17,305 in this case, or about US\$0.85 per W_p . These prices are for bulk purchases by BREB of hundreds of SWPs at a time. Taking the energy generation and amortizing the price over 25 years bringing everything to present value, we find that the life cycle cost of energy after 25 years is about 3.8 cents per kWh (US\$). Even in a subsidized electric market for irrigation this LCOE is competitive. Since water is pumped for irrigation only for about 5 months a year and not every day, the excess energy when not pumped is worth more than the electricity only used for irrigation. Simple system payback of the initial \$17.3k investment cost is achieved at about 9.8 years at current Bangladesh net metered rates (US\$0.0514/kWh), which were only

adopted in August, 2020. This assumes one inverter replacement after 15 years; the AC pump and PV modules should last over a quarter century. There may be additional farmer costs for new irrigation piping and boreholes, but these will vary from farmer to farmer and are not part of the power system LCOE analysis.

Table 2. SWP System Cost Breakdown (15 HP pump and 20.4 kWp PV array)

15 HP PV System Cost Breakdown with Tax			
US\$/Wp	% Costs		TOTAL COST US\$
\$ 0.27	31.5%	PV Modules	\$ 5,448
\$ 0.09	10.5%	Pump Inverter	\$ 1,819
\$ 0.06	7.0%	Pump & Motor	\$ 1,212
\$ 0.14	16.7%	Mounting Structures	\$ 2,890
\$ 0.01	1.7%	OC Protection/Wire	\$ 293
\$ 0.00	0.3%	Design	\$ 57
\$ 0.17	20.3%	Installation	\$ 3,510
\$ 0.01	1.2%	Commissioning	\$ 212
\$ 0.02	2.7%	Tax PV installation	\$ 462
\$ 0.07	8.1%	Tax SWP Goods	\$ 1,402
\$ 0.85	100.0%	SubTotal PV System Costs	\$ 17,305
		\$/Wp	\$ 0.85

Based on annual energy savings alone, the PVPS levelized life cycle cost per kWh generated the value of the electricity generated amortized over 25 years would be approximately \$0.038 per kWh, or about 3/4 of the grid net metered rates. The SWP grid-tied PV energy production would also help with peak shaving opportunities to displace BREB daytime loads, as well as improving grid power quality at the end of the grid where these systems are typically located.

Table 3. Amortized Net Present Value of Grid-Tied 20.4 kWp SWP over 25 years

Item	Year	PV Array Degradation	PV Energy Production kWh/yr	Grid Price \$/kWh	Electricity Value Saved \$	PVIF	Net Present Energy Value \$
1. Costs	0	0.80%					
		100%	26,682	0.05139	\$ 1,371	1.00	\$ 1,371
	1	99.2%	26,469	0.05293	\$ 1,401	1.01	\$ 1,415
	2	98.4%	26,256	0.05452	\$ 1,431	1.02	\$ 1,460
	3	97.6%	26,042	0.05615	\$ 1,462	1.03	\$ 1,506
	4	96.8%	25,829	0.05784	\$ 1,494	1.04	\$ 1,555
	5	96.0%	25,615	0.05957	\$ 1,526	1.05	\$ 1,604
	6	95.2%	25,402	0.06136	\$ 1,559	1.06	\$ 1,655
	7	94.4%	25,188	0.06320	\$ 1,592	1.07	\$ 1,707
	8	93.6%	24,975	0.06510	\$ 1,626	1.08	\$ 1,761
	9	92.8%	24,761	0.06705	\$ 1,660	1.09	\$ 1,816
	10	92.0%	24,548	0.06906	\$ 1,695	1.11	\$ 1,873
	11	91.2%	24,334	0.07113	\$ 1,731	1.12	\$ 1,932
	12	90.4%	24,121	0.07327	\$ 1,767	1.13	\$ 1,992
	13	89.6%	23,908	0.07546	\$ 1,804	1.14	\$ 2,053
	14	88.8%	23,694	0.07773	\$ 1,842	1.15	\$ 2,116
	15	88.0%	23,481	0.08006	\$ 1,880	1.16	\$ 2,182
	16	87.2%	23,267	0.08246	\$ 1,919	1.17	\$ 2,251
	17	86.4%	23,054	0.08493	\$ 1,958	1.18	\$ 2,318
	18	85.6%	22,840	0.08748	\$ 1,998	1.20	\$ 2,390
	19	84.8%	22,627	0.09011	\$ 2,039	1.21	\$ 2,463
	20	84.0%	22,413	0.09281	\$ 2,080	1.22	\$ 2,538
	21	83.2%	22,200	0.09560	\$ 2,122	1.23	\$ 2,615
	22	82.4%	21,986	0.09846	\$ 2,165	1.25	\$ 2,695
	23	81.6%	21,773	0.10142	\$ 2,208	1.26	\$ 2,776
24	80.8%	21,559	0.10446	\$ 2,252	1.27	\$ 2,860	
25	80.0%	21,346	0.10759	\$ 2,297	1.28	\$ 2,944	
Total 25 Year			624,370		\$ 46,879		\$ 53,848
					SWP LCOE Generation Value	\$ 0.038	/kWh

7. CONCLUSIONS

In summary, solar water pumping (SWP) technology ensures sustainable and effective access to water for irrigation, livestock watering and drinking water supply for smallholder farmers in Bangladesh. The key barriers for generating large scale commercial sales of SWP systems are subsidized electric tariffs, subsidized diesel fuel, and financial access to credit. The technology with properly designed and sized systems is reliable and mature. SWP systems costs have dropped by 50 percent over the past decade, but still require a somewhat higher initial capital investment than conventional diesel pumps. The life cycle cost analysis showed that the cost of energy from a grid-tied grid tied SWP system is about half of current electric tariffs amortized over a 25 year period at a cost of about US\$0.026 per kWh. Efforts to commercialize SWP technology for irrigation are still developing in Bangladesh, but Bangladesh but have a higher value by embedding SWP technologies into value chain projects, which support farmers to increase income through improved yields and growing high value crops off season. Challenges include lack of awareness about the technology, upfront capital costs, and absence of technical repair services that are being addressed through the BREB SPPAI demonstration project and partnerships with farmers and technology providers.

8. ACKNOWLEDGEMENTS

The *Photovoltaic Pumping for Agricultural Irrigation* (SPPAI) subproject is a component of the Asian Development Bank Loan-2769: Power System Efficiency Improvement Project. Loan 2769 approved on 11 August 2011 for \$300 million from ADB's ordinary capital resources (OCR) to help replace energy-inefficient thermal power plants and expand renewable energy in Bangladesh. The SPPAI project is implemented by the Bangladesh Rural Electrification Board (BREB) with technical assistance provided by Sheladia Associates and Sodev.

9. REFERENCES

- (ADB, 2017) Feasibility Study, Proposed Bangladesh: Power System Efficiency Improvement Project (Off-grid Solar Pumping Component, September.
- (Al-Amin, 2017) Al-Amin, & Tanni, Tasmiah & Rahman, Dr.Md & Asaduzzaman, Miah & Al Matin, Md Abdullah. A Study on the Present Scenario of Solar Irrigation in Bangladesh. *International Journal of Scientific and Engineering Research*. 8.
- (BADC, 2019) Bangladesh Agricultural Development Corporation, Minor Irrigation Survey Report 2018-19, Dhaka, Bangladesh
- (IRENA, 2016), Solar pumping for irrigation: Improving livelihoods and sustainability, June
- (Foster, 2013) R. and A. Cota, "Solar Water Pumping Advances and Comparative Economics," Solar World Congress, International Solar Energy Society (ISES), Quintana Roo, Mexico, November 3-7, 7 pp.
- (Sheladia, 2019) "Feasibility Study Review: Proposed Bangladesh: Power System Efficiency Improvement Project (Off-grid Solar Pumping Component), Dhaka, Bangladesh, May 27, 2019.
- (World Bank, 2016) <http://www.worldbank.org/en/results/2016/10/07/bangladesh-growing-economy-through-advances-in-agriculture>
- (World Bank, 2016) Solar pumping Pumps: A New Way of Agriculture in Bangladesh, Dhaka, Bangladesh.

Zero Emissions Network; A Pilot Program for Carbon Emissions Reduction

Sarah Townes¹, Rahim Khoie², and Panteli Stathopoulos¹

¹American Solar Energy Society
2525 Arapahoe Ave #E4-253
Boulder, CO 80302
stownes@ases.org

²Department of Electrical and Computer Engineering
University of the Pacific
Stockton, CA 95211
rkhoie@pacific.edu

Abstract

Public awareness of the disastrous consequences of continued rise in global carbon emissions reached a peak in 2019 with masses of people participating in Climate Strikes in more than 4,500 locations spanning 150 countries across the United States and the globe. The stage is therefore set for taking the matter to the people at a local level. In this paper, we report a pilot program: the Zero Emissions Network (ZEN), the newest program addition to the American Solar Energy Society (ASES), through which emissions reducing technologies such as solar electricity generation, green roofs, electric bicycles, geo-thermal HVAC, and re-planting of native flora using flight offset dollars are made more readily available and affordable, especially to lower income clients and communities. Student interns from the University of Colorado (CU), are the driving work force of the project, and we are working towards a sister chapter at the University of the Pacific (PACIFIC) in Stockton, CA.

The program solicits funding from both local and national sources for:

- a) providing micro-grants to low-income individuals and small businesses to help them afford solar electricity and other emissions-reducing technologies,
- b) building an information kiosk and web-based data center where all ZEN and ASES participants can get information on emissions reduction strategies and technologies, as well as track their overall greenhouse gas emissions to see how their investments in progressive technologies and lifestyle changes are reducing their greenhouse gas (GHG) emissions and those of their community.

Keywords: Zero Emissions Network, Monitoring and reducing GHG Emissions, Distributed Local Solar Generation

1. Introduction

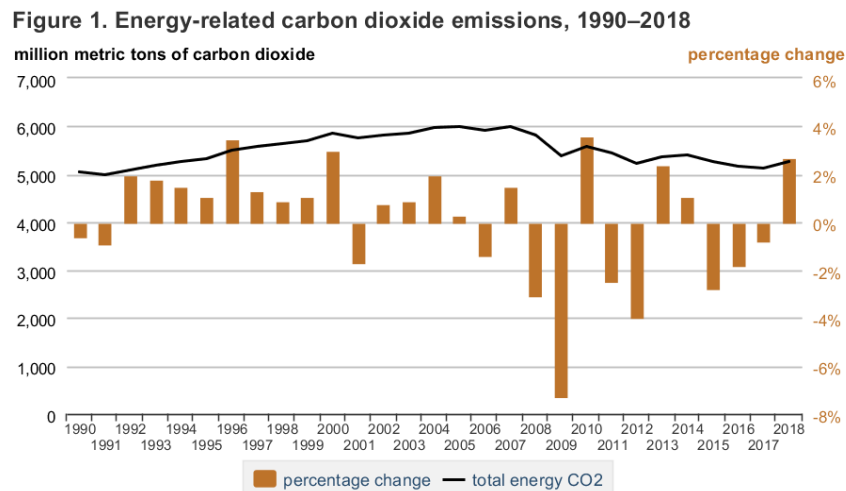
The Zero Emissions Network is a pilot project initiated by ASES and has attracted a strong core team determined to help the public take steps toward lowering their carbon emissions in many areas of life. In summary our 3-fold goals are:

- 1) Through micro-grants help elevate lower income communities to realize their place as leaders in GHG reduction within the environmental movement.
- 2) Help each location town by town, city by city, county by county, to track and see progress reducing their community's GHG emissions.
- 3) Educate and empower ourselves as ZEN team members, ASES members and ZEN participants, to track and take actions day by day which reduce our own GHG emissions so that we can serve as mentors and be examples for others who are ready to change their habits and help heal our precious atmosphere.

The project seeks funding from local and national sources and distributes the funds to local customers for installation of small to medium size distributed solar electricity generation and other GHG reducing technologies. The rapid and initial success of the ZEN program in securing its first two grants indicates the readiness of funding sources to help with this project. The project has very low overhead and is scalable to the availability of the local funding sources and the local needs of its customers. We hope that our presentation to the SOLAR 2020 audience will result in significant interest in replicating the project in other locales, especially by participating students, faculty, and solar industry representatives. Finally, Zero Emissions must be a global goal, and as important as it is to reduce local emissions, it is only through a massive global effort that we will achieve Zero Emissions, and hence the need for implementation of the ZEN program and similarly action-oriented models across the U.S. and the globe.

2. The need for ZEN project

The total U.S. carbon emissions was on a declining trend between 2007 and 2016 as shown in Fig. 1 (U.S. EIA, 2020).



 Source: U.S. Energy Information Administration, *Monthly Energy Review*, October 2019, Table 11.1, Carbon Dioxide

Fig. 1. Total and percentage of change in the U.S. energy-related carbon dioxide emissions. (U.S. EIA, 2020)

After peaking at 5983 Million Metric Tons (MMT) in 2007, the total U.S. carbon emissions reached a trough of 5171 MMT in 2016. In fact compared to 2005-levels, the total U.S. emissions dropped by 7% and 13% in 2010 and 2016, respectively. The drop continued in 2017 at 14% below 2005 levels. This is a significant decline by any measure. Various researchers have cited reasons for this decline, including:

- decline in the U.S. economy output in the years following the financial crisis of 2008-2009 (Peters, et. al. 2012) (Guardian, 2010), and (Murray and Maniloff, 2015).

- increase in use of natural gas (Feng, et. al., 2015) and (De Gouw, et. al., 2014)
- federal regulations imposed by the Obama Administration (Adler, 2011) (McCarthy and Copeland, 2016),
- and state-mandated regulations, and in particular, the Renewable Portfolio Standards (LBL, 2016).

However, as shown in Fig. 1, there was an up-tick (about 3% rise) in U.S. emissions in 2018. In that same year, the National Oceanic and Atmospheric Administration in its 2018 Report on “Climate Change: Current and Projected Impacts on the U.S.” called for the need for removal of existing carbon from the atmosphere to prevent the projected climate disasters by 2050 (NOAA, Fahey 2018). This call came at the time when a large number of deregulatory actions were being taken by the current administration in federal energy policies and especially in relation to electricity generation from coal. These actions include (Brookings Institution, 2019) and (National Geographic, 2020):

- Relaxing the rules on emission of greenhouse gases in new coal-fuel power plants.
- Relaxing the rules on producing mercury and other air-toxins by coal-burning power plants.
- Repealing Clean Power Plan, and
- Postponing enforcement of many Environmental Protection Agency (EPA) regulations.

In the absence of any federal mandate on reducing U.S. carbon emissions, and in light of recent federal energy deregulations by the present administration, and in particular, deregulation of the coal industry, the action of states in mandating emissions reduction has become the most important measure by state governments in reducing U.S. emissions. This action, referred to as the Renewable Portfolio Standard (RPS), requires utility companies to produce a certain percentage of their electricity from renewable resources. We previously reported the effects of enactment of RPS laws by the states in lowering emissions (Khoie, Calderon, 2018).

Considering the present circumstances, and in light of the warning by NOAA on the need for removal of carbon from the atmosphere, it is imperative that we get the public (the end users) involved in efforts to not only reduce their own emissions to zero, but also help remove carbon from the atmosphere. The Zero Emissions Network (ZEN) project aims to do just that: taking the cause to the public at micro-scale.

3. The ZEN history

In 2018, Sarah Townes was asked to moderate the Policy in Action session of the National Solar Conference (SOLAR 2018). The resounding message she received from many world renowned speakers was consistent and clear:

- The scientific urgency for the need to reduce greenhouse gas emissions and save our climate was thoroughly, credibly established.
- The technology necessary to reduce emissions was readily available.
- The economic modelling for how to make the transition to renewable energy sources was finally well established.
- What was missing were federal government initiatives and public engagement.

In other words, drastically reducing carbon emissions was both urgently necessary and completely doable, but missing two essential components: people and the federal government. This realization was further enhanced by her personal experience living in one of the most wealthy, educated, and theoretically progressive cities in the U.S. (Boulder, CO) where neither she nor any person she knew had made their lifestyle net zero emissions, or even tracked their carbon footprint enough to bring it close to that mark. In her experience most people made small efforts where convenient, but mostly bought what they wanted to buy, flew where they wanted to fly, ate what they wanted to eat, drove their cars, turned on the gas burning heater in winter and so on.

Further motivation for this project was the work presented by Rahim Khoie in SOLAR 2018 Conference (Khoie, Calderon, 2018) in which he conducted a study of the effects of RPS in several states which **proved that progress in emissions reduction was being made due to state mandates and local initiatives**. Though counter-productive policies by the federal government were moving us away from reducing green-house-gases (GHG) as a nation, still the city and state programs showed decisive progress.

This caused Sarah Townes to propose to her organization, the American Solar Energy Society (ASES), that a new program be created to help ASES members nationwide and in the headquarter city of Boulder, CO take decisive action to reduce their GHG emissions. This proposal was passed by the board in January of 2019.

4. Accomplishments

The following is a partial list of what has been accomplished so far:

1. We created a fantastic team of interns from the University of Colorado, Boulder (CU, Boulder) Environmental Studies Program, and together they created an online guide specific to Boulder for how to track and reduce carbon emissions. Months of dedicated research went into this very practical and doable set of suggestions. Areas of focus include home energy use, transportation, diet, and Natural Solutions carbon offsets.
2. We created a team of students from the University of the Pacific (Stockton, California) to conceptualize, design, and build a CO₂ monitoring kiosk that provides information on local, national, and global concentration of CO₂ in the atmosphere.
3. We met with city sustainability leaders and told them of our program and our goals, and received suggestions from them on how best to implement our ideas. In turn we promised to drum up support for their ambitious Climate Mobilization Action Plan which the City of Boulder recently rolled out.
4. We applied for and received a grant from the Left Coast Fund with which we purchased \$20,000 worth of subscriptions to Jack's Solar Garden, a wonderful energy CSA and regenerative agriculture farm. These subscriptions we will allocate to 10 lower income individuals & families in Boulder who will receive a monthly discount on their electric bill, and simultaneously reduce their carbon footprint with solar.
5. We have been awarded a second \$25,000 allocation with which we plan to purchase a solar array and trailer for El Costeño Oaxacan food truck. The owner Moises Santos has already outfitted his business with a full complement of resource saving devices to track and reduce consumption of water, food waste, and electricity. We are proud to be able to add solar panels to this wonderfully sustainable enterprise.
6. One of our team members helped submit two grant applications to fund an electric vehicle charging station in North Boulder that will serve a lower income community where most people do not have a garage to plug an electric vehicle into.
7. We are in the process of creating a Natural Solutions carbon offset fund, where local citizens can offset their GHG emissions by investing in local plants. This can include building green roofs, investing in local sustainable agricultural projects such as Dharma's Garden, and local reforestation projects.
8. We ourselves as a team have begun tracking our individual consumption habits and GHG emissions. This is incredibly humbling and eye opening. We wish everyone were as aware of their consumption and its effect on their life as we are, for example, aware of how much money we make, what we wear, and how we vote.

We currently have an application in with Boulder County asking the county to host a CO₂ kiosk which will educate citizens about the city's greenhouse gas emissions. The design specifications of a prototype of this kiosk is provided in this paper. When fully assembled, this kiosk will be placed in the heart of the downtown Pearl Street pedestrian mall. We would be delighted if SOLAR 2020 attendees to used our design to replicate and build this kiosk to be installed in their locale.

5. The CO₂ Kiosk

A team of students from the University of the Pacific has designed the necessary electronic components of the CO₂ kiosk as part of their senior project capstone course. The assigned project description provided to the student was: “Design and build a Carbon Dioxide Kiosk that displays the local, national, and global levels of carbon dioxide in the atmosphere. The requirements of the system are: solar powered, updating data once every 24 hours, measure and display carbon dioxide content of the local atmosphere in parts per million, be visible from 100 yards, and acquire and display the national and global CO₂ data from reliable sources, and particularly from the U.S. Energy Information Agency websites (U.S. EIA): <https://www.eia.gov/environment/emissions/carbon/>.”

A behavioral description of the electronic system of the CO₂ kiosk is shown in Fig. 2. The system requires no input, as it is designed to operate somewhat autonomously and in perpetuity. The output of the system are the three CO₂ levels; local, national, and global, which are displayed on a panel which is readable from a distance of up to 100 yards. The system consists of 6 subsystems: CO₂ sensor, solar panels, microcontroller, power storage and power conditioning, data storage, and software.

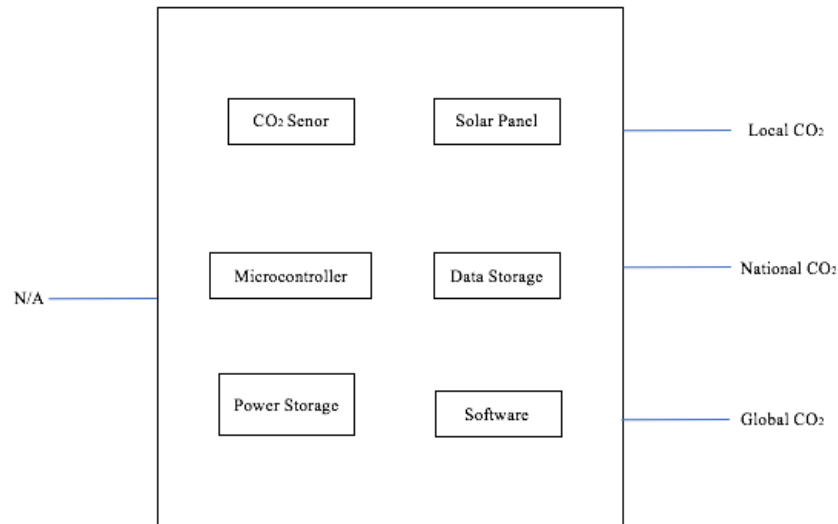


Figure 2: Behavioral design of the CO₂ Kiosk showing its input/output behavior.

A functional description of the electronic system of the CO₂ kiosk at various levels is shown in Fig. 3. The main components of the system are:

- 1) The CO₂ sensor module which uses a light tube consisting of an infrared source and an infrared sensor used for detection of the CO₂ content in the air at the locale. A low pass filter is used to reduce the interference noise. The signal from the sensor is further amplified and is received by the microcontroller for processing and storage.
- 2) The microcontroller module which receives, processes, and displays the data.
- 3) The display module that is powered from a DC source and is controlled by the microcontroller. This module consists of three display panels for local, national, and global CO₂ data.
- 4) The power module which consists of a solar panel, a rechargeable battery, and voltage regulator at various DC levels for the microcontroller module and the display module.

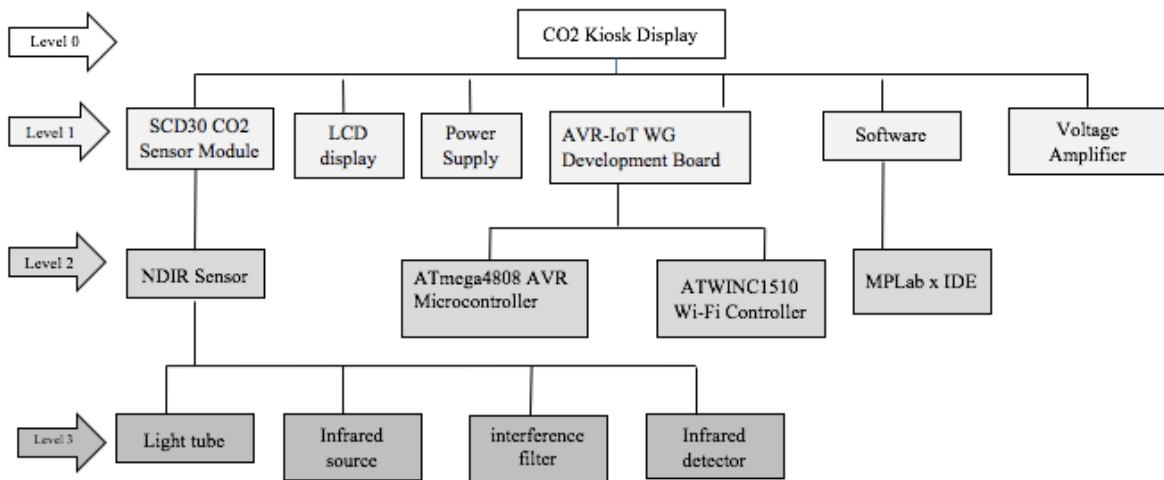


Figure 3: Functional description of the electronic system of the CO2 kiosk at 4 abstraction levels.

- 5) The Wi-Fi module which is used to access websites for data on national and global CO2 data.
- 6) The software module which consists of required programs to run the microcontroller and the Wi-Fi modules.

The modules listed above have been partially tested and or simulated to ensure that the design is viable. Each component of the modules has been thoroughly researched in order to identify the optimal parts in terms of the required cost and power usage. Additional information about the hardware and software components of the system will be provided upon request: email Rahim Khoie at rkhoie@pacific.edu.

6. The ZEN Website

The ZEN project is based on the idea that if people could comprehend the size of their carbon footprint they might be more inclined to reduce it. Then if someone reaches out a personal hand with mentorship and money to encourage their efforts, they cannot help but make progress. These principles have guided the programs within the Zero Emissions Network. A carbon tracker was built to estimate an individual's carbon footprint. Research was conducted in order to understand ways to reduce that footprint. A micro-grant program was created to support investment in green technology. A carbon offset program is underway, making it possible for people to reach net-zero in a non-intrusive way.

At ZEN we believe that knowledge and action are necessary tools to combat climate change. The ZEN website (<https://www.ases.org/zen-program/>) summarizes multifaceted topics that are related to environmental degradation and community involvement. We recognize solutions, leaving the decision to act to the people. The ZEN team plans to reach people digitally, through a solid space at the kiosk, through the ASES network, and via personal relationships. The following is a brief bullet point description of information the public will be able to gather by visiting the ZEN website.

- The “What We Offer” page outlines current and future services provided by the ZEN team (<https://www.ases.org/what-we-offer/>). This page outlines the ZEN micro grant program, the carbon offset program, and soon a carbon tracker.

- The ZEN micro grant program subsidizes subscriptions to Jack's Solar Garden, a holistic solar garden with integrated agriculture. These grants are reserved for low-income individuals who want to be a part of the renewable energy solution. Subscribing to Jack's Solar Garden reduces your carbon footprint and lowers your energy bill!
- The ZEN carbon offset program is a work in progress. When this program is fully realized it will direct funds to carbon sequestration projects. Individuals can buy into this program to offset their carbon emissions. This tool will be vital in helping people reach net zero emissions.
- The ZEN carbon tracker is a tool which is necessary to track an individual's carbon emissions. With this tool people can track their progress in reducing their emissions. We are currently refining it as our own team members track our individual carbon footprint, and plan to publicize the finished version this year.
- At the heart of our work is a section of the website titled "How to Reduce Emissions" (<https://www.ases.org/reduce-emissions/>). This section seeks to answer two basic questions: What are common carbon emitting activities, and what are carbon reducing activities. These questions are answered with respect to transportation, home energy, and diet.
- Another important section is related to local government and local utilities (<https://www.ases.org/zen-local-government/>). This section breaks down what local governments climate related goals are and their plans to achieve them. Also, information related to the local utilities is presented in this section. Both government and utilities play a large role in carbon planning and emissions. It is vital to be aware of these institutions and the means by which citizens have power to change them.
- One very useful and progressive section of the website is titled "Solutions" (<https://www.ases.org/zen-solutions/>). This section is entirely dedicated to local organizations that lower carbon emissions through natural solutions and innovations. These organizations help people to lower their carbon footprint.

7. Conclusions

One of the most inspiring discoveries of our work is the ever-growing list of how each effort to reduce GHG emissions improves the quality of life for the participant. To give just a few examples:

- bicycling over driving improves health and happiness,
- electric vehicles reduce noise pollution and cost less to maintain,
- air drying clothes lengthens their usable lifespan,
- eating local and sustainably grown food builds community and personal health,
- Connecting with others around reducing emissions builds strong relationships on a super positive foundation.

We find that each and every climate action taken brings direct positive results in our lifestyle.

Perhaps the greatest aspect of this project has been the sense of joy and comradeship with which our teams have carried out our mission to help reduce GHG emissions. We have a great time together when we meet, and we sleep better at night knowing that we are making progress in reducing our carbon footprint and helping others to do the same.

8. Acknowledgments

The authors wish to thank and acknowledge the passion, dedication and hard work of the following group of young engineers and scientists who have made tremendous contributions to the success of this project:

Kiosk:

Giselle Aranda, Electrical Engineering, University of the Pacific

Grace Hamada, Engineering Physics, University of the Pacific

Grant Writing:

Alyssa Kalac, Major in Environmental Studies, Minor in Physical geography and Business, CU Boulder

Transportation:

Taylor Heisler, Major in Environmental Studies, CU Boulder

Joseph Wajrowski, Major in Environmental Studies, CU Boulder

Taylor Bartlett, Major in Environmental Studies, CU Boulder

Website Coordinating:

Zach Zalesne, Major in Environmental Studies, Minor in Philosophy, CU Boulder

Alison Dilworth, Major in Environmental Studies, Minors in Business and Atmospheric and Oceanic Studies, CU Boulder

Carbon Tracking:

Daniel Hood, Major in Environmental Studies, CU Boulder

Sean Davidson, Major in Environmental Studies, CU Boulder

Diet and Agriculture:

Eliane Bach, Double Major in Environmental Studies and Ecology & Evolutionary Biology, CU Boulder

Home Energy:

John Shapland, Major in Environmental Studies, CU Boulder

Outreach:

Michele Wolff, Major in Environmental Studies, Minor in Spanish, CU Boulder

Carbon Tracker:

Remi Akinwonmi, BA in Mechanical Engineering, Minor in Renewable Energy, Federal University of Agriculture, Abeokuta, Nigeria

Carbon Sequestration:

Adrienne Hodgson, Major in Environmental Studies, CU Boulder

Taylor Heisler, Major in Environmental Studies, CU Boulder

Local Utilities and Government:

Teli Stathopoulos, Major in Environmental Studies, Minor in Business and Atmospheric and Oceanic Studies, CU Boulder

9. References

Adler, J. 2011. Heat expands all things: The proliferation of greenhouse gas regulation under the Obama administration. *Harvard Journal of Law and Public Policy*, 421. <http://heinonline.org/>, Accessed March 2018.

Brookings Institution, 2019. "Tracking deregulation in the Trump era," Friday, April 12, 2019, <https://www.brookings.edu/interactives/tracking-deregulation-in-the-trump-era/> Accessed: April 2019.

De Gouw, J. A., Parrish, D.D., Frost, G. J., and Trainer, M., 2014. "Reduced emissions of CO₂, NO_x, and SO₂ from US power plants owing to switch from coal to natural gas with combined cycle technology." *Earth's Future* 2, no. 2 (2014): 75-82.

Feng, K., Davis, S., Sun, L., and Hubacek, K. 2015. Drivers of the U.S. CO₂ emissions 1997–2013. *Nature Communications*, 21 July 2015, Open Source. <https://www.nature.com/articles/ncomms8714.pdf>.

Guardian, The, 2010. Global emissions of carbon dioxide drop 1.3%, say international Scientists. <https://www.theguardian.com/environment/2010/nov/21/carbon-emissions-fall-report>, Accessed March 2018.

Guardian, The, 2010. Global emissions of carbon dioxide drop 1.3%, say international Scientists. <https://www.theguardian.com/environment/2010/nov/21/carbon-emissions-fall-report>, Accessed March 2018.

Khoie, R. and Calderon, A., 2018. "Forecasting Carbon Emissions in States of Hawaii, California, Colorado, and Florida; The Effects of States' Renewable Portfolio Standards," Published in Proceedings of SOLAR 2018, *American Solar Energy Society 47th National Solar Conference and Summit*, Boulder, Colorado, August 5-8, 2018.

LBL, 2016. Electricity Markets and Policy Group. Renewable Portfolio Standards Resources. Lawrence Berkeley National Laboratory. 2016. Available: <https://emp.lbl.gov/projects/renewables-portfolio>. Accessed March 2018.

McCarthy, J. and Copeland C. 2016. EPA Regulations: Too Much, Too Little, or On Track? Congressional Research Service, Library of Congress, December 30, 2016 <https://fas.org/sgp/crs/misc/R41561.pdf>. Accessed March 2018.

Murray, Brian C., and Maniloff, P., 2015. "Why have greenhouse emissions in RGGI states declined? An econometric attribution to economic, energy market, and policy factors." *Energy Economics* 51 pp. 581-589.

National Geographic, 2020. <https://news.nationalgeographic.com/2017/03/how-trump-is-changing-science-environment/>. Accessed June 2020.

National Oceanic and Atmospheric Administration, 2018. David Fahey, "Climate Change: Current and Projected Impacts on the U.S.," ASES SOLAR 2018, Pathways to the Renewable Energy Transformation, August 5-8, 2018, Boulder, CO. See: <https://www.noaa.gov/climate-data-and-reports>.

Peters, G. Marland, G., Le Quéré, C., and Boden, T. 2012. Rapid growth in CO₂ emissions after the 2008–2009 global financial crisis. *Nature Climate Change*, 2012, <https://www.nature.com/articles/nclimate1332>, Accessed March 2018.

SOLAR 2018. *American Solar Energy Society 47th National Solar Conference and Summit*, Boulder, Colorado, August 5-8, 2018.

U.S. EIA, 2020. U.S. Energy Information Agency, 2020. <https://www.eia.gov/environment/emissions/>

Emerald City 100% Renewable Energy Plan

Steven B. Smiley

Energy Economist (ret.)
Omena, Michigan (USA)
Smiley27@earthlink.net

Abstract

This paper presents the practical policy and project implementation steps of a 10-year conceptual plan to transition the heat and electric power systems of Traverse City, Michigan to 100% renewable energy. Pitched as “Emerald City”, it proposes the deployment of a mix of solar, wind and bioenergy systems—coupled with energy storage, energy efficiency, demand management, mini-district heat, and optimal control strategies. Potential city specific renewable energy, efficiency and storage projects are outlined, representing an abundance of choices for citizens and stakeholders working together, or as autonomous actors. The author, the developer of the first green pricing program in the United States (US), argues that green pricing programs are no longer appropriate, and should be replaced. The Traverse City renewable energy plan can be accomplished with minimal electrical distribution infrastructure changes through the following strategies: targeting a 300% increase in electric energy distribution, displacing natural gas in a 7,800 heating degree day (HDD) climate, and applying the concepts of the “Harmonious Grid” (NW Energy Coalition), “Link and Sync” (C. Gruenwald – Blattner Energy), and Green RE-Heat (Smiley)—with focus on thermal energy storage. Unique policy applications such as unlimited solar net metering, flexible and targeted climate/carbon fees, maximizing on-bill financing for efficiency, solar, energy storage, and fuel switching, can also help achieve 100% renewable energy while lowering and fixing energy costs indefinitely.

Keywords: 100% Renewable Energy, carbon fees, on-bill financing, harmonious grid

1. Introduction

This “Emerald City” 100% renewable energy plan for Traverse City, Michigan is a 10-year “concept plan” of how to make a small city of 15,000 100% renewable energy heated and powered. The focus is on very practical steps, describing the community energy profile, promulgating policy, identifying projects, financing, and then implementing these policies, systems, and projects. This is a conceptual plan because, since extensive detailed research and project development work will be required by utility staff, analysts, engineers, and financiers.

Economists, when writing policy should state their foundational political economic principles relevant to their study. Here are four which provide a framework for my plan:

- “All energy choices and prices are based on politics and policy”. John Pestle (ret. energy attorney).
- “Make the market your slave, not your master.” Frede Hvelplund, Aalborg University, DK
- 21st Century economics must be, “distributive and regenerative”. Kate Raworth; *Doughnut Economics* (2017)
- “Wealth is regenerated solar radiation.” R. Buckminster Fuller; *Operating Manual for Spaceship Earth* (1969)

Backed by green bonds, green banks, climate fees, and on-bill utility financing, the capital bottleneck can be removed releasing the tremendous latent demand for clean energy by local citizens of all income levels—investing in conjunction with the municipal electric utility. Unlimited and unrestricted solar net metering can help rapidly expand

Smiley

solar energy within the city limits, with full net metering for residential customers and adjusted net metering for large commercial installations. I project that the impact on utility revenues will be less than one percent with an unrestricted solar net metering program. Planned community solar, as well as utility scale wind and solar installations can generate roughly three times the present electric energy consumption in Traverse City. Flexible and targeted “climate crisis cost recovery” fees will be uniquely applied, positive on-peak, and negative off-peak so that off-peak period electricity will out-compete natural gas for space and water heating. Quick response combined heat and power (CHP) biogas engines, with thermal storage, enough to run the city on average (35 MWe), with load control and as emergency back-up will be installed throughout the city. This can displace the emergency back-up generators that represent roughly 50% of the city electric load, sitting idle over 99% of the time—representing a tremendous economic waste. Thermal and electric battery storage will be distributed throughout the city with thousands of controlled hot water tanks (both large and small), and electric battery systems. Electric vehicles will be phase in with incentives and low-cost time of use (TOU) charging rates. Distribution grid modernization will be conducted, including retrofitting distribution substations for bi-directional control and at least one large utility-scale wind and utility-scale solar collection substation. A broadband monitored “grid harmonization” control plan will be implemented as outlined by methodologies such as Charley Gruenwald’s “Link and Sync” and the Brattle Group. Any excess renewable energy can be sold into the regional grid to help avoid curtailment. With climate fees phased out over 10 years energy costs will lower than present and fixed indefinitely.

2. Geography, Resources, Economic and Energy Profile

“Emerald City” is based on the geographic, economic and energy characteristics of Traverse City, Michigan. Traverse City currently has a population of 15,000, covering 8.7 square miles, in a humid continental climate with 7,794 (F) HDD and 458 (F) cooling degree days, situated at 44 degrees north latitude. The solar resource is 1,350 kW-hrs/m²/year and the wind resource category is IEC Class IIIA on surrounding higher ground. It is not the sunniest or windiest place, but there is a good seasonal balance with twice as much wind in the winter and twice as much sun in the summer (see Figure 1). The windiest hour on average is 3 PM, aligning with peak period electric use. Adequate feedstock for biofuels is available.

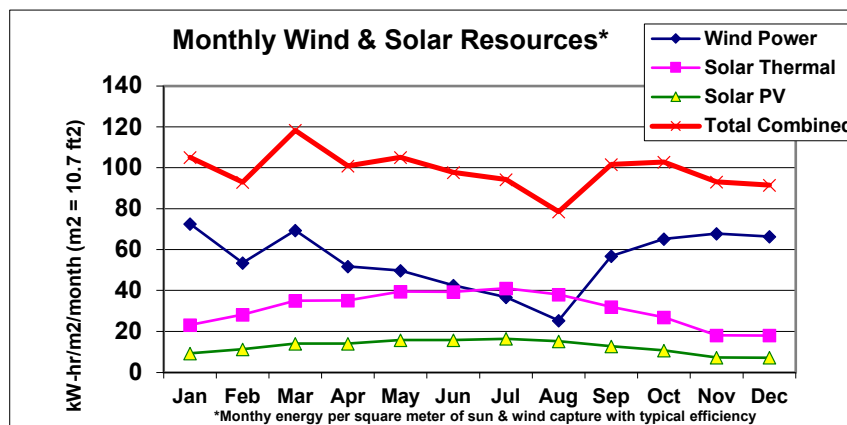


Figure 1

Smiley

2.1. Energy and Economic Profile

Currently, in Emerald City, 93% of the non-transportation-related energy is natural gas (64%) and coal (29%) respectively (see Figure 2). Wind and solar account for roughly 5% with land-fill gas and natural gas combustion turbines (CT) filling in the balance of the generation mix.

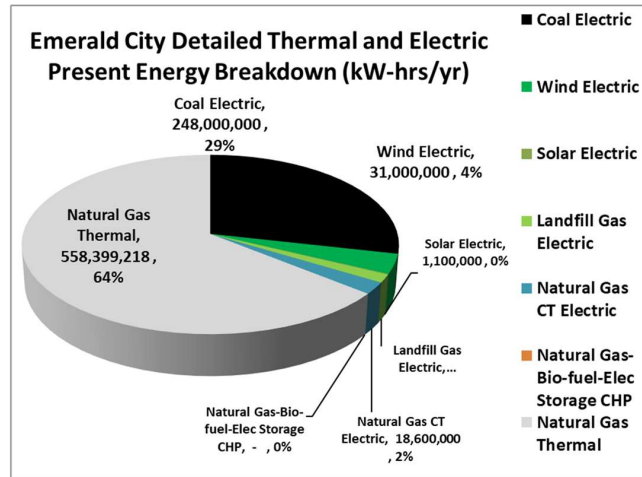


Figure 2

The summer peak is roughly 70 MW's, the average load is 40 MW and the base load (night-time) is roughly 25 MW (see Figure 3). Annual electric consumption is roughly 310 million kilowatt-hours (kW-h) and annual natural gas use is roughly 560 million kW-h.

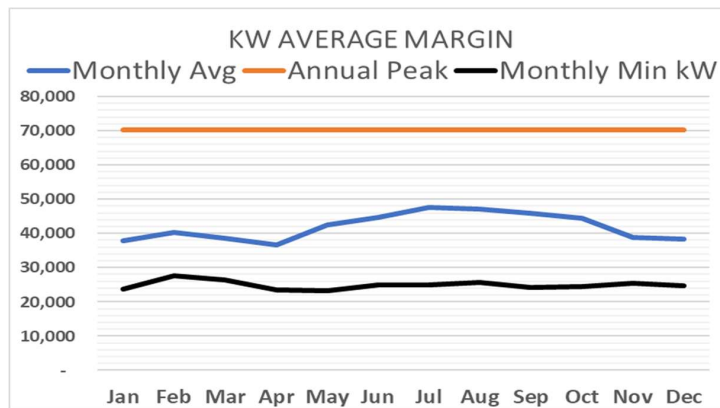


Figure 3

The customer economic electric profile shows important distinctions with 87% of the metered customers residential and the balance of 13% commercial, institutional, and industrial (see Figure 4). In contrast to this, 87% of the electric revenues (see Figure 5) are commercial, institutional, and industrial. Put another way, with residential consumers representing only 20% of revenues, if they cut their electric use 50%, it would only impact utility revenues by 10%.

The annual electric expense is roughly \$35 million, and the natural gas expense is roughly \$20 million--with a total annual community expense of \$55 million. Transport fuels have not been estimated.

Smiley

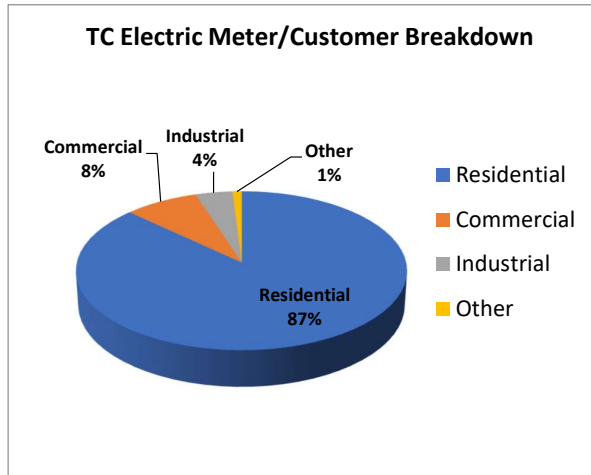


Figure 4

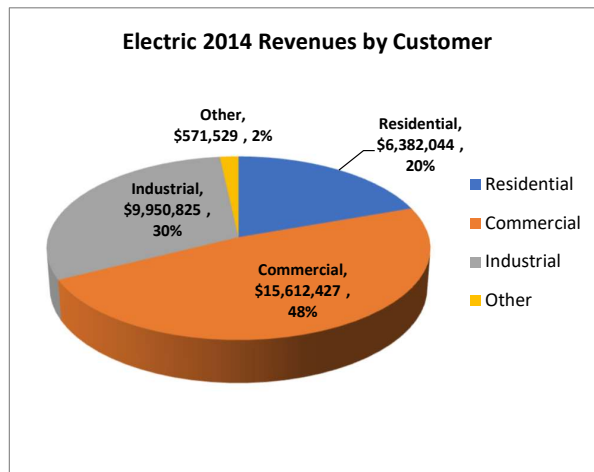


Figure 5

Next, Figure 6 illustrates a typical winter daily electric demand profile with peak rated capacity, hourly demand, and a net capacity. The peak capacity available is higher in the winter due to colder temperatures. The net capacity availability which reaches 55 MW during the night-time raises the question, “is this enough electric capacity to heat the city--eliminating natural gas use?” One might conclude that it is, especially with the leverage provided by heat pumps. But even without heat pumps, low cost electric resistant heat systems can meet the need most of the time. Therefore, with the existing electric distribution capacity, we can heat the city, including both space and water heating. With this, we can use thermal energy storage for space and water heating, one of the least cost energy storage systems. Thousands of controlled domestic hot water heaters and a few large commercial hot water storage systems (i.e. 3 MW hot water boilers with variable load controls) can meet the demand.

Smiley

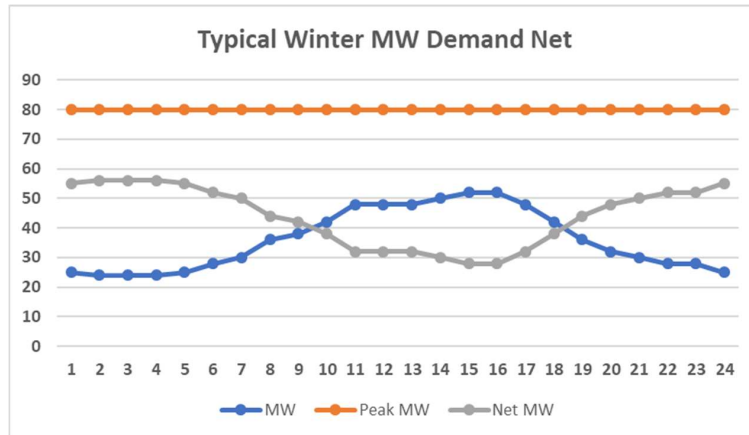


Figure 6

3. Policy

3.1. Unlimited Solar Net Metering

All limits should be removed on solar net metering. Presently there is a 20-kW size limit, with annual metered kW-hours as the basis for maximum system sizing. For residences, even if 20% of the city's homes, churches, businesses, and multifamily units had 100% net zero solar the impacts, on the community owned municipal utility would be less than 1% of revenues. The reason the impacts on utility revenues are insignificant are fourfold. First, residential customers make up only 20% of the total utility revenues so with tree lined shaded streets, roof space and orientation limitations, it is estimated that only 20% of properties have reasonable solar access resulting in 4% solar potential. Second, most properties will not have adequate roof or yard space to offset annual kW-h, further limiting the residential solar output. Third, excess solar generation is automatically consumed by the nearest non-solar neighbor with near zero distribution expenses, a neighbor who pays the full retail price plus a proposed climate fee for that solar energy. And fourth, since solar is typically generated during peak periods, peak period distribution capacity is increased while power quality is improved.

More importantly, commercial, and industrial consumers should be allowed to maximize solar opportunities on their properties. For larger solar installations, with economies of scale, a lower solar value can be implemented (basically a fair feed-in-tariff), but it must be enough to "make a market", at minimum the 10% return on investment we guarantee our monopoly investor owned utilities (IOU's). With this, the net revenue effects on the community can be near zero.

3.2. Community Solar

In this tree lined city solar opportunities in residential neighborhoods are limited by shading, with the trees providing beauty, oxygen, and free air conditioning (passive solar cooling!) for the community. Therefore, community solar, whether cooperatively owned or utility customer owned, provides an important element of a 100% renewable energy plan. Importantly, since larger community solar projects are lower cost, there should never be a solar premium on a utility bill, but at minimum, an equal offset on the electric bill. If a utility consumer buys into a community solar project, dedicating a portion of their electric bill to the investment in the solar project, they should have a net lower electric bill. This provides opportunities for lower-income citizens. For citizens that are not metered consumers independent cooperatively owned larger solar systems provide an investment opportunity. Citizens have tremendous latent demand to invest in solar locally if the program is fair and promoted aggressively by the utility.

Smiley

3.3. Climate Crisis Recovery Fee

A “climate crisis recovery fee” (CCRF) is proposed as an alternative to a carbon fee. Most electric utilities have guaranteed rate adjustment fees generally called “power service cost recovery” (PSCR). When fossil fuel supply costs go up or down, adjustments are automatically made to rates. A variable and flexible CCRF is proposed as part of investment fund raising for the municipal utility, to offset external environmental and social costs associated with pollution, to account for distribution system retrofits, and as a mechanism for fuel switching from natural gas to electricity. This CCRF is much more than a carbon fee and it is not calculated based on avoided tons of carbon. The CCRF benefits accrue much beyond carbon avoidance. The CCRF is a flexible and variable fee that varies with time of use electric rates, with the fee high during on-peak periods, moderate during intermediate periods and negative during off peak periods. The CCRF should be phased in over roughly three years, reaching, for example 3 cents per kWh on-peak and negative 1 cent per kWh off peak. The goal is to raise revenues on balance but to push off peak electric rates low, below the cost of natural gas with simple electric resistance heat values, roughly 4 cents per kWh. This provides the basis for clean nighttime and weekend electricity to out-compete natural gas for space and water heating, provide an incentive for thermal energy storage, and low-cost off-peak storage for electric vehicle charging, electric busses, and other electric battery applications, such as landscape equipment, tools, forklifts, phone and computer chargers.

With heat pumps, whether ground source, water source, or air source for heating and cooling, the electric energy value is at least doubled, cutting the thermal value of the 4 cents per kWh off-peak electricity to 2 cents per kWh. Electric vehicle fuel at 4 cents per kW-hour is half of the cost of gasoline at the pump, and during the weekends there are 65 hours of off-peak low-cost electricity to fuel EV's.

3.4. On-Bill Financing

On-bill financing for efficiency and solar PV is another critical component for distributing equitable investment resources towards the 100% renewable energy goal. On-bill utility financing, with the assistance of green banks, can capture the benefits and financial markets that traditional banks have ignored. Emerald City experimented with on-bill financing and many cities are conducting pilot projects, yet none have added solar PV to their programs. With no credit checks, just an electric bill, all income levels can participate. One's ability to pay for efficiency and solar is demonstrated by one's ability to pay their electric bill. This provides access to solar energy for all income levels. The program must be set up, so the net electric bill stays the same or is lower. If fuel switching retrofits are included, as it should be, the net gain from the elimination of natural gas systems can reduce the total energy costs. The goal is to eliminate natural gas and replace it with renewable energy. Overall, total energy costs will be lower.

On-bill financing (that can provide added revenues to the utility) must have a long enough term to ensure the total cost (electric and gas) to the consumer is lower than before the financing. “On mortgage” financing is an excellent comparison example with the potential demonstrated by the Grand Traverse Habitat for Humanity Depot project where the lower-income homeowners have their grid tied solar systems powering all of their electricity and HVAC on a net annual basis, with the cost of solar in the 30 year mortgage—adding only \$35 per month, fixed for 30 years. This is clean energy security and financial security for these lower-income residences. Since we finance natural gas equipment in the mortgage, why not solar equipment?

3.5. Rebates

Rebate programs are a critical incentive for implementing energy efficiency, solar systems, thermal and electric storage. Rebates are cheap way for a utility to buy “nega-watts” and to incentivize solar deployment and energy storage. Emerald City, like most electric utilities, has a good rebate program in place that simply requires expansion to include fuel switching from natural gas to electric HVAC systems, thermal and electric storage systems, demand management systems, electric vehicles, and their charging systems.

Smiley

3.6. Time of Use Rate Reform

Emerald City has time of use (TOU) rates for some customer classes. TOU meters must be provided to all customer classes with new TOU rate structures. If necessary, an intermediate period can be added to the off-peak and on-peak periods. The on-peak period is from 10 am to 5 pm, weekdays. All other times, including weekends and holidays are considered off-peak. Off-peak primary service high load factor commercial kWh energy rates average 5 cents per kWh. With grid harmonization, high off-peak energy use, and fuel switching and storage, most rate payers will become “high load factor” consumers, justifying the low off-peak rates for all customer classes.

3.7. Develop Grid Harmonization Inside the Distribution System

Grid harmonization is a generic phrase for various control methodologies to optimize the utilization of renewable energy, energy storage systems and to balance loads. One example is monitoring wind energy to switch on thermal storage systems during a cold windy night when marginal cost wind power nears 2 cents per kWh. Grid harmonization starts from the inside out, peak shaving, and managing demand, while monitoring renewable generation and prices. A graphical example of such a grid harmonization system is shown below in Figure 7, referencing Charlie Gruenwald’s “Link and Sync” plan. However, the Emerald City plan would exclude the MISO transmission portion and be focused on the distribution side of the utility.

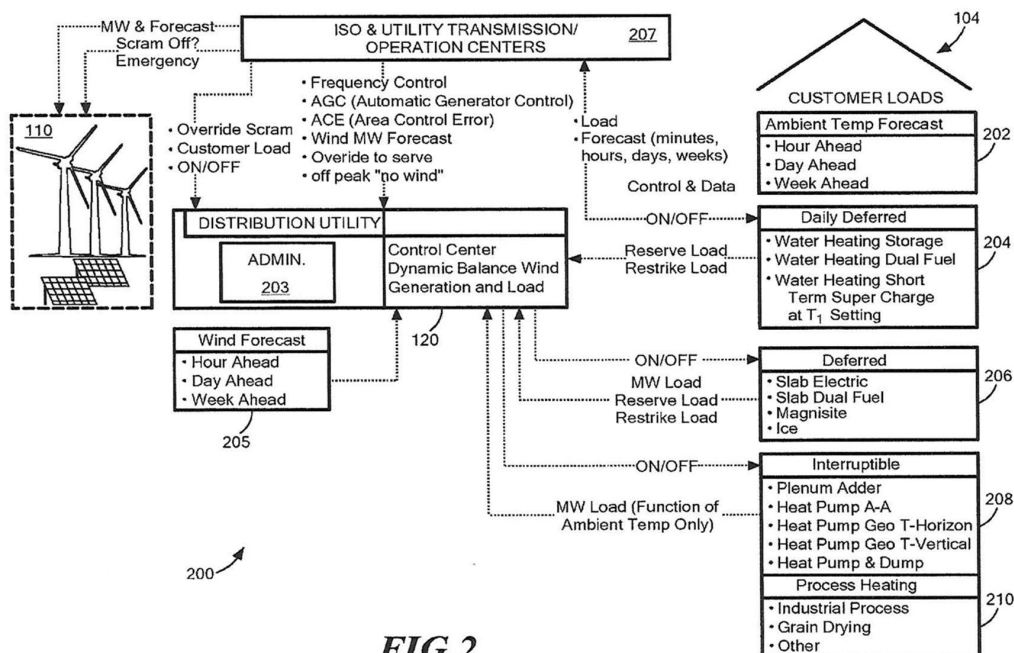


FIG. 2

Figure 7

Smiley

Electrical building codes need to be modernized in conjunction with solar and demand management systems. Solar electric interconnection guidelines and electric service sizing requirements are irrational, especially with new demand management systems. The electrical load on the average Emerald City residence is 7 amperes. A standard 100-amp electric service should not need expansion in the typical residence.

Electric utilities, for the most part, can control their own electric generation and distribution inside the distribution substations. The large multi-state Mid-Continent Independent System Operator, (MISO) has costs and control of transmission level electric system activities. New generation outside the utility distribution system must meet MISO planning, interconnection and operating requirements, and project owners must pay fees to participate the system. The MISO queue for generation is long, due in part for the high demand for cost-effective new renewable energy. By focusing on renewable energy projects inside the distribution system MISO complications and costs can be avoided.

3.8. Ban on New Natural Gas Lines

With electricity out competing natural gas for existing HVAC systems it makes both economic and environmental sense to phase out natural gas and place a ban new natural gas connections, while developing biogas systems (i.e. green gas) for special cases. Bans on new natural gas pipeline connections are being implemented in many cities for environmental, cost and safety reasons. Replacing old leaking natural gas lines is waste of money and they should be shut off for financial and safety reasons while the consumers convert to all electric systems.

3.9. Green Bonds, Banks, and Other Financing

Green Bonds, Green Banks, and other financing sources such as PACE (property assessed clean energy financing) should be implemented. Munis can raise capital with green bonds, usually as much as needed, within the fiduciary regulatory limits on municipal bonds. The green bonds can be promoted and sold locally to maximize the local economic benefits. A local green bank, whether independent of banks or a special division of local banks should be established, with special expertise and focus on green energy systems from generation sources, energy storage, fuel switching, efficiency applications, mechanical and electrical retrofits.

4. Projects

Projects consist of three primary generation sources, solar energy, wind energy and combined heat and power (CHP) biogas engines. Projects will also include grid harmonization infrastructure with thermal and electric energy storage plants and systems. The 100% percent net annual energy target is roughly 870 million kWh. The proposed target generation mix is 300 million kWh of solar energy, 400 million kWh of wind energy, and roughly 170 million kWh of CHP generation. The tables below (see Tables 1-3) breakdown potential installations and capacity. It should be noted that even during a low wind, low sun day the energy available from the three primary generation sources can meet the city average energy needs.

Energy efficiency measures and practices are an important component of projects, but they should not take precedence over renewable energy generation. While the potential for energy efficiency is significant, actual results do not match the potential. Commercial and industrial consumers who make up over 70% of the city energy consumption typically do not place energy efficiency as a high priority in their capital and operating expense decision making. First, there are many competing financial needs in a business, so when there are excess revenues a business manager may decide to hire another worker or buy a new production machine rather than invest in energy efficiency measures. Second, energy costs for many businesses are a small part of the operating budget, often small in comparison to labor, insurance, and taxes. Businesses will take the easy low hanging fruit, such as LED lamps, but more aggressive actions, such as window replacement, is complicated and expensive. Energy efficiency measures and practices will reduce the

Smiley

eventual total amount of renewable generation and energy storage projects, and this is important, but they do not change the fundamental fossil fuel, carbon intensive energy delivery system.

Incumbent electric utilities will argue that 100% renewable energy is not possible in the near term because of long-term contracts and debt obligations for fossil fuel and atomic generation. These contracts and debt must be renegotiated, bought-out or cancelled as soon as possible. During the 2008-2009 financial crisis millions of citizens lost their homes and property due to no fault of their own - they simply had to default and walk away. With the climate crisis we must be prepared to do the same with our underwater coal and atomic power plants that are costing citizens hundreds of millions of dollars every year, just in the upper Midwest. The state legislatures of Illinois, Indiana and Ohio have forced their citizens to unfairly subsidize these emitting power generation sources. In the largest power plant bond default in the 1980's, the Washington Public Power System defaulted on \$2.5 billion in bonds and yet survived and prospered. The contracts and debt on dirty, underwater power plants need to be cancelled as soon as possible to make room for lower cost renewable energy.

Local ownership and control are paramount to maximize community economic benefits and to dispatch the renewable energy resources to optimize grid harmonization. Utility-scale solar arrays and wind turbines must be merchant power plants wholly owned and controlled by the city utility. The traditional power purchase agreement (PPA) used by electric utilities is an economically dysfunctional, tax avoidance based, financial approach that discourages local ownership, drains money out of the community, increases economic inequality, and makes permitting projects more difficult. Community ownership brings community acceptance. While tax credits do help account for the environmental benefits and non-market external costs and, as such, are justified, these financial benefits must be made available to all non-profit organizations, municipalities, and other public entities. Recently proposed 2020 federal legislation (House Bill 2) attempts to correct this flaw in our clean energy incentive programs—and would be a boost to non-profit public renewable energy projects. Nevertheless, a municipal utility can compete with tax advantaged PPA's by utilizing long-term, lower interest financing and utilizing their own or hired project development expertise. The Emerald City utility and public works department must staff up with policy and project development expertise, basically energy “concierges” to guide the advancement of the 100% renewable energy plan.

4.1. Solar Energy

Solar energy systems inside the city need to be quickly advanced to push the energy inside out to reduce loads on distribution substations and increase distribution capacity.

There are four project types for solar electric implementation. First, there are individual property owners investing on their own (with or without utility on-bill financing), including residential, multifamily, condominiums, and businesses. Second, non-profit public and government consumers, including schools, governmental buildings, churches, and public facilities represent a project type. A third type are community and cooperative solar projects. And fourth, utility-scale installations. The following list includes examples of solar site opportunities in Emerald City. 80% of the solar energy generation is projected to come from utility scale, large commercial and community solar projects. With economies of scale these projects provide the most cost-effective, dispatchable and controllable solar systems—with costs comparable to the utility's present “avoided cost.”

Smiley

Table 1

SOLAR ELECTRIC	Acres	Installed KW	Capacity Factor	Energy (kWh/yr)	kW on Cloudy day	Est. Capital Cost (\$million)
Airport / Aero Park Drive Area	125	25,000	0.18	39,420,000	2,500	31.3
Solar PV - NMC/CHS/Civic Center	10	2,000	0.18	3,153,600	200	2.5
GT Commons Solar PV	10	2,000	0.18	3,153,600	200	2.5
South Hwy 31 Solar PV - West JR High/Meijer/...	250	50,000	0.18	78,840,000	5,000	62.5
Sub-station Solar PV w/ 22 MW PPA +TWP FARMS)	400	70,000	0.18	110,376,000	7,000	87.5
M72 V44 Wind Site Solar PV - 3 MW +	15	3,000	0.18	4,730,400	300	3.8
Distributed "Community Solar PV" (with established policy)	50	10,000	0.18	15,768,000	1,000	12.5
Distributed net metering residential/commercial/institutional	100	20,000	0.15	26,280,000	2,000	35.0
Schools: T Heights, G Loomis, CGS, EE, etc	6	1,200	0.18	1,892,160	120	1.5
West Bay Abandoned Coal Yard--Solar	0.25	140	0.18	220,752	14	0.2
Industrial Sites; trackers and single axis large net metering	15	3,000	0.18	4,730,400	300	3.8
SOLAR TOTAL	807	161,340		288,564,912	16,134	\$ 243

Since many utility customers (~80%) do not have optimal solar access on their property, community or cooperatively owned solar projects are essential to provide opportunities and distributed benefits for all citizens. As demonstrated by many of the good community solar project models, the investment can be handled on one’s electric bill with on-bill financing. Shares purchased for the lower cost solar energy should reduce one’s electric bill, so the total electric bill is the same or lower than before, without the solar investment. For those without electric bills, shares can be provided for cooperatively owned projects. There are dozens of good community solar project models and the State of Minnesota has some of the best examples. Community or cooperatively owned solar allow the electric utility to optimize the location and size of the systems to aid in grid harmonization. For instance, a 10 MW community solar array can be placed on a 10 MW distribution circuit that can essentially zero out a distribution substation—leveraging more capacity on the distribution circuit.

4.2. Wind Energy

With the recent rapid development of tall tower, large rotor, high capacity factor wind turbines that operate at around 50% capacity factors, generating electricity roughly 90% of the time, the cost of wind energy out-competes all energy sources, averaging 4-5 cents per kWh in moderate winds, with a marginal cost on a windy day approaching 2 cents per kWh—without tax incentives (see Figure 8).

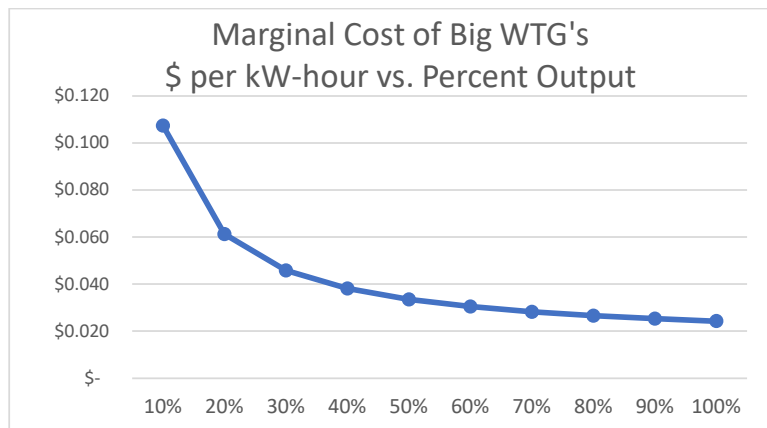


Figure 8

Smiley

The moderate winds on the city’s surrounding hills specify IEC Class IIIA wind turbines that will generate at a high capacity factor with rotor diameters of roughly 150 meters, nominally rated at 4 MW’s peak capacity. The windiest hour is 3 pm and the windiest months are in the fall and winter, from October to April.

Here, 21 wind turbines are proposed in addition to the existing five, 2 MW wind turbines (10 MW total) that were contracted under a PPA several years ago. The proposed wind projects are classified as distributed wind, where one to four turbines are grouped together, typical for this terrain and landscape with small farm parcels. Distributed wind projects in multiple townships are not attractive for international wind developers who develop based on large wind farms in vast agricultural areas owned by outside investors, selling the energy under power purchase agreements. Such large wind farm projects reduce community economic benefits that come with locally owned distributed wind energy. The local utility has, or can hire, the expertise needed to develop and install distributed wind projects.

Table 2

COMMERCIAL WIND	Number	Installed KW	Capacity Factor	Energy (kWhr/yr)	kW on Low Wind Day	Est. Capital Cost (\$million)
Existing Heritage 10 MW	5	10,000	0.3	26,280,000	500	\$ -
City Distributed Wind Projects	1	4,200	0.48	17,660,160	210	\$ 7
Garfield Twp Wind	2	8,400	0.48	35,320,320	420	\$ 14
Elmwood Township	4	16,800	0.48	70,640,640	840	\$ 29
Long Lake Township	4	16,800	0.48	70,640,640	840	\$ 29
East Bay Township	2	8,400	0.48	35,320,320	420	\$ 14
Acme Township	4	16,800	0.48	70,640,640	840	\$ 29
Peninsula Township	1	4,200	0.48	17,660,160	210	\$ 7
Blair Township	3	12,600	0.48	52,980,480	630	\$ 21
WIND TOTAL	26	98,200		397,143,360	4,910	\$ 150

4.3. Combined Heat and Power

Combined Heat and Power (CHP), gas engines are low cost and relatively easy to install providing a dispatchable generation source. While the goal is to run the engines on biogas, initial planning and installations can begin on natural gas if necessary. Intelligently designed and operated CHP systems will run between 80-90% efficient, displacing other natural gas systems of lower efficiency, and providing a net gain in efficiency and reduced emissions. It is proposed the CHP plants be dispersed throughout Emerald City, roughly 5 MW each units, totaling 35 MW’s, installed near large thermal loads and distribution substations. This includes schools, the college, public works, hospitals, and industrial consumers of hot water for process, domestic water, and space heating. Large hot water storage tanks, combined with the gas engines, can also be heated with excess wind and solar energy. The primary role of the CHP system is as a load balancing source, sized approximately to the average city electric load which can also run in the event of grid outages. The engines will be dispatched to run when there is inadequate wind, solar and battery storage. The long-term goal is to build one or more biogas production plants (as part of the city waste handling system), generating green gas from the local organic waste stream including such sources as food waste, process waste, agricultural waste, and septic system waste. Examples of such biogas plants are found at Lemvig, Denmark and Trollhatten, Sweden.

Smiley

Table 3

			Capacity Factor	Energy (kWh/Yr)	Est. Capital Cost (\$million)
COMBINED HEAT AND POWER (CHP) NG-Biogas-Thermal Storage					
College/Schools/CHS/EE/CC/MC Hospital/District heat	1	5,000	0.5	21,900,000	\$ 5
Aero Park /Coast Guard/ District heat	2	10,000	0.5	43,800,000	\$ 10
Hillshire Foods/BATA/District Heat	1	5,000	0.5	21,900,000	\$ 5
GT Commons/Munson Hosp/W Jr High/Meijer/ District Heat	1	5,000	0.5	21,900,000	\$ 5
Public Works/Library/Waste Water Plant/District heat	1	5,000	0.5	21,900,000	\$ 5
Cone Drive/Oryana/Govt Center/Downtown/District Heat	1	5,000	0.5	21,900,000	\$ 5
TOTAL	7	35,000		153,300,000	\$ 35

4.4. Investment Criteria

The total capital expenditure for full implementation, with grid infrastructure retrofits and grid harmonization systems, can approach \$450 million. With annual community energy expenses of approximately \$55 million (without transport), investing \$450 million from public and private sources makes economic sense. One can ask the simple question; “how much would one invest to earn \$55 million a year?” The logical answer will far exceed \$450 million.

The appropriate investment criteria vary with the project type and investor. These include non-profit public works, including schools, churches, hospitals, municipal services (including the utility); individual net metered properties including residences, multifamily apartments, condominium associations, and renters; commercial for-profit business; and cooperative or community solar projects.

For public works, such as utility-scale solar systems or large public systems, benefit/cost analysis should be conducted. Selecting a project is a simple matter of conducting benefit/cost analysis on proposed system alternatives to find the best value for the community.

For net metered solar consumers, especially with long-term, on-bill or other financing, no investment analysis is required as the solar system cost is already budgeted. The budget is one’s utility bill, which is paid either way, a lifetime energy mortgage or debt that can be off-set and eliminated once the solar system is paid for. The Grand Traverse Habitat for Humanity Depot project is a good example, where the cost of the solar systems, providing 100% net-metered energy for all electric and HVAC systems, is included in the 30-year mortgage adding only \$35 per month, fixed. This is affordable energy security that distributes solar to lower-income citizens.

Commercial for-profit solar installations, where the solar system generation is beyond offsetting one’s own electric consumption, become an earning investment. The municipal utility must provide a fair price for the solar to “make a market”. Since all IOU’s are guaranteed roughly a 10% return on investment, all businesses investing in solar should be treated the same, or better. Solar energy prices should be scaled to make a market accounting for economies of scale. The German feed-in-tariff program provides a good model, with long-term guaranteed prices, and priority to the grid. With tax advantages accounted for, private or public organizations, can simply conduct a standardized analysis to insure the minimum 10% return on investment.

Smiley

5. Conclusions

The following graph (Figure 9) illustrates the ten-year planned changes.

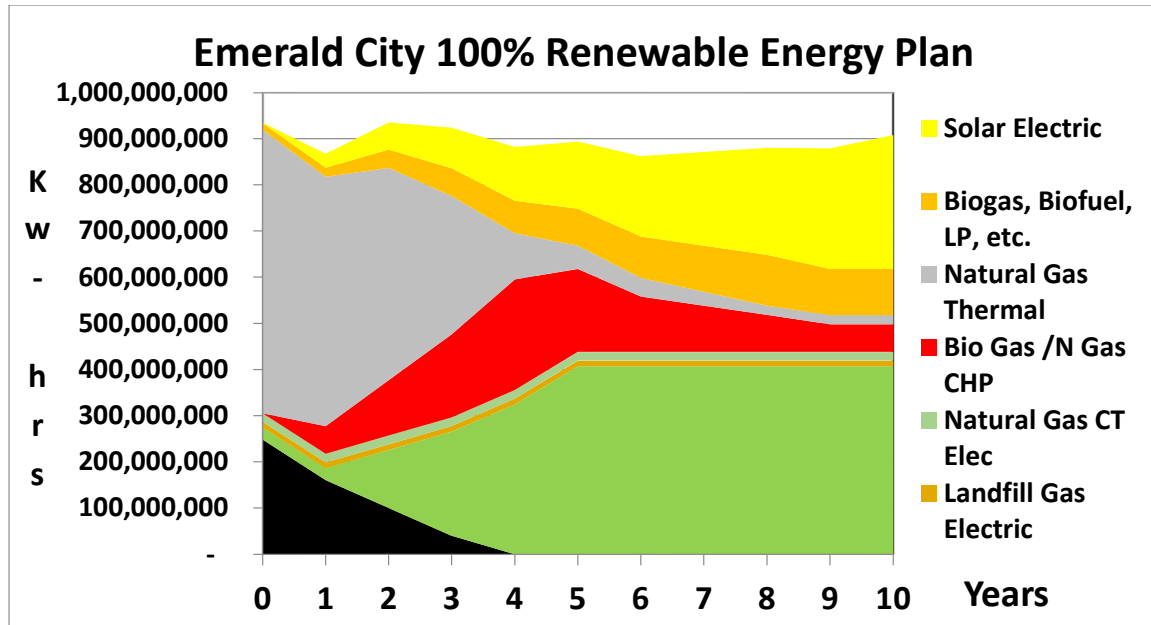


Figure 9

With green financing mechanisms, green bonds, green banks and utility on-bill financing, Emerald City can achieve a distributive and regenerative energy economy with energy security, economic and environmental justice. The public utility will as much as triple its electric distribution to displace natural gas and gasoline, increasing quantity and quality at a lower unit cost. With unlimited solar net metering, community solar and wind projects, waste to biogas CHP, harmonized with distributed energy storage, all citizens, rich and poor, will have the opportunity to benefit, bathed under the abundance of solar energy.

Utilizing a climate crisis fee, positive and negative, with the marginal cost of wind energy near 2 cents per kWh, natural gas will be eliminated for the most part, keeping \$20 million a year in citizens' pockets to pay for more efficiency measures and green electricity to heat, cool and power the community.

It is irrefutable, that at some point our communities will be 100% renewable energy heated and powered. It may be 10-20 years before polluting fossil fuels are physically, economically, or politically gone. Yet we are in a race against time. Now that wind and solar and other distributed renewable energy sources are the least cost option, every delay is costly to society and the environment. Community power is the fastest path for a sustainable future, where metered results can be achieved quickly. Communities do not need permission or legislation from the state or national government. With results demonstrating meaningful solutions we address the climate crisis and provide hope, abating the anxiety and depression inflicting our communities, in turn reenergizing the community.

Hourly Solar Radiation Estimation Using Data Mining and Generalized Regression Neural Network Models

Yacob G. Hiben^{1, 2*}, Mulu B. Kahsay¹, Johan Lauwaert²

¹Thermal and Energy Systems Chair, School of Mechanical and Industrial Engineering, Mekelle University, Endayesus Campus, Mekelle, Ethiopia

²Department of Electronics and Information Systems, Faculty of Engineering and Architecture, Ghent University, iGent-tower, Technologiepark-Zwijnaarde 15, 9052 Ghent-Zwijnaarde

yacob.gebreyohannes@mu.edu.et

Abstract

Accurate information on solar radiation intensity is essential for the development of solar energy projects. The real-time solar radiation measurement on smaller time intervals is preferred for some precise data. However, since the values are greatly affected by the time and location and the calibration and maintenance work is costly, only professional institutes will perform this type of measurement for short periods. As such, usually properly recorded radiation data are hardly available in most developing countries like Ethiopia. This leads to the requirement of using estimation models established by climatological and geographical parameters of locations. Among various models, hourly solar radiation estimation models are important for much more accurate prediction because of the detailed changes that can be recorded in a day. In this study, Data Mining (DM) and Generalized Regression Neural Network (GRNN) methods were proposed. The correlation coefficients for the models were determined using calculated sun-earth parameters and measured irradiance in Mekelle, Ethiopia. The methods of statistical analysis were used to evaluate and verify the performance of the models. The study showed that the calculated variable coefficients of the DM model and $G_{GRNN} = 0.62 + 0.57 (G_{mes})$ can predict the nature of hourly solar radiation in the study area. The GRNN method showed better estimation compared to the DM technique. The DM technique also showed a better estimation for clear sky days. The limitations for accurate prediction of the models could be mainly due to the short-term measured average solar radiation values and the outlier input features of the training data space. Hence, further study is recommended for effective predictions, especially for cloudy days.

Keywords: Solar radiation, Estimation models, DM, GRNN, Mekelle

1. Introduction

The solar radiation collected by a surface on earth varies on seasonal (daily or monthly) basis due to the presence of clouds and the Sun position. It also varies on an hourly basis due to the east to the west relative position of the sun (Bekele, 2009). Accurate information on solar radiation intensity is, therefore, essential for the development of solar energy projects as well as long-term performance and economic analysis of solar energy systems at a given location. For some precise researches, the real-time measured solar radiation data recorded on smaller time intervals are preferred. However, the values are greatly affected by the time and location in addition to the costly calibration and maintenance work. Usually, only professional research institutes and universities will perform this type of measurement for short periods (Zhang et al., 2017). Thus, in most developing countries like Ethiopia, properly recorded solar radiation data are hardly available.

Without properly recorded solar radiation data, estimation models are necessary to convert the available climatological and geographical data. Through investigating the literature, a large proportion of studies are to estimate the solar radiation for impending days and hours (Zhang et al., 2017; Lauret et al., 2015; Hocaoglu et al., 2008). Since an hour is commonly the smallest time interval in the measurements of official meteorological stations, hourly data represents more information and is more useful for different applications (Khatib et al., 2015). Thus, the effective estimations of hourly solar energy capacity through the statistically tested estimation models play an important role in the design and application of solar systems (Duffie, 2013).

Among various models and parameters, Data Mining (DM) models proposed by Liu and Jordan and verified by Collares-Pereira and Rabel formulated using the concept of sun-earth angle, climatological parameters, and geographical parameters have been used to determine hourly solar radiation patterns from daily solar radiation data (Khatib et al., 2015; Bulut et al., 2007; Koussa et al., 2009; Fletcher et al., 2007; Raja, 1994; Trabea et al., 2000;

Rietveld, 1978; Ravinder Kumar et al., 2005). Many studies have also applied Artificial Neural Networks (ANNs) to estimate solar radiation. The ANNs used to estimate solar radiation have similar configurations and are much more complex than an empirical model in terms of their computational work. Their basic principle is to correlate the input features with the target output in applying different selectable approaches. The variables in an ANN model include the input, the number of layers and neurons, training algorithm, and transfer function. Any modification in the variables can create a new ANN model, so it is necessary to develop appropriate rules to compare these ANN models. Since all of the ANNs have their pros and cons, there is no perfect algorithm for a neural network that can solve all problems. The ANNs algorithm is chosen depending on the task. As such, the Generalized Regression Neural Network (GRNN) was employed in this study. This method is a much more efficient algorithm for small datasets and the network uses lazy learning that does not require iterative training but just stores parameters and uses them to make predictions (NeuPy-2019, n.d.; Specht, 1991).

The objective of this study is, therefore, to analyze and validate empirical DM and GRNN models for hourly solar radiation estimation using measured irradiance and calculated sun-earth parameters. The study also aims to show the effectiveness of the models for hourly solar radiation estimation. Data was collected permitting direct computerized data recording by automated measurement procedures to obtain more precise results in Mekelle University's main campus, Ethiopia. A description of proposed models was made from literature. This was followed by the determination of the model's unknown coefficients and statistical tests. Computational Microsoft Excel spreadsheets and Python programming language were used for data treatment, conditioning, and analysis. The output of the study appreciates achieving the most appropriate model and will have significant importance in terms of promoting solar energy applications.

2. Materials and Methods

2.1. Sun-Earth Parameters

Location is represented by geographical coordinates in degrees as latitude (ϕ) and longitude (λ). The solar angle parameters represented as the declination (δ), hour angle (ω), and sunset (ω_s) angles in degrees are used to describe Sun motion. The Earth trajectory around the Sun is an ellipse with the Sun being one of its foci represented by the Sun elevation h and the Sun azimuth ψ in degrees. The relations among the parameters are summarized in Table 1 (Prescott, 1940; Angstrom, 2007; Ulfat et al., 2008; Türkiye Bilimsel ve Teknik Araştırma Kurumu. et al., 2004; Iqbal, 1980; Şen, 2008).

Tab. 1: Sun motion and Earth trajectory Equations

Parameter	Equation	Remark
Sunset hour angle	$\omega_s = \cos^{-1}(-\tan \phi \tan \delta)$	ω_s is the sunshine duration.
	$\delta = 23.45 \sin (0.9863 * (248+n_d))$ n_d is the day number	ϕ is the angle between the location and the equator. δ is the angle between the sun and the equatorial plane of the earth.
Hour angle	$\omega = 15 (T_{solar} - 12 \text{ hour})$	ω is the angular displacement of the sun from the focal point and it defines the true solar time.
True solar time	$T_{solar} = T_{loc} + (EoT + \left(\frac{D_{hg}}{\text{degree}}\right) [(LSMT - \lambda)])/60$	T_{solar} (hr) is given by daily apparent motion of the true or observed sun. It depends on the interval between two successive returns of the sun to the local meridian.
	T_{loc} is the local time (hr) EoT is the Equation of Time (min) D_{hg} is the time difference (advance of 4 min per degree) LSMT is the Local Standard Meridian Time	
	$EoT = 9.87\sin(2B) - 7.53\cos(B) - 1.5\sin(B)$ $B = (360^0/365) (n_d - 81)$ B is a factor	EoT is the difference between apparent and mean solar times, both taken at a given longitude for the same real instant of time.
	$LSMT = 15^0 * \text{Time zone}$	LSMT is a reference meridian

		used for a particular time zone. It is similar to the prime meridian used for Greenwich Mean Time (GMT).
		λ is the angle between the meridian of the location with the standard meridian.
Sun elevation	$h = \sin^{-1}(\sin(\varphi) \sin(\delta) + \cos(\varphi) \cos(\delta) \cos(\omega))$	h is the angle between the horizontal plane with the Sun direction. The value $h = 0$ is at sunrise and sunset; it varies between 90° (zenith) and 90° (nadir).
Sun azimuth	$\Psi = \sin^{-1}(\cos(\delta) \sin(\omega) / \cos(h))$	ψ is the angle on the horizontal plane, being the projection of the Sun direction with the direction to the south. The azimuth is between $-180^\circ \leq \Psi \leq 180^\circ$.
Hourly extraterrestrial radiation	$I_o = \frac{12 * 3600 * G_{sc}}{\pi} \left[1 + 0.033 * \cos\left(\frac{360n_d}{365}\right) * \left[\cos \varphi \cos \delta \sin(\omega_2 - \omega_1) + \frac{\pi(\omega_2 - \omega_1)}{180} \sin \varphi \sin \delta \right] \right]$	G_{sc} , solar constant (i.e 1367W/m^2) is the amount of solar energy per unit time on a unit area at the mean distance of the earth from the sun normal to the direction of propagation of the radiation outside the atmosphere.

2.2. Solar Radiation Data and Processing

The measurement site is located in Mekelle University's main campus, Ethiopia at an altitude of 2208m. The two major seasons in the site are dry and wet. These seasons run from October to May and June to September, respectively. Considering the climate of the site, solar irradiance data were collected at ten minutes interval from March 2018 to October 2019. The solar irradiance data is recorded by the SPN1 sunshine Pyranometer recorder with an accuracy of +/-5%.

Computational Microsoft Excel spreadsheet was employed to process the solar data as required for analysis. The recorded data are checked for errors and inconsistencies. Assessment to correct or remove errors or uncertainty that may lead to biased and misleading of the results were done. Errors resulted from data logger time shifts and missing single data are corrected and all other unnecessary and null data out of the objective were canceled for fast and easy handling of missing values. Then, a computer program using the Python programming language was employed for data analysis. From the raw data set, hourly and daily average statistics were made for the solar irradiance data.

2.3. Solar Radiation Estimation Models

The estimation of average hourly solar radiation was tried based on the parameters and ground recorded data from the measurement site applying DM and GRNN models. These analyses were made using Python programming language.

i. Data Mining (DM) Model

Empirical models are developed for hourly solar radiation data mining using daily solar radiation data. Liu and Jordan proposed (1) for the estimation of hourly solar radiation (Duffie, 2013; Khatib et al., 2015).

$$\frac{G_h}{G_D} = \frac{\left(\frac{\pi}{24}\right) (\cos \omega - \cos \omega_s)}{\sin \omega_s - \left(\frac{2\pi\omega_s}{360}\right) \cos \omega_s} \quad 1$$

Where G_h is mean hourly solar radiation and G_D is mean daily solar radiation.

Collares-Pereira and Rabel verified the correlation given in (1) and propose (2) for estimating mean hourly solar radiation.

$$\frac{G_h}{G_D} = (a + b \cos \omega) \frac{\left(\frac{\pi}{24}\right) (\cos \omega - \cos \omega_s)}{\sin \omega_s - \left(\frac{2\pi\omega_s}{360}\right) \cos \omega_s} \quad 2$$

Where the coefficient $a = 0.409 + 0.5016 \sin(\omega_s - 60)$ and $b = 0.6609 - 0.4767 \sin(\omega_s - 60)$.

ii. Generalized Regression Neural Network (GRNN)

ANNs are a numerical modeling technique inspired by the biological neural system and is capable of processing non-linear relationship, data sorting, pattern detection, optimization, clustering, and simulation. It is called a "black box" modeling technique because it does not present a physical explanation about the question. The calculation units of ANNs are interconnected neurons in the layers. In terms of configuration, the model usually contains an input layer, a hidden layer, and output layer. In terms of the process of data manipulation, it mainly consists of two stages: training section and testing section. In the training section, the ANNs finish learning and storing the pattern information of the existing database. In the testing section, the ANNs recall the information to produce output based on a particular input database (Zhang et al., 2017). As such, the GRNN was employed to search for a relationship among variables which is one of the most important fields in statistics and machine learning. There are many regression methods available. Linear regression is one of them and is chosen for this task. The parameters for the proposed GRNN model are listed in Table 2 (NeuPy-2019, n.d.; Specht, 1991).

Tab. 2: GRNN model methods

SN	Method	Remark
1	Define input features and target output	$T_{solar}, \omega, \psi, h, I_o,$ and G_h
2	Normalization	The network is sensitive when one input feature has higher values than the other one. Input data normalization is required before training.
3	Learning rate	The network is sensitive to the learning rate (Standard deviation [Std]) value. Std should be on the range of input features for good prediction.
4	Training	The network stores all the information about the data (x_{train}, y_{train}) for the prediction.
5	Test	The network returns prediction per each sample in the input (x_{test}).

2.4. Statistical Evaluation Gauges

The corresponding estimated values of the models are compared with measured values using the statistical tests to ensure proper evaluation and check the estimation ability of the proposed models. The performance of the models was compared by Mean Absolute Error (MAE) and Root Mean Square Error (RMSE). The coefficient of correlation (R) was used to compare the depth of the correlation between the estimated and ground measured solar radiation (Nguyen et al., 1997).

The MAE defined using (3) yields deviation of the estimated and measured radiation values.

$$MAE = \left(\frac{1}{n}\right) \sum |G_{est} - G_{mes}| \quad (3)$$

Where n is the number of data considered, G_{est} is the estimated value of mean hourly radiation, and G_{mes} is the measured value of mean hourly radiation.

The RMSE defined using (4) yields the same idea of deviation between estimated and measured radiation values.

$$RMSE = \sqrt{\frac{\sum (G_{est} - G_{mes})^2}{n}} \quad (4)$$

The R is defined using the statistical formula in (5):

$$R = \frac{\sum (G_{est} - \bar{G}_{est})(G_{mes} - \bar{G}_{mes})}{\sqrt{\sum (G_{est} - \bar{G}_{est})^2 \sum (G_{mes} - \bar{G}_{mes})^2}} \quad (5)$$

The MAE values can be negative or positive for under and overestimations, respectively. Errors are added up neglecting the signs to obtain the mean. Thus, the long-term performance of the correlations is determined by allowing a comparison of the actual deviation term by term. This is useful to care for outliers in the data. The RMSE values are always positive and zero in the ideal case. It gives a short-term performance of the correlations

by allowing a term by term comparison of the actual deviation. This is useful to care for unexpected values in the data. The R values are always less than one and one in the ideal case. It is useful to measure if the model is good or not.

3. Results and Discussion

3.1. Solar Data and Models Parameters

The geographical and astronomical parameters of the measurement site are summarized in Table 3.

Tab. 3: Geographical and astronomical parameters of the measurement site

Parameter	Value
Latitude (φ) in degrees	13.33
Longitude (λ) in degrees	39.30
Local time (T_{loc}) in hours	00:00 - 23:00
Time zone in hours	GMT + 3
Number of days (n_d)	Between 1 for 1 st of January and 365 for 31 st of December

The statistics of the collected data are summarized in Table 4.

Tab. 4: Measured data statistics

Indicator	Global Irradiance (Wm^{-2})
Count	76616.00
Mean	253.49
Std	347.55
Max	1408.07
Min	1.05

The processed measured data for the analysis using the selected GRNN model are summarized in Table 5.

Tab. 5: Processed GRNN model data

Parameter	Description
Training data	70%
Test data	30%
Range of normalized input features	[-4, 3]
Range of Std	[0.1, 1.1]

The model empirical relations were used to calculate the DM model features of the measurement site shown in Figure 1 (a and b).

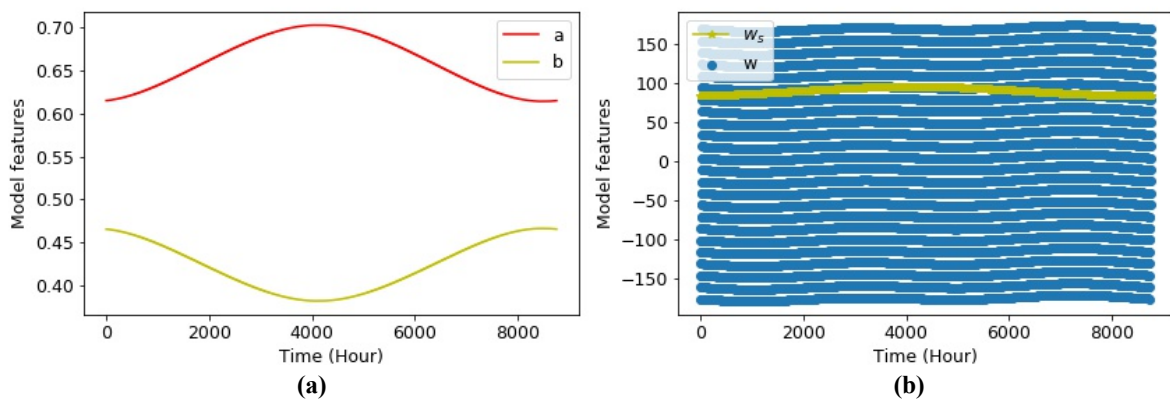


Fig. 1: DM model feature values (a) Coefficients a and b, (b) W and W_s .

The Python code was run to train the network for different learning rates by varying the standard deviation (Std) using the normalized input features. The Mean Square Error (MSE) that minimized the actual test target and network output was used to compare the performance of the GRNN method as can be seen from Figure 2.

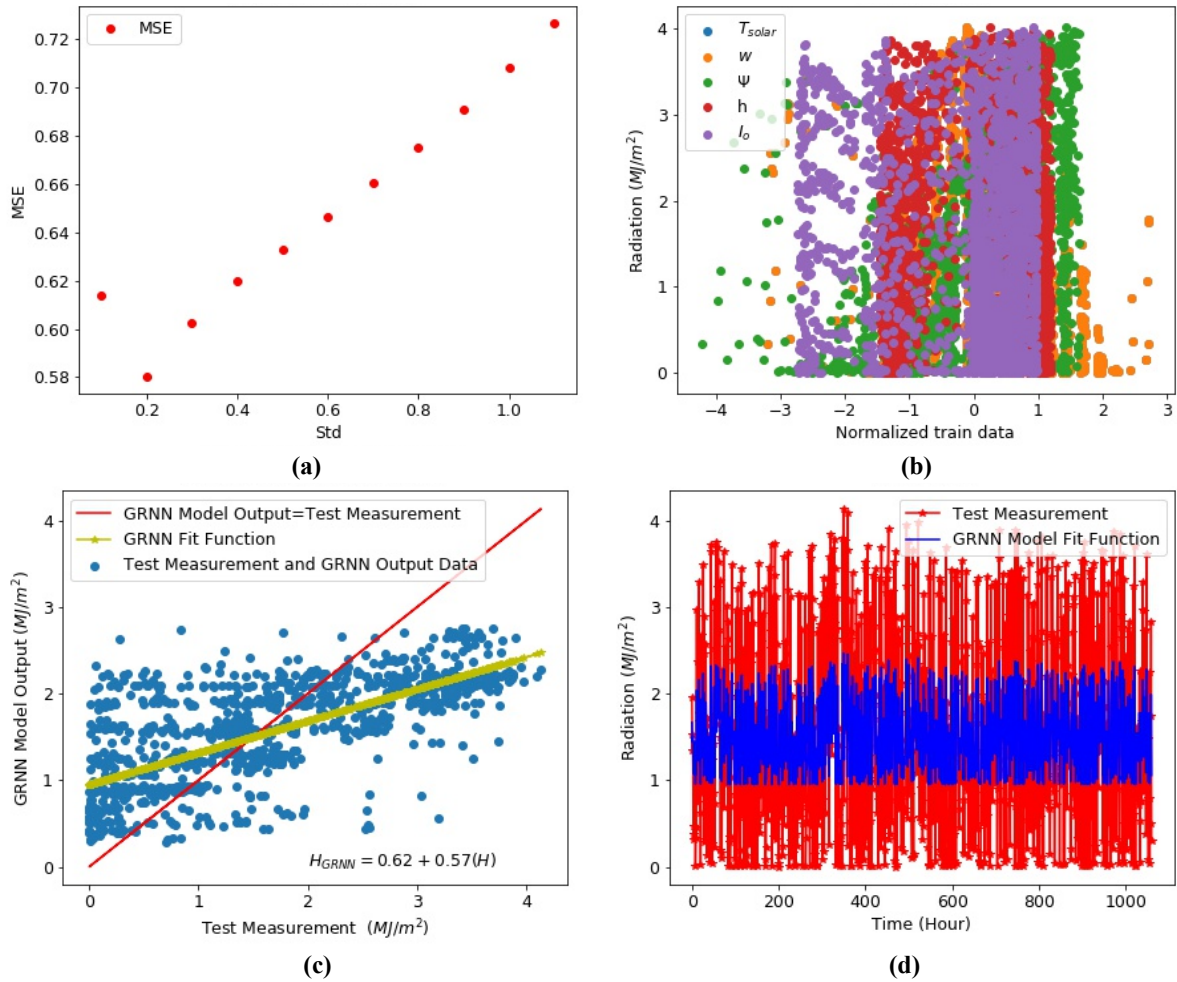


Fig. 2: GRNN learning and test (a) MSE, (b) Training data, (c) Network correlation factor, (d) Test data

From Figure 2a, the MSE subsequently receded to a lower value as the Std become 0.2 to show superior performance. As a result, the measured solar radiation can be related to the final trained neural network output after a test data in Figure 2d by $G_{GRNN} = 0.62 + 0.57(G_{mes})$. From Figure 2c, it is possible to see that the estimation match is acceptable, although not perfect for a wide range of solar radiation values. Some points on the lower and higher radiation measurements seem to diverge from the regressed line. This might arise due to the presence of data points far from other training points which are not representative of all input space. Analysis of the scatter plot for the training data in Figure 2b clearly shows the case.

3.2. Solar Radiation and Statistical Tests

The calculated extraterrestrial solar radiation and the re-sampled measured solar radiation data from the Python script file written for the analysis are shown in Figure 3.

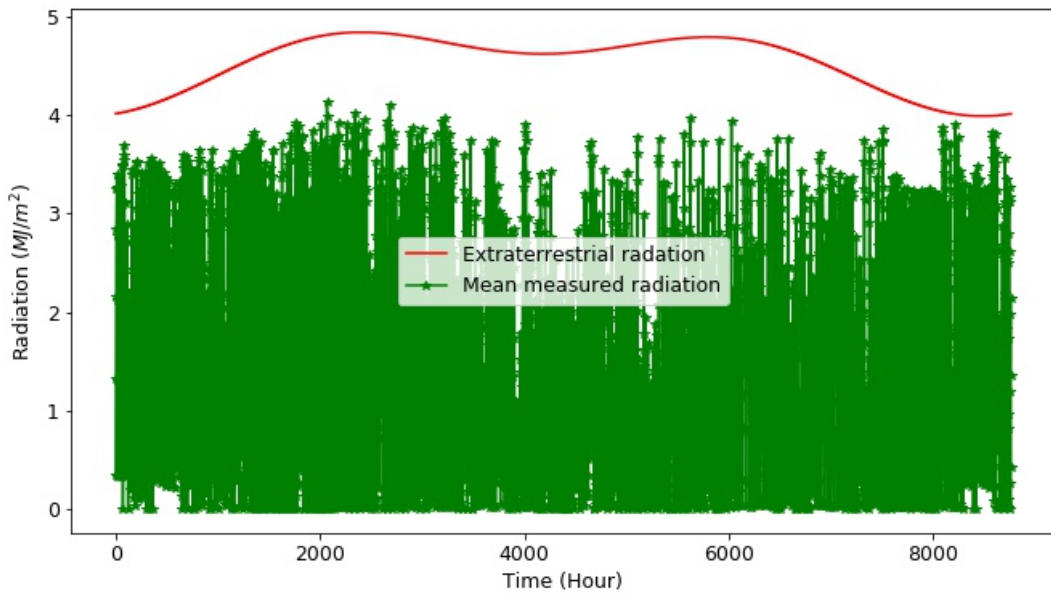


Fig. 3: Hourly extraterrestrial and measured radiation

The average hourly solar radiation from the DM model and corresponding variable feature values, the parallel measured values, and the corresponding difference (delta) values are shown in Figure 4.

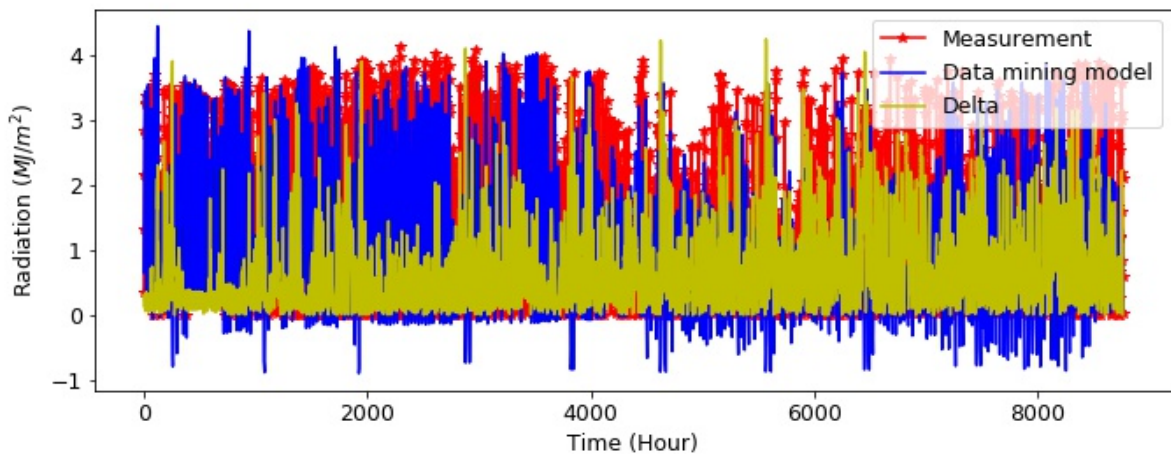


Fig. 4: Measured and DM extracted hourly solar radiation

The average hourly solar radiation from the GRNN model, the parallel measured values, and the corresponding difference (delta) values are given in Figure 5.

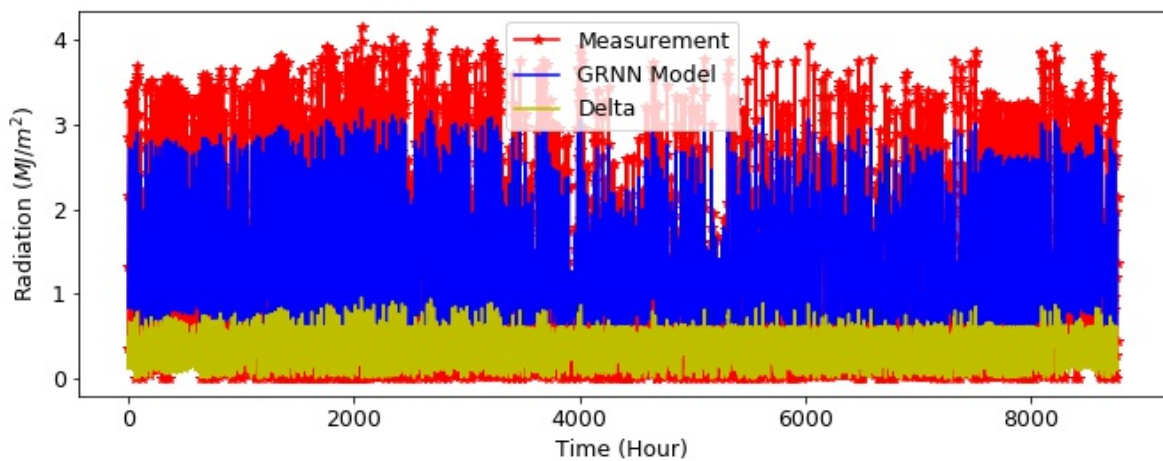


Fig. 5: Measured and GRNN predicted hourly solar radiation

The statistical tests (MAE, RMSE, and R) for comparison of estimations were determined and the results are summarized in Tables 6.

Tab. 6: The statistical test results of estimations

Indicator	DM	GRNN
MAE	0.74	0.42
RMSE	1.03	0.50
R	0.77	0.83

From the results of the statistical tests, it is clear that the GRNN model predicted the hourly solar radiation more successfully. This is in line with the large number of studies that had applied ANN to estimate solar radiation that concluded ANN models were more accurate than empirical models (Rajesh Kumar et al., 2015; Yadav et al., 2014; Qazi et al., 2015). However, it is possible to see that the estimation matches are not perfect. This could be because of the needs to consider the scattering, absorption, and reflection of the atmospheric components in detail becomes more difficult for the process of accurate hourly solar radiation estimation.

Looking in to further details in Figure 6, the prediction accuracy of the proposed GRNN model (Figure 6a and Figure 6b) is low for the lower and higher solar radiation measurements of both clear sky and cloudy days. Hourly solar radiation for clear sky days (Figure 6c) is predicted well by the DM model. However, a bad prediction is observed for cloudy days (Figure 6d) using the DM model.

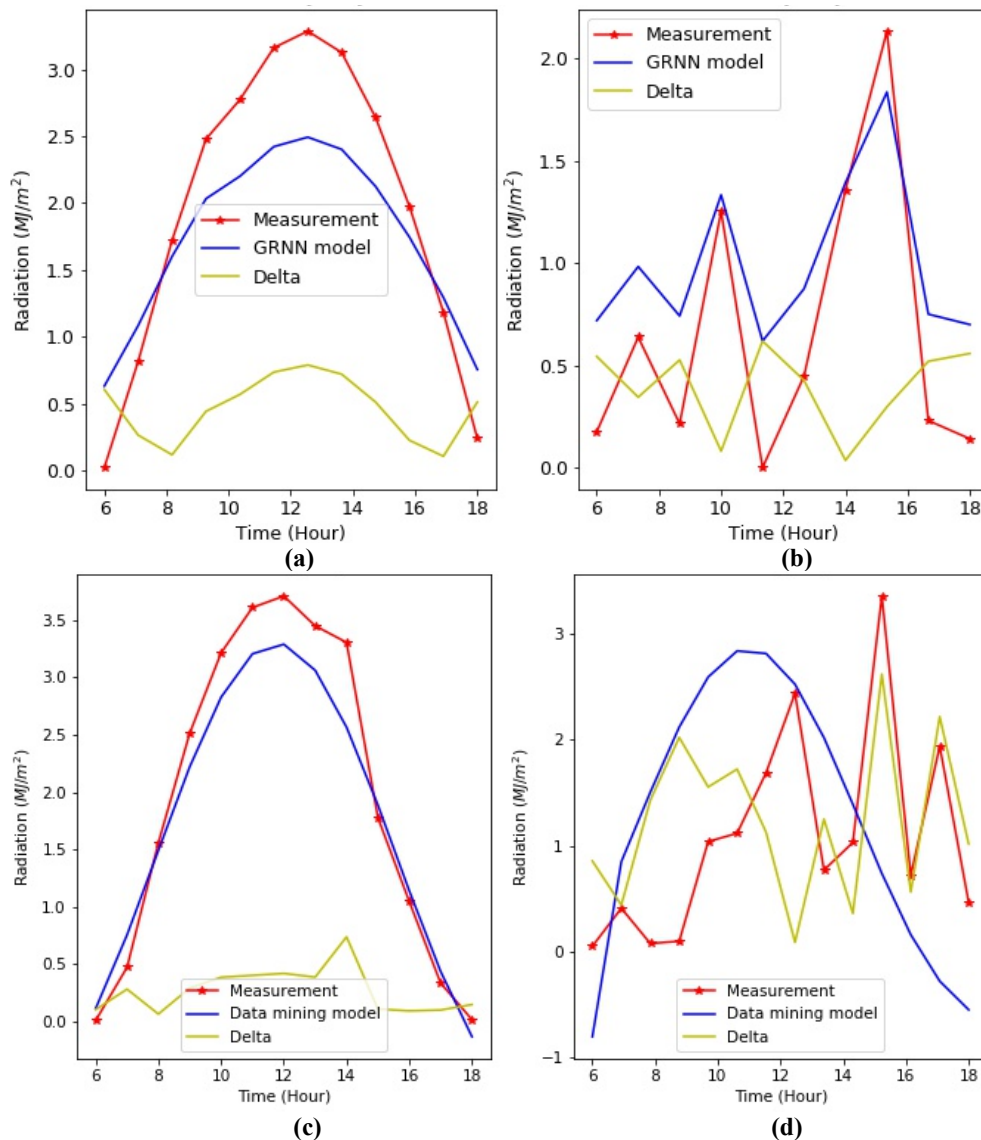


Fig. 6: Typical hourly solar radiation (a) GRNN clear sky, (b) GRNN cloudy (c) DM clear sky, (d) DM cloudy

The prediction accuracy of the proposed GRNN model is affected by the uneven distribution of the input features on the training data space. The prediction accuracy of the DM model is affected due to the mean daily solar radiation value of the measured data. This could be mainly due to unstable solar radiation levels caused by the difference in cloud formation and atmospheric conditions at different times.

The variation in estimation is usually solved by adding shifting constants to the models. Moreover, to improve the generalization capability of the proposed neural network and the accuracy of the GRNN model, only points that span the whole training data space could be considered. Since ground measured data recorded for a short period cannot provide valuable information, the variation is usually solved using long-term average data. Estimation results improved in this way could become more acceptable.

4. Conclusions

The study aims at evaluating the appropriateness and effectiveness of DM and GRNN models for the prediction of hourly solar radiation collected at the earth's surface. To select the most appropriate model for Mekelle University's main campus solar measurement site, estimation models have been collected from the literature. Measured irradiance and calculated sun-earth parameters of the site were used for the analysis. The performance of the employed models was evaluated and compared based on the statistical gauges MAE, RMSE, and R. According to the results, the models can predict the nature of the hourly solar radiation with reasonable accuracy using variable DM model coefficients and $G_{GRNN} = 0.62 + 0.57 (G_{mes})$. The estimation matches are not perfect because of the need to consider the scattering, absorption, and reflection of the atmospheric components. The GRNN model shows better prediction compared to DM. The proposed hourly DM model also showed acceptable prediction for clear sky days as compared to cloudy sky days. The limitations for accurate prediction of the models are the outlier input features of the training data space and the daily average solar radiation of the measured data. This could be mainly due to the short-term average values of the measured solar radiation. These limitations could be solved by removing outlier data from the training data space and adding shifting constants to the models. Furthermore, the limitations could be improved by using long-term average solar radiation measurements. As such, further study is recommended for a thorough treatment of the models to consolidate with this study for effective estimation of hourly solar radiation in the study area and elsewhere with comparable climatic conditions.

5. Acknowledgments

The authors would like to acknowledge EnPe capacity 5 and CoE in REWiSE projects for the funds to establish the solar radiation measurement instrumentation of Mesele Hayelom's Ph.D. study and the Ph.D. study of the first author, respectively.

6. References

- Angstrom, A. (2007). Solar and terrestrial radiation. Report to the international commission for solar research on actinometric investigations of solar and atmospheric radiation. *Quarterly Journal of the Royal Meteorological Society*, 50(210), 121–126. doi: 10.1002/qj.49705021008
- Bekele, G. (2009). *Study into the potential and feasibility of a standalone solar-wind hybrid electric energy supply system*. Skolan för industriell teknik och management, Kungliga Tekniska högskolan.
- Bulut, H., & Büyükalaca, O. (2007). Simple model for the generation of daily global solar-radiation data in Turkey. *Applied Energy*, 84(5), 477–491. doi: 10.1016/J.APENERGY.2006.10.003
- Duffie, J. A. and W. A. B. (2013). *Solar Engineering of Thermal Processes* (Fourth Ed). USA: John Wiley & Sons.
- Fletcher, A. L., & Moot, D. J. (2007). Estimating daily solar radiation in New Zealand using air temperatures. *New Zealand Journal of Crop and Horticultural Science*, 35(1), 147–157. doi: 10.1080/01140670709510179
- Hocaoğlu, F. O., Gerek, Ö. N., & Kurban, M. (2008). Hourly solar radiation forecasting using optimal coefficient 2-D linear filters and feed-forward neural networks. *Solar Energy*, 82(8), 714–726. doi: 10.1016/j.solener.2008.02.003
- Iqbal, M. (1980). Prediction of hourly diffuse solar radiation from measured hourly global radiation on a horizontal surface. *Solar Energy*, 24(5), 491–503. doi: 10.1016/0038-092X(80)90317-5
- Khatib, T., & Elmenreich, W. (2015). A Model for Hourly Solar Radiation Data Generation from Daily Solar

- Radiation Data Using a Generalized Regression Artificial Neural Network. *International Journal of Photoenergy*, 2015, 1–13. doi: 10.1155/2015/968024
- Koussa, M., Malek, A., & Haddadi, M. (2009). Statistical comparison of monthly mean hourly and daily diffuse and global solar irradiation models and a Simulink program development for various Algerian climates. *Energy Conversion and Management*, 50(5), 1227–1235. doi: 10.1016/J.ENCONMAN.2009.01.035
- Kumar, Rajesh, Aggarwal, R. K., & Sharma, J. D. (2015). Comparison of regression and artificial neural network models for estimation of global solar radiations. In *Renewable and Sustainable Energy Reviews* (Vol. 52, pp. 1294–1299). Elsevier Ltd. doi: 10.1016/j.rser.2015.08.021
- Kumar, Ravinder, & Umanand, L. (2005). Estimation of global radiation using clearness index model for sizing photovoltaic system. *Renewable Energy*, 30(15), 2221–2233. doi: 10.1016/J.RENENE.2005.02.009
- Lauret, P., Voyant, C., Soubdhan, T., David, M., & Poggi, P. (2015). A benchmarking of machine learning techniques for solar radiation forecasting in an insular context. *Solar Energy*, 112, 446–457. doi: 10.1016/j.solener.2014.12.014
- NeuPy-2019. (n.d.). *Documentation — NeuPy*. 2019. Retrieved from <http://neupy.com/pages/documentation.html>
- Nguyen, B. T., & Pryor, T. L. (1997). The relationship between global solar radiation and sunshine duration in Vietnam. *Renewable Energy*, 11(1), 47–60. doi: 10.1016/S0960-1481(96)00122-X
- Prescott, J. A. (1940). Evaporation from a water surface in relation to solar radiation. *Transactions of the Royal Society of South Australia*, 61(1), 114–118. Retrieved from <https://ci.nii.ac.jp/naid/10025613338/>
- Qazi, A., Fayaz, H., Wadi, A., Raj, R. G., Rahim, N. A., & Khan, W. A. (2015). The artificial neural network for solar radiation prediction and designing solar systems: A systematic literature review. In *Journal of Cleaner Production* (Vol. 104, pp. 1–12). Elsevier Ltd. doi: 10.1016/j.jclepro.2015.04.041
- Raja, I. A. (1994). Insolation-sunshine relation with site elevation and latitude. *Solar Energy*, 53(1), 53–56. doi: 10.1016/S0038-092X(94)90605-X
- Rietveld, M. R. (1978). A new method for estimating the regression coefficients in the formula relating solar radiation to sunshine. *Agricultural Meteorology*, 19(2–3), 243–252. doi: 10.1016/0002-1571(78)90014-6
- Şen, Z. (2008). *Solar energy fundamentals and modeling techniques: Atmosphere, environment, climate change and renewable energy*. London: Springer London. doi: 10.1007/978-1-84800-134-3
- Specht, D. F. (1991). A General Regression Neural Network. *IEEE Transactions on Neural Networks*, 2(6), 568–576. doi: 10.1109/72.97934
- Trabea, A. A., & Shaltout, M. A. M. (2000). Correlation of global solar radiation with meteorological parameters over Egypt. *Renewable Energy*, 21(2), 297–308. doi: 10.1016/S0960-1481(99)00127-5
- Türkiye Bilimsel ve Teknik Araştırma Kurumu., F., & ULFAT, I. (2004). Turkish journal of physics. In *TURKISH JOURNAL OF PHYSICS* (Vol. 28, Issue 5). Scientific and Technical Research Council of Turkey. Retrieved from <https://journals.tubitak.gov.tr/physics/abstract.htm?id=7176>
- Ulfat, I., Ahmed, F., Javed, F., Usman, A., & Kanwal, F. (2008). *Recital of Some Existing Sunshine-Based Models of Global Solar Radiation for Selected Stations of Punjab, Pakistan: A Comparative Study* (Vol. 36). Retrieved from <http://uok.edu.pk/kujs/docs/7-08.pdf>
- Yadav, A. K., & Chandel, S. S. (2014). Solar radiation prediction using Artificial Neural Network techniques: A review. In *Renewable and Sustainable Energy Reviews* (Vol. 33, pp. 772–781). Elsevier Ltd. doi: 10.1016/j.rser.2013.08.055
- Zhang, J., Zhao, L., Deng, S., Xu, W., & Zhang, Y. (2017). A critical review of the models used to estimate solar radiation. In *Renewable and Sustainable Energy Reviews* (Vol. 70, pp. 314–329). Elsevier Ltd. doi: 10.1016/j.rser.2016.11.124

B

Barber, E.

Long Term Output Deterioration of Grid-Tied PV Systems 27

Bose, A.

The Carbon Emissions of Wind Power: A Study of Emissions of Windmill in the Panhandle... 99

Brandvold, A.

Carbon Footprint in the Design Studio, a Paradigm Shift 56

Brownson, J.R.S.

Occupational Risks Associated with Solar Installations: A Review 49

C

Calderon, A.

Forecasting Carbon Emissions in Seven Eastern States of the United States: The Effects... 86

Committee, N.O.

ASES SOLAR 20/20: Renewable Energy Vision Conference, Proceedings Introduction 1

D

Duan, Q.

Estimating Hourly Solar NIR Irradiance Using Meteorological Data for Sustainable... 80

Utilizing Solar Infrared-Induced Photothermal Heating on Building Windows in Winter 18

Duroha, J.

Occupational Risks Associated with Solar Installations: A Review 49

F

Feng, Y.

Development of a Spectral Integral Method for Analyzing Solar Effects through Windows... 74

Estimating Hourly Solar NIR Irradiance Using Meteorological Data for Sustainable... 80

Foster, R.

Sustainable Solar Water Pumping for Irrigation in Bangladesh 121

G

Gebreyohannes, Y.

Hourly Solar Radiation Estimation Using DM and GRNN Models 155

H

Hall, J.

A New National Database for Solar Resource Assessment Compiled from Ground-Based... 40

K

Kahsay, M.B.

Hourly Solar Radiation Estimation Using DM and GRNN Models 155

Khoie, R.

Forecasting Carbon Emissions in Seven Eastern States of the United States: The Effects... 86

The Carbon Emissions of Wind Power: A Study of Emissions of Windmill in the Panhandle... 99

Zero Emissions Network: A Pilot Program for Carbon Emissions Reduction 133

L

Lauwaert, J.

Hourly Solar Radiation Estimation Using DM and GRNN Models 155

M

Macht, G.

Occupational Risks Associated with Solar Installations: A Review 49

Mansy, K.

Carbon Footprint in the Design Studio, a Paradigm Shift 56

O

Olson, G.

New Ways to Combine Solar Thermal with Geothermal 32

P

Phillips, J.

Carbon Footprint in the Design Studio, a Paradigm Shift 56

R

Ragheb, A.

A Framework to Reduce Dust Problems on PV Modules in the US Climatic Zones 2

Rahman, M.

Sustainable Solar Water Pumping for Irrigation in Bangladesh 121

S

Saltsman, J.

The Carbon Emissions of Wind Power: A Study of Emissions of Windmill in the Panhandle... 99

Sayed, S.I.

Sustainable Solar Water Pumping for Irrigation in Bangladesh 121

Schwaen, R.

House in a House 110

Smiley, S.

Emerald City 100% Renewable Energy Plan 142

Spector, T.	
<i>Carbon Footprint in the Design Studio, a Paradigm Shift</i>	56
Stathopoulos, P.	
<i>Zero Emissions Network: A Pilot Program for Carbon Emissions Reduction</i>	133
Stavy, M.	
<i>Is Hydrogen Energy Storage Ready for Prime Time on the North American Grid? A Guide</i>	63
Stivers, J.	
<i>Carbon Footprint in the Design Studio, a Paradigm Shift</i>	56

T

Townes, S.	
<i>Zero Emissions Network: A Pilot Program for Carbon Emissions Reduction</i>	133

W

Wang, J.	
<i>Development of a Spectral Integral Method for Analyzing Solar Effects through Windows</i>	74
<i>Estimating Hourly Solar NIR Irradiance Using Meteorological Data for Sustainable</i>	80
<i>Utilizing Solar Infrared-Induced Photothermal Heating on Building Windows in Winter</i>	18
Wang, N.	
<i>Development of a Spectral Integral Method for Analyzing Solar Effects through Windows</i>	74

Y

Young, B.	
<i>Emergency Power For All Disasters</i>	10
Yu, Y.	
<i>New Ways to Combine Solar Thermal with Geothermal</i>	32

Z

Zhang, E.	
<i>Utilizing Solar Infrared-Induced Photothermal Heating on Building Windows in Winter</i>	18
Zhao, Y.	
<i>Utilizing Solar Infrared-Induced Photothermal Heating on Building Windows in Winter</i>	18